



NASA CR-152,323

**NASA CR-152323**

NASA-CR-152323  
19800017771

# **An Advanced Panel Method for Analysis of Arbitrary Configurations in Unsteady Subsonic Flow**

**Arthur R. Dusto and Michael A. Epton  
Boeing Commercial Airplane Company  
Seattle, Washington**

**Prepared for  
Ames Research Center  
under contract NAS2-7729**

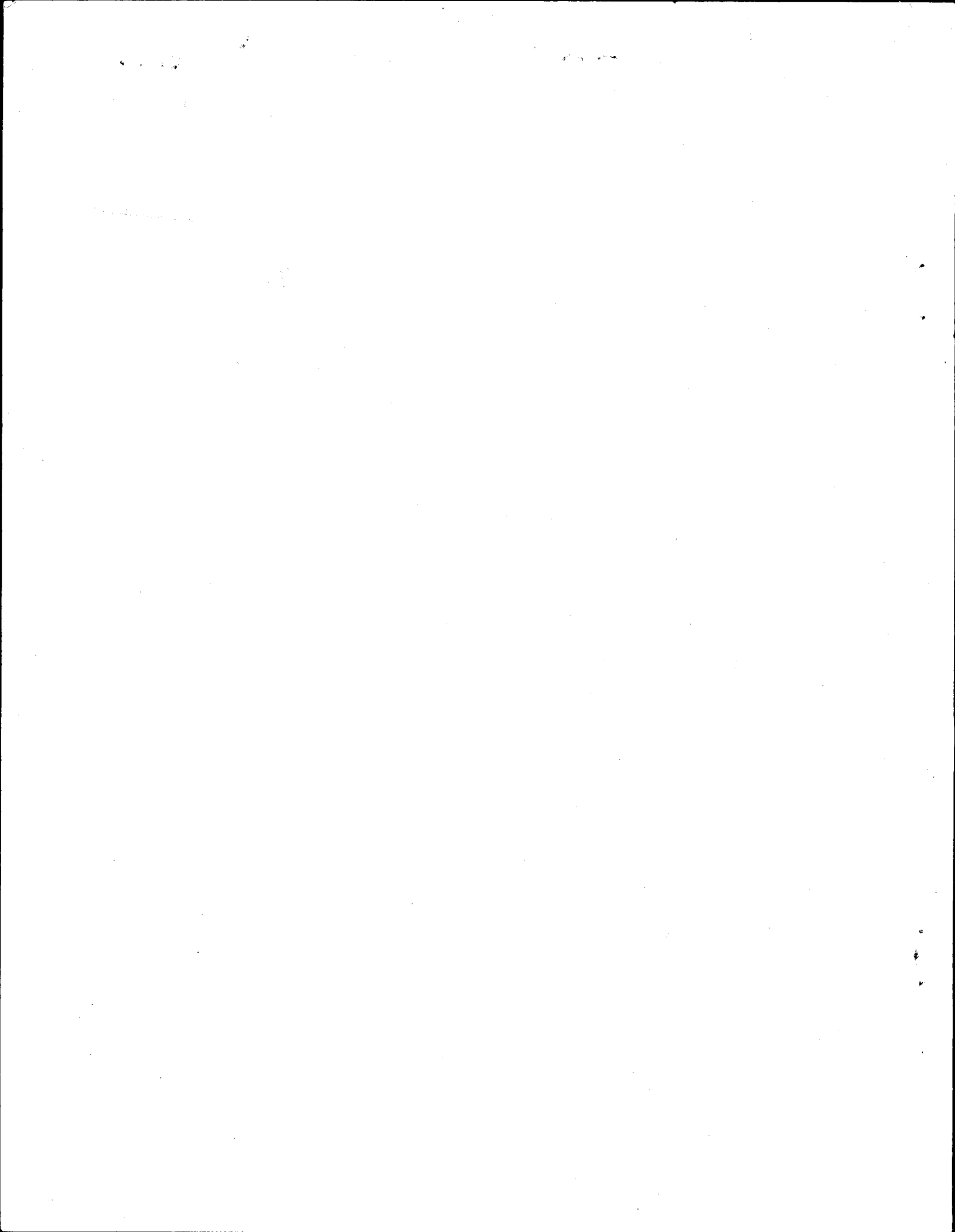
**NASA**  
National Aeronautics and  
Space Administration

**1980**

**LIBRARY COPY**

**JUL 19 1980**

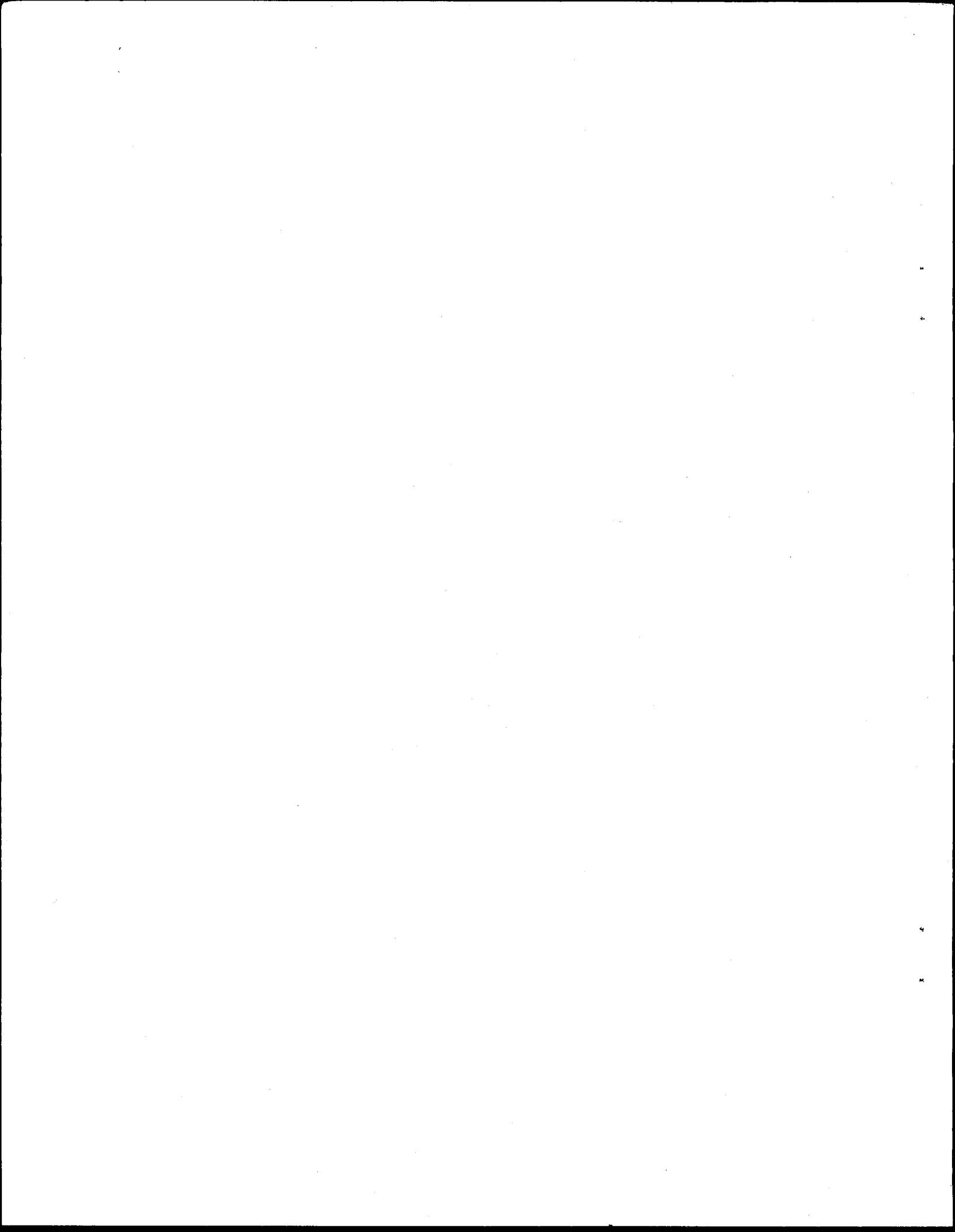
**LANGLEY RESEARCH CENTER  
LIBRARY, NASA  
HAMPTON, VIRGINIA**



1 Report No <b>NASA CR 152323</b>	2. Government Accession No.	3 Recipient's Catalog No.	
4. Title and Subtitle <b>An Advanced Panel Method for Analysis of Arbitrary Configurations in Unsteady Subsonic Flow</b>		5 Report Date <b>February 1980</b>	
		6. Performing Organization Code	
7. Author(s) <b>Arthur R. Dusto and Michael A. Epton</b>		8. Performing Organization Report No <b>D6-48846</b>	
		10. Work Unit No.	
9 Performing Organization Name and Address <b>Boeing Commercial Airplane Company P. O. Box 3707 Seattle, Washington 98124</b>		11 Contract or Grant No <b>NAS2-7729</b>	
		13. Type of Report and Period Covered <b>Contractor Report March 1976 - Feb. 1980</b>	
12. Sponsoring Agency Name and Address <b>NASA-Ames Research Center Moffett Field, California 94035</b>		14. Sponsoring Agency Code	
15 Supplementary Notes <b>Technical Monitor: Larry L. Erickson</b>			
16 Abstract  An advanced method is presented for solving the linear integral equations for subsonic unsteady flow in three dimensions. The method is applicable to flows about arbitrary, nonplanar boundary surfaces undergoing small amplitude harmonic oscillations about their steady mean locations. The problem is formulated with a wake model wherein unsteady vorticity can be convected by the steady mean component of flow. The geometric location of the unsteady source and doublet distributions can be located on the actual surfaces of thick bodies in their steady mean locations. The method is an outgrowth of a recently developed steady flow panel method and employs the linear source and quadratic doublet splines of that method.			
17. Key Words (Suggested by Author(s)) <b>Analysis Panel Method Higher Order Potential Flow Influence Coefficient Subsonic Linear Three Dimensional Unsteady</b>		18. Distribution Statement  <b>Unclassified-Unlimited</b>	
19. Security Classif. (of this report) <b>Unclassified</b>	20. Security Classif. (of this page) <b>Unclassified</b>	21. No. of Pages <b>196</b>	22. Price*

\*For sale by the National Technical Information Service, Springfield, Virginia 22151

*N 80-26270 #*



# CONTENTS

	Page
1.0 SUMMARY .....	1
2.0 INTRODUCTION .....	3
3.0 UNSTEADY FLOW PANEL METHOD .....	7
3.1 Coordinate Systems and Surface Motion .....	7
3.2 Unsteady Flow Boundary Value Problem .....	10
3.3 Integral Solution to Unsteady Flow Problems .....	15
3.4 Aerodynamic Influence Coefficients .....	19
3.5 Unsteady Flow Problem Formulation .....	28
4.0 DISCUSSION OF RESULTS .....	37
5.0 COMPUTER CODE USER'S GUIDE .....	75
6.0 CONCLUSIONS .....	89
APPENDIX A GENERAL THEORY OF FLOW .....	91
APPENDIX B APPROXIMATE LINEAR THEORY OF FLOW .....	109
APPENDIX C DERIVATION OF INTEGRAL EQUATION FORMULATION OF THE UNSTEADY FLOW PROBLEM .....	122
APPENDIX D. EVALUATION OF AERODYNAMIC INFLUENCE COEFFICIENTS. .	147
APPENDIX E. SECOND ORDER DERIVATIVES OF THE VELOCITY POTENTIAL .....	192
REFERENCES .....	195

## FIGURES

Figure		Page
1	Surface of Integration and Domain of Dependence .....	4
2	Typical Configuration Surface Panel Arrangement .....	5
3	Compressibility Coordinate System and Uniform Freestream Vector.....	7
4	Local Panel Coordinate System .....	7
5	Surface Displacement .....	8
6	Panel Approximation to Surface of Integration .....	20
7	Approximate Surface Discontinuity .....	20
8	Two Triangular Subpanels of A Quadrilateral Panel .....	21
9	Eight Triangular Subpanels, Panel Center Local Coordinate System, and Nine Canonical Points .....	21
10	Subpanel Approximation to Surface of Integration .....	22
11	Source Evaluation Points at the Center of the Panel and Its Neighboring Panels .....	24
12	Doublet Evaluation Points at the Center of the Panel and Its Neighboring Panels .....	24
13	Network Grid Point Numbering .....	30
14	Abutting Networks .....	30
15	Network Control Points .....	31
16	Surfaces of a Lifting Body and Its Wake .....	33
17	Surfaces of a Lifting Body and Its Wake .....	35
18	Planform of Test Wing .....	38
19	Thin Wing Unsteady Lifting Pressure Comparison at 18.1% Semi-span .....	39
20	Thin Wing Unsteady Lifting Pressure Comparison at 51.2% Semi-span .....	40
21	Thin Wing Unsteady Lifting Pressure Comparison at 81.7% Semi-span .....	41
22	Thin Wing Unsteady Lifting Pressure Comparison at 97.7% Semi-span .....	42
23	Panel Spacing on Test Wing .....	43
24	Test Wing with Partial Span Flaps .....	46
25	Chordwise Distribution of Lifting Pressure Coefficient, Case 1 .....	47, 48
26	Chordwise Distribution of Lifting Pressure Coefficient, Case 2 .....	49, 50
27	Chordwise Distribution of Lifting Pressure Coefficient, Case 3 .....	51, 52
28	Paneling of Test Wing with Split Trailing Edge Flap .....	54
29	Clevenson-Leadbetter T-tail, .....	55
30	Paneling of Clevenson-Leadbetter T-tail .....	57
31	Planforms of Horizontal and Vertical Fin of Davies T-tail .....	58
32	Planforms of Horizontal Tail and Vertical Fin of Stark T-tail .....	61
33	Paneling of Stark T-tail .....	62
34	Panel Arrangement for Thick Test Wing .....	65
35	Thick Wing Unsteady Lifting Pressure Comparison at 18.1% Semi-span .....	66
36	Thick Wing Unsteady Lifting Pressure Comparison at 51.2% Semi-span .....	67
37	Thick Wing Unsteady Lifting Pressure Comparison at 81.7% Semi-span .....	68
38	Thick Wing Unsteady Lifting Pressure Comparison at 97.7% Semi-span .....	69

## FIGURES (CONCLUDED)

Figure		Page
39	Paneling of Typical Transport Configuration .....	72
40	Doublet-lattice Paneling of Typical Transport Configuration .....	74
41	Airplane Configuration Oscillating in Pitch .....	78
42	Example Subroutine CBET .....	81
43	Wake Panel Spacing .....	85
44	Singularity Parameters Along Wake Streamline Coordinates .....	86
45	Aerodynamic Surface Variation in Time .....	98
46	Control Surface for Computing Aerodynamic Force .....	100
47	Surface of Discontinuity .....	101
48	Wake Surface Motion .....	104
49	Unsteady Surface Displacement .....	118
50	Representation of Field and Surface Points .....	148
51	Region of Integration Corresponding to a Panel Edge .....	154

## TABLES

Table		Page
1	Effect of Panel Density on Thin Wing Forces .....	45
2	Swept, Thin Wing Hinged Flap Hinge Moment Amplitude and Phase Errors .....	53
3	Generalized Forces on Clevenston-Leadbetter T-tail Oscillating in Yaw .....	56
4	Comparison of Davies T-tail Generalized Force Coefficients .....	59
5	Davies T-tail Generalized Force Coefficient Amplitude and Phase Errors .....	60
6	Comparison of Stark T-tail Generalized Force Coefficients .....	62
7	Computed Vs. Exact Values of Velocity Potential and Its Derivatives at Surface of A Sphere .....	64
8	Truncation Coefficients and Zeros of Constrained Tschebycheff Polynomials ..	176
9	Maximum Admissible Phase Variation .....	177
10	Admissible Panel Phase Variation Related to Truncation Errors .....	187

# SYMBOLS

## LATIN SYMBOLS

$a$	determinant of the components of $a_{\alpha\beta}$
$a_{\alpha\beta}$	fundamental surface tensor
$\vec{a}_i$	covariant base vectors of compressibility coordinate system
$\vec{a}^i$	contravariant base vectors of compressibility coordinate system
$a_j^i$	elements of transformation from local panel coordinate system to compressibility coordinate system
$\vec{a}_\beta$	covariant base vectors of surface coordinates
$\vec{a}^\beta$	contravariant base vectors of surface coordinates
$A_{ij}$	aerodynamic influence coefficient
$A_j^i$	elements of transformation from compressibility coordinate system to local panel coordinate system
$\hat{b}_i$	unit base vectors of scaled coordinate system
$c$	speed of sound, m/sec
$\hat{c}$	unit vector in the direction of undisturbed freestream
$C_p$	specific heat at constant pressure, J/K
$C_p$	pressure coefficient
$C_v$	specific heat at constant volume, J/K
$\vec{D}$	displacement vector, m
$e$	internal energy density, $m^2/sec^2$
$e_{ijk} = e^{ijk}$	permutation symbol
$E_j^i$	elements of Prandtl-Glauert transformation
$\&_j^i$	elements of inverse Prandtl-Glauert transformation
$\vec{F}$	aerodynamic force vector, n

$g$	determinant of covariant metric tensor
$g_{ij}$	covariant metric tensor of compressibility coordinates
$g^{ij}$	contravariant metric tensor of compressibility coordinates
$G^{ij}$	cofactors of $g_{ij}$
$i$	$\sqrt{-1}$
J	abbreviation for joule
$k$	reduced frequency,
K	abbreviation for Kelvin
M	Mach number
m	abbreviation for meter
$n$	normal coordinate of a surface, position in the direction of $\hat{n}$ ; also, abbreviation for newton
$\hat{n}$	unit vector normal to a surface (unit of length of scaled coordinates)
$n_c$	conormal coordinate of a surface, m
$\vec{n}_c$	surface conormal vector, m
$\hat{N}$	unit vector normal to a surface (unit of length in compressibility coordinates), m
$N$	magnitude of $\hat{N}$ in the measure of the scaled coordinates
$p$	pressure, $n/m^2$
P	field point
$q$	dynamic pressure, $n/m^2$
Q	surface point
$Q^+, Q^-$	limiting position approaching Q from side of surface where $n$ is positive, negative
R	distance from P to Q, m
$R = C_p - C_v$	ideal gas constant, J/K
$\vec{r}$	position vector relative to origin of coordinates, m
t	time, sec

$t_j^i$	elements of orthogonal transformation from scaled coordinates to local panel coordinates
$T_j^i$	elements of orthogonal transformation from local panel coordinates to scaled coordinates
$\vec{u}$	velocity of a surface point, m/sec <sup>2</sup>
$u_n$	surface speed of displacement along the surface normal, m/sec
$\vec{U}_0$	freestream velocity, m/sec
$U_0$	magnitude of freestream velocity, m/sec
$\vec{V}_c$	total flow velocity, m/sec
$\vec{V}_m$	mean flow velocity at a surface of velocity discontinuity, m/sec
$\vec{w}$	perturbation mass flux vector, Kg/m <sup>2</sup> · sec
$W$	wake surface
$\vec{W}$	mass flux vector, Kg/m <sup>2</sup> · sec
$x, y, z$	coordinate lines of compressibility coordinate system, m
$\bar{x}, \bar{y}, \bar{z}$	coordinate lines of scaled coordinate system
$x^i$	indical notation for $x, y, z$ coordinate lines, m
$\bar{x}^i$	indical notation for $\bar{x}, \bar{y}, \bar{z}$ coordinate lines

### GREEK SYMBOLS

$\hat{\alpha}_i$	unit base vector of local panel coordinate system
$\beta = \sqrt{1 - M^2}$	compressibility factor
$\gamma = C_p/C_v$	ratio of specific heats
$\delta_{ij}$	kronecker delta
$\epsilon_{ijk} = \sqrt{g} e_{ijk}$	covariant permutation tensor
$\epsilon^{ijk} = \frac{1}{\sqrt{g}} e^{ijk}$	contravariant permutation tensor
$\vec{\theta}$	surface rotation vector, radians
$\mu^*$	complex amplitude of doublet strength, m <sup>2</sup> /sec
$\xi, \eta, \zeta$	coordinate lines of local panel coordinate system

$\xi^i$	indicial notation for $\xi, \eta, \zeta$ coordinate lines
$\rho$	fluid mass density, $\text{Kg/m}^3$
$\sigma^*$	complex amplitude of source strength, $\text{m/sec}$
$\Sigma$	surface
$\partial\Sigma$	perimeter of $\Sigma$
$\phi$	perturbation velocity potential, $\text{m}^2/\text{sec}$
$\psi_0$	elementary solution to Laplace's equation, $1/\text{m}$
$\psi^*$	complex amplitude of elementary solution to Helmholtz's equation, $1/\text{m}$
$^*\psi$	difference of $\psi_0$ and $\psi^*$ , $1/\text{m}$

$\bar{\omega} = \omega/U_0$  reduced frequency for a unit characteristic length

$\Omega = \bar{\omega}M_0/\beta^2$  Helmholtz's coefficient

### OPERATORS

$\frac{d}{dt} = \frac{\partial}{\partial t} + \vec{V}_c \cdot \vec{\nabla}$  material (or Eulerian) derivative,  $1/\text{sec}$

$\frac{D}{Dt} = \frac{\partial}{\partial t} + \vec{U}_0 \cdot \vec{\nabla}$  linearized material derivative,  $1/\text{sec}$

$\vec{\nabla}$  gradient,  $1/\text{m}$

$\nabla^2$  Laplacian,  $1/\text{m}^2$

$\frac{\delta}{\delta t} = \frac{\partial}{\partial t} + \vec{u} \cdot \vec{\nabla}$  time rate of change apparent to a surface point,  $1/\text{sec}$

$( )_x, ( )_y, ( )_z$  partial derivation with respect to  $x, y, z$ ,  $1/\text{m}$

$( )_{,i}$  covariant with respect to  $i$ th spatial coordinate,  $1/\text{m}$

$( )_0$  freestream value of  $( )$

$( )_s$  steady value of  $( )$

$( )_u$  unsteady value of  $( )$

$( )^+ = ( )_u$  value of  $( )$  in the limit approaching a surface point  $Q$  from the side of the surface where  $n$  is positive

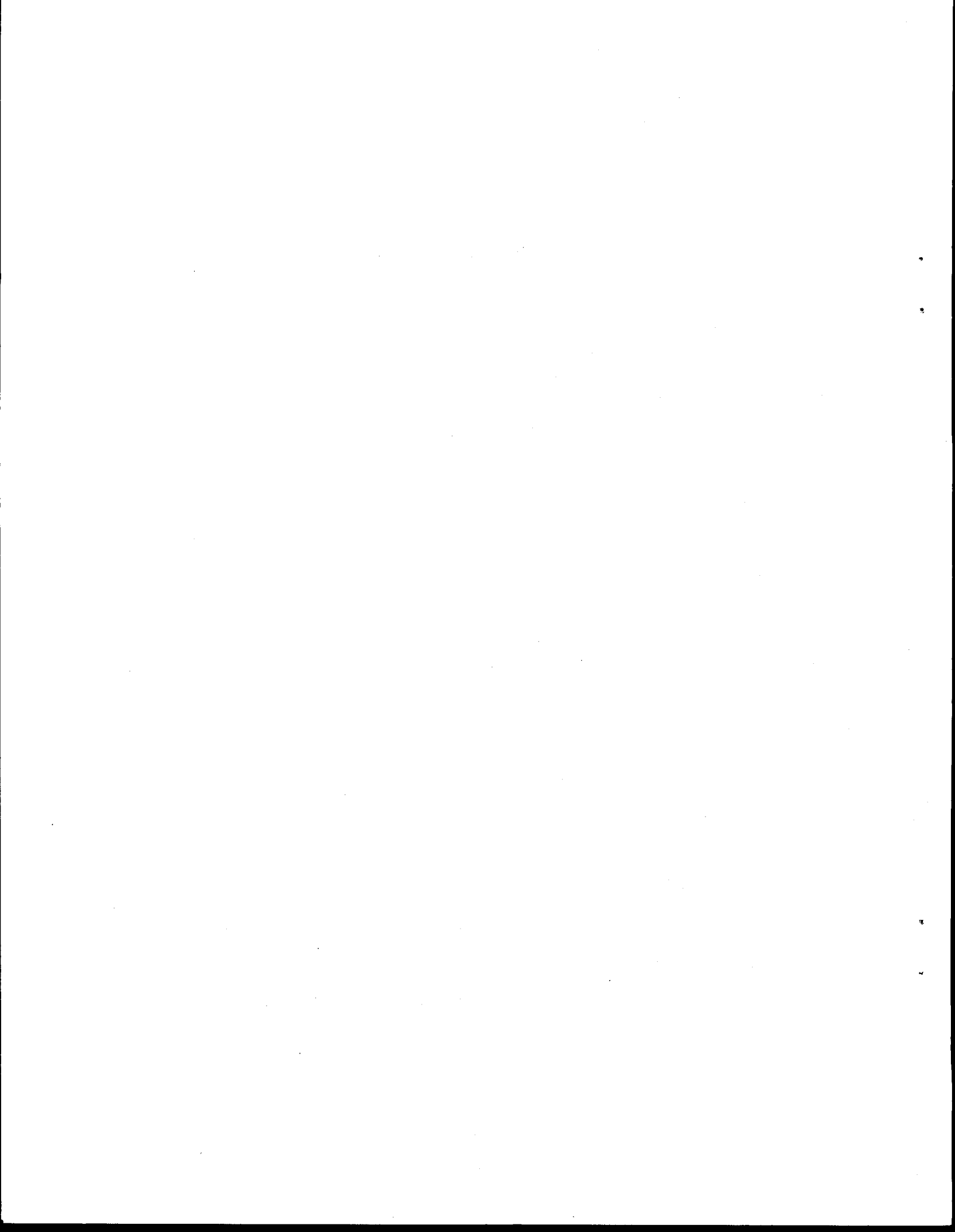
$( )^- = ( )_1$	value of $( )$ in the limit approaching a surface point $Q$ from the side of the surface opposite that where $n$ is positive
$( )_m = 1/2 (( )^+ + ( )^-)$	mean value of $( )$ across a surface
$\  ( ) \  = (( )^+ - ( )^-)$	jump in value of $( )$ across a surface
$( )^*$	complex amplitude of $( )$
$\bar{( )}$	$( )$ as a function of scaled coordinates
$\tilde{( )}$	$( )$ as a function of local panel coordinates (except in app. D)
$O( )$	order of magnitude of $( )$
$R( )$	real part of the complex quantity $( )$
$( )U( )$	union of two sets of quantities
$\text{IMAG}( )$	imaginary part of $( )$
$( )\epsilon( )$	$( )$ is an element of $( )$

#### MATRIX SYMBOLS

$[ ]$	rectangular matrix
$\{ \}$	column matrix
$[ ]^{-1}$	matrix inverse
$[ ]^T$	matrix transpose

#### VECTOR SYMBOLS

$\cdot$	scalar product
$\times$	cross product
$   $	magnitude
$\vec{( )}$	vector
$\hat{( )}$	vector of unit magnitude



## 1.0 SUMMARY

This report presents a panel-type influence coefficient method which solves the linear integral equations of unsteady, small disturbance, subsonic, potential flows. The method is applicable to flows about arbitrary, nonplanar bodies having flow boundary surfaces undergoing small amplitude harmonic oscillations. The flow boundary surfaces are paneled (i.e., subdivided into small quadrilateral surface segments) and polynomial distribution splines of unsteady sources and doublets are defined for each panel. The method is an outgrowth of a recently developed steady flow panel method and employs the linear source and quadratic doublet splines of the steady flow method.

Since the flow boundary surfaces are undergoing small amplitude harmonic motion, they have mean steady locations relative to which their unsteady motion is described. As a consequence, the unsteady flow problem is formulated as a small disturbance to a mean steady flow, and the mean steady flow is the flow about the arbitrary, nonplanar boundary surfaces in their steady mean locations. This formulation of the unsteady flow problem follows from a Taylor series expansion of the unsteady flow boundary conditions about the steady mean flow boundary conditions. The result is an unsteady flow problem which depends on an underlying steady mean component of flow and which contains boundary conditions evaluated at the steady mean locations of the boundary surfaces. The boundary conditions are such that the unsteady flow analyst can incorporate important features into the flow model which are not available in the usual theory of linearized flow.

One of the important features of the formulation is the wake model; the wake can be an arbitrarily shaped surface along which the unsteady vorticity can be convected arbitrarily. This feature is useful when modeling the unsteady flow about complex configurations, for example, those consisting of wing-body-tail combinations. When the usual wake model, consisting of free stream convection of the wake vorticity, is employed for such a configuration, the tail cannot be correctly positioned relative to vorticity in the wing wake. Using the present panel method, if the analyst can determine the appropriate steady mean wing wake surface streamlines which follow the contour of the steady mean body surface, then he can solve the problem with the unsteady vorticity in the wing wake convected along those streamlines using the steady mean convection speed. Using this wing wake model rather than that of the usual linear theory, the unsteady wing wake vorticity location and phase relative to the tail more closely represents the physics of the problem.

A second important feature of the formulation stems from the geometric location of the unsteady source and doublet distributions; they can be located on the actual surfaces of thick bodies in their steady mean locations. The usual linear theory places these distributions on mean defining surfaces which are restricted to being cylindrical with the generator of these cylindrical surfaces aligned with the undisturbed freestream. This restriction is a consequence of having expanded the boundary conditions about the freestream. In the present panel method, the boundary conditions are expanded about the steady mean component of flow; hence, the sources and doublets are distributed on the boundary surfaces in their steady mean locations. Since the unsteady flow disturbances are emitted by the unsteady source and doublet distributions, the panel method allows the unsteady disturbances to be emitted from locations which are significantly closer to their actual physical locations. Even so, the panel method still suffers from another defect of the usual linear theory, namely, that disturbances propagate with the freestream speed of sound. Regardless of this error, however, the panel method can circumvent part of the error in the computation of the cause-and-effect phase relation of unsteady disturbances emitted from the boundary surfaces of thick bodies.

Only the second of the aforementioned features of the panel method is demonstrated in the report, namely, that thick aerodynamic surfaces can be paneled on their actual, mean steady locations. The first feature, which allows a more accurate wake model, is not demonstrated because the steady flow computational capability required for computing the mean steady flow wake location and vorticity convection was not available. The unsteady flow about a wing-body-tail-nacelle configuration has been computed and the wake surface was deformed so that it follows the body contours; however, the wake deformation is the result of an engineering judgement and was not a result of an actual steady flow computation.

The primary objective of the work was to demonstrate the capability for modeling unsteady flow about realistic aircraft geometries using paneling on the actual surfaces of thick bodies. That objective was achieved.

## 2.0 INTRODUCTION

This report describes a panel method for evaluating the unsteady, subsonic flow about a solid body which is of arbitrary shape and which is undergoing harmonic oscillation in a uniform freestream. The method is an outgrowth of the steady flow panel method described by Reference 1, "A Higher Order Panel Method for Linearized Supersonic Flow." The method has been implemented as a computer program by modifying the computer program of ref. 1, but only the subsonic capability of that computer program has been extended to unsteady flow. The modification is such that, if the unsteady flow program is executed for a harmonic frequency of zero, the two computer programs yield identical results. The validity of the unsteady flow panel method has been tested by comparing computed results with wind tunnel test results and with results computed by other subsonic, unsteady flow prediction methods. Those comparisons are shown in sec. 4 of this report. Sec. 5 contains a supplement to the user's manual for the method of ref. 1, i.e., "User's Manual, Subsonic/Supersonic Advanced Panel Pilot Code," ref. 2. From the point of view of the program user, the two programs are so similar that a separate user's manual for the unsteady panel method is neither necessary or desirable.

The unsteady flow panel method is described in sec. 3 with references to appendices containing the details of its derivation. The description is divided into five parts, viz., sec. 3.1 - sec. 3.5. Sec. 3.1 introduces coordinate systems and the method used to describe unsteady surface motion. Sec. 3.2 describes the unsteady flow boundary value problem. That boundary value problem is derived in App. B as a linear unsteady flow theory approximating the general theory of unsteady flow appearing in App. A.† Sec. 3.3 describes the integral equation, which represents a general solution to the unsteady flow boundary value problem. The integral equation is derived from Helmholtz's theorem in app. C.

Sec. 3.4, sec. 3.5, and app. D, together, describe the panel method of reducing the integral equation to a determinate system of linear, complex algebraic equations. The solution to this system of equations provides a solution to the unsteady flow problem.

In essence the unsteady panel method is a method for constructing approximate solutions to Helmholtz's equation, viz.,

$$\nabla^2 \phi^* + (i\Omega)^2 \phi^* = 0$$

where  $\phi^*$  is the complex amplitude of a potential and  $\Omega$  is a constant referred to as the Helmholtz coefficient.

The solution is constructed in a domain,  $V$ , enclosed by a surface,  $\Sigma$ , by means of Helmholtz's theorem, ref. 3, viz.,

$$\frac{1}{4\pi} \iint_{\Sigma} \left\{ \sigma^*(Q) \frac{e^{-i\Omega R}}{R} - \mu^*(Q) \frac{\partial}{\partial n} \left( \frac{e^{-i\Omega R}}{R} \right) \right\} ds = \phi^*(P)$$

where  $\sigma^*(Q)$  and  $\mu^*(Q)$  represent, respectively, the complex amplitudes of sources and doublets distributed on the surface,  $\Sigma$ , and

$$R = |\vec{R}' - \vec{R}|$$

† This development is significant in that it leads to the so-called "nonlinear boundary conditions."

where  $\vec{R}$  is the position of a field point P while  $\vec{R}'$  is the position of a point Q on the surface of integration  $\Sigma$ . Also,

$$\frac{\partial}{\partial n} ( ) = \hat{n} \cdot \vec{\nabla} ( )$$

where  $\hat{n}$  is a unit vector which is normal to  $\Sigma$  and which is directed from a point Q on  $\Sigma$  and into the volume enclosed by  $\Sigma$ , see fig. 1.

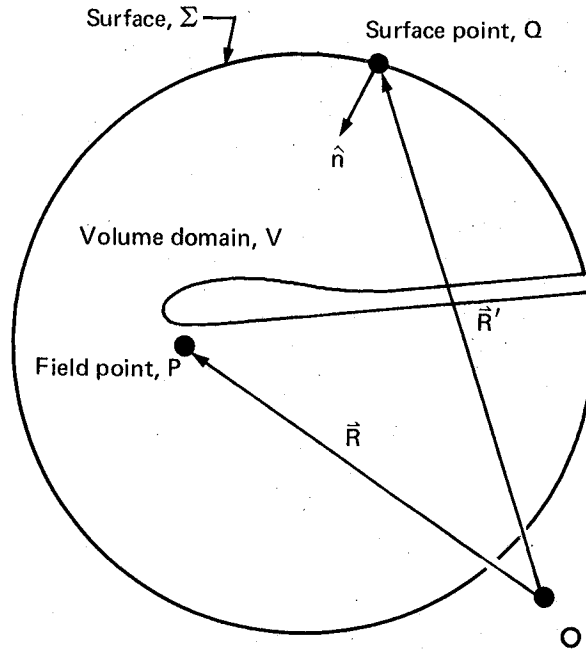


Figure 1. – Surface of Integration and Domain of Dependence

The theory of unsteady flow underlying the panel method is based on the linear, small disturbance flow equation. This flow equation, as shown in sec. 3.2, can be related to Helmholtz's equation by changes in the dependent and independent variables. Helmholtz's theorem, therefore, provides a general solution to the unsteady flow equation. A particular solution is obtained by requiring  $\phi^*$  to satisfy boundary conditions which are usually specified on the surface of integration  $\Sigma$ .

As noted above, the panel method reduces the integral contained in Helmholtz's theorem to a linear, complex algebraic expression. As shown in sec. 3.3, for unsteady flow about an aircraft in an unbounded atmosphere, Helmholtz's theorem reduces to a surface integral over the aerodynamic and wake surfaces of the aircraft. The quantities

$$-\frac{1}{4\pi} \frac{e^{-i\Omega R}}{R} \quad \text{and} \quad \frac{1}{4\pi} \frac{\partial}{\partial n} \left( \frac{e^{-i\Omega R}}{R} \right)$$

appearing in Helmholtz's theorem are kernel functions describing the complex amplitudes of the potentials induced at P due to, respectively, a unit source and a unit doublet located at Q. As noted above, the complex quantities

$$\sigma^*(Q) \text{ and } \mu^*(Q)$$

multiplied by those kernel functions are the distribution strengths of the sources and doublets distributed on  $\Sigma$ . These distribution strengths are the unknowns of the flow problem and they are determined by requiring  $\phi^*(P)$  to satisfy the boundary conditions of the flow problem. The panel method is applied by subdividing the surface of integration into quadrilateral panels, fig. 2. The source and doublet distributions are approximated on each panel by a truncated power series, e.g.,

$$\sigma^*(Q) = \sigma_0^* + \sigma_\xi^* \xi + \sigma_\eta^* \eta$$

where  $\xi, \eta$  are the coordinates of a surface point Q and where  $\sigma_0^*, \sigma_\xi^*, \sigma_\eta^*$  are the complex coefficients of the terms of the truncated power series. The surface integral is now evaluated for each panel to obtain an expression for  $\phi^*(P)$ . This expression is a complex algebraic equation in terms of the power series coefficients. The power series coefficients are related by a least squares fit to the values of  $\sigma^*$  and  $\mu^*$  at discrete points on the surface. These values are collectively called the singularity parameters and they are the unknowns of the problem.

The flow problem can be expressed symbolically in terms of the singularity parameters as

$$\phi^*(P) = \sum_j A_j^*(P) \lambda_j^*$$

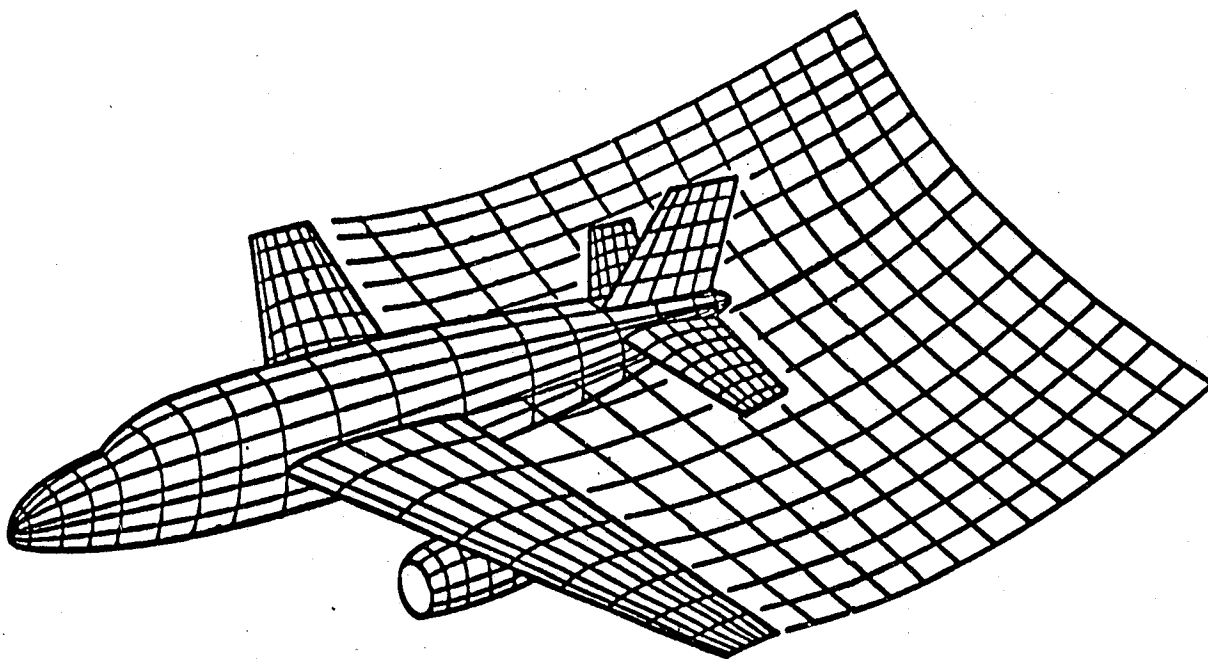


Figure 2. — Typical Configuration Surface Panel Arrangement

where  $\lambda_j^*$  denotes the  $j$ th singularity parameter. When the values of this expression or of the gradient of this expression are specified by the boundary conditions at a sufficient number of points, a determinate system may be obtained, for example,

$$\phi_i^* = \sum_j A_{ij}^* \lambda_j^*,$$

and that system may be solved for the unknown singularity parameters. The flow characteristics which constitute a solution to the unsteady flow problem are then computed making use of the computed values of the singularity parameters.

The panel approximations employed in the present, unsteady flow panel method are identical with those of the steady flow panel method for ref. 1. In general, source distributions vary linearly and doublet distributions vary quadratically on each panel; but, depending on the distance of the field point from the panel, the linear and quadratic distributions are defined over: (1) eight triangular subpanels of the quadrilateral panel, (2) two triangular subpanels of the quadrilateral panel, or (3) the quadrilateral panel itself. In any case the aerodynamic influence coefficients,  $A_{ij}^*$ , are evaluated by carrying out the integrations, appearing in Helmholtz's theorem. These integrations are carried out independently over each panel region for which the source and doublet distribution approximations are defined. This operation leads to values of potential and potential gradient at field points where boundary conditions are applied. The resulting integrals relate these field point values to unit values of the coefficients in the power series approximations to the source and doublet distributions; they, in turn, are related by the least squares fit to the singularity parameters.

The integrals involved in evaluating the influence coefficients are decomposed in such a manner, app. D, that every integral which must be evaluated is related to two fundamental integrals. The integrands of these fundamental integrals are approximated by a series of constrained Tschebycheff polynomials. The result is a sequence of integrals which are integrable in closed form. The number of series terms required to achieve a specified accuracy for this approximation depends on the magnitude of the Helmholtz coefficient,  $\Omega$ , and on the panel size; an error analysis of the approximation appears in app. D. The series approximations are such that the integrands and the limits of integration appearing in the series terms are independent of the Helmholtz coefficient; thus, the formulation, like that of ref. 4, would allow the integrals to be evaluated, saved, and recombined sequentially to produce aerodynamic influence coefficients for a sequence of Helmholtz coefficient values (i.e., a sequence of harmonic frequency values). The computer code, however, was not structured to allow this type of sequential computation.

### 3.0 UNSTEADY FLOW PANEL METHOD

#### 3.1 COORDINATE SYSTEMS AND SURFACE MOTION

The unsteady flow boundary value problem and the panel method for its solution are described in terms of two coordinate systems:

- (1) Compressibility coordinate system –  $x, y, z$
- (2) Local panel coordinate system –  $\xi, \eta, \zeta$

The compressibility coordinate system is a rectangular, Cartesian system which is an inertial reference frame translating with a steady velocity in the negative  $x$  direction relative to the undisturbed fluid, fig. 3; thus, there appears to be a uniform freestream in the positive  $x$  direction.

As noted in sec. 2 and illustrated by fig. 2, the aerodynamic surfaces and the wake surfaces are subdivided into a large number of segments called panels. Each segment of surface represented by a panel is approximated by one or more flat panels. A local panel axis system is defined for each flat panel. This coordinate system is related to the compressibility coordinates by a transformation such that the  $\xi, \eta$  coordinate plane is parallel with the plane of the flat panel and such that the  $\zeta$  axis is normal in relation to it, fig. 4. The coordinate transformation, relating the local panel and compressibility systems, is described in app.C.

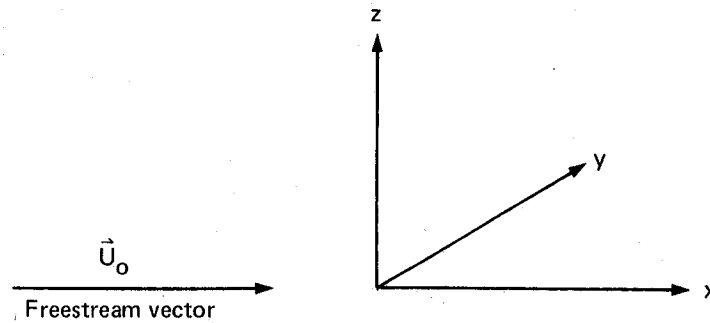


Figure 3. – Compressibility Coordinate System and Uniform Freestream Vector

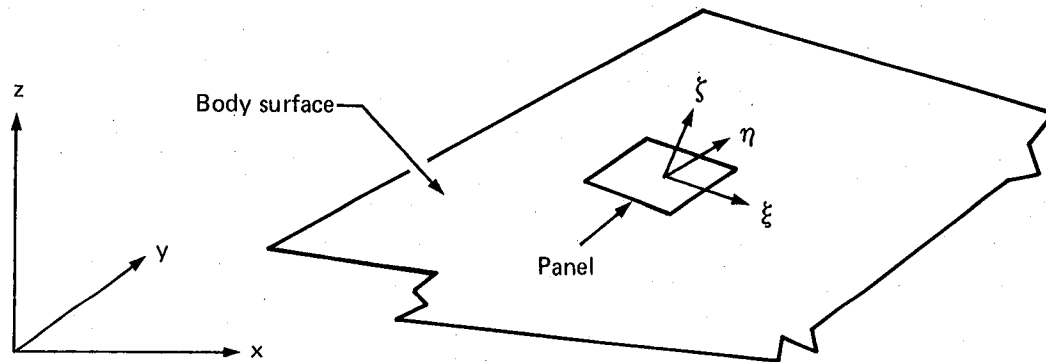


Figure 4. – Local Panel Coordinate System

The above notation (i.e.,  $x, y, z$ ) for denoting the coordinate lines of the compressibility system is different from that of ref. 2, "User's Manual, Subsonic/Supersonic Advanced Panel Pilot Code." Since ref. 2 is used in conjunction with sec. 5 of this report as a user's manual for the unsteady panel method code, this difference in notation should be carefully recognized. Ref. 2 employs  $x, y, z$  to denote the coordinate lines of the global coordinate system which is used as a basis for describing body surfaces and flow properties. The coordinate lines of the compressibility system are denoted by  $x_c, y_c, z_c$ . In this report the global coordinate system is mentioned only in sec. 5.

The analytical statement of the flow boundary conditions requires an analytical description of the aerodynamic and wake surfaces. This description is expressed in terms of surface points defined by surface coordinates which are the local panel coordinates introduced above. The surface coordinates appear as the parameters in the Gaussian description of the surface (ref. 5, p. 183), viz.,

$$\vec{R} = \vec{R}(\xi, \eta, t).$$

If  $\eta$  and  $t$  are held fixed while  $\xi$  is varied, then the position vector,  $\vec{R}$ , traces out a spatial curve on the surface as the surface appears at the instant of time  $t$ . This curve is a surface coordinate line corresponding with the  $\xi$  parameter. Surface coordinate lines corresponding with the  $\eta$  parameter are constructed by holding  $\xi$  and  $t$  fixed, and varying  $\eta$ . A surface coordinate system is seen to be formed by  $\xi$  and  $\eta$  and a surface point is defined by a pair of values for  $\xi, \eta$ .

Unsteady motions of the surfaces are described by an unsteady displacement of the surfaces from steady mean locations, fig. 5. Let  $Q$  denote an arbitrary surface point of the steady mean location

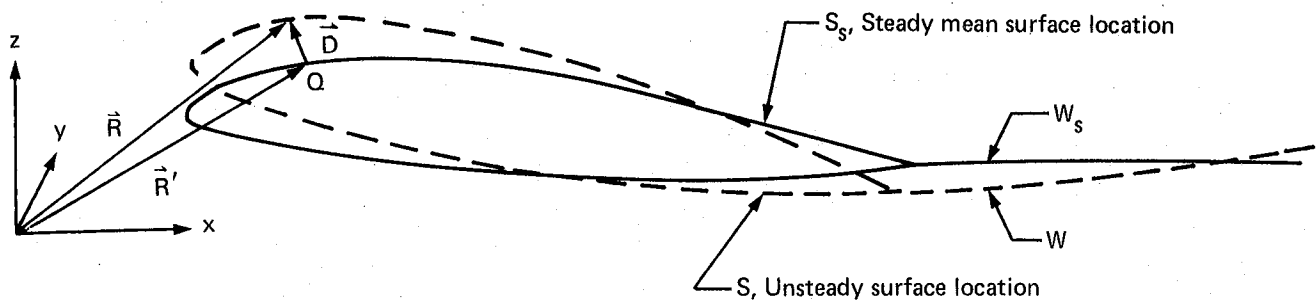


Figure 5. — Surface Displacement

of a surface. This point has the steady position  $\vec{R}'$  relative to the compressibility coordinate system. Unsteady surface motion is introduced by allowing this surface point to have the unsteady (i.e., time dependent) position  $\vec{R}$ . The surface point therefore undergoes the following time dependent displacement:

$$\vec{D} = \vec{R} - \vec{R}' \quad (1)$$

The velocity of the surface point, viz.,

$$\vec{u} = \frac{\partial \vec{D}}{\partial t} \quad (2)$$

where  $\xi, \eta$  are held fixed, is then used to compute the speed of displacement of the surface in the direction of the surface normal, i.e.,

$$u_n = \hat{n} \cdot \frac{\partial \vec{D}}{\partial t} \quad (3)$$

where  $\hat{n}$  is the unit vector normal to the moving surface at the surface point.

The unsteady flow theory used in the panel method is an approximate theory which, as shown in app. B, follows by assuming that the displacement,  $\vec{D}$ , is small everywhere on the surfaces and by assuming that the harmonic motion, i.e.,

$$\frac{1}{U_0} \frac{\partial \vec{D}}{\partial t} = i\bar{\omega} \vec{D}^* e^{i\omega t} \quad \text{where } \bar{\omega} = \omega/U_0,$$

is such that the frequency of the motion satisfies

$$|\bar{\omega} \vec{D}^*| \ll O(|\vec{D}^*|); \quad (4)$$

hence,

$$\bar{\omega} \ll O(1).$$

From the assumed smallness of  $\vec{D}$  the following approximations are taken to be valid (cf. app. B):

$$\vec{\theta} \approx \frac{1}{2} (\vec{\nabla} \times \vec{D}) \quad \text{is a first order approximation to surface rotation,}$$

$$\hat{n} \approx \hat{n}_s + \theta \times \hat{n}_s \quad \text{is the unit vector normal to the moving surface, and}$$

$$u_n \approx \hat{n}_s \cdot \frac{\partial \vec{D}}{\partial t} \quad \text{is the speed of displacement of the moving surface.}$$

### 3.2 UNSTEADY FLOW BOUNDARY VALUE PROBLEM

The flow is assumed to be compressible, inviscid, irrotational, and isentropic. Under these assumptions the motion of the fluid may be described in terms of a velocity potential satisfying the well known, nonlinear flow equation shown as equation (A.17) of app. A. In the approximate theory, however, disturbances to the uniform freestream are assumed to be sufficiently small that the nonlinear flow equation may be approximated by the small disturbance flow equation, viz.,

$$\nabla^2 \phi = \frac{1}{c_0^2} \frac{D^2 \phi}{Dt^2} \quad (5)$$

where

$$\frac{D}{Dt} \equiv \frac{\partial}{\partial t} + U_0 \frac{\partial}{\partial x}$$

and  $\phi$  is the disturbance velocity potential which is related to the flow velocity as follows:

$$\vec{V}_c = \vec{U}_0 + \vec{\nabla} \phi. \quad (6)$$

The panel method is predicated on the separation of the velocity potential into two components, viz.,

$$\phi = \phi_s + \phi_u \quad (7)$$

where the velocity potential  $\phi_s$  is independent of time and describes the flow if the speed of displacement,  $u_n$ , of every surface point vanishes for a sufficiently long period of time. The velocity potential  $\phi_u$  is that of the unsteady component of flow arising as a consequence of nonzero  $u_n$ .

The steady velocity potential is required to satisfy the steady form of eq. (5), viz.,

$$(1 - M_0^2)(\phi_s)_{xx} + (\phi_s)_{yy} + (\phi_s)_{zz} = 0, \quad (8)$$

and the boundary conditions of the approximate theory of steady flow described by ref. 1. Those boundary conditions are as follows:

$$\vec{W}_s \cdot \hat{n}_s = 0 \text{ on } S_s \text{ and } W_s \quad (9)$$

where (ref. 1, sec 3.10)  $S_s$  and  $W_s$  denote, respectively, the aerodynamic and wake surfaces. The aerodynamic and wake surfaces, in the present application, coincide with the steady mean locations of those surfaces. The vector  $\vec{W}_s$  represents the mass flux of the steady component of flow which is given the following first order approximation (ref. 1, sec. 3.1):

$$\vec{W}_s = \rho_0 (\vec{U}_0 + \vec{w}_s) \quad (10)$$

where, in turn,

$$\rho_0 \vec{w}_s = \rho_0 \left( \vec{\nabla} \phi_s - \hat{i} M_0^2 (\phi_s)_x \right) \quad (11)$$

and the quantity  $\rho_0 \vec{w}_s$  is the perturbation mass flux of the steady component of flow.

In addition to this boundary condition, across wake surfaces the pressure coefficient is required to be continuous, i.e.,

$$[[C_p]] = 0 \text{ on } W_s. \quad (12)$$

The boundary condition shown as eq. (12) is applied using the following second order approximation for the pressure coefficient:

$$C_p = (p_s - p_0) \left( \frac{1}{2} \rho_0 U_0^2 \right)^{-1} \approx - \frac{1}{U_0^2} \left[ 2U_0 (\phi_s)_x + \vec{\nabla} \phi_s \cdot \vec{\nabla} \phi_s - M_0^2 ((\phi_s)_x)^2 \right]. \quad (13)$$

This approximation is chosen because (as shown by sec. 3.3, ref.1) it satisfies Euler's equations so that the momentum integral (ref. 1, eq. 24) is valid; as a consequence, the aerodynamic force is computed as follows:

$$\vec{F}_s = \frac{1}{2} \rho_0 U_0^2 \iint_{S_s} C_p \hat{n}_s ds, \quad (14a)$$

when the pressure coefficient is approximated by eq. (13). Similarly, the moment of the aerodynamic pressure is computed as

$$\vec{M}_s = \frac{1}{2} \rho_0 U_0^2 \iint_{S_s} C_p \vec{R}_s \times \hat{n}_s ds \quad (14b)$$

where  $\vec{R}_s$  describes position on the mean steady surface and  $\hat{n}_s$  is the unit normal.

The unsteady potential,  $\phi_u$ , must satisfy eq. (5) and the following boundary conditions derived in app. B:

$$\vec{w}_u \cdot \hat{n}_s = -\vec{W}_s \cdot (\vec{\theta} \times \hat{n}_s) - (\vec{D} \cdot \vec{\nabla} \vec{W}_s) \cdot \hat{n}_s + \rho_s u_n \text{ on } S_s \text{ and } W_s \quad (15)$$

where (app. B, eq. (21))

$$\vec{w}_u = \rho_0 \left( \vec{\nabla} \phi_u - \frac{M_0^2}{U_0} \frac{D}{Dt} (\phi_u) \hat{i} \right) \quad (16)$$

and (app. B, eq.(B.15))

$$\rho_s = \rho_o \left( 1 - \frac{M_o^2}{U_o} (\phi_s)_x \right) \quad (17)$$

In addition, across wake surfaces the unsteady disturbance pressure must be continuous, i.e.,

$$\llbracket C_{p_u} \rrbracket = 0 \text{ on } W_s, \quad (18)$$

when the unsteady disturbance pressure coefficient, i.e.,

$$C_{p_u} = (p - p_s) / \left( \frac{1}{2} \rho_o U_o^2 \right), \quad (19)$$

is approximated as follows:

$$C_{p_u} \approx - \frac{1}{\frac{1}{2} \rho_o U_o^2} \left( \rho_s (\phi_u)_t + \vec{W}_s \cdot \vec{\nabla}(\phi_u) \right) \quad (20)$$

where eq.(B.29) has been introduced into eq.(19). Finally, the unsteady disturbance aerodynamic force is computed by integrating the pressure at the aerodynamic surfaces, viz.,

$$\vec{F}_u = \frac{1}{2} \rho_o U_o^2 \iint_{S_s} C_{p_u} \hat{n}_s ds \quad (21)$$

when the pressure coefficient is given by eq. (20).

Harmonic time dependence is imposed by substituting

$$\vec{D} = \vec{D}^* e^{i\omega t} \quad (22)$$

and

$$\phi_u = \phi'^* e^{i\omega t} \quad (23)$$

into the flow equation and boundary conditions. The result of that substitution into the flow equation shown as eq. (5) is as follows:

$$\nabla^2 \phi'^* = M_o^2 \left( (i\bar{\omega})^2 \phi'^* + 2i\bar{\omega} \phi'^* + \phi'_{xx} \right) \quad (24)$$

where the freestream direction has been chosen to be sufficiently close to the direction of the  $x$  axis of the compressibility coordinate system that the components of

$$\left( \left( \frac{\vec{U}_0}{U_0} \right) \cdot \vec{\nabla} \phi'^* - \phi'_{x^*} \right)$$

have negligible order of magnitude. The result of substituting eq.(22) and eq.(23) into the boundary condition shown as eq. (15) is as follows †:

$$\vec{w}'^* \cdot \hat{n}_s = -\vec{W}_s \cdot (\vec{\theta}^* \times \hat{n}_s) - (\vec{D}^* \cdot \vec{\nabla} \vec{W}_s) \cdot \hat{n}_s + \rho_s u_n^* \text{ on } S_s \text{ and } W_s \quad (25)$$

where  $\vec{W}_s$  (cf. eq. (10)) may contain a small component of freestream incidence,

$$\vec{w}'^* = \rho_o (\vec{\nabla} \phi'^* - M_o^2 (i\bar{\omega} \phi'^* + \phi'_{x^*}) \hat{i}), \vec{\theta}^* = \frac{1}{2} (\vec{\nabla} \times \vec{D}^*), \text{ and } u_n^* = i\bar{\omega} U_o \vec{D}^*; \quad (26)$$

while the wake boundary condition shown as eq. (12) becomes

$$[[C_p^*]] = 0 \text{ on } W_s \quad (27)$$

where

$$C_p^* = -\frac{1}{\frac{1}{2} \rho_o U_o^2} (\rho_s i\bar{\omega} U_o \phi'^* + \vec{W}_s \cdot \vec{\nabla} \phi'^*). \quad (28)$$

A modified complex potential amplitude,  $\phi^*$ , is introduced by letting

$$\phi'^* = \phi^* e^{i\bar{\omega} x M_o^2 / \beta^2}. \quad (29)$$

Substituting eq. (29) into equations (24) - (28) leads to the following problem in which the flow equation assumes the form of Helmholtz's equation, viz.,

$$\beta^2 \phi_{xx}^* + \phi_{yy}^* + \phi_{zz}^* + \Omega^2 \beta^2 \phi^* = 0 \quad (30)$$

where

$$\Omega = \bar{\omega} M_o / \beta^2$$

† As shown in sec. 4.3, the method for computing the steady component of flow is not sufficiently accurate for computing the term  $(\vec{D}^* \cdot \vec{\nabla} \vec{W}_s) \cdot \hat{n}_s$ . This term, therefore, is retained in the analysis but is not actually evaluated in the test cases of sec. 4.

and the boundary conditions appear as

$$\vec{w}^* \cdot \hat{n}_s = \left[ -\vec{W}_s \cdot (\vec{\theta}^* \times \hat{n}_s) - (\vec{D}^* \cdot \vec{\nabla} \vec{W}_s) \cdot \hat{n}_s + \rho_s u_{n1}^* \right] e^{-i\bar{\omega}x} M_o^2 / \beta^2 \quad \text{on } S_s \text{ and } W_s \quad (31)$$

where

$$\vec{w}^* = \rho_o \left( \beta^2 \phi_x^* \hat{i} + \phi_y^* \hat{j} + \phi_z^* \hat{k} \right) \quad (32)$$

Further, eq. (28) becomes

$$\llbracket C_p^* \rrbracket = 0 \quad \text{on } W_s \quad (33)$$

where

$$C_p^* = -\frac{2}{U_o} \left[ \left( i\bar{\omega} / \beta^2 \right) \phi^* + \frac{1}{\rho_o} \vec{W}_s \cdot \vec{\nabla} \phi^* \right] e^{i\bar{\omega}x} M_o^2 / \beta^2 \quad (34)$$

As will be seen in the following, a more useful form for the wake boundary condition follows by substituting eq. (34) into eq. (33). The desired form is given by

$$\left( i\bar{\omega} / \beta^2 \right) \mu^* + \frac{1}{\rho_o} \vec{W}_s \cdot \vec{\nabla} \mu^* = 0 \quad \text{on } W_s \quad (35)$$

where

$$\mu^* \equiv \llbracket \phi^* \rrbracket.$$

Letting

$$w_s \frac{\partial}{\partial \ell} = \frac{1}{\rho_o} \vec{W}_s \cdot \vec{\nabla} \quad (36)$$

where  $\ell$  is a coordinate line along a mean steady flow streamline on the wake surface and where

$$w_s \equiv \left| \frac{1}{\rho} \vec{W}_s \right|$$

is the magnitude of the nondimensional mass flux at the wake surface, one may write the following identity:

$$\left[ \left( i\bar{\omega} / \beta^2 w_s \right) \mu^* + \frac{\partial \mu^*}{\partial \ell} \right] e^{\left[ \left( i\bar{\omega} / \beta^2 \right) \int d\xi / w_s \right]} = \frac{\partial}{\partial \ell} \left( e^{i\bar{\omega}x} / \beta^2 \right).$$

Integrating along the steady streamline  $\ell$  from  $\ell = c$ , the boundary condition becomes

$$\mu^*(\ell, s) = \mu^*(c, s) e^{\left[ \left( i\bar{\omega} / \beta^2 \right) \int_c^\ell d\xi / w_s \right]} \quad (37)$$

where  $s$  is a wake surface coordinate which is orthogonal to  $\ell$ .

This expression evaluates the doublet strength at any point on a wake surface in terms of the value of the doublet strength at  $\ell = c$ . As noted at the close of app. A, the doublet strength at the trailing edge of the lifting surface, from whence the wake emanates, is equal to the circulation on the lifting surface. This condition, when combined with that shown as eq. (37), allows the wake surface doublet distributions to be treated as known functions of the source and doublet distributions on the non-wake surfaces. This treatment of the wake doublet distribution is used in the following section.

### 3.3 INTEGRAL SOLUTION TO UNSTEADY FLOW PROBLEMS

As shown by app. C, Helmholtz's theorem provides a solution to eq. (30), i.e., the flow equation expressed in terms of the modified potential introduced by eq. (29). The solution provides the value of complex potential,  $\phi^*$ , at a point P interior to a volume V surrounded by the surface  $\Sigma$ , whereon unsteady sources and doublets are distributed. Letting Q represent a surface point of  $\Sigma$ , the solution appears as follows:

$$\iint_{\Sigma} \left[ \sigma^*(Q) \psi^*(P, Q) + \mu^*(Q) \frac{\partial}{\partial n'_c} (\psi^*(P, Q)) \right] ds' = \phi^*(P) \quad (38)$$

where

$$\psi^*(P, Q) = -\frac{1}{4\pi R} e^{-i\Omega R}, \quad (39)$$

$$R = \left[ (x' - x)^2 + \beta^2 (y' - y)^2 + \beta^2 (z' - z)^2 \right]^{1/2}, \quad (40)$$

Q is a surface point with coordinates  $x', y', z'$ ,

P is a spatial point with coordinates  $x, y, z$ ,

$$\frac{\partial}{\partial n'_c} = \vec{n}'_c \cdot \vec{\nabla}', \quad (41)$$

and

$$\vec{n}'_c = \beta^2 (\hat{n} \cdot \hat{i}) \hat{i} + (\hat{n} \cdot \hat{j}) \hat{j} + (\hat{n} \cdot \hat{k}) \hat{k}.$$

The vector  $\vec{n}_c$  is the conormal vector of  $\Sigma$  defined such that, as shown by app. C,

$$\frac{\partial}{\partial n_c'} = \beta^2 \left( \hat{n} \cdot \hat{i} \right) \frac{\partial}{\partial x'} + \left( \hat{n} \cdot \hat{j} \right) \frac{\partial}{\partial y'} + \left( \hat{n} \cdot \hat{k} \right) \frac{\partial}{\partial z'}$$

The function  $\psi^*$  is an elementary solution to eq. (30) except at Q because  $\psi^*$  becomes singular as P approaches Q on the surface  $\Sigma$ . Multiplying this function by the factor employed to obtain the modified potential, viz.,

$$e^{-i\Omega M_o (x' - x)},$$

results in

$$\phi_s^* = -\frac{1}{4\pi R} e^{-i\Omega [M_o (x' - x) + R]} \quad (42)$$

This equation appears as eq. (4.24) in ref. 6 where it is shown to represent the complex amplitude of the potential induced at point P due to a unit strength, harmonically fluctuating source located at the point Q.

A solution to the boundary value problem posed in the preceding section, i.e., sec. 3.2, is constructed by choosing the singularity distributions,  $\sigma^*(Q)$  and  $\mu^*(Q)$ , such that  $\phi^*$  satisfies the flow boundary conditions. The boundary conditions are specified at the aerodynamic surface,  $S_s$ , the upper and lower surfaces of the wake,  $W_u$  and  $W_l$ , and, at the far-field surface,  $\Sigma_\infty$  - the latter being an arbitrarily shaped surface located at a large distance from the aerodynamic surface. The original surface,  $\Sigma$ , therefore is represented as

$$\Sigma = S_s \cup W_u \cup W_l \cup \Sigma_\infty \quad (43)$$

where  $\cup$  denotes a union.

The far-field boundary conditions require that the potential and its normal derivative vanish at  $\Sigma_\infty$ . These boundary conditions are satisfied by requiring  $\sigma^*(Q)$  and  $\mu^*(Q)$  to vanish for points Q on  $\Sigma_\infty$ ; as a consequence, the integral equation for  $\phi^*$  reduces to an integral over  $S_s$ ,  $W_u$ , and  $W_l$ .

As shown in app. C, the source and doublet distribution strengths are related to the potential as follows:

$$\begin{aligned} \sigma^*(Q) &= \left[ \left[ \partial \phi^* / \partial n_c \right] \right] \\ \mu^*(Q) &= \left[ \left[ \phi^* \right] \right] \end{aligned} \quad (44)$$

where, for example,

$$[[\phi^*]] \equiv \phi^*(Q^+) - \phi^*(Q^-)$$

denotes the jump (or difference) in the limiting values of  $\phi^*$  as  $Q$  is approached from either side of the surface. Applying the second of eq. (44) to the wake surfaces leads to

$$\mu^*(Q_u) = \phi^*(Q_u^+) - \phi^*(Q_u^-) \text{ on } W_u$$

and

$$\mu^*(Q_\ell) = \phi^*(Q_\ell^+) - \phi^*(Q_\ell^-) \text{ on } W_\ell.$$

Letting the surface  $W_\ell$  approach the surface  $W_u$ , in the limit

$$\phi^*(Q_u^-) = \phi^*(Q_\ell^-)$$

so that one may define

$$[[\phi^*]] \equiv \phi^*(Q_u^+) - \phi^*(Q_\ell^+)$$

as the jump in potential across the wake. Similarly, one may define

$$[[\partial\phi^*/\partial n_c]] \equiv (\partial\phi^*/\partial n_c)|_{Q_u^+} - (\partial\phi^*/\partial n_c)|_{Q_\ell^+}.$$

Further, noting that

$$\left(\frac{\partial}{\partial n_c}\right)_u = -\left(\frac{\partial}{\partial n_c}\right)_\ell, \quad (45)$$

the integrals over  $W_u$  and  $W_\ell$  can be expressed as a single integral over the surface  $W_u$ , viz.,

$$\iint_{W_u} \left( [[\partial\phi^*/\partial n_c]] \psi^* + [[\phi^*]] \partial\psi^*/\partial n'_c \right) ds.$$

The wake boundary conditions are shown by eq. (31). If eq. (31) is evaluated at either side of the wake surface and the evaluations are subtracted from one another, then we have the following result:

$$\llbracket \vec{w}^* \cdot \hat{n}_s \rrbracket = 0 \quad \text{on } W_s.$$

From eq. (32) and eq. (41) it follows that this expression may be written as follows:

$$\llbracket \frac{\partial \phi^*}{\partial n_c} \rrbracket = 0 \quad \text{on } W_s. \quad (46)$$

As a consequence of eq. (46), the first term of the wake integral integrand is seen to vanish.

Using the above, the integral shown by eq. (38) becomes as follows:

$$\phi^*(P) = \iint_{S_s} \left[ \sigma^*(Q) \psi^*(P,Q) + \mu^*(Q) \frac{\partial}{\partial n'_c} \psi^*(P,Q) \right] ds' + \iint_{W_s} \mu^*(Q) \frac{\partial}{\partial n'_c} \psi^*(P,Q) ds' \quad (47)$$

where the upper surface of the wake,  $W_u$ , is identified as  $W_s$ , thereby distinguishing that side to be the side where  $n_c$  is positive. Also, as a consequence of eq. (37), eq. (47) becomes

$$\phi^*(P) = \iint_{S_s} \left[ \sigma^*(Q) \psi^*(P,Q) + \mu^*(Q) \frac{\partial}{\partial n'_c} \psi^*(P,Q) \right] ds' + \phi_w^*(\mu^*(c,s)) \quad (48)$$

where

$$\phi_w^*(\mu^*(c,s)) = \iint_{W_s} \mu^*(c,s) e \left[ \left( i\bar{\omega} / \beta^2 \right) \int_c^l d\xi / w(\xi,s) \right] \frac{\partial}{\partial n'_c} \psi^*(P,Q) ds'$$

and  $\mu^*(c,s)$  denotes the doublet strength (or jump in potential,  $\llbracket \phi^* \rrbracket$ ) along the edge of the aerodynamic surface from which the wake surface emanates.

### 3.4 AERODYNAMIC INFLUENCE COEFFICIENTS

The concepts involved in the panel method have been introduced in section 2.0, where it was indicated that the objective of the panel method is to reduce an integral equation and its associated boundary conditions to a determinate system of algebraic equations. The surfaces of integration are subdivided into panels and the unknown functions under the integral sign (viz., the singularity strength distribution functions) are approximated on each panel by polynomial functions of the surface coordinates  $\xi$ ,  $\eta$ . The coefficients of these polynomial functions are expressed in terms of a finite number of singularity parameters. The resulting expression is integrated over each panel to obtain influence coefficients which, when used with the boundary conditions, yield an algebraic system of equations containing the singularity parameters as the unknowns of the problem.

The integral equation for the unsteady flow problem is shown by eq. (48) and the associated boundary conditions are given by eq. (31) and eq. (37). The panel method for reducing this problem to a system of algebraic equations is essentially that of ref. 1. The paneling of the surfaces of integration and the panel approximations to the unknown surface functions are identical with those of ref. 1. The kernel functions of the integral equation, however, are not identical with those of ref. 1; hence, different methods for evaluating the panel integrals are required. Regardless of this distinction there is a very close relationship with the panel method of ref. 1. Because of this close relationship only the methods for evaluating the panel integrals are completely developed in this report with the details of that development contained in app. D. This section presents only an overview of the panel method.

The surface panels are defined by covering the actual surfaces of integration by a number of grids (cf., fig. 2) and these grids are called networks. The surface points at intersections of the grid lines (called grid points) are the quantities used to define the panels, cf. sec. 4.1 of ref. 1. The grid points of each network of panels are numbered by a double index system (M,N) which assumes that the grid points of a network are arranged in columns and rows even though the grid may not be rectangular, cf. sec. 1.1 of ref. 2. If a surface of integration covered by a network has finite curvature, the panels are not actually segments of the curved surface; they lie close to the surface, but even their corner points need not coincide with the grid points, cf. fig. 6. The panels are flat or they are made up of several flat segments called subpanels; therefore, the panels are assembled to form a surface which is an approximation to the actual surface of integration when that surface has curvature.

Actually, depending on the distance from the panel to the point where its influence is being evaluated (i.e., the field point), one of three different surface of integration panel approximations is used. Letting  $D$  represent the panel diameter (viz., twice the distance from the panel center to its farthest corner) and letting  $R_0$  represent the distance from the panel center to the field point, the choice of panel approximation is as follows:

- (1) If  $R_0 \geq 0.75D$ , then each panel is represented by the quadrilateral whose corners are formed by projecting four contiguous grid points to their average plane (ref. 1, sec. 4.4). If the surface of integration has curvature, then the lines forming the edges of two adjacent panels need not coincide but need merely to intersect one another at their midpoints (cf. fig. 7). This approximate surface of integration, therefore, may be discontinuous at the panel edges.

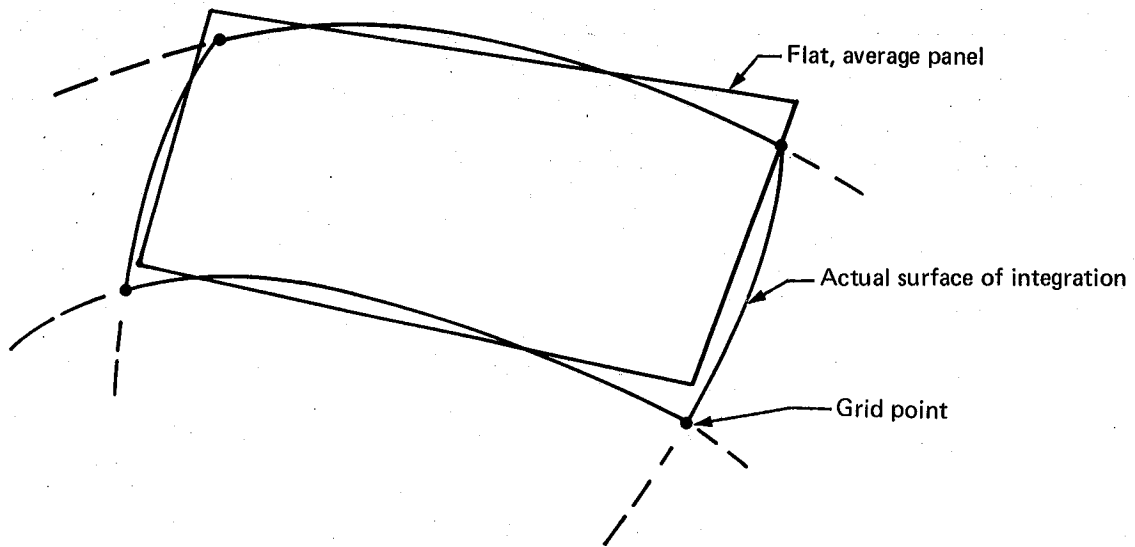


Figure 6. — Panel Approximation to Surface of Integration

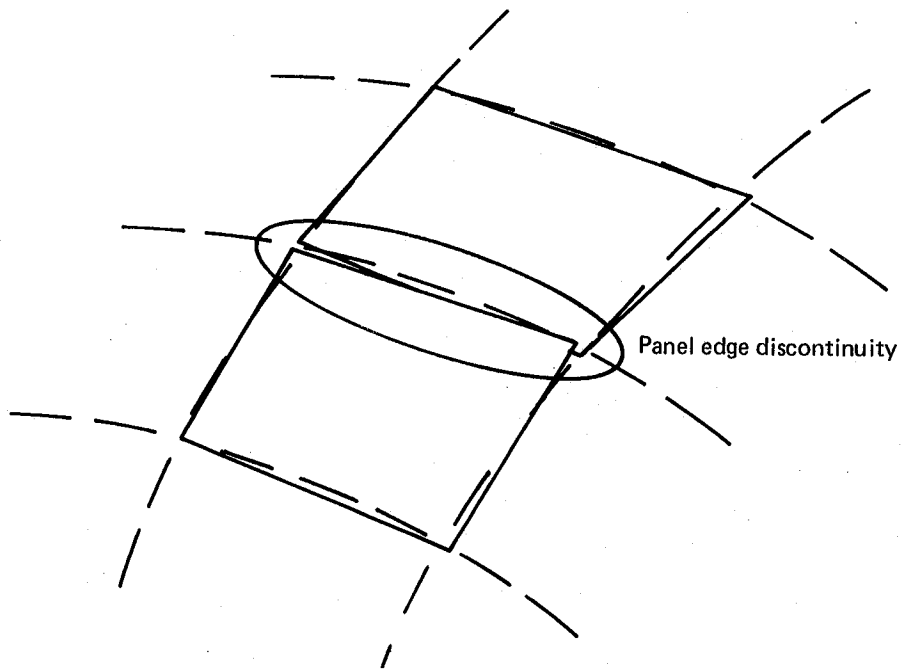


Figure 7. — Approximate Surface Discontinuity

- (2) If  $0.45D \leq R_0 < 0.75D$ , then the quadrilateral – viz., the four sided region formed by lines connecting four contiguous grid points – is represented by two plane triangular subpanels having vertices at the grid points and one edge formed by the diagonal, fig. 8. Since there are two diagonals, there are two possible surface approximations contained in this arrangement. Both approximations are used, in that, panel influences are computed using both surface approximations and the quadrilateral panel influence is defined as the average influence.

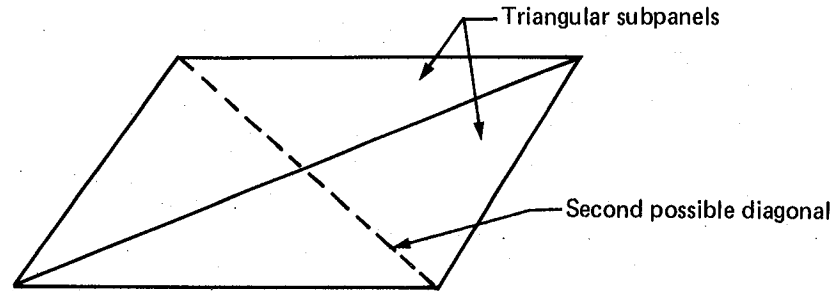


Figure 8. – Two Triangular Subpanels of a Quadrilateral Panel

- (3) If  $R_0 < 0.45D$ , then the quadrilateral is subdivided into eight triangular subpanels, fig. 9. The four interior subpanels lie in the average plane, while only the interior edge of an outer subpanel lies in the average panel plane. The exterior vertices of the outer subpanels are made to coincide with the grid points. This arrangement, like (2), above, causes the approximate surface of integration to be continuous at the panel edges. This continuity allows an approximate doublet distribution formulation having continuity at the panel edges, see sec. 4.2, ref. 1.

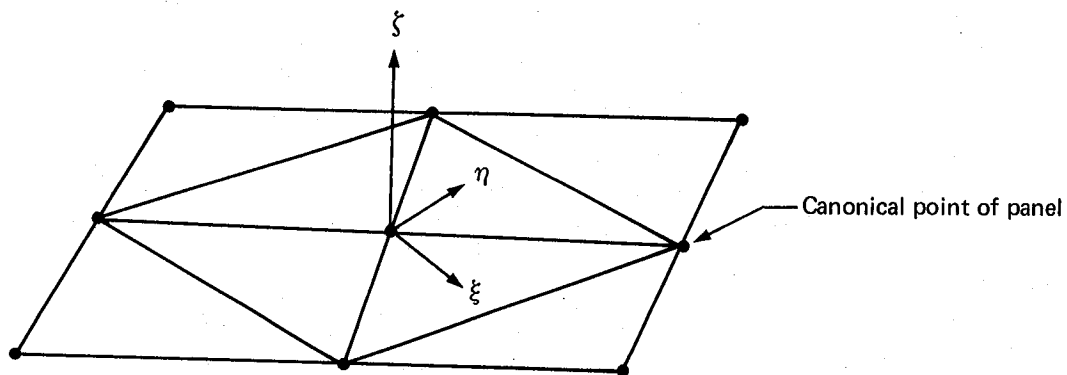


Figure 9. – Eight Triangular Subpanels, Panel Center Local Coordinate System, and Nine Canonical Points

The panel approximating-functions for the source and doublet distributions are polynomial functions of local panel coordinate systems defined for each flat quadrilateral panel and each flat triangular subpanel. The coordinate lines of a local panel system are denoted as  $\xi$ ,  $\eta$ ,  $\zeta$  and the  $\xi$ ,  $\eta$  coordinate plane is chosen to coincide with the plane of a flat quadrilateral panel or a flat triangular subpanel. For case (1), above, the origin of the local coordinates is at the center of the quadrilateral. For case (2), above, the origin for each triangular subpanel is at the vertex opposite the side forming the diagonal of the quadrilateral. For case (3), the origin is at the center of the quadrilateral when the local coordinates are related to the inner four subpanels, fig. 9, and at the outer vertices when related to outer four subpanels, fig. 10.

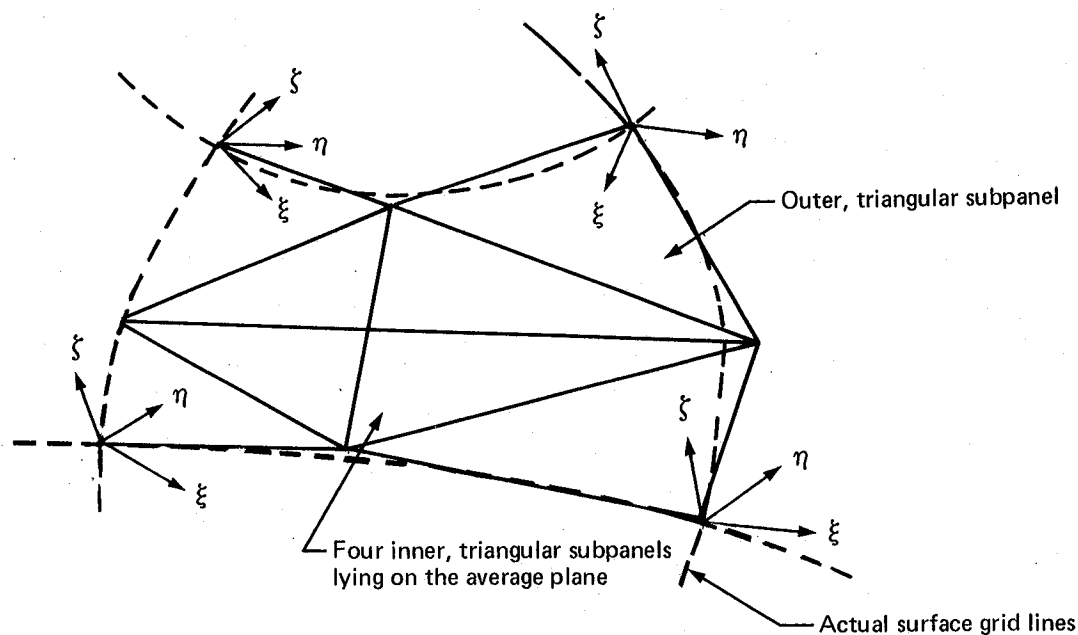


Figure 10. — Subpanel Approximation to Surface of Integration

The polynomial approximating-functions for the source and doublet distributions are as follows:

Source,

$$\sigma^*(Q) = \sigma_0^* + \sigma_\xi^* \xi + \sigma_\eta^* \eta \tag{49}$$

Doublet,

$$\mu^*(Q) = \mu_0^* + \mu_\xi^* \xi + \mu_\eta^* \eta + \frac{1}{2} \mu_{\xi\xi}^* \xi^2 + \mu_{\xi\eta}^* \xi\eta + \frac{1}{2} \mu_{\eta\eta}^* \eta^2 \tag{50}$$

where  $Q$  is the surface point with coordinates  $\xi, \eta$ . The values of the coefficients in these polynomials are found by fitting the polynomials to the values of the source and doublet distributions at the nine canonical points of the quadrilateral shown by fig. 9. The values at these nine points are denoted as

$$\begin{aligned} & \text{(e)} \\ & \sigma_i^* = \sigma^*(Q_i) \text{ for } i = 1, \dots, 9 \end{aligned} \tag{51}$$

and

$$\begin{aligned} & \text{(e)} \\ & \mu_i^* = \mu^*(Q_i) \text{ for } i = 1, \dots, 9. \end{aligned} \tag{52}$$

For each panel and subpanel the coefficients are related to the canonical values by matrix expressions of the following form:

$$\begin{Bmatrix} \sigma_0^* \\ \sigma_\xi^* \\ \sigma_\eta^* \end{Bmatrix}_k = \begin{bmatrix} \text{(e)} \\ (\text{RR})_{jik} \end{bmatrix} \begin{Bmatrix} \text{(e)} \\ \sigma_i^* \end{Bmatrix} \tag{53}$$

and

$$\begin{Bmatrix} \mu_0^* \\ \mu_\xi^* \\ \mu_\eta^* \\ \mu_{\xi\xi}^* \\ \mu_{\xi\eta}^* \\ \mu_{\eta\eta}^* \end{Bmatrix}_k = \begin{bmatrix} \text{(e)} \\ (\text{QQ})_{jik} \end{bmatrix} \begin{Bmatrix} \text{(e)} \\ \mu_i^* \end{Bmatrix} \tag{54}$$

where the index  $j$ , in eq. (53) and eq. (54), ranges over the elements of the column matrices of polynomial coefficients, the index  $i$  ranges over the canonical values required to determine the polynomial coefficients, and the index  $k$  identifies the subpanel over which the approximating polynomial is defined.

The canonical values of the source and doublet distributions on a panel are determined from a least squares fit of the polynomials shown by eq. (49) and eq. (50) to the values of the distributions at the panel center and the centers of the neighboring panels. In the case of a panel source distribution the points of evaluation are those shown by fig. 11, while in the case of a panel doublet distribution the points of evaluation are those shown by fig. 12. The distribution values at these points are referred to as the panel singularity parameters; and, for a panel source distribution, they are nine in number and denoted as

$$\overset{(e)}{\sigma_\alpha^*} \text{ for } \alpha = 1, \dots, 9. \tag{55}$$

For a panel doublet distribution the panel singularity parameters are twenty-one in number and are denoted as

$$\overset{(e)}{\mu_\alpha^*} \text{ for } \alpha = 1, \dots, 21. \tag{56}$$

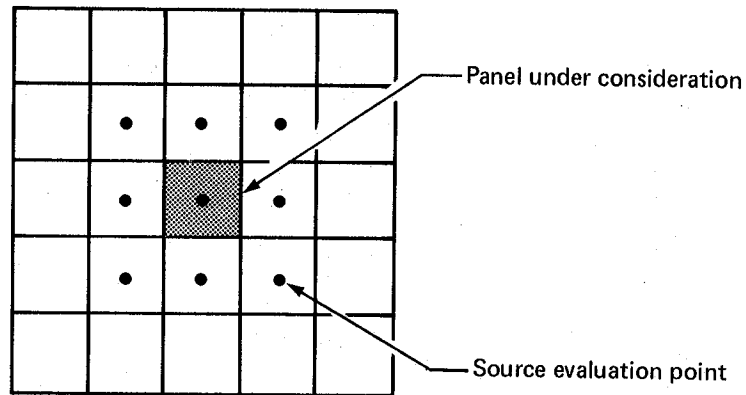


Figure 11. — Source Evaluation Points at the Center of the Panel and Its Neighboring Panels

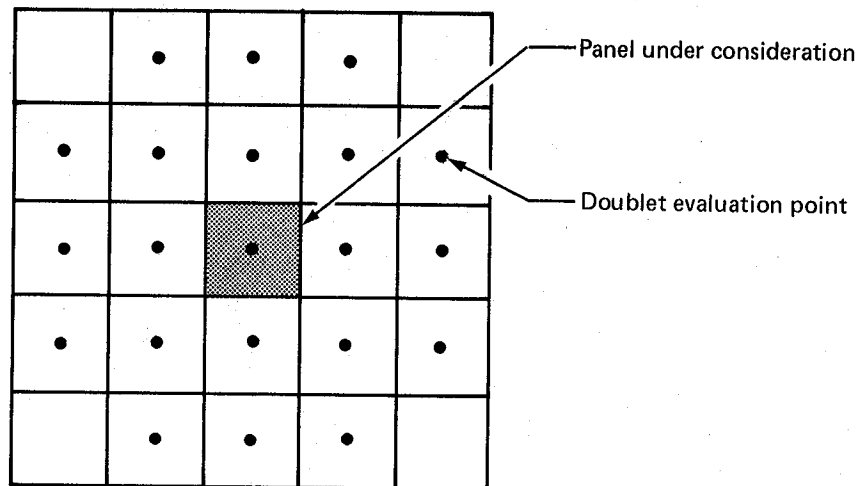


Figure 12. — Doublet Evaluation Points at the Center of the Panel and Its Neighboring Panels

The least squares fit to these panel singularity parameters, when evaluated at the canonical points of the panel, yield the following matrix relations:

$$\begin{Bmatrix} \sigma_i^* \\ \sigma_\alpha^* \end{Bmatrix} = \begin{bmatrix} \text{(e)} \\ (\text{ASTS})_{i\alpha} \end{bmatrix} \begin{Bmatrix} \sigma_\alpha^* \end{Bmatrix} \quad (57)$$

and

$$\begin{Bmatrix} \mu_i^* \\ \mu_\alpha^* \end{Bmatrix} = \begin{bmatrix} \text{(e)} \\ (\text{ASTD})_{i\alpha} \end{bmatrix} \begin{Bmatrix} \mu_\alpha^* \end{Bmatrix} \quad (58)$$

Taken together, eq. (49), eq. (50), eq. (53), eq. (54), eq. (57), eq. (58) describe the source and doublet distribution approximations on each subpanel of a quadrilateral, and this description is in terms of the panel source and doublet singularity parameters defined by eq. (55) and eq. (56).

In the implementation of eq. (56) the points of evaluation appear to be 25 in number, because a double index system is used to enumerate the evaluation points. The double index system ranges over five columns and five rows of grid points in order to identify the twenty-one evaluation points. In other words, the evaluation points for each panel span five rows and five columns, and this leads to a single index ranging from one to twenty five.

Having approximated the surfaces of integration by networks of panels and having replaced the unknown functions describing the source and doublet distributions by approximating functions defined independently over each panel or subpanel, panel influence coefficients may be defined. Letting  $\Sigma_e$  represent the surface area of the eth panel and letting  $\sigma_e^*$  and  $\mu_e^*$  represent the approximating functions on the panel, the panel influences at the field point  $P$  are defined as follows:

$$\phi_S^*(P) = \iint_{\Sigma_e} \sigma_e^* \psi^* ds' \quad (59)$$

$$\phi_D^*(P) = \iint_{\Sigma_e} \mu_e^* \frac{\partial}{\partial n_c} \psi^* ds' \quad (60)$$

$$\vec{v}_S^*(P) = - \iint_{\Sigma_e} \sigma_e^* \vec{\nabla}' \psi^* ds' \quad (61)$$

$$\vec{v}_D^*(P) = - \iint_{\Sigma_e} \mu_e^* \frac{\partial}{\partial n_c} \vec{\nabla}' \psi^* ds' \quad (62)$$

where

$$\vec{\nabla} \psi^* = -\vec{\nabla}' \psi^* \quad (63)$$

because, as shown by eq. (40),  $\psi^*$  is a function of the coordinates of two points, P and Q, and the unprimed gradient is with respect to the coordinates of P while the primed gradient is with respect to the coordinates of Q.

Appendix C contains the development whereby these integrals are expressed in the local panel coordinates and the results are shown as equations (C.128) through (C.136). The procedures for evaluating these integrals appear in app. D; they lead to a reduction of eqs. (59) through (63) to algebraic expressions evaluated at a finite number of points called control points, see sec. 3.4 and sec. 4, ref. 1. These expressions are evaluated at control points located essentially at the singularity parameter evaluation points described above (see sec. D.1, app. D); if they are evaluated at the  $i$ th control point and combined with eqs. (49) through (58), they provide the following relations:

$$\begin{Bmatrix} \phi_S^* \\ \vec{v}_S^* \end{Bmatrix}_i = \sum_{\alpha=1}^9 \sum_{j=1}^3 \begin{matrix} (e) \\ (DVDS^*)_{ij} \end{matrix} \begin{matrix} (e) \\ (ASTS)_{j\alpha} \end{matrix} \begin{matrix} (e) \\ \sigma_\alpha \end{matrix}^* \quad (64)$$

and

$$\begin{Bmatrix} \phi_D^* \\ \vec{v}_D^* \end{Bmatrix}_i = \sum_{\alpha=1}^{21} \sum_{j=1}^3 \begin{matrix} (e) \\ (DVDD^*)_{ij} \end{matrix} \begin{matrix} (e) \\ (ASTD)_{j\alpha} \end{matrix} \begin{matrix} (e) \\ \mu_\alpha \end{matrix}^* \quad (65)$$

where the superscript (e) indicates the values of the quantities associated with the  $e$ th panel. The subscript  $i$  now indicates the  $i$ th control point.

The indices  $\alpha$ , appearing in eqs. (64) and (65), range over the singularity parameter evaluation points neighboring the  $e$ th panel. These equations and this index assignment scheme are set up exclusive of the arrangement of the panels when they are used to assemble an approximation to a surface of integration. A separate index assignment scheme is used to identify the singularity evaluation points on the actual surface (cf., secs. 4.1 and 4.2 of ref. 1 — particularly, the discussion related to figs. 13 and 14). The terms “panel singularity parameters” and “global singularity parameters” are used. The values of the source and doublet distribution strengths appearing in eqs. (64) and (65) are referred to as panel singularity parameters; thus, a single isolated panel is under consideration and the panel singularity parameters at points on and neighboring that panel determine the doublet and/or source distribution on the panel. The values of the source and doublet distribution at the singularity evaluation points on the assembled surface are referred to as global singularity parameters. Incidence relations are used to relate the indices of the panel singularity parameters to those of the global singularity parameters. These relations appear as follows:

$$i = (IID)_\alpha^{(e)} \text{ for } \alpha = 1, \dots, 21 \quad (66)$$

and

$$j = (IIS)_\alpha^{(e)} \text{ for } \alpha = 1, \dots, 9 \quad (67)$$

where  $i$  is the global index corresponding to the  $\alpha$ th doublet strength value for the  $e$ th panel and, similarly,  $j$  is the global index corresponding to the  $e$ th panel. These relations can be viewed as column matrices, one for each panel; the  $\alpha$ th entry of  $[(IID)\alpha]$  is then the global index of a doublet evaluation point on the assembled surface where the  $\alpha$ th panel singularity point of the  $e$ th panel is to be located.

The incidence relations shown by eqs. (66) and (67) are used to incorporate eqs. (64) and (65) into a single matrix expression, viz.,

$$\begin{Bmatrix} \vdots \\ \phi^* \\ \vec{v}^* \\ \vdots \end{Bmatrix}_A = [(DSDFS^*)_{ij}] \{\lambda_j^*\} \quad (68)$$

where  $\lambda_j^*$  is the  $j$ th global singularity parameter. The coefficient matrix appearing in eq. (68) is called the aerodynamic influence coefficient matrix and this coefficient matrix contains the coefficients denoted as  $A_{ij}^*$  in sec. 2.0. The left hand member contains the complex amplitudes of the potential and the velocity (in terms of the modified potential, viz., eq. (29)) evaluated at the control points. However, as shown by app. C, sec. C.2, the potential and the velocity are discontinuous at the control points because the control points lie on surfaces containing the source and doublet distributions. The subscript A, appearing in eq. (68), denotes the fact that the values computed by eq. (68) are the average of the limiting values found by approaching the surface from above and below, viz.,

$$(\phi_i^*)_A = \frac{1}{2} (\phi_u^* + \phi_\ell^*)_i \quad (69)$$

and

$$(\vec{v}_i^*)_A = \frac{1}{2} (\vec{v}_u^* + \vec{v}_\ell^*)_i. \quad (70)$$

The discontinuities in potential and velocity at a surface of source and doublet distribution are as follows:

For doublet distributions:

$$\phi_u^* - \phi_\ell^* = \mu^* \quad (71)$$

and for source distributions:

$$\left( \frac{\partial \phi^*}{\partial n_c} \right)_u - \left( \frac{\partial \phi^*}{\partial n_c} \right)_\ell = \sigma^*; \quad (72)$$

thus, the potential and velocity at the upper side of the surface are found as follows:

$$\phi_u^* = (\phi^*)_A + \frac{1}{2}\mu^*. \quad (73)$$

Noting that

$$\vec{v}_u^* - \vec{v}_\ell^* = \vec{\nabla}\mu^* + \vec{n}_c \left[ \left( \frac{\partial\phi^*}{\partial n_c} \right)_u - \left( \frac{\partial\phi^*}{\partial n_c} \right)_\ell \right] = \vec{\nabla}\mu^* + \vec{n}_c \sigma^*, \quad (74)$$

the velocity at the upper side of the surface is found to be

$$\vec{v}_u^* = (\vec{v}^*)_A + \frac{1}{2}(\vec{n}_c \sigma^* + \vec{\nabla}\mu^*);$$

and, at the lower side of the surface, similarly,

$$\phi_\ell^* = (\phi^*)_A - \frac{1}{2}\mu^* \quad (75)$$

$$\vec{v}_\ell^* = (\vec{v}^*)_A - \frac{1}{2}(\vec{n}_c \sigma^* + \vec{\nabla}\mu^*) \quad (76)$$

As a comment regarding eqs.(69) and (70), the average of the limiting values are not actually computed in the manner indicated by those equations. Although the integral describing the influence of a panel on a point located on the panel is singular, the singular behavior of the two integrals implied by the right hand numbers of eqs. (69) and (70) cancel one another. The result of this cancellation is a single, regular integral. This regular integral is evaluated to obtain the average influence, cf., ref. 1, sec. 3.7.

### 3.5 UNSTEADY FLOW PROBLEM FORMULATION

As a preliminary to this section, consider the network arrangement for describing the panels on the surface of a configuration (cf. sec. 4, ref. 1 and sec. 1.1, ref. 2). The panels are described in terms of networks consisting of rows and columns of panels. Each network covers a portion of the surface of a configuration without overlapping the surface covered by another network; thus, every panel on the surface of a configuration is a member of one and only one network. For example, the right half of a symmetric wing surface and its wake could be covered by four networks consisting of the upper wing surface, the lower wing surface, a surface closing the tip, and the wake surface.

The panels of a single network are all of one type; that is, every panel of a particular network is either a source panel, a doublet panel, or a combined source-doublet panel. If one portion of a configuration surface is to have only sources distributed on it while a second portion is to have only doublets distributed on it, then these two portions of surface must be covered by different networks: one a source network, the other a doublet network.

As already noted, a network is a two dimensional array of panels, fig. 13. The grid points, which form the corners of the panels of a network, are enumerated by the indices (M,N) where M is the grid point row number, while N is the grid point column number. Although it would appear from this that a network always has four sides, one side of a network can be collapsed into a single point so that the collapsed side has zero length. When the edge (or side) of a network is collapsed, all panels along that edge must have a collapsed edge such that they are three sided and have one corner point

located at the point representing the collapsed edge of the network. This requirement is consistent with the requirement that every row and column of grid points of a network must have the same number of members. If the collapsed edge of a network corresponds with the column direction of indexing grid points and the network has  $M$  rows of grid points, then the point representing the collapsed edge is counted  $M$  times in the indexing scheme. Also, if a network edge has finite length, then the edges of every panel lying on that network edge must have a finite length even though the length of each panel edge can be different from the others.

Recall from the preceding that the unit vector normal to the surface appears in the boundary conditions of the flow problem; thus, in order to formulate a flow problem one must have a facility for specifying which side of a surface is to be that of positive normal (i.e., the upper side of the surface). This facility is provided for each network by the grid point numbering system. Let  $\vec{M}$  and  $\vec{N}$  denote vectors, respectively, in the grid point row and column directions (fig. 13). The side of the surface in the direction of the cross product  $(\vec{N} \times \vec{M})$  is called the upper side (or positive side) of the surface and this is the side of positive unit normal vector for the portion of surface covered by the network. The opposite side is called the lower (or negative) side.

Network surfaces do not overlap one another and the edges of networks are either free edges of surfaces or edges which abut other network edges. Since surfaces can contain narrow gaps, a convention is used to distinguish between a physical gap and an abutment of two network edges on a continuous surface. The convention is as follows: The edge of a network is a continuous curve consisting of straight line segments. If the two curves representing the edges of two networks are identical (within the accuracy of the computations), then the two network edges abut one another. Along any straight line segment of the network edge curves, the number and location of the grid points can differ between the abutting networks (except at the line segment ends) but these intermediate grid points must lie precisely on the line segment, fig. 14. If these conditions are not satisfied, then the two networks do not abut one another and a surface gap (or discontinuity) is introduced.

The control points of typical networks are shown by fig. 15. A source network has panel center control points only; while a doublet network has both panel center and network edge control points.† Boundary conditions are applied at these points specifying: (1) the value of a flow parameter obtained as a value of an aerodynamic influence coefficient (e.g., the normal component of the unsteady perturbation mass flux vector at the upper side of the network) or (2) the value of a source or doublet distribution. The network edge control points play the role of outer evaluation points, see app. C of ref. 1; they are used to impose continuity on the doublet distribution between abutting networks of doublet panels, see sec. 6.0, ref. 1.

The aerodynamic surface boundary condition which appears as eq. (31) and which is derived in app. B is expressed as follows:

$$\vec{w}^* \cdot \hat{n}_s = B^* \quad \text{on } S_s$$

where

$$B^* = \left[ -\vec{W}_s \cdot (\vec{\theta}^* \times \hat{n}_s) - (\vec{D}^* \cdot \vec{\nabla} \vec{W}_s) \cdot \hat{n}_s + \rho_s u_n^* \right] e^{-i\vec{\omega} \times M_0^2 / \beta^2} \quad (31)$$

† Wake surfaces are represented by doublet networks; and, in the case of a wake-doublet network, control points occur only along one edge, cf., the discussion concerning figures 16 and 17.

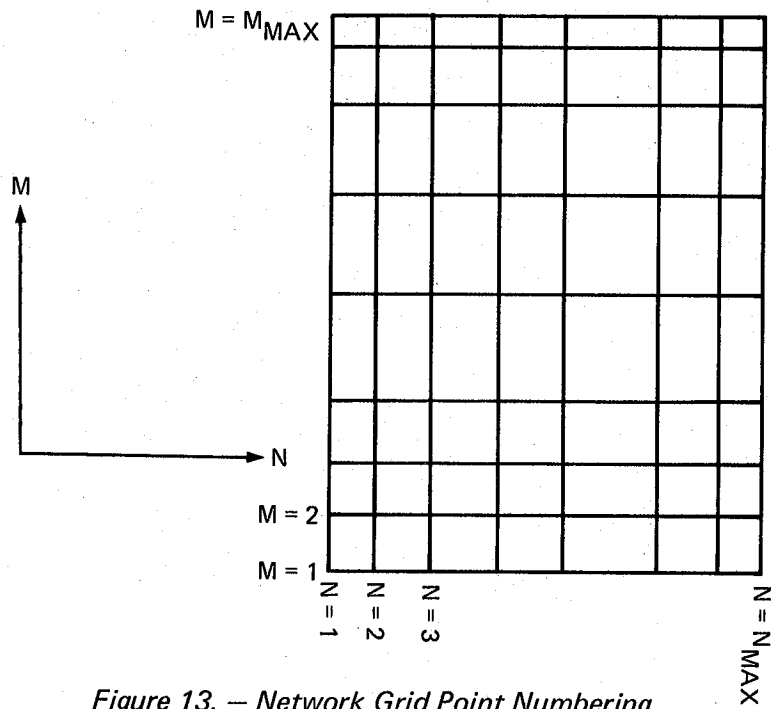


Figure 13. — Network Grid Point Numbering

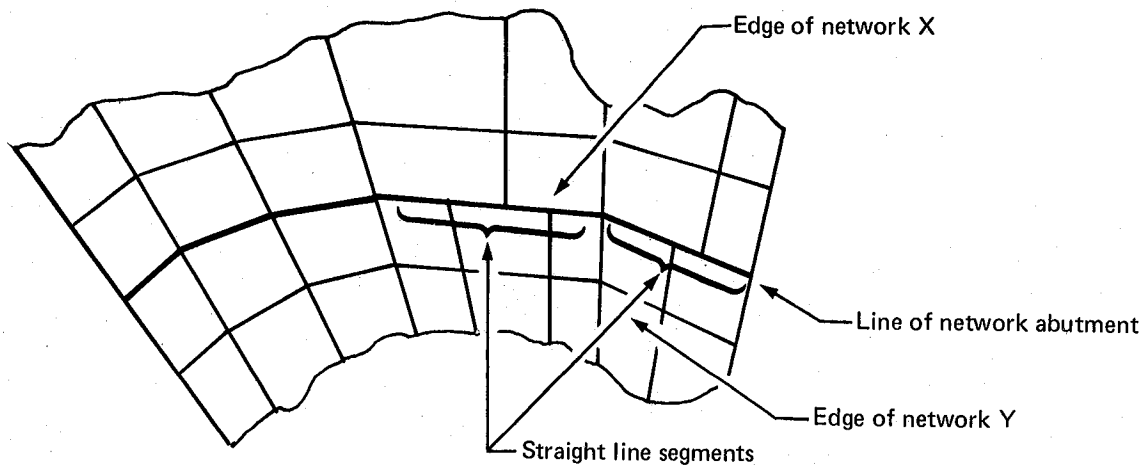


Figure 14. — Abutting Networks

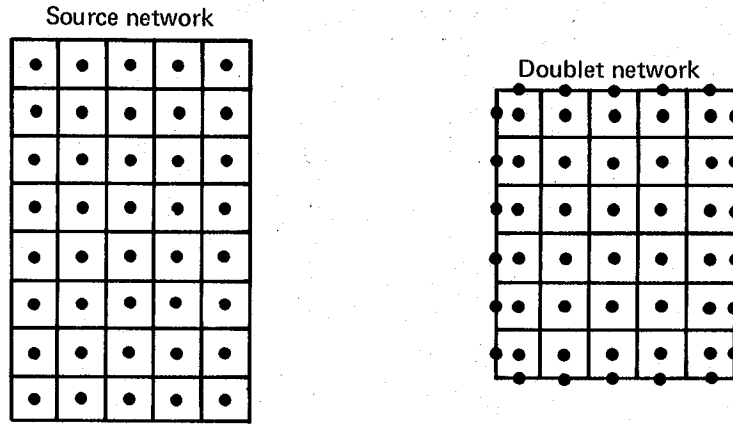


Figure 15. — Network Control Points

This boundary condition must be satisfied at each of the aerodynamic surface network control points. Referring to eqs. (32) and (41), the left hand number of eq. (31) can also be expressed in terms of the mean steady surface conormal vector such that

$$\vec{n}_c \cdot \vec{\nabla} \phi^* = B^* \quad \text{on } S_s ; \quad (77)$$

hence, assuming that this boundary condition is to be satisfied at the upper surface of a network, it is evaluated, using eq. (72), as follows:

$$\vec{n}_c \cdot \left( \vec{v}_A^* + \frac{1}{2} \vec{n}_c \sigma^* + \frac{1}{2} \vec{\nabla} \mu^* \right)_u = B^* \quad \text{on } S_s . \quad (78)$$

Eq. (78) represents a special form of the following general boundary condition:

$$C_u (\vec{w}_u^* \cdot \hat{n}) + \vec{T}_u \cdot \vec{v}_u^* + D_u \phi_u^* + C_\ell (\vec{w}_\ell^* \cdot \hat{n}) + \vec{T}_\ell \cdot \vec{v}_\ell^* + D_\ell \phi_\ell^* = B^* . \quad (79)$$

If the coefficients of the flow parameters are given the following values:

$$C_u = 1 , \quad \vec{T}_u = \vec{T}_\ell = C_\ell = D_u = D_\ell = 0 ,$$

then eq. (79) reduces directly to eq. (78).

Consider, as an example, the Morino-type boundary conditions (ref. 2, sec. 1.31) for an aerodynamic body having finite thickness, i.e., a body whose surface encloses a volume of space. These boundary conditions are such that the unsteady disturbance potential is made to vanish everywhere in the enclosed volume. The networks on the surface are chosen as combined source-doublet networks and their grid point indices are chosen such that the lower side of the network surfaces are at the interior of

the body. If  $\phi_\ell^*$  is set to zero at the doublet control points, then  $\phi^*$  will vanish at the lower side of the surface; and, therefore,  $\phi^*$  will vanish everywhere throughout the enclosed volume. Since, as shown by eq. (71), the doublet strength is equal to the jump in potential at the surface, i.e.,

$$\mu^* = \phi_u^* - \phi_\ell^* ,$$

the doublet strength is equal to the potential at the upper side of the surface, viz.,

$$\mu^* = \phi_u^* ,$$

because

$$\phi_\ell^* = 0 .$$

Also, from eq. (72)

$$\sigma^* = \left( \frac{\partial \phi^*}{\partial n_c} \right)_u - \left( \frac{\partial \phi^*}{\partial n_c} \right)_\ell ;$$

but, because

$$\left( \frac{\partial \phi^*}{\partial n_c} \right)_\ell = 0 ,$$

the source strength is equal to the normal component of perturbation mass flux at the upper side of the surface, viz.,

$$\sigma^* = \left( \frac{\partial \phi^*}{\partial n_c} \right)_u$$

or

$$\sigma^* = \left( \hat{n} \cdot \vec{w}^* \right)_u$$

where eqs. (32) and (41) have been used to introduce the mass flux vector.

The Morino-type boundary conditions are implemented, using the general form of the boundary condition shown as eq. (79), by the following choice of coefficients:

At doublet control points

set  $D_\ell = 1$  and all other coefficients set to zero.

At source control points

set  $C_u = 1$  and set  $B^* =$  (right hand side of eq. (31) )

and all other coefficients set to zero.

The evaluation of the right hand side of eq. (31) requires the values of the mass flux vector, the mass flux vector gradient, and the mass density of the fluid in the steady mean component of flow. These quantities must be obtained from a separate solution to the steady mean flow problem, cf. sec. 5.2.

In the case of thin wing theory (ref. 7, Chapter 13) the steady mean component of flow is simply the undisturbed freestream. In that case the aerodynamic surface boundary condition, viz., eq. (31), reduces to the following:

$$\vec{w}^* \cdot \hat{n}_s = \left[ -\hat{i} \cdot (\vec{\theta}^* \times \hat{n}_s) + u_n^* / U_o \right] e^{-i\bar{\omega}x M_o^2 / \beta^2} \text{ on } S_s \quad (80)$$

where  $S_s$  is a cylindrical surface with generator parallel with the  $x$  axis. Only doublet networks are required on  $S_s$  and the boundary condition is expressed by setting  $C_\rho = 0.5$ ,  $C_u = 0.5$ , and  $B^*$  equal to the right hand member of eq. (80) evaluated at the doublet control points. All other coefficients of the boundary condition are set to zero.

As indicated by eq. (48), the unsteady wake surface boundary condition is not an independent boundary condition, in that the doublet distribution on the wake is determined on its entire surface by its value along its upstream edge. The wake is a surface emanating from the edge of a lifting body, fig. 16, and the Kutta condition requires that the discontinuity in potential across the wake surface and across the lifting surface be continuous at the lifting surface trailing edge. The wake is represented by doublet networks; and, since the doublet strength is equal to the jump in potential, i.e.,

$$\mu^*(Q) = \phi_u^*(Q) - \phi_l^*(Q) \quad \text{for } Q \text{ on } W_s,$$

the wake doublet strength along the network edges which abut a lifting surface must be equal to the jump in potential across the lifting surface along the line of abutment. If the lifting body is represented by thin wing theory, then the lifting body is an infinitesimally thin lifting surface represented by doublet networks. In this case, letting  $Q_s$  represent a point on the lifting surface and letting  $Q_w$  represent a point on the wake, if  $Q_s$  and  $Q_w$  approach the same point on the abutment line between the lifting surface and the wake, then in the limit we require that

$$\mu^*(Q_s) = \mu^*(Q_w), \quad (81)$$

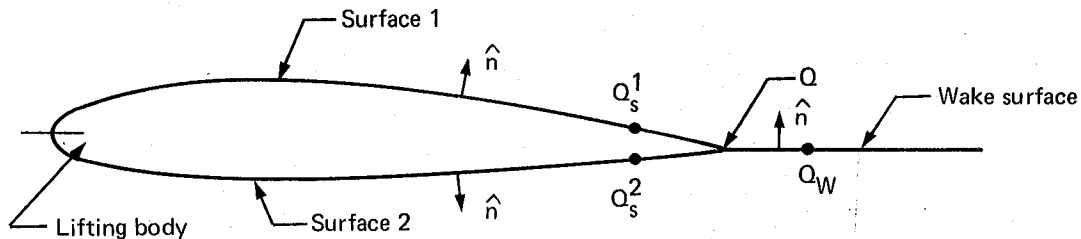


Figure 16. — Surfaces of a Lifting Body and Its Wake.

and this expression represents the Kutta condition requirement. If the lifting surface is thick and is represented by Morino-type boundary conditions such that

$$\mu^* (Q_s^1) = \phi_{u^*} (Q_s^1)$$

and

$$\mu^* (Q_s^2) = \phi_{u^*} (Q_s^2)$$

where  $Q_s^1$  and  $Q_s^2$  represent points on the two surfaces shown by fig. 16, then in the limit as the three points  $Q_s^1$ ,  $Q_s^2$  and  $Q_w$  all approach the same point on the line of abutment with the wake we require that

$$\mu^* (Q_s^1) - \mu^* (Q_s^2) = \mu^* (Q_w); \quad (82)$$

and this expression, in addition to eq. (37), represents the Kutta condition requirement.†

As noted above, the doublet strength distribution on a wake network is determined by the conditions along the upstream edge of the network. This determination is described by eq. (37), viz.,

$$\mu^* (\ell, s) = \mu^* (c, s) e^{-i\bar{\omega} / \beta^2} \tau (\ell, s) \text{ on } W_s \quad (37)$$

where

$$\tau (\ell, s) = \int_c^\ell \frac{d\xi}{w_s (\xi, c)}$$

and

$$w_s \equiv \left| \vec{W}_s \right| \frac{1}{\rho_o U_o}$$

is the magnitude of the mean steady mass flux vector divided by the freestream mass flux. The parameter  $\ell$  is a coordinate line along the mean steady flow streamline at the wake surface,  $s$  is a coordinate line orthogonal to  $\ell$ , and  $c$  is the value of  $\ell$  at the upstream edge of the wake network, see fig. 17. Eq. (37) can be seen to specify the doublet distribution everywhere on a wake network in terms of the doublets' strength along the upstream edge.

If, as in the case of the usual linear theory, the mean steady flow is simply the undisturbed freestream, then eq. (37) reduces to

$$\mu^* (x, s) = \mu^* (c, s) e^{-i\bar{\omega} (x-c)} \quad (83)$$

† As a result of numerical approximations involved in the evaluation of eq. (82), a modified form of the Morino-type boundary conditions is required for approximating the Kutta condition, cf., sec. 4.4.

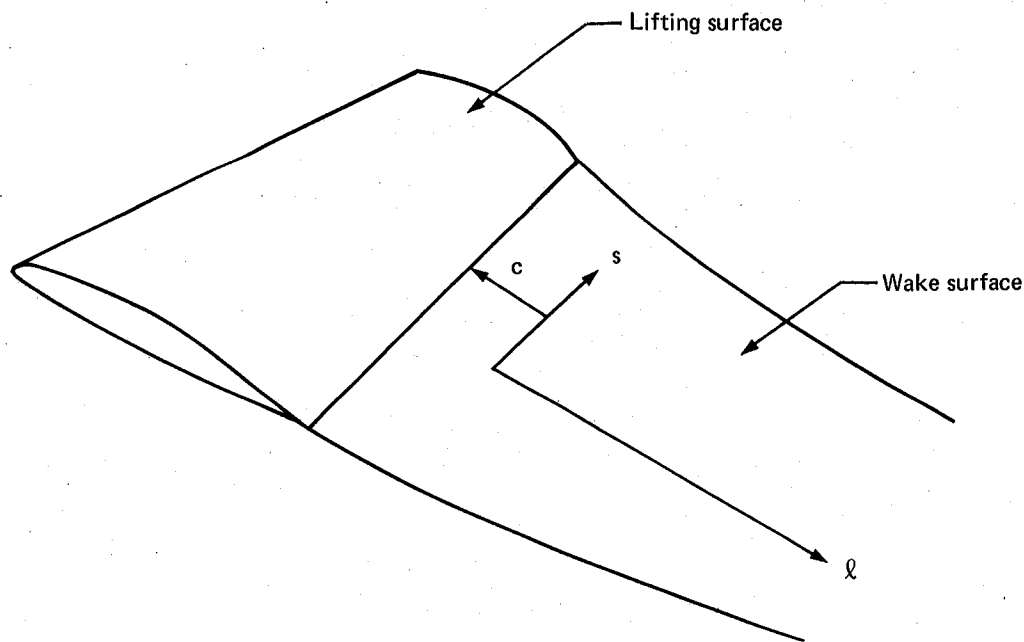


Figure 17. — Surfaces of a Lifting Body and Its Wake

the  $x$  coordinate. The results computed in the following section have all been computed using this doublet distribution on the wake surface networks. The theory and its implementation as a computer program provide for the wake model shown as eq. (37), but the steady flow analysis capability for generating the parameters required to evaluate eq. (37) has not yet been developed.

The evaluation of eq. (37) requires a solution to a nonlinear steady flow problem. The steady flow method of solution provided by ref. 1 is based on a wake which is a cylindrical surface with generator parallel with the undisturbed freestream direction. This wake representation provides a first order approximation to a solution satisfying the exact wake boundary conditions developed in app. A, viz.,

$$[[p]] = 0 \text{ on } W \quad (\text{A.35})$$

and

$$\vec{V}_m \cdot \hat{n} = 0 \text{ on } W; \quad (\text{A.48})$$

however, it does not provide the data required to evaluate eq. (37).

In the exact theory eq. (A.35) requires pressure to be continuous across the wake and eq. (A.48) requires the mean velocity at the wake surface to be tangent to the wake surface. A plausible formulation of these boundary conditions, which is consistent with the approximations involved in eq. (37), consists of replacing the pressure in eq. (A.35) with the second order approximation shown by eq. (B.8) and of replacing the flow velocity appearing in eq. (A.48) with the approximate mass flux vector shown by eq. (B.4). An iterative solution is required in which the wake surface location is adjusted until these approximate forms of the wake boundary conditions are satisfied.

Presuming success for the solution of the problem, the solution would provide the spatial coordinates of the wake surface (viz.,  $\ell$ ,  $s$ ) and the mean of the steady mass flux vector along the wake surface (viz.,  $W_s$ ). These quantities then provide a means for evaluating the unsteady flow wake boundary condition shown as eq. (37).

Regardless of how the wake surface is approximated, the doublet strength varies along a streamline coordinate deviating only slightly from a harmonic function of the coordinate distance. Recalling that the panel approximation to the doublet strength distribution is a quadratic function of the local panel coordinates, cf. eq. (50), it can be seen that the wake paneling must be sufficiently dense in the streamwise direction that the panel-wide quadratic provides an accurate least squares approximation to the harmonic variation. A panel density of sixteen panels per wave length of harmonic doublet variation has been used in the example cases described in sec. 4.

## 4.0 DISCUSSION OF RESULTS

This section presents computed results which demonstrate the validity of the approximations contained in the unsteady flow panel method, primarily, the approximation to the unsteady kernel function described in app. D. This emphasis on the validity of the kernel function approximation stems from the fact that the method is an outgrowth of the steady flow panel method of ref. 1. The approximation to the unsteady kernel function is the primary feature leading to this outgrowth; hence, the demonstration of its validity is a central consideration in establishing the validity of the unsteady flow panel method.

The demonstration cases consist of configurations of four different types:

- (1) thin, planar lifting surfaces;
- (2) thin, nonplanar lifting surfaces;
- (3) bodies of finite thickness; and
- (4) combinations of (2) and (3).

Demonstration cases of type (1) are the primary basis for validating the unsteady kernel function approximation. The reason for this is the availability of an accurate, alternate method as a basis of comparison, viz., that of ref. 8. A T-tail is typical of a type (2) configuration and three different T-tails are evaluated and compared with alternate methods of evaluation. A type (3) configuration is represented by a wing with sources and doublets distributed on its actual surfaces in their mean steady locations. The lift distribution on this wing as a thick body is compared with the lift distribution on the same wing treated as a thin body, type (1). A type (4) configuration is represented by a twin engined transport configuration.

### 4.1 APPLICATION OF PANEL METHOD TO PLANAR, THIN WINGS

As noted in the preceding, in the case of thin lifting surfaces, when the boundary conditions are completely linearized, the steady mean component of flow consists of the undisturbed freestream. The aerodynamic surface and wake boundary conditions shown by eqs. (31) and (35), reduce to those shown by eqs. (80) and (83); and the panel method reduces to a method for evaluating the flow governed by thin wing theory, e.g., chapter 13 of ref. 7. The problem is formulated entirely in terms of doublet networks on the lifting surfaces and on the surfaces of their wakes. For the case of a single, planar lifting surface the acceleration doublet method of ref. 8 provides a well validated, independent method for evaluating thin wing theory; hence, it provides a basis for testing the validity and accuracy of the panel method doublet network for in-plane computations.

Figure 18 shows the planform of the right hand wing of a test case wing, which is symmetric about the  $x$  axis. The wing is oscillating in pitch about the midpoint of the root chord with a reduced frequency of 0.3577 in a uniform flow with a Mach number of 0.6. Figures 19 through 22 show the real and imaginary parts of the lifting pressure coefficient chordwise distribution at

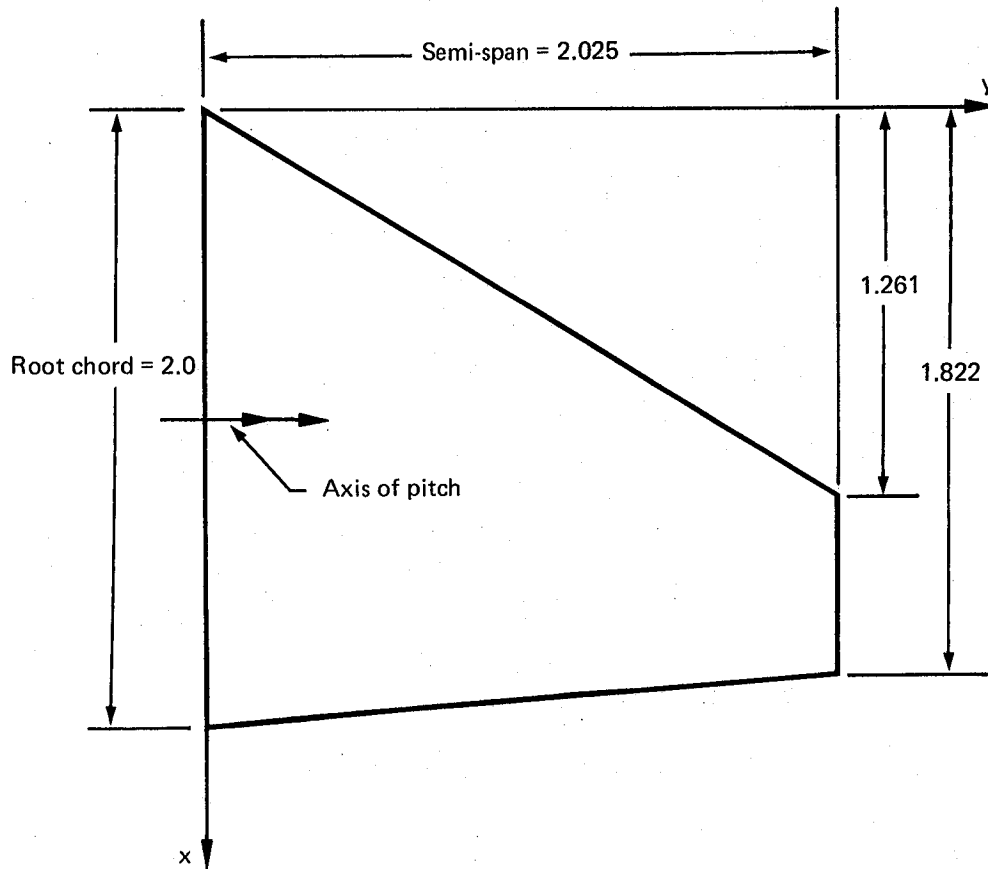


Figure 18. — Planform of Test Wing

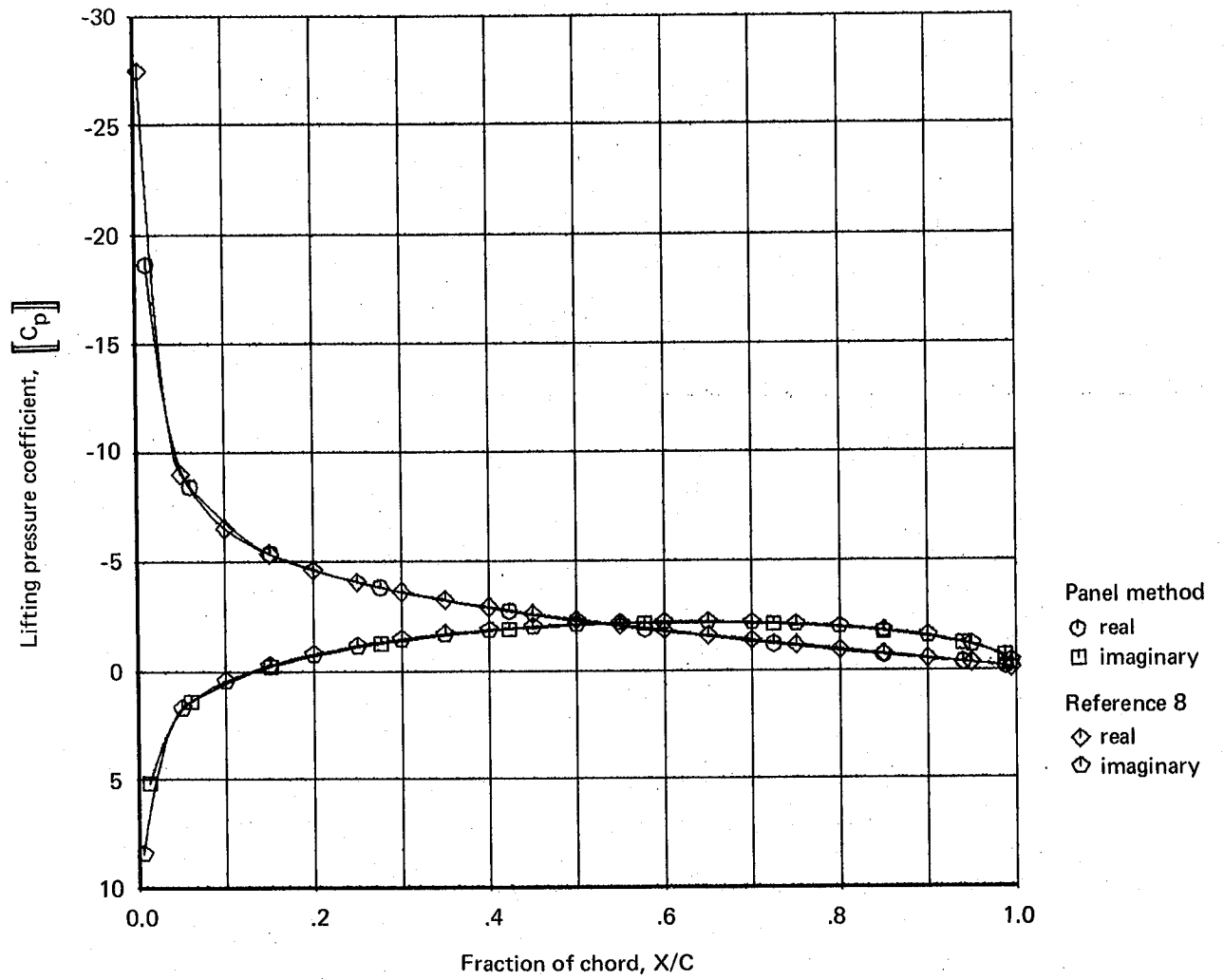


Figure 19. — Thin Wing Unsteady Lifting Pressure Comparison at 18.1% Semi-span

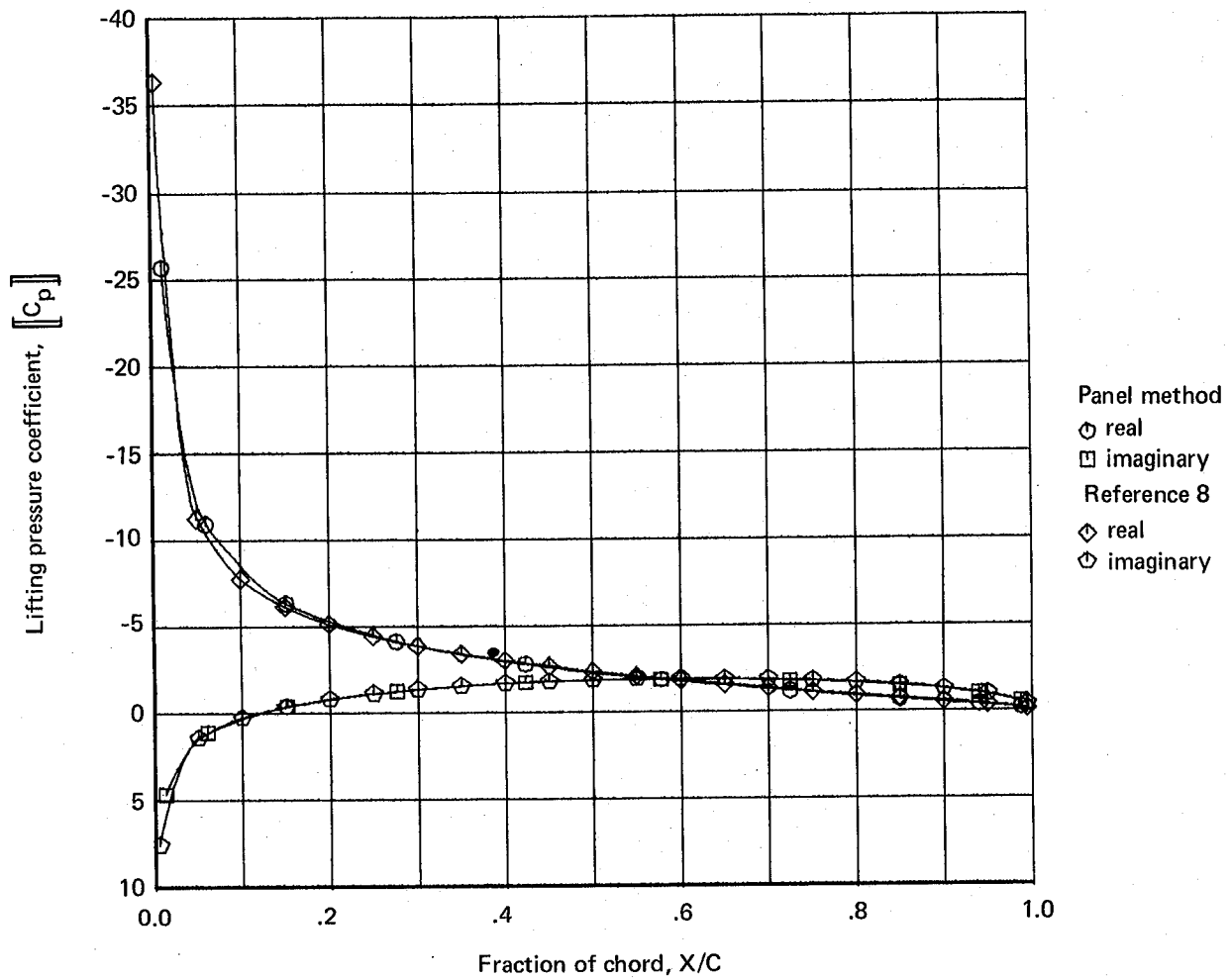


Figure 20. — Thin Wing Unsteady Lifting Pressure Comparisons at 51.2% Semi-span

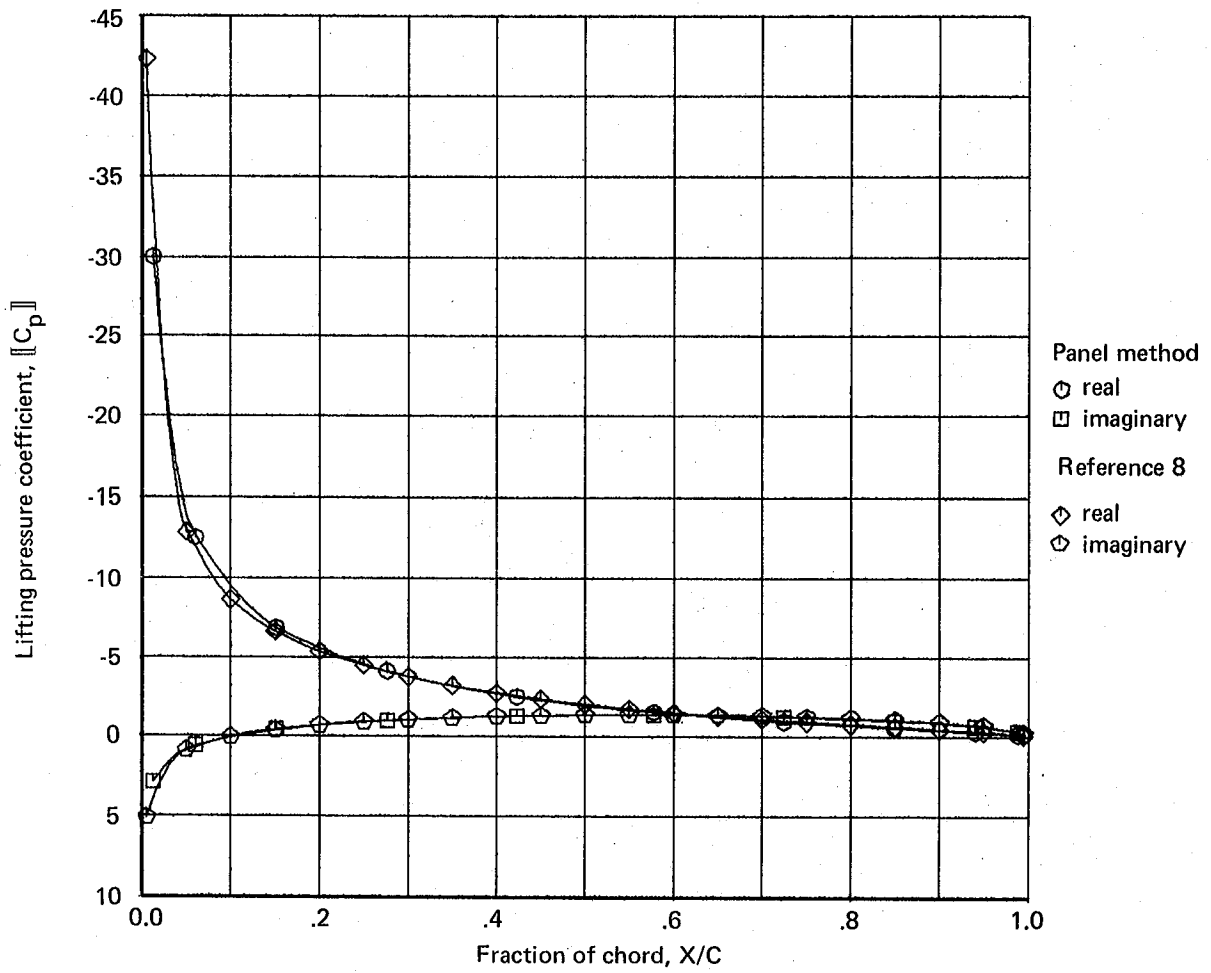


Figure 21. — Thin Wing Unsteady Lifting Pressure Comparison at 81.7% Semi-span

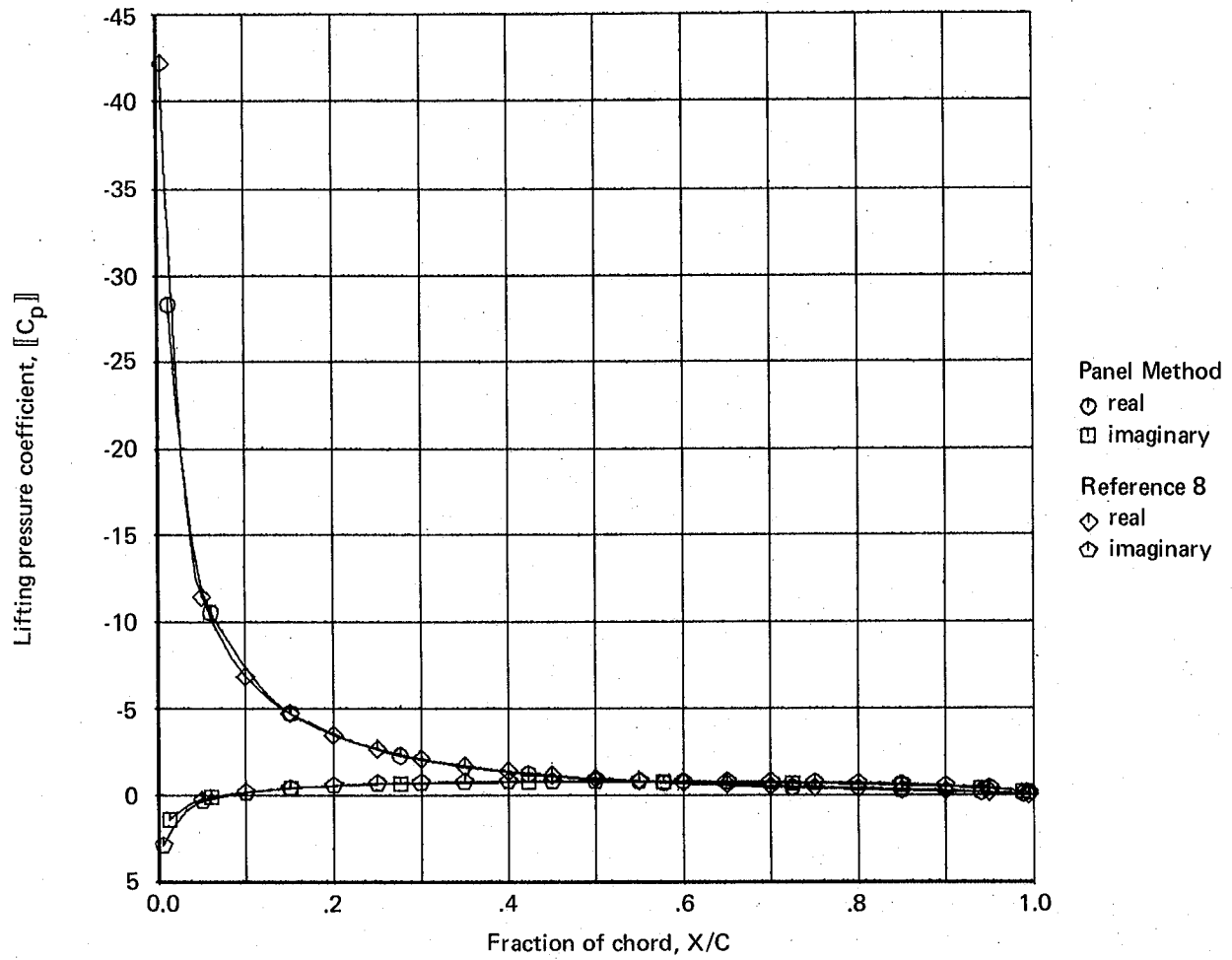


Figure 22. — Thin Wing Unsteady Lifting Pressure Comparison at 97.7% Semi-span

four spanwise locations (viz., at 18.1, 51.2, 81.7, and 97.7 percent of semi span from the root). The plotted values shown on the figure as circles and squares are, respectively, the real and imaginary lifting pressure coefficients computed by the panel method using 100 panels on the right hand wing. The panel spacing is such that there are ten panels in both the spanwise and chordwise directions; letting  $b = 4.05$  denote the span, the chordwise edges of the panels are located at the following points along the  $y$  coordinate direction:

$$y(N) = \frac{b}{2} \sin\left(\frac{S\pi}{2}\right) \quad (84)$$

where

$$s = (N - 1)/(NMAX - 1) \quad (85)$$

and  $NMAX = 11$  while  $N = 1, \dots, NMAX$ . The  $x$  coordinates of spanwise panel edges are spaced along each chord lines as follows:

$$\xi(M)/c = \frac{1}{2} (1 - \cos(s\pi)) \quad (86)$$

where  $c$  is the local chord length,  $\xi$  is the distance from the trailing edge, and

$$s = (M - 1)/(MMAX - 1) \quad (87)$$

where  $MMAX = 11$  and  $M = 1, \dots, MMAX$ . Fig. 23 shows the resulting panel spacing.

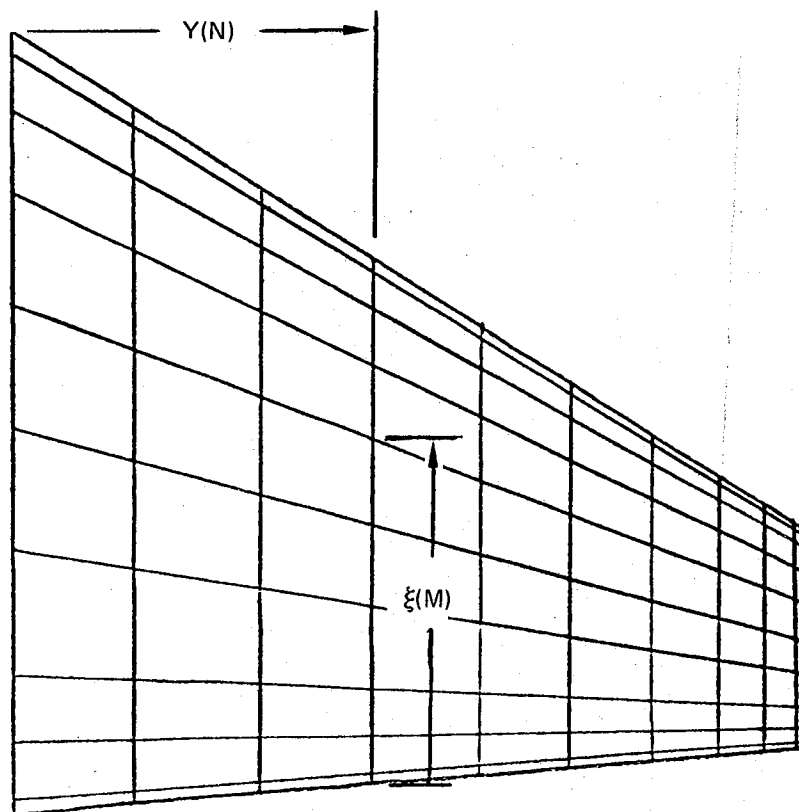


Figure 23. — Panel Spacing on Test Wing

Figures 19 through 22 show the panel method predicted pressure distribution compared with that predicted by the method of ref. 8. This method is based on a solution to the unsteady flow problem in terms of the acceleration doublet kernel function and distribution functions defined over the entire wing planform; it is a sufficiently well validated method that the close agreement shown between it and the panel method validates the panel method for application to planar, lifting surfaces.

Table 1 shows the effect of panel density on the values of the predicted unsteady pressures acting on the test wing. The effect is evaluated on the basis of the errors in the unsteady lift, pitching moment and rolling moment. This error evaluation is expressed as the relative error in the magnitudes of the lift and the moments, and the absolute error in their phase angles. When the wing has 375 panels, viz., 25 chordwise panel spaces and 15 spanwise panel spaces, the panel method yields the following:

Lift Force:

$$|C_L^*| = \frac{|L^*|}{q S_{REF}} = 3.6235$$

where  $|L^*|$  is the magnitude of the complex lift force on the right hand wing,  $S_{REF} = 2.5465$

square semi root chord lengths, and  $q$  is the dynamic pressure. The lift phase angle is

$$\varphi_L = 17.099^\circ$$

Rolling Moment:

$$|C_\ell^*| = \frac{|\ell^*|}{q B_{REF} S_{REF}} = 1.5672$$

where  $|\ell^*|$  is the magnitude of the complex rolling moment on the right hand wing about the x-axis and  $B_{REF} = 1.9463$  semi root chord lengths. The rolling moment phase angle is

$$\varphi_\ell = 14.852^\circ$$

Pitching Moment:

$$|C_m^*| = \frac{|m^*|}{q C_{REF} S_{REF}}$$

where  $|m^*|$  is the magnitude of the complex pitching moment about the pitch axis at  $x = 1.0$  and  $C_{REF} = 1.308$  semi root chord lengths.

The amplitude and phase errors are evaluated relative to the values of these quantities computed for the wing with 375 panels.

Table 1. — Effect of Panel Density on Thin Wing Forces

Panel density		Lift coefficient		Roll coefficient		Pitch coefficient	
Chordwise	Spanwise	Relative amplitude error (percent)	Absol. phase error (deg)	Relative amplitude error (percent)	Absol. phase error (deg)	Relative amplitude error (percent)	Absol. phase error (deg)
M	N						
2	2	1.2882	3.7643	-4.3078	3.5575	-1.4574	1.3216
3	2	.0672	2.3262	-3.3658	1.3043	-1.0146	-.0571
4	2	-.5647	1.7591	-2.9070	.5999	-3.2965	-.8675
6	2	-.7855	1.2611	-2.7774	.2514	-3.0980	-.9688
10	2	-.3229	.9876	-2.7966	.2817	-.0434	.0365
3	3	.0096	1.7587	-1.2023	1.0720	-6.9601	-4.7459
4	3	-.5304	1.1990	-1.1313	.4498	-6.1607	-3.1378
6	3	-.8324	.7316	-1.1493	.0848	-5.4025	-2.4572
10	3	-.5755	.5154	-1.0051	.0396	-2.5278	-1.1698
4	4	-.9754	1.0403	-1.5814	.5754	-7.4157	-3.8772
6	4	-1.3384	.5922	-1.7217	.2047	-6.1414	-2.6490
10	4	-1.1723	.4087	-1.5706	.1310	-3.0597	-1.0612
15	4	-.9496	.3714	-1.4320	.1594	-1.0267	-.1956
6	6	-1.1424	.3999	-1.4593	.2290	-6.3652	-2.8913
10	6	-1.0397	.2371	-1.3294	.1242	-3.1733	-1.1056
15	6	-.8520	.2100	-1.1682	.1299	-1.2578	-.2654
20	6	-.7375	.2077	-1.0765	.1425	-.3041	.1269
10	10	-.5940	.0770	-.7108	.0478	-3.2516	-1.3135
15	10	-.4169	.0572	-.5361	.0401	-1.3554	-.4615
20	10	-.3069	.0576	-.4276	.0463	-.4553	-.0839
15	15	-.1727	-.0043	-.1689	-.0084	-1.3835	-.5627
20	15	-.0661	-.0049	-.0604	-.0022	-.4829	-.1993
25	15	0.0000	0.0000	0.0000	0.0000	0.0000	0.0000

Figure 24 shows a second test wing. This is a swept wing having no taper, a twenty-five degree angle of sweep, and partial span trailing edge flaps having chord lengths equal to thirty per cent of the total wing chord. This wing was tested for various combinations of flap and wing oscillatory motions and the results of those tests are reported by ref. 9. The real and imaginary parts of the unsteady pressure coefficient were measured along the chord lines shown as dashed lines on fig. 24. The measured pressure coefficient distributions are compared with distributions computed by the panel method in fig. 25 through 27. The surface paneling arrangement is shown in fig. 28.

The flow velocity is less than 100 feet per second; hence, the flow was taken to be incompressible. There are five different cases of flap and wing oscillation, which are as follows:

- (1) Both flaps oscillating with the same phase and amplitude (viz., 0.82 degrees)
- (2) Outer flap oscillating (amplitude: 0.66 degrees), inner flap and wing stationary.

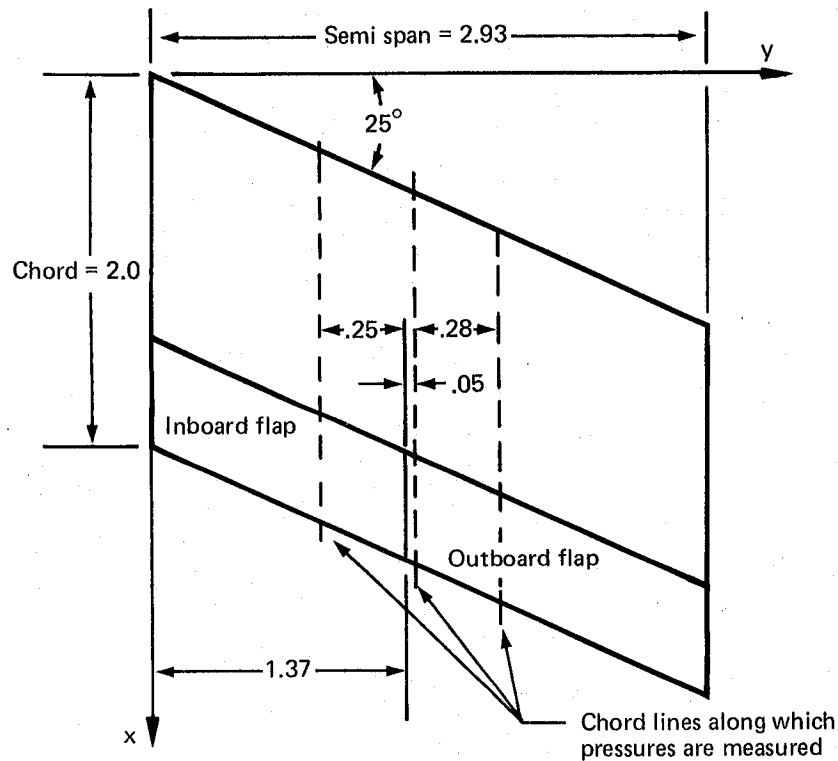
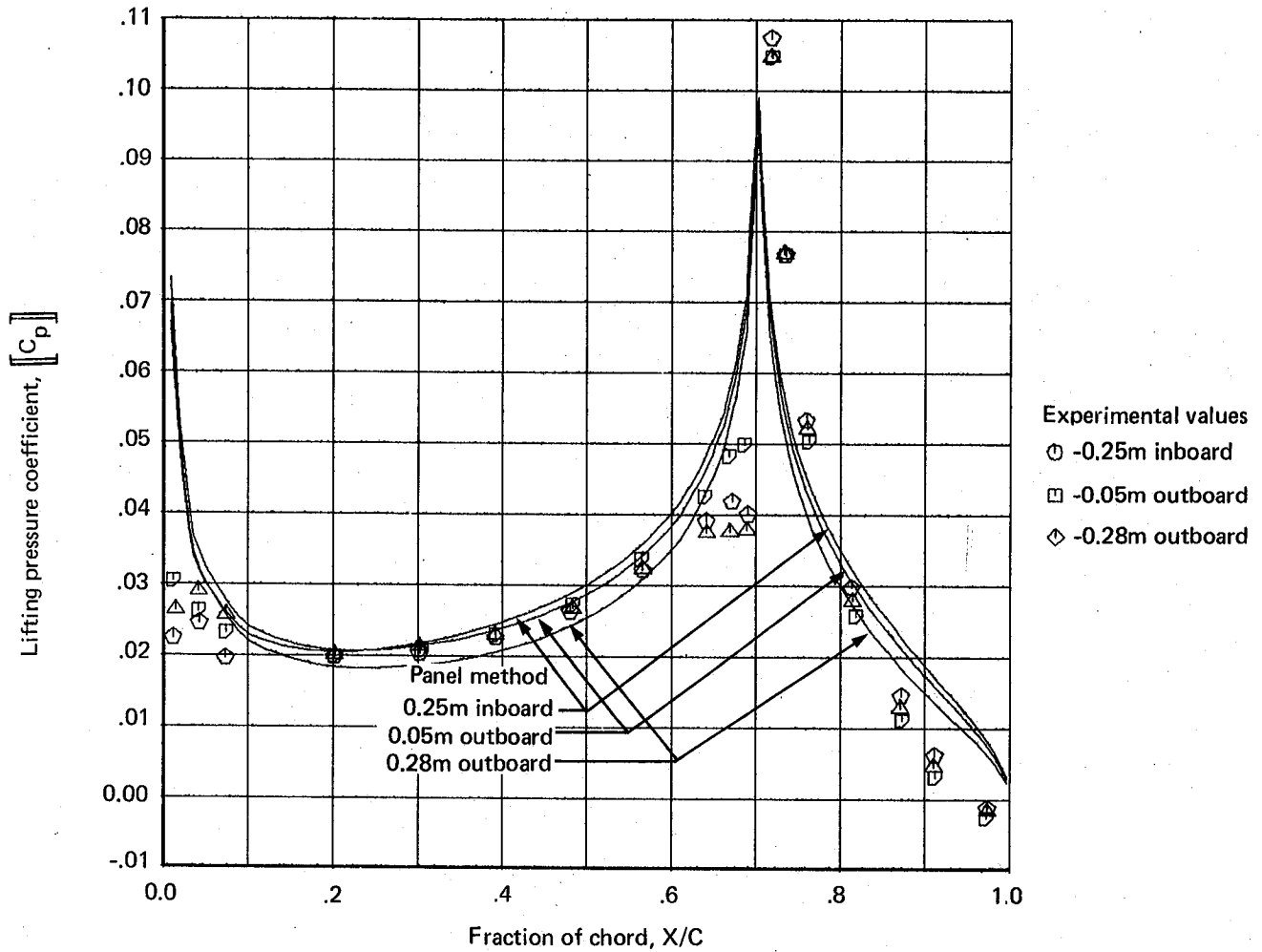


Figure 24. — Test Wing with Partial Span Flaps



a. REAL PART

Figure 25. — Chordwise Distribution of Lifting Pressure Coefficient, Case 1.

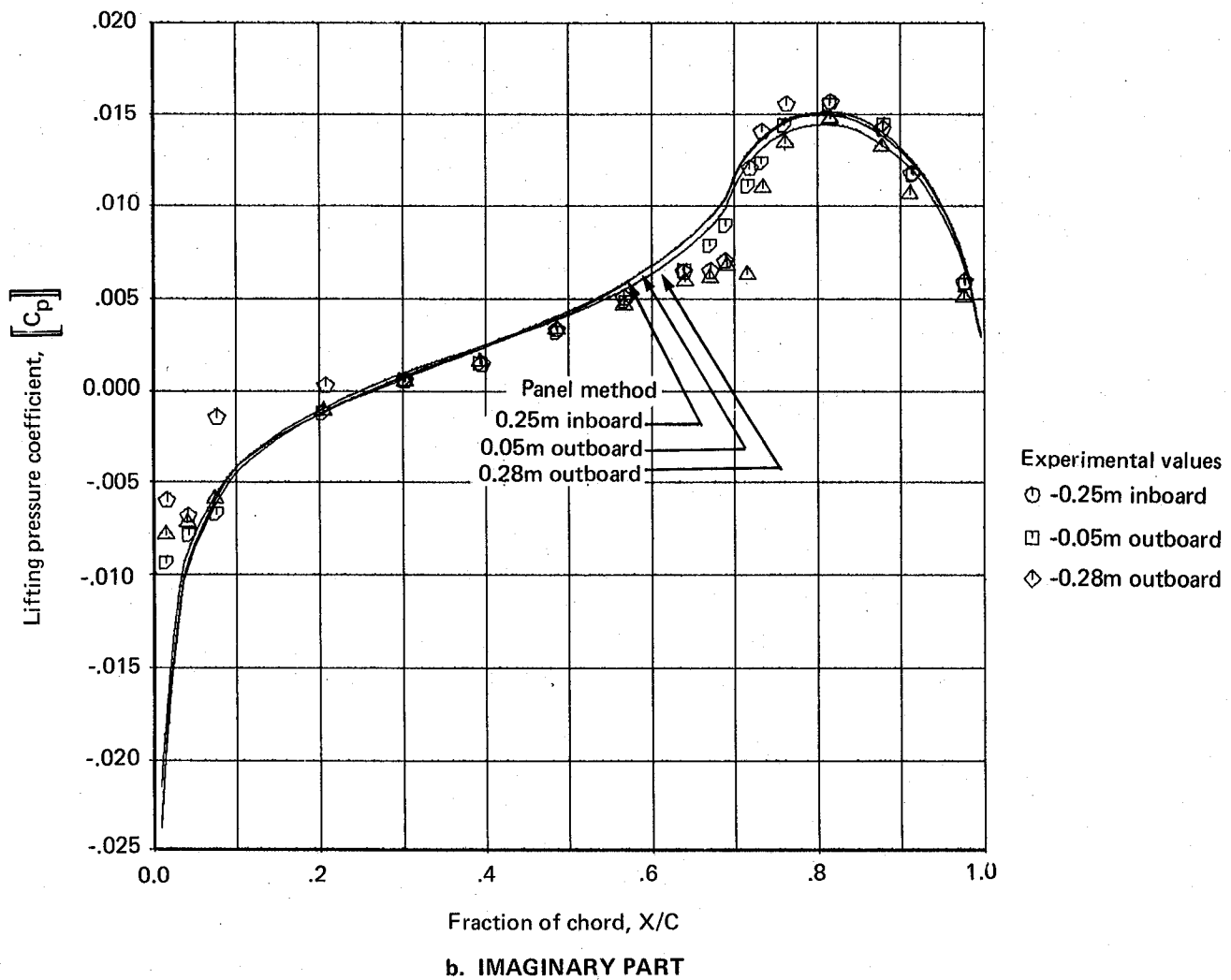
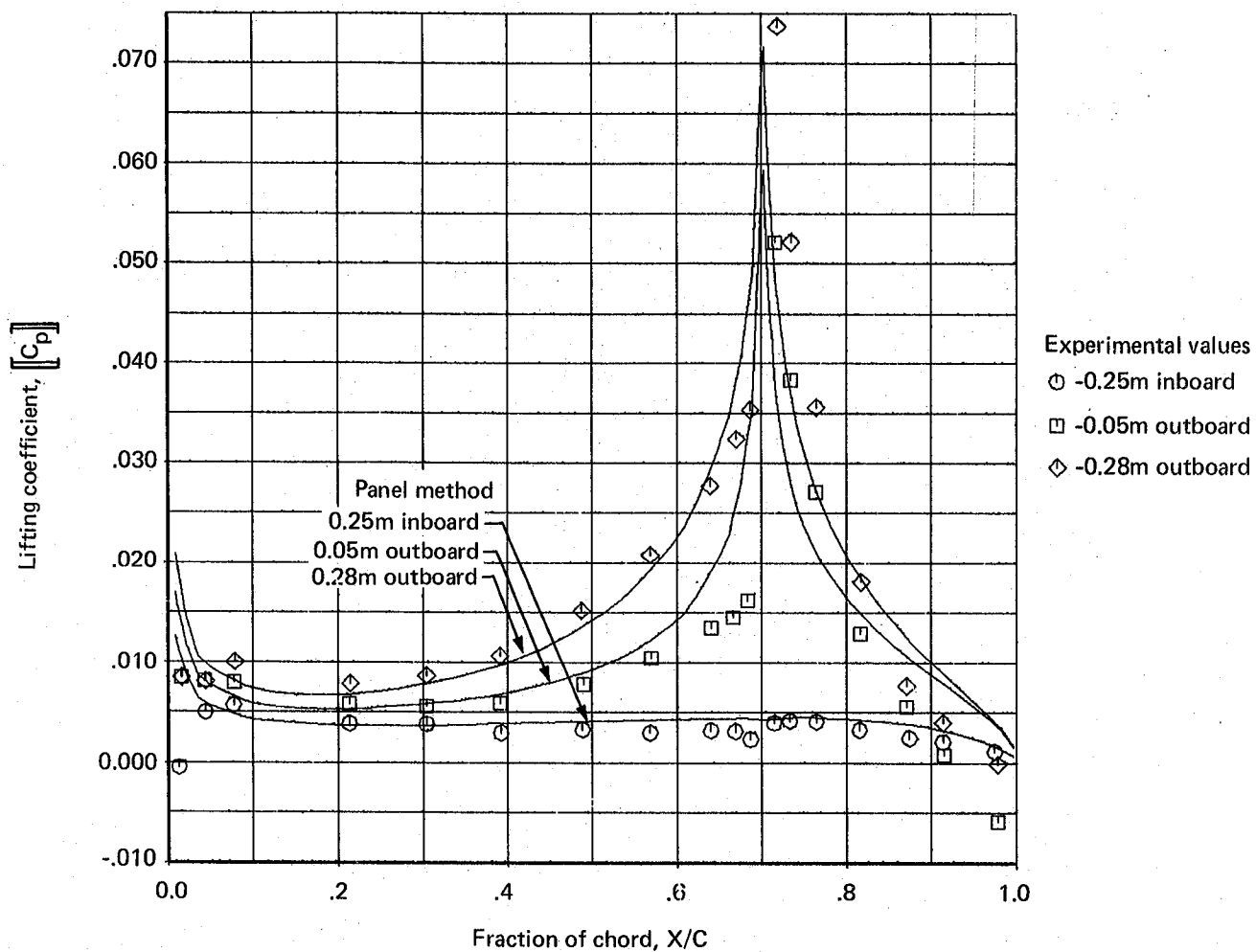
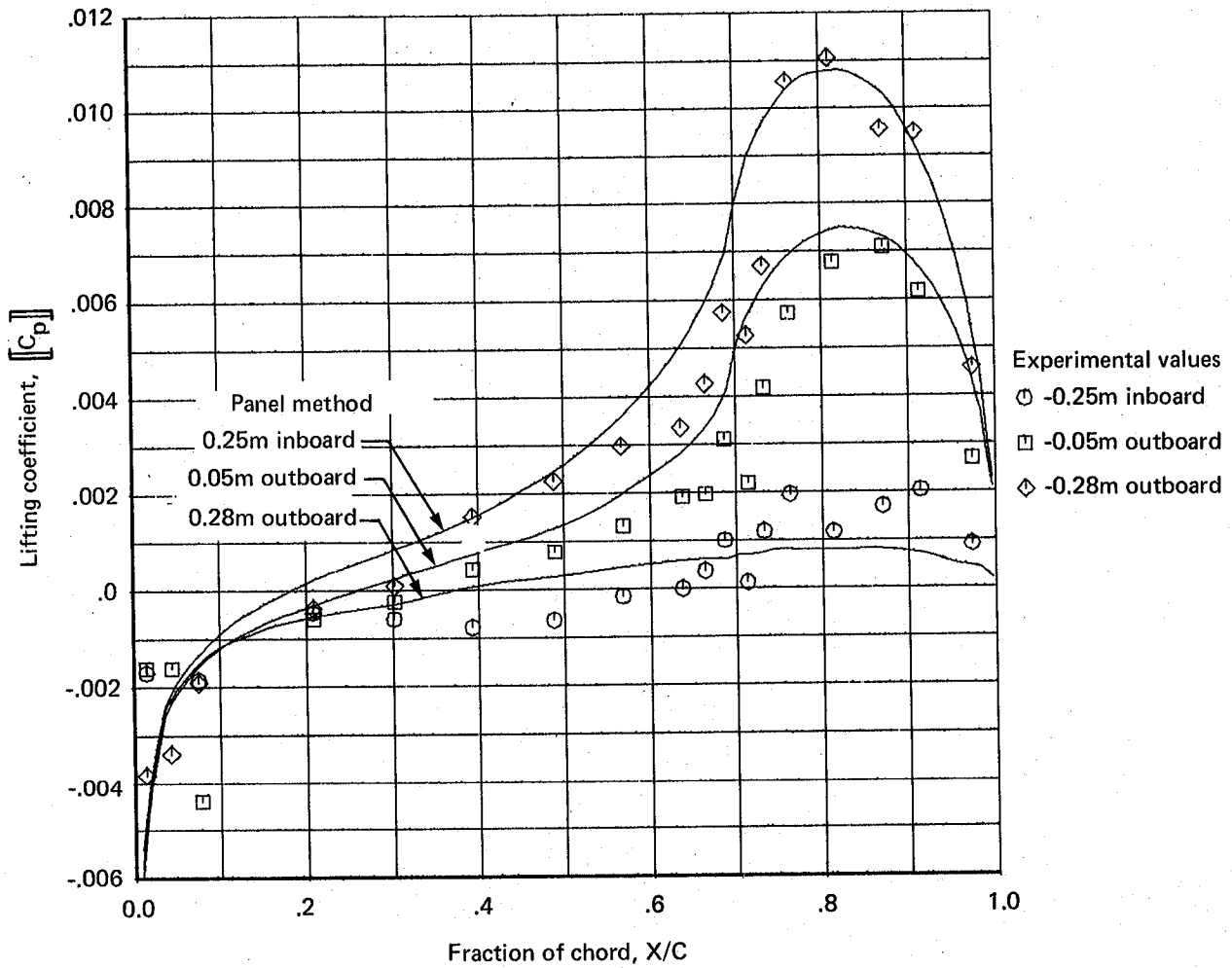


Figure 25. — Chordwise Distribution of Lifting Pressure Coefficient, Case 1.



a. REAL PART

Figure 26. — Chordwise Distribution of Lifting Pressure Coefficient, Case 2.



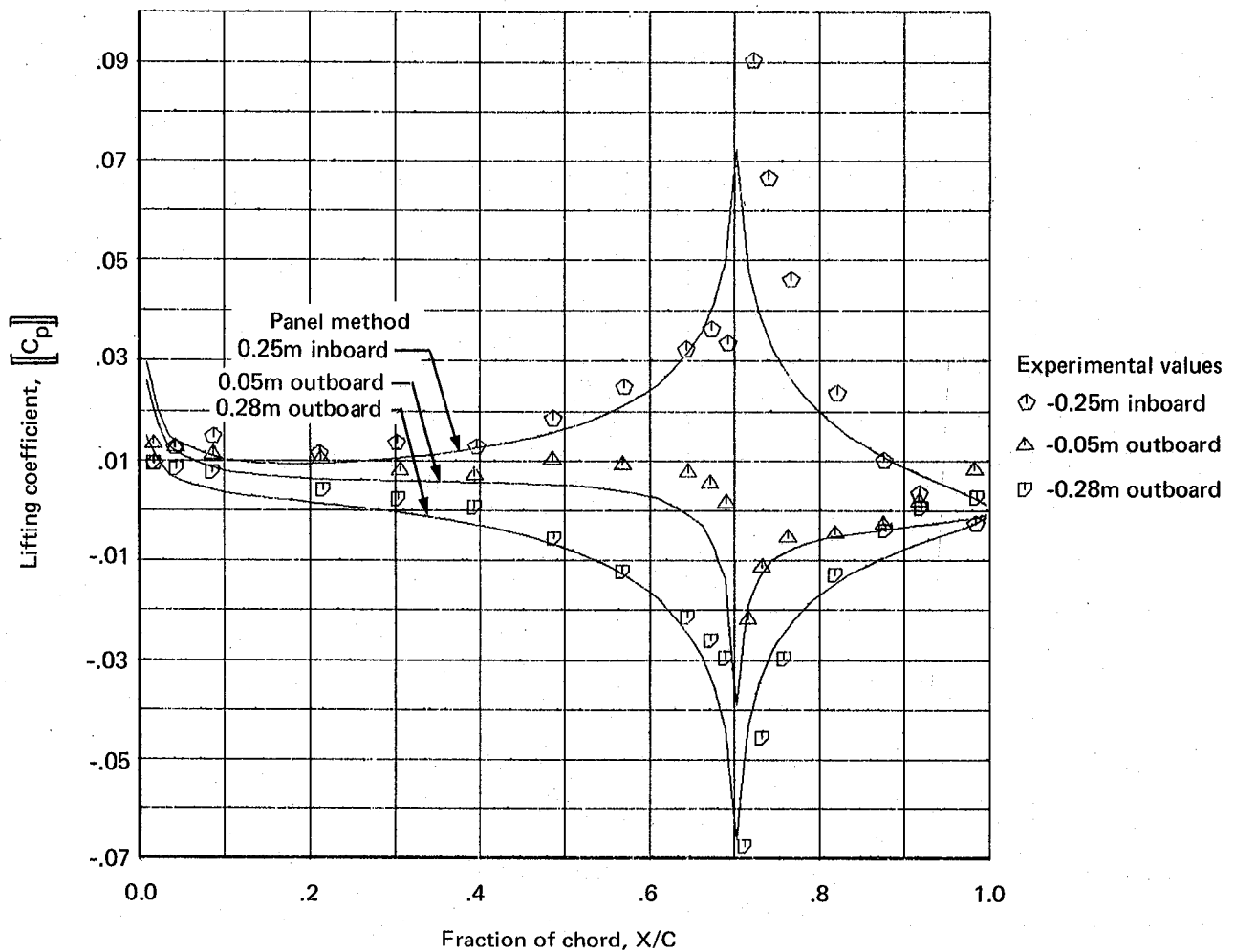
b. IMAGINARY PART

Figure 26. — Chordwise Distribution of Lifting Pressure Coefficient, Case 2.

- (3) Inner flap oscillating (amplitude: 0.67 degrees), outer flap oscillating (amplitude: 0.65 degrees) in anti-phase with inner flap, wing stationary.

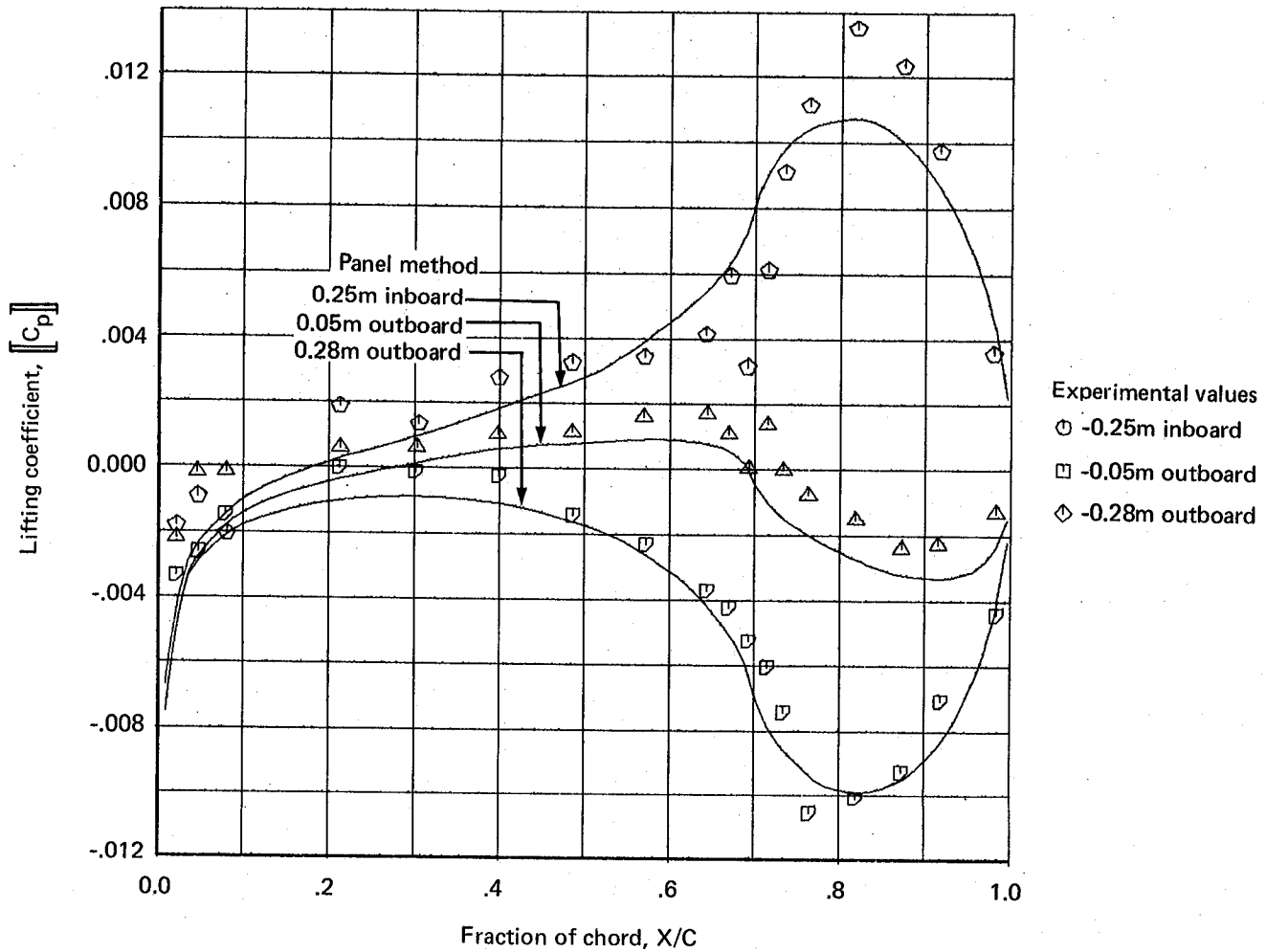
In each case the reduced frequency of the oscillatory motion is 0.372.

The comparisons shown by fig. 25 through 27 demonstrate the capability of the panel method to evaluate the lifting pressure distributions induced by oscillating trailing edge flaps. Table 2 further demonstrates that capability; it shows the variation in the amplitude of the control surface hinge moments for several panel densities. This variation is shown as the error in hinge moment amplitude relative to that computed for the most densely paneled case. This table also shows the absolute error in predicted phase angle, again, regarding the phase angle of the most densely paneled case as the point of reference.



(a.) REAL PART

Figure 27. — Chordwise Distribution of Lifting Pressure Coefficient, Case 3



(b.) IMAGINARY PART

Figure 27. — Chordwise Distribution of Lifting Pressure Coefficient, Case 3

Table 2. — Swept, Thin Wing Hinged Flap Hinge Moment Amplitude and Phase Errors

Panel density		Mode shape number	Inboard flap		Outboard flap	
Chordwise M	Spanwise N		Relative amplitude error (percent)	Absol. phase error (deg)	Relative amplitude error (percent)	Absol. phase error (deg)
3	3	1	8.3573	-1.0627	7.0874	-2.3467
4	4		6.8592	- .5331	3.6825	-1.4808
5	5		3.9411	- .3346	1.9150	-1.0299
7	7		1.6780	- .1575	.4573	- .3566
10	7		.0910	- .0180	- .6030	.1481
10	10		0.0000	0.0000	0.0000	0.0000
3	3	2	21.9326	-17.4810	6.7727	-2.7354
4	4		8.9168	-10.3497	3.6726	-1.7837
5	5		4.0357	-6.1419	1.7157	-1.1981
7	7		1.4196	-2.0295	.3400	- .4614
10	7		.3209	-1.1490	- .7575	.1303
10	10		0.0000	0.0000	0.0000	0.0000
3	3	3	10.6967	-1.6447	6.2658	-3.2233
4	4		7.9253	- .9786	3.5864	-2.1791
5	5		4.5119	- .6171	1.4140	-1.4031
7	7		1.8492	- .2542	.1613	- .5891
10	7		.2118	- .0640	- .9636	.1196
10	10		0.0000	0.0000	0.0000	0.0000

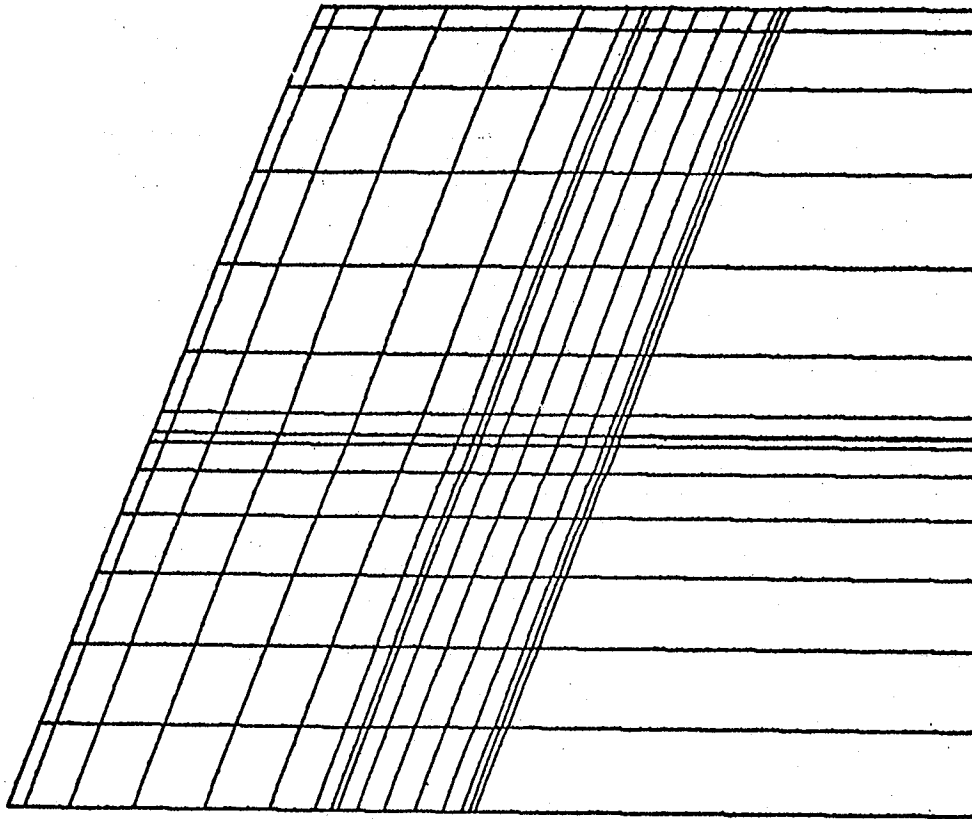


Figure 28. — Paneling of Test Wing with Split Trailing Edge Flap

#### 4.2 APPLICATION OF PANEL METHOD TO NON PLANAR, THIN LIFTING SURFACES

The panel method is validated for this type of configuration by computing the unsteady aerodynamic forces on three different T-tail configurations undergoing oscillatory motions. These are T-tails which have been evaluated by the alternative methods described by ref. 10 through 13.

The first T-tail evaluated is shown by fig. 29. This T-tail is tested oscillating in yaw about an axis along the mid chord line of the vertical surface and the test results are contained in ref. 10. The tail oscillates with a reduced frequency of 0.105 in a uniform freestream having a Mach number of 0.376. Table 3 shows the values of the amplitude and phase angle of the following generalized aerodynamic force coefficients from three sources:

- $C_{y,\psi}$ : side force coefficient due to yaw
- $C'_{\ell,\psi}$ : rolling moment coefficient of the horizontal surface abouts its center line due to yaw
- $C_{\ell,\psi}$ : rolling moment coefficient of the T-tail about the root of the vertical due to yaw
- $C_{n,\psi}$ : yawing moment coefficient due to yaw

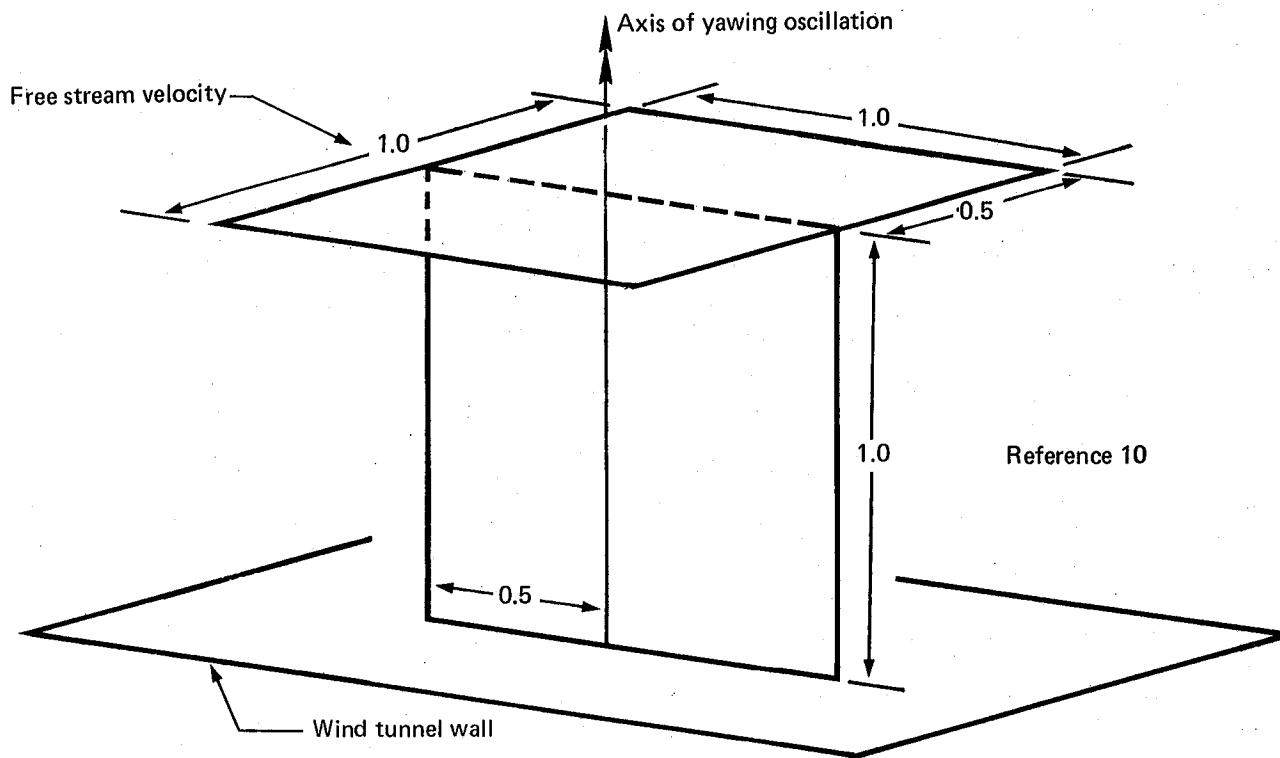
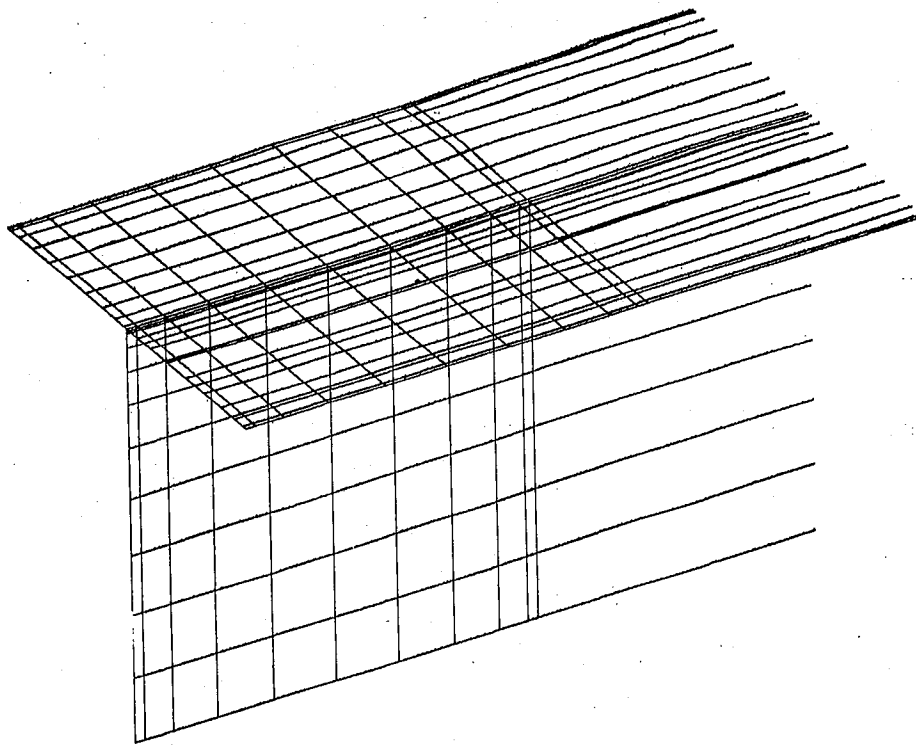


Figure 29. — Clevenson-Leadbetter T-tail

One set of values appearing in table 3 is that from the experiment of ref. 9, the second set was computed by the method of ref. 11, and the third set was computed by the panel method using the paneling shown by fig. 30.

Table 3. — Generalized Forces on Clevenson-Leadbetter T-tail Oscillating in Yaw

	$C_{Y,\psi}$		$C'_{\ell,\psi}$		$C_{\ell,\psi}$		$C_{n,\psi}$	
	Amp.	Phase	Amp.	Phase	Amp.	Phase	Amp.	Phase
Experiment, reference 11	1.306	- 1.0°	-0.264	-4.0°	-2.74	- 1.0°	.616	- 8.0°
Theory, reference 10	1.16	-12.0°	Not Available		-1.914	12.0°	.621	-11.0°
Panel method, 10x10 panels	1.224	4.0°	-0.277	2.11°	-2.57	3.95°	.632	- 5.97°



*Figure 30. — Paneling of Clevenson-Leadbetter T-Tail*

Figure 31 shows the T-tail of ref. 11. The side force, yawing moment, and rolling moment coefficients for this tail are evaluated for five different modes of motion. The five modes of motion are described in terms of mode shapes expressed in terms of the coordinate system shown on figure 31. For points on the horizontal they are as follows:

$$Z_1 = 0$$

$$Z_2 = 0$$

$$Z_3 = y$$

$$Z_4 = 0$$

$$Z_5 = 2 (1.5041)y$$

For points on the vertical they are as follows:

$$y_1 = 1$$

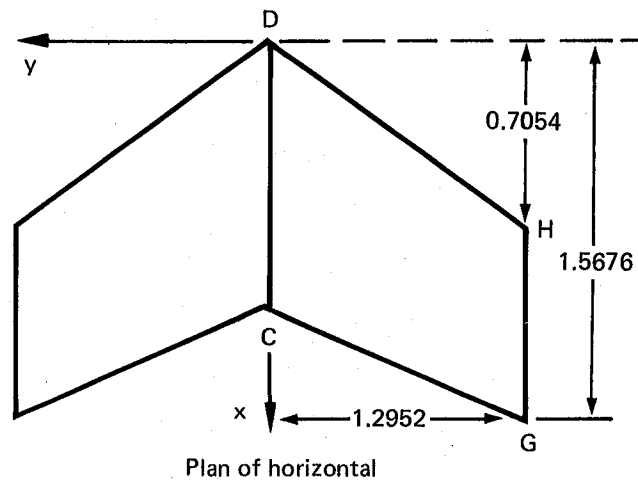
$$y_2 = x$$

$$y_3 = (1.5041 - Z)$$

$$y_4 = X(1.5041 - Z)$$

$$y_5 = (1.5041 - Z)^2$$

The oscillatory motions all have a reduced frequency of 0.5 based on the root chord length of the tailplane, and the flow Mach number is 0.8.



Reference 11

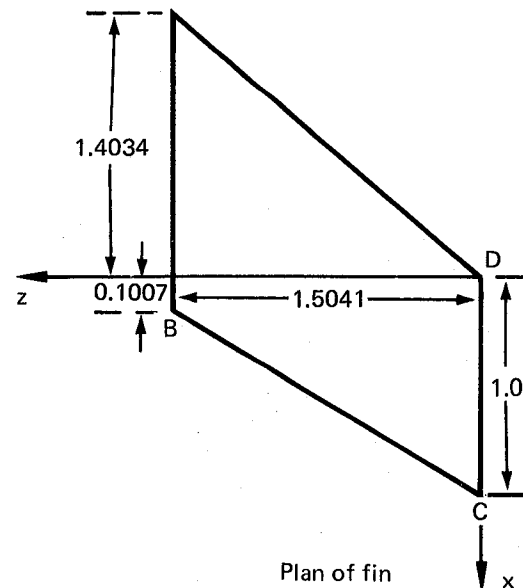


Figure 31. — Planforms of Horizontal and Vertical Fin of Davies T-tail

Table 4 lists the values of the real and imaginary parts of the three generalized aerodynamic force coefficients corresponding to the first, second, and third mode shapes, viz.,  $C_y$ ,  $C_n$ , and  $C_\ell$  with the yawing moment,  $n$ , taken about the  $z$  axis shown on fig. 31 and the rolling moment,  $\ell$ , taken about the root chord line of the fin. Complex values for these three coefficients relative to each of the above five modes of motion are shown by table 4 and the values shown are those presented by ref. 11 along with the corresponding values computed by the panel method. The panel arrangement is essentially that shown by fig. 30 with 11 panel spaces in the spanwise direction and 13 panel spaces in the chordwise direction of each of the three lifting surfaces making up the T-tail. Table 5 shows the effect of varying the panel density on the predicted aerodynamics of this T-tail. Table 5 shows the relative error in the amplitudes and the absolute error in the phase angles for four different panel densities, treating the most densely paneled case as the basis. The results of ref. 11 are included also, again, using the most densely paneled as a base for comparison.

Table 4. — Comparison of Davies T-tail Generalized Force Coefficients

Coefficients		Mode 1		Mode 2		Mode 3		Mode 4		Mode 5	
		Real	Imag	Real	Imag	Real	Imag	Real	Imag	Real	Imag
$C_y$ Side force	Ref. 11	.2164	-1.0246	-2.0977	-.7804	.1589	-.9654	-1.700	-.6946	.1529	-1.2249
	P.M.*	.2236	-1.0490	-2.2056	-.8461	.1431	-.9327	-1.8105	-.7158	.1058	-1.0671
$C_n$ Yawing moment	Ref. 11	-.0129	.3185	.6847	-.1498	.0261	.1489	.3520	-.1612	.0529	.0703
	P.M.*	-.0327	.3049	.6776	-.2869	.0673	.1274	.3361	-.2926	.0937	.0317
$C_\ell$ Rolling moment	Ref. 11	.0859	-1.0942	-2.2202	-.6104	.1759	-1.6627	-2.0574	-.7025	.3505	-3.0422
	P.M.*	.0872	-1.0582	-2.2048	-.6527	.0761	-1.3939	-2.0616	-.6969	.0641	-2.2815

\* P.M. — Panel method computed result

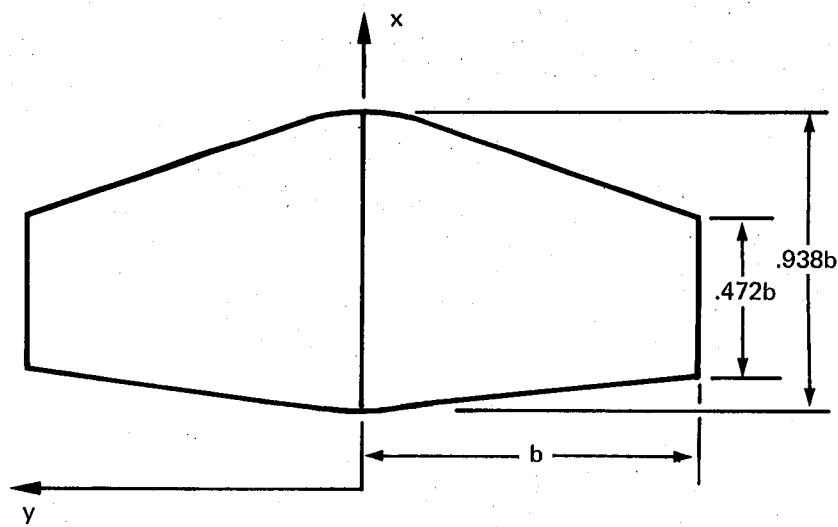
Figure 32 shows the T-tail which is evaluated by ref. 12 for oscillatory sideslip, yaw, and roll. Let  $L_{\mu\nu}^*$  denote the following generalized complex aerodynamic force coefficients:

$$L_{\mu\nu}^* = \frac{1}{4\pi\bar{q}b} \iint H_\mu H_\nu^* ds$$

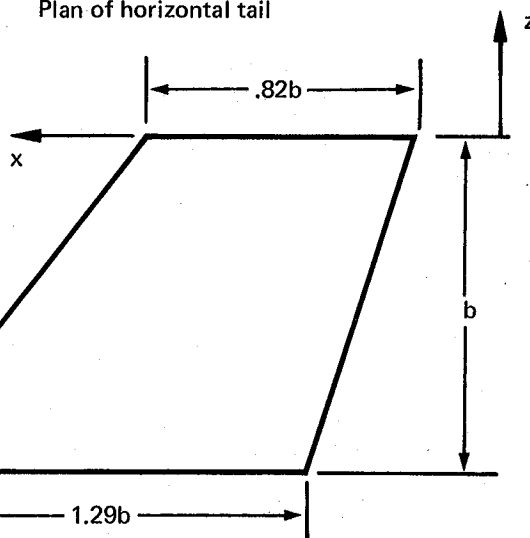
where  $H_\mu$  for  $\mu = 1, 2, 3$  describes the T-tail surface displacement for unit yaw, sideslip, and roll while  $H_\nu^*$ , for  $\nu = 1, 2, 3$  describes the complex amplitude of the surface distribution of lifting pressure induced by unit yaw, sideslip, and roll. Table 6 compares the values of these generalized force coefficients computed by the method of ref. 12 with the values computed

Table 5. — Davies T-tail Generalized Force Coefficient Amplitude and Phase Errors

Panel density		Mode shape	Side force coefficient		Roll moment coefficient		Yaw moment coefficient	
Chordwise	Spanwise	Number	Relative amplitude error (percent)	Absol. phase error (deg)	Relative amplitude error (percent)	Absol. phase error (deg)	Relative amplitude error (percent)	Absol. phase error (deg)
M	N							
4	4	1	.7113	1.7037	6.7321	2.0443	-13.7859	2.6247
		2	2.1025	1.2369	8.1898	1.6755	-8.2479	-3.0742
		3	6.0527	-.4840	19.5132	1.6025	-17.9444	-17.0173
		4	3.3682	.6625	9.1164	1.2442	-3.6290	-7.8951
		5	13.6220	-2.9102	29.5909	1.7166	25.8300	-37.0972
10	4	1	-2.3728	-.0500	2.3127	.0467	-4.2382	.9793
		2	-2.2320	-.2738	2.5290	-.3496	-3.4322	-.9620
		3	2.9433	-1.8463	17.0718	-.2244	-11.4497	-5.3214
		4	-2.5776	-.5884	1.1952	-.5656	-1.6913	-.7936
		5	11.5950	-4.0580	29.6109	-.0907	-.2585	-31.5162
10	9	1	.3192	-.0389	1.7467	-.0757	-1.8769	.3091
		2	.3685	-.0522	1.9557	-.1367	-1.3871	-.4019
		3	1.3557	-.2629	4.4635	.0119	-3.1876	-1.6598
		4	.7066	-.0961	1.9844	-.1043	-.8659	-.9761
		5	2.6007	-.8238	6.5778	.1386	-.6875	-6.1689
13	11	1	0.0000	0.0000	0.0000	0.0000	0.0000	0.0000
		2	0.0000	0.0000	0.0000	0.0000	0.0000	0.0000
		3	0.0000	0.0000	0.0000	0.0000	0.0000	0.0000
		4	0.0000	0.0000	0.0000	0.0000	0.0000	0.0000
		5	0.0000	0.0000	0.0000	0.0000	0.0000	0.0000
		(Reference 11)						
		1	-2.3647	-.1070	3.3698	-.2220	3.9500	-3.8021
		2	-5.2558	-.5810	.1391	-1.1181	-4.7483	10.6073
		3	3.6854	.6242	19.7713	2.9140	4.9185	17.9035
		4	-5.6725	.6525	-.1000	.1753	-13.1200	16.4364
		5	15.1142	1.4530	34.1712	4.9629	-11.0567	34.3475



Plan of horizontal tail



Plan of vertical tail

Reference 12

Figure 32. — Planforms of Horizontal Tail and Vertical Fin of Stark T-tail

using the panel method. The panel method values are based on a computation using the panel arrangement shown by fig. 33. The comparisons are shown in table 6 for two different values of reduced frequency of motion, viz., 0.2 and 0.3. These reduced frequency values are based on the definition of ref. 12 using one third of the semi-span of the horizontal tail as the characteristic length. Also included in table 6 are comparison values computed using the doublet lattice method; those values are taken from ref. 13.

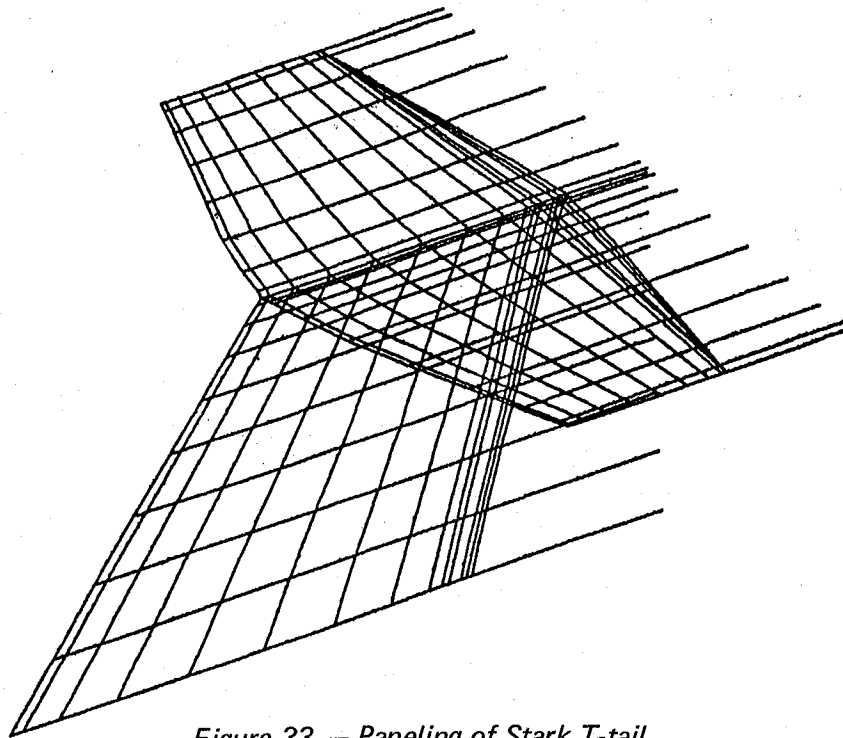


Figure 33. — Paneling of Stark T-tail

Table 6. — Comparison of Stark T-tail Generalized Force Coefficients

Coefficients		Yawing		Sideslipping		Rolling	
		Real	Imag	Real	Imag	Real	Imag
K = 0.2							
Yawing moment	Ref. 12	-.0961	-.4811	.0412	-.0300	.0125	.0239
	P.M.	-.0528	-.4773	.0456	-.0228	.0126	.0237
	Ref. 13	-.0837	-.5270	.0470	-.0278	.0137	.0257
Side force	Ref. 12	-.6108	-.3625	.0241	-.1211	.0158	-.0295
	P.M.	-.5422	-.3721	.0305	-.1098	.0166	-.0270
	Ref. 13	-.6270	-.3965	.0297	-.1260	.0171	-.0318
Rolling moment	Ref. 12	-.1247	-.1151	.0134	-.0255	.0179	-.0497
	P.M.	-.1176	-.1210	.0149	-.0249	.0177	-.0478
	Ref. 13	-.1270	-.1266	.0154	-.0269	.0186	-.0529
K = 0.3							
Yawing moment	Ref. 12	-.0690	-.7736	.0973	-.0549	.0315	.0403
	P.M.	-.0489	-.7260	.1056	-.0282	.0291	.0396
Side force	Ref. 12	-.6471	-.5592	.0562	-.1895	.0379	-.0449
	P.M.	-.5015	-.5691	.0749	-.1587	.0382	-.0386
Rolling moment	Ref. 12	-.1344	-.1729	.0299	-.0415	.0411	-.0770
	P.M.	-.1168	-.1820	.0328	-.0390	-.0401	-.0715

### 4.3 GRADIENT OF STEADY MEAN MASS FLUX VECTOR

Before proceeding to a discussion of results from thick wing or wing-body flow problems, a discussion of one of the influences of the underlying steady mean component of flow is required. An additional approximation is introduced by deleting one of the boundary condition terms which is not computed with sufficient accuracy by the panel method of ref. 1.

The aerodynamic surface and wake surface boundary conditions shown by eq. (31) contain the following term involving the gradient of the mass flux vector:

$$(\vec{D} \cdot \vec{\nabla} \vec{W}_s) \cdot \hat{n}_s = \left[ \vec{D} \cdot \vec{\nabla} \left( \vec{\nabla} \phi_s - \hat{i} M_o^2 (\phi_s)_x \right) \right] \cdot \hat{n}_s.$$

The value of this term depends on the second order derivatives of steady mean velocity potential, and its accurate evaluation places stringent requirements on the accuracy of the steady mean flow solution. As noted in the preceding, the steady mean component of flow is computed by the panel method of ref. 1. If that method is not sufficiently accurate, then this term cannot be included in the unsteady panel method formulation.

The accuracy of the steady panel method was tested by computing second order derivatives of the velocity potential at the surface of a sphere in an uniform, incompressible flow. These computed values were then compared with values computed from the exact solution to this flow problem, i.e.,

$$\phi = \frac{a^3 x}{2r^3}$$

where  $a$  is the radius of the sphere and  $r$  is the distance from the center of the sphere to the point where the potential is evaluated, viz.,

$$r = (x^2 + y^2 + z^2)^{1/2}.$$

The spherical surface was approximated by 968 panels. Twenty-two panels were uniformly spaced in rows along meridian lines running from the forward stagnation point to the aft stagnation point and there were forty-four such panel rows around the circumference of the sphere. The problem was solved using Morino type boundary condition, cf. sec. 3.4; hence, the potential and its first and second order derivatives with respect to the local panel coordinates were readily evaluated at each panel center from the solution doublet distribution.

The exact solution to the flow problem was differentiated with respect to the compressibility coordinates, and the components of the derivatives were transformed to the local panel coordinates. The derivatives of the potential, with respect to the local panel surface coordinates, should then compare with those computed by the panel method. For a typical meridian line row of panels the results are as shown in table 7.

Table 7. — Computed Vs. Exact Values of Velocity Potential and Its Derivatives at Surface of A Sphere

$\theta(\text{deg.})^*$	$\phi$	$\phi_{\xi}$	$\phi_{\eta}$	$\phi_{\xi\xi}$	$\phi_{\xi\eta}$	$\phi_{\eta\eta}$
4.09	.49835**	.02183	-.00004	-.84453	-.03974	.06799
	.50130***	.03542	.00007	-1.51171	.00001	-1.51163
12.27	.48831	.10618	-.00271	-.47719	.01194	-.87561
	.49126	.10565	.00018	-1.48240	.00004	-1.48164
20.45	.46835	.17415	-.00406	-.46848	.01045	-.81333
	.47134	.17400	.00026	-1.42409	.00010	-1.42214
28.67	.43886	.23910	-.00530	-.43757	.00909	-.76325
	.44191	.23920	.00031	-1.33751	.00017	-1.33408
36.82	.40041	.29923	-.00601	-.38881	.00749	-.69249
	.40350	.29997	.00033	-1.22384	.00024	-1.21893
45.00	.35381	.35313	-.00632	-.33226	.00580	-.61314
	.35683	.35505	.00032	-1.08480	.00031	-1.07870
53.18	.29998	.40006	-.00606	-.26680	.00413	-.51912
	.30278	.40317	.00029	-.92269	.00038	-.91597
61.36	.23999	.43905	-.00519	-.19756	.00460	-.41078
	.24242	.44327	.00024	-.74049	.00045	-.73386
69.55	.17510	.46891	-.00415	-.13673	.00543	-.30231
	.17697	.47433	.00018	-.54180	.00049	-.53603
77.73	.10662	.48936	-.00291	-.08068	.00555	-.19175
	.10778	.49553	.00011	-.33082	.00053	-.32659
85.91	.03591	.49993	-.00129	-.02526	.00543	-.07203
	.03631	.50633	.00004	-.11223	.00055	-.11003

\* Meridian angle from forward stagnation point

\*\* Computed value

\*\*\* Exact value

Except at the first panel, which is closest to the stagnation point, the value of the potential and its gradient are computed with sufficient accuracy to be regarded as a satisfactory steady flow solution for the purpose of evaluating the surface pressure distribution. The second order derivatives, however, are considerably in error over the entire meridian line. Because of these large errors, the boundary condition term described at the beginning of this subsection was deleted in the boundary conditions of the demonstration cases.

#### 4.4 APPLICATION OF THE PANEL METHOD TO WINGS OF FINITE THICKNESS

Figure 34 shows the panel arrangement of a test case wing having finite thickness. This wing has the planform shown by fig. 18 and an airfoil section that is 4.8 percent thick at a point 40 percent of the chord aft of the leading edge. The thickness of this wing is sufficiently small that the lifting pressure induced on its surface as a result of harmonic flow incidence is accurately predicted by the thin wing theory method of ref. 8. Using the paneling shown by fig. 34 the lifting pressure has been computed, satisfying the unsteady thick wing flow theory shown by eqs. (30) through (35). The wing is oscillating in pitch about a spanwise line through its mid-root chord point with a reduced frequency of 0.3577. The lifting pressure coefficient distributions along four chord lines are shown by figs. 35 through 38. These figures provide a comparison of the real and imaginary parts of the pressure with those computed by the method of ref. 10. Since the thick wing panel method should yield results in this case which are nearly identical with results from the method of ref. 8, the close correlations shown by fig. 35 through 38 imply validation of the panel method.

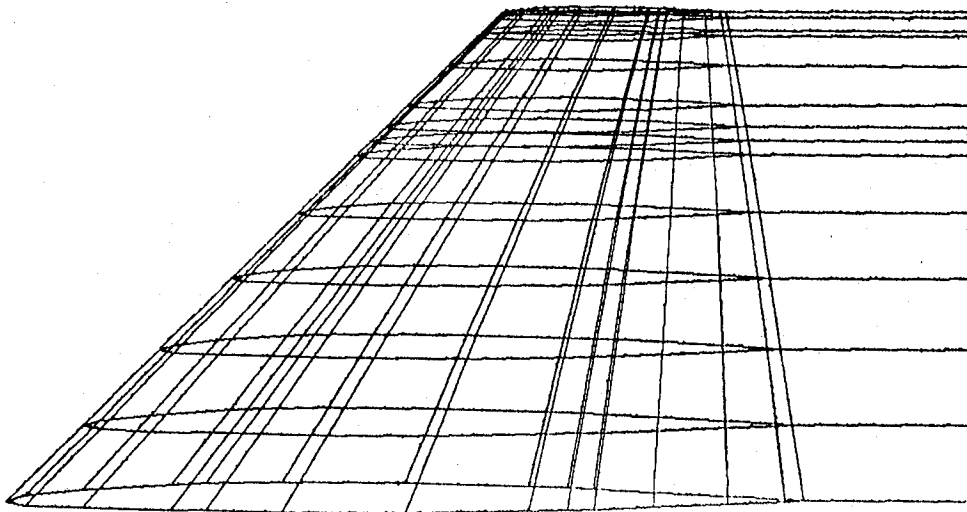


Figure 34. — Panel Arrangement for Thick Test Wing

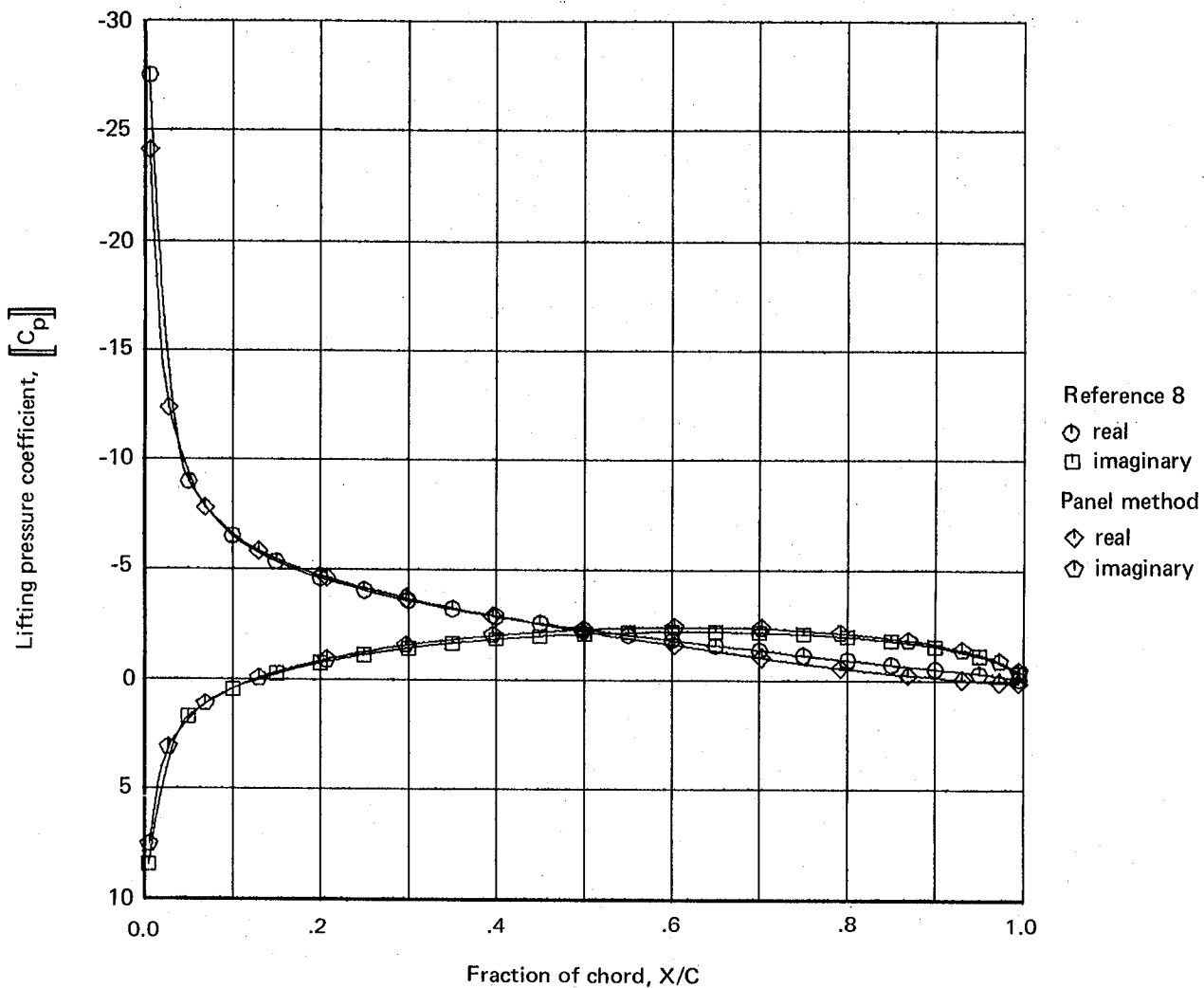


Figure 35. — Thick Wing Unsteady Lifting Pressure Comparison at 18.1% Semi-span

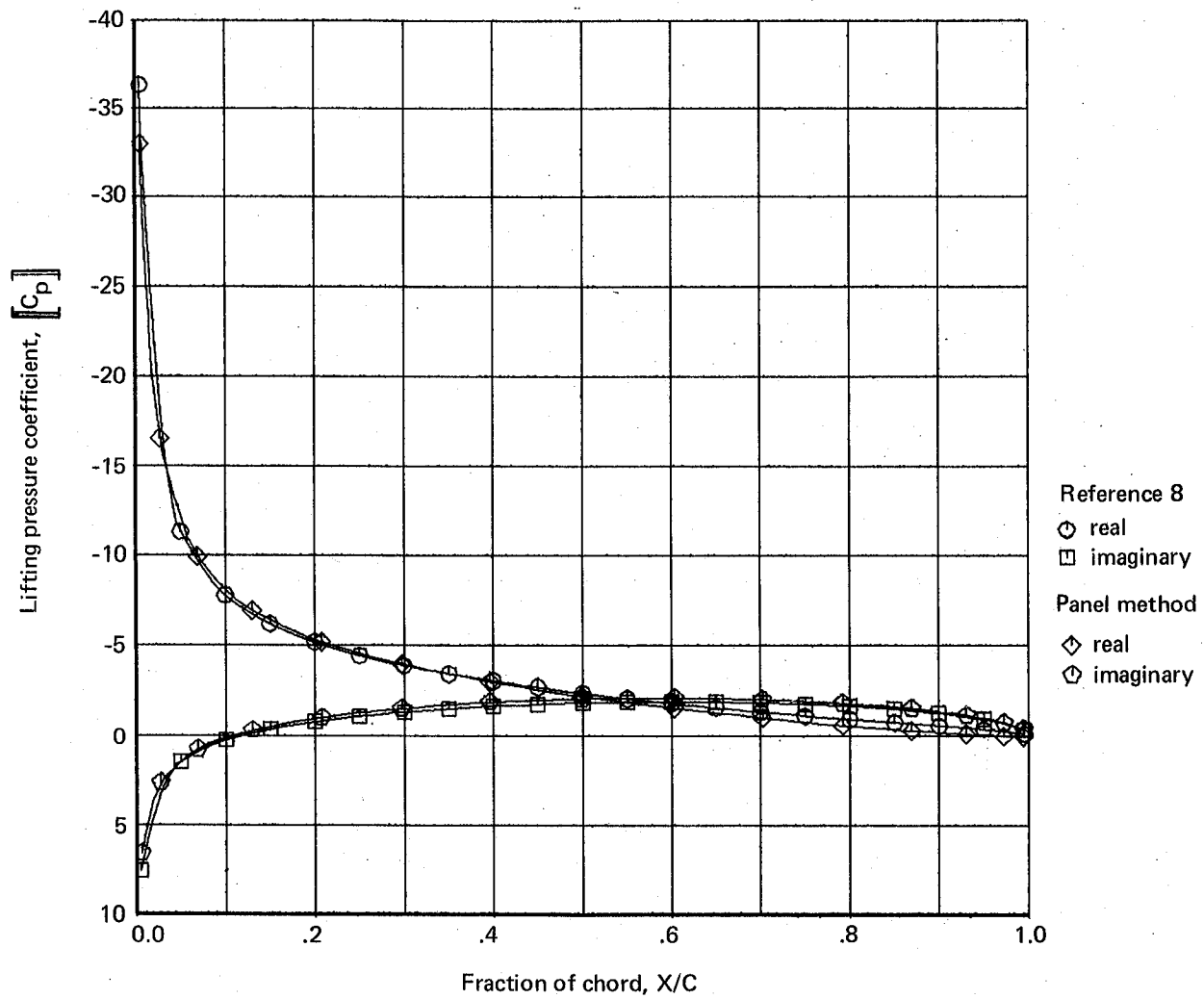


Figure 36. — Thick Wing Unsteady Lifting Pressure Comparison at 51.2% Semi-span

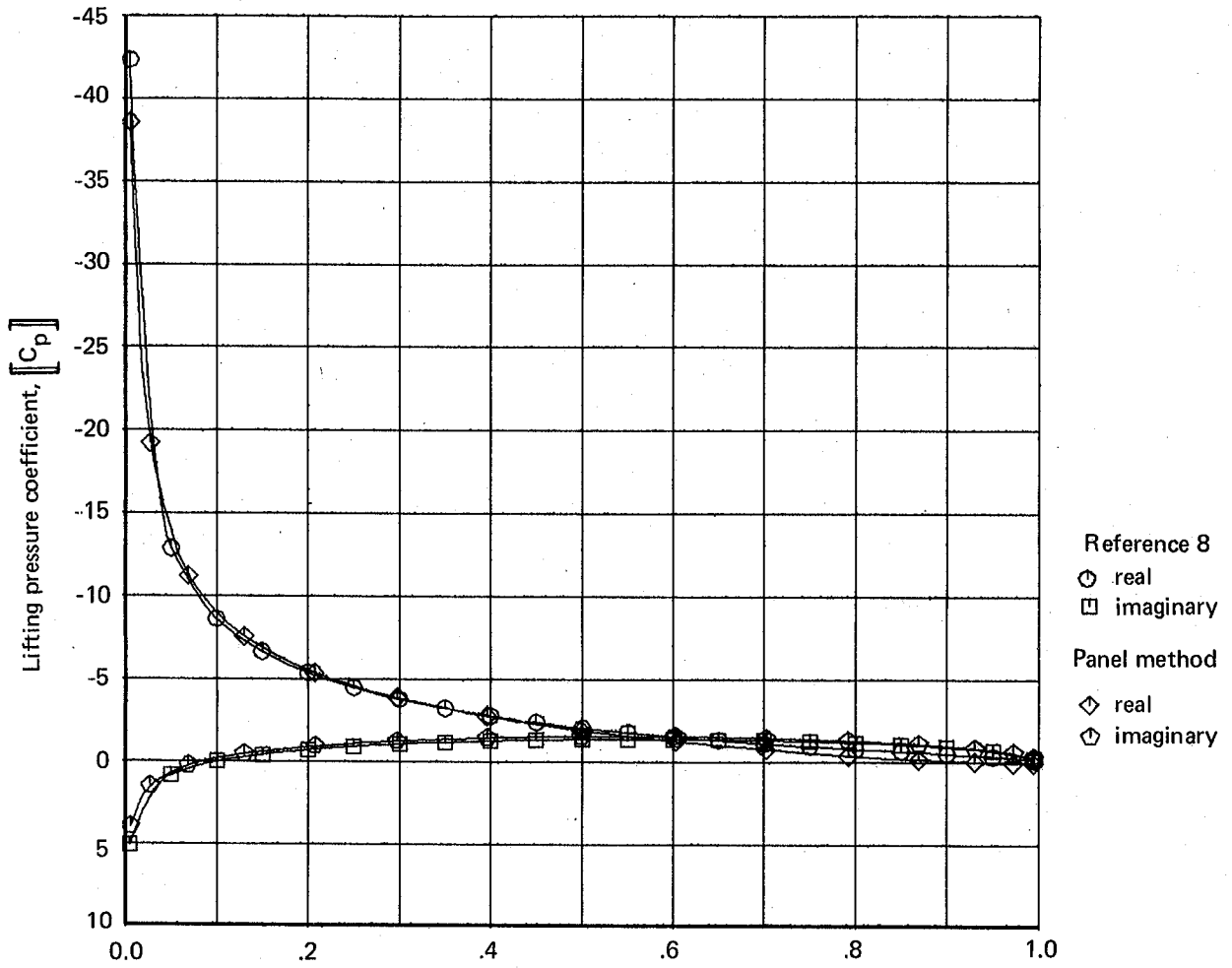


Figure 37. - Thick Wing Unsteady Lifting Pressure Comparison at 81.7% Semi-span

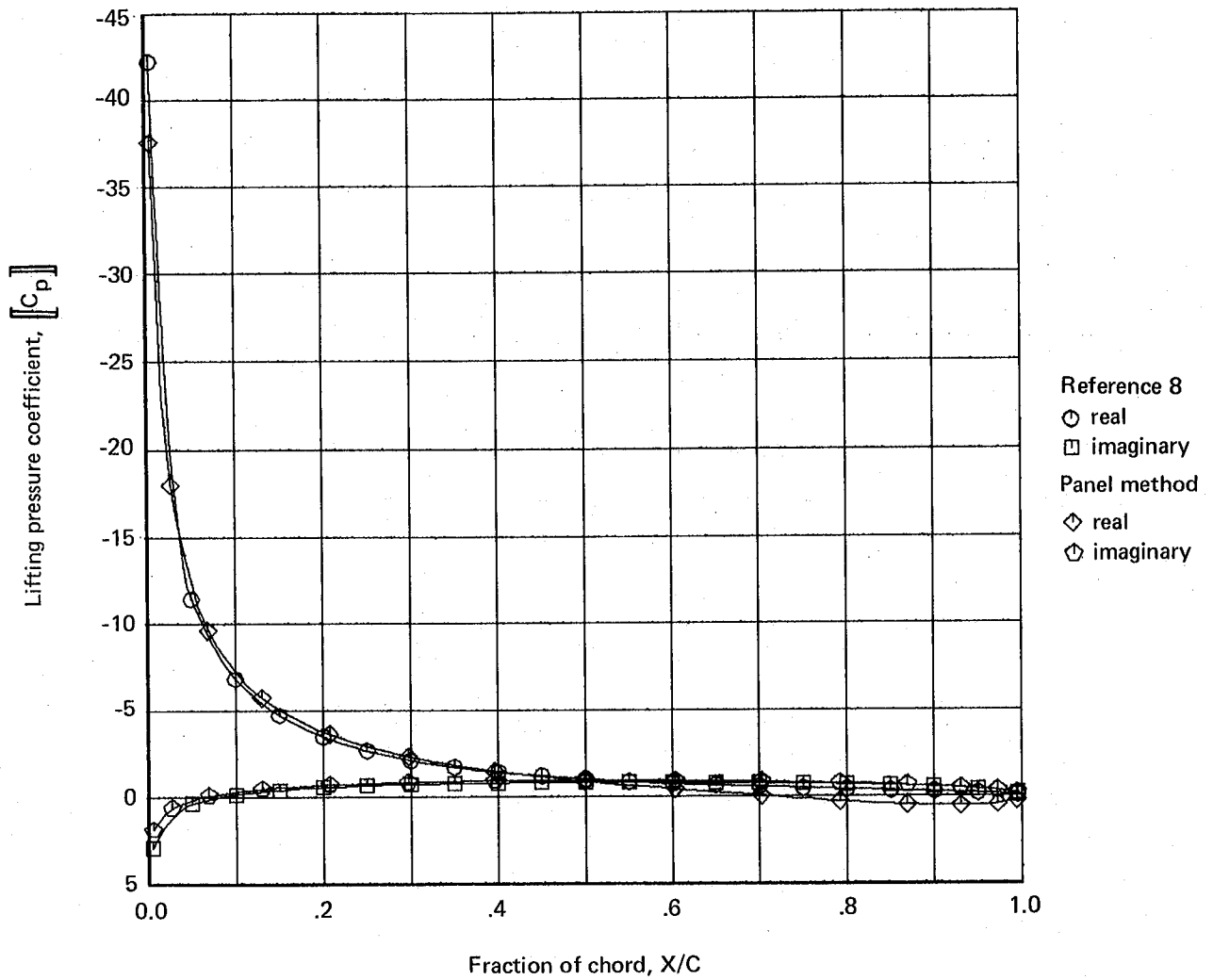


Figure 38. — Thick Wing Unsteady Lifting Pressure Comparison at 97.7% Semi-span

This wing flow problem was computed using the Morino-type boundary conditions described in one of the examples of sec. 3.5. The wing is represented by distributions of unsteady sources and doublets on the upper and lower surfaces of the wing and on a surface which closes its tip. The strengths of the sources are set equal to the unsteady flow incidence and the unsteady disturbance velocity potential is required to vanish at all points interior to the wing surface. A direct application of these boundary conditions in the panel method, however, does not lead to an accurate representation of the flow in the neighborhood of the wing trailing edge. This problem was corrected by a modification of the Morino-type boundary conditions; the nature of the problem and its remedy are described in the following.

The panel method is applied by defining three networks of panels covering the wing surface: (1) the upper surface, (2) the lower surface, and (3) the tip closure surface. As indicated above these are combination source-doublet networks; and, in the terminology of ref. 2, sec. 2.4, these three networks are typed as follows:

$$\text{NTS}(K) = 1 \text{ and } \text{NTD}(K) = 12 \text{ for } K=1,2,3.$$

These networks have control points at the panel centers and at the mid-points of the panel edges which are also network edges, cf., fig. 15. Two boundary conditions are required at each panel center control point and a single boundary condition is required at each network edge control point.

Again, using the terminology of ref. 2, sec. 2.4., the Morino-type boundary conditions are imposed by setting the boundary condition parameters as follows:

at panel center control points (ref. 2, tables 2.2 and 2.3):

$$\begin{aligned} \text{NLOPT1} &= 5 \\ \text{NROPT1} &= 5 \\ \text{NLOPT2} &= 7 \\ \text{NROPT2} &= 2 \end{aligned}$$

at network edge control points:

$$\begin{aligned} \text{NLOPT1} &= 0 \\ \text{NLOPT2} &= 7 \\ \text{NROPT2} &= 2 \end{aligned}$$

This specification of the boundary condition parameters causes the source strength to be set equal to the flow incidence at panel centers and causes the disturbance potential to vanish at limiting points approaching the control points from the interior of the wing.

The doublet strength values at control points at the edges of two adjoining networks are used, in part, to enforce continuity of the doublet strength between the adjoining networks across their abutting edges, ref. 1, sec. 6.0. In the present case of the thick wing, the doublet strength on the

wake along its upstream edge is forced to match the sum of the doublet strengths of the upper and lower wing surface networks along their line of abutment with the wake. At the edge control points of the upper and lower surface networks, however, if the Morino-type boundary conditions are imposed, causing  $\phi_\zeta^*$  to vanish at these points, the Kutta condition fails to be correctly satisfied. This failure is a failure of the boundary conditions to correctly determine the direction of the disturbed flow at the wing trailing edge. The flow should be tangent to the wake surface at this edge; but, because eq. (82) is not satisfied precisely at the wake line of abutment, the flow direction can be in a direction significantly different from that of the tangent to the wake surface. This failure is remedied by requiring the flow to be tangent to the upper surface of the wing at the edge control points.

At the edge control points along the trailing edge of the upper surface network, the boundary condition parameters (ref. 2, tables 2.2 and 2.3) are given the following values:

$$NLOPT1 = 0$$

$$NLOPT2 = 3$$

$$NROPT2 = 2$$

As a result,

$$\vec{w}_\zeta^* \cdot \hat{n} = 0$$

at edge control points of the upper surface along the wake and this condition causes the unsteady flow to have a direction tangent to this surface along its trailing edge.

#### 4.5 APPLICATION OF THE PANEL METHOD TO A WING-BODY-TAIL-NACELLE CONFIGURATION

Figure 39 shows the paneling for a typical subsonic, twin engine transport with the following characteristics:

Wing area = 297.0 square meters (2759 square feet)

aspect ratio = 8.71

taper ratio = 0.267

sweep @ C/4 = 31.5 degrees

dihedral = 6 degrees

root chord = 856.7 cm (337.3 inches)

tip chord = 228.6 cm (90.0 inches)

MAC = 603.18 cm (237.474 inches)

span = 47.24 m (1860.0 inches)

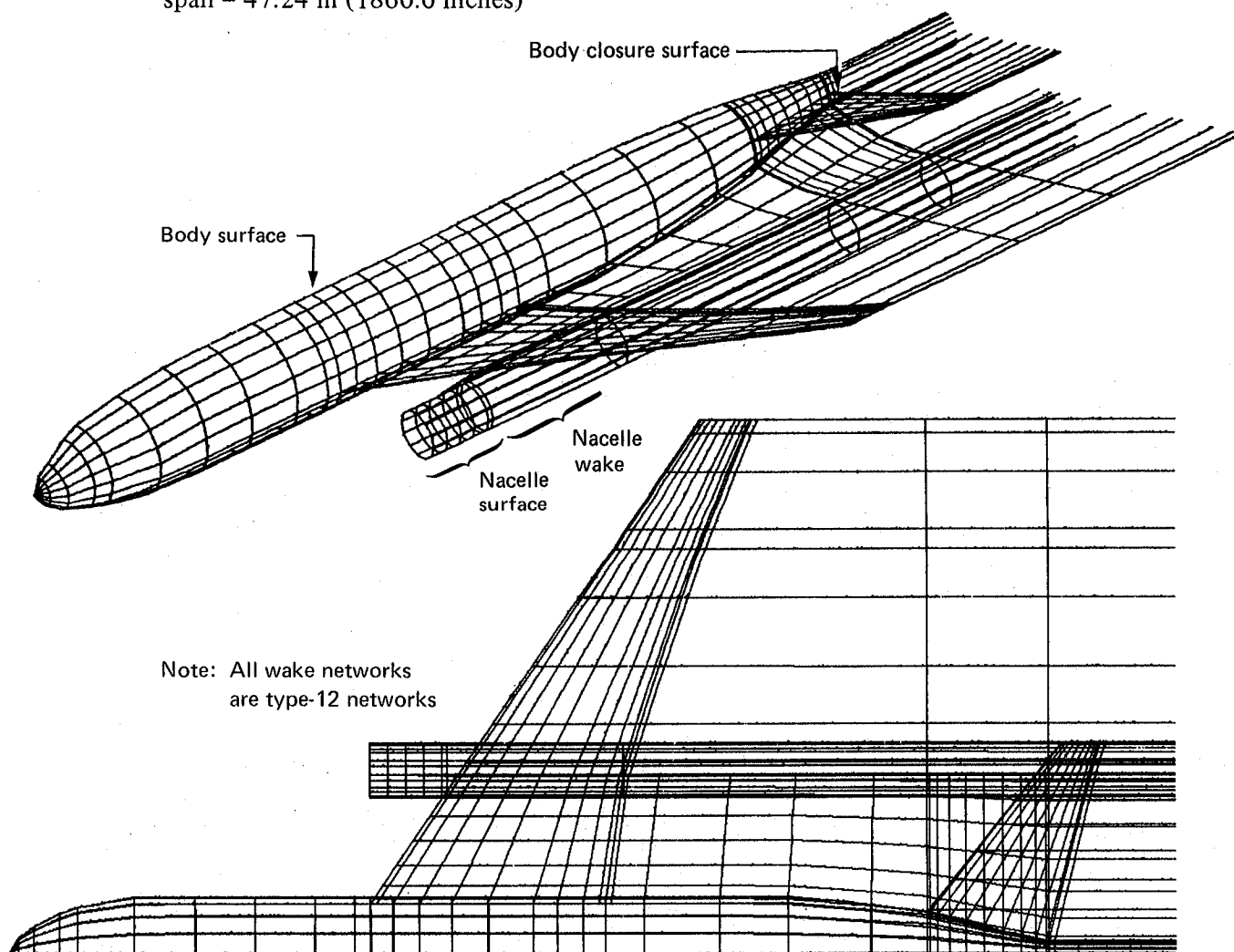


Figure 39. — Paneling of Typical Transport Configuration

Horizontal tail area = 89.3 square meters (830 square feet)

aspect ratio = 4.50

taper ratio = .250

sweep @ C/4 = 33 degrees

dihedral = 7 degrees

root chord = 662.4 cm (260.8 inches)

tip chord = 165.6 cm (65.2 inches)

MAC = 463.6 cm (182.5 inches)

span = 1863.0 cm (733.4 inches)

tail arm = 2053 cm (808.4 inches)

tail volume coefficient = 0.926

Body cross section maximum width = 502.9 cm (198.0 inches)

maximum height = 541.0 cm (213.0 inches)

The body is represented by sources and doublets distributed directly on the actual surface except on the closure section aft of the horizontal tail. A cylindrical wake surface with generator parallel with the undisturbed freestream emanates from the aft body surface simulating flow separation from the body surface at the body station where the trailing edge of the horizontal tail intersects the body. The body closure surface is simply a flat surface normal to the freestream and at the leading edge of the body separation wake. Morino-type boundary conditions, cf. sec. 3.4, are applied at the body surface; hence, the source distribution strength is set equal to the complex amplitude of the unsteady flow incidence at the body surface and the unsteady potential is set to zero at the body interior. Source and doublet panels are also placed on a surface which closes the aft body interior to the cylindrical wake separation surface. This body closure surface is a flat surface normal to the freestream direction. The unsteady disturbance potential is set to zero at either side of the body closure surface, thereby, causing the doublet strength to vanish but providing a source distribution together with control points along the edge of the body closure surface adjacent to the wake surface. These boundary conditions lead to undisturbed freestream flow interior to the cylindrical wake separation surface.

At the wing, tail, and nacelle surfaces thin lifting surface boundary conditions are applied. The effects of thickness and the effect of a mean steady component of flow are ignored. A nacelle is treated, essentially, as a ring wing, and it is on a strut having a wake.

Figure 40 shows the paneling of the transport used in a doublet-lattice computation. The body paneling shows the surface of interference for the body. The actual body was represented by unsteady line doublets to generate its slender body theory aerodynamic influence.

The transport is assumed to be oscillating in pitch about a point 848.3 inches aft of the nose of the body. The reduced frequency was chosen as 0.0174 so as to be typical of the short period frequency of an aircraft of this type. The flow Mach number was chosen as 0.87.

The complex amplitude of the lift and pitching moment coefficients induced by the pitch oscillation were computed by both the panel method and the double-lattice method. The results are summarized as follows:

panel method	doublet-lattice method
$1/2 C_L^* = (3.5033) + i(.0647)$	$1/2 C_L^* = (3.0022) + i(.1301)$
$1/2 C_M^* = -(15.4742) - i(.75279)$	$1/2 C_M^* = -(13.2033) - i(.9273)$

where the pitching moment is about a point 234.95 cm (92.5 inches) forward of the nose. The solution to this problem required approximately 1000 CPU seconds on the Ames CDC 7600 computer.

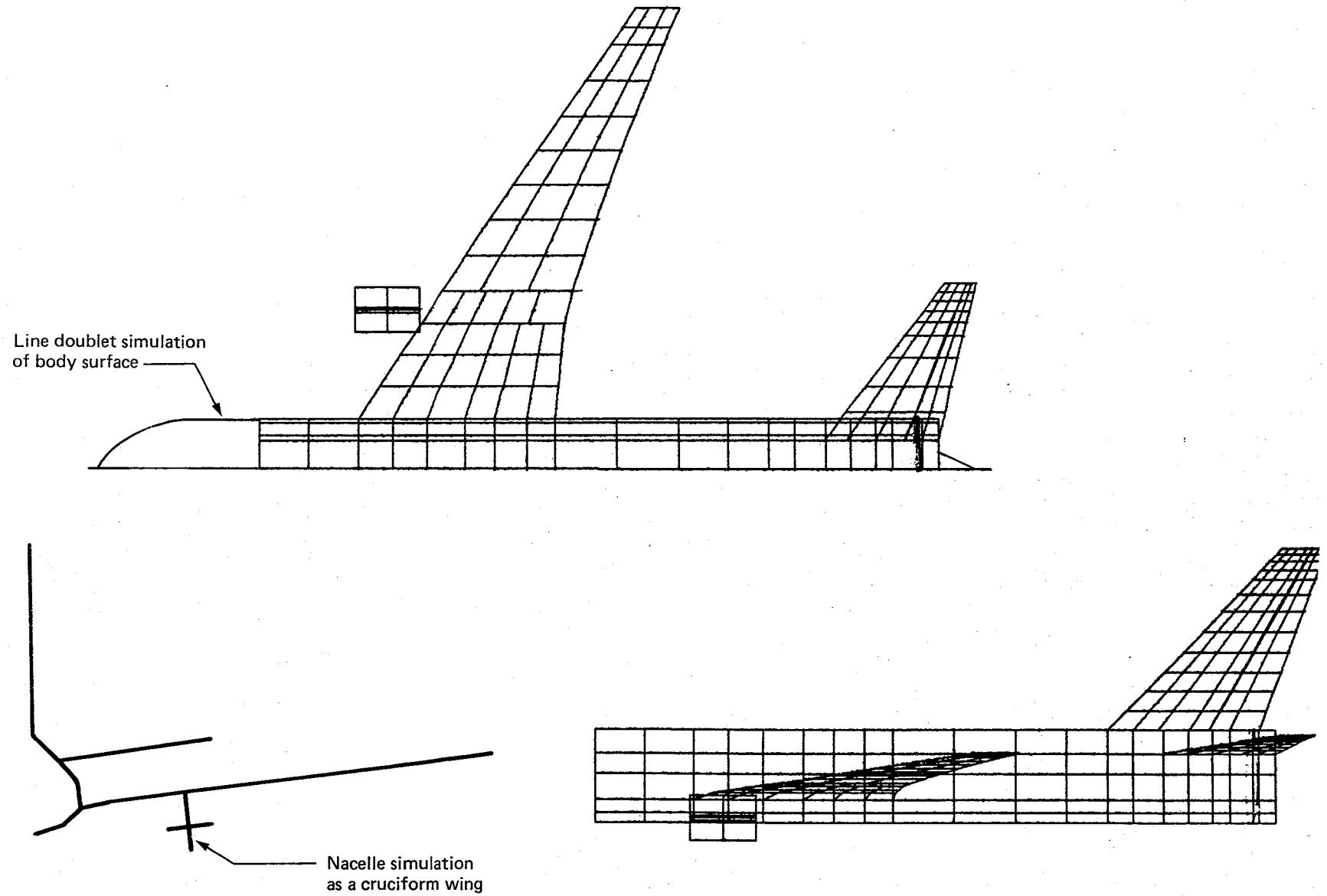


Figure 40. — Doublet-lattice Paneling of Typical Transport Configuration

## 5.0 COMPUTER CODE USER'S GUIDE

The computer program of the unsteady panel method is a modified form of the steady flow panel method computer program described by ref. 1 and 2.† Input data for executing the unsteady flow program is nearly identical with the input data required by the steady flow program; hence, this section is written as a supplement to the user's manual of the steady flow program, viz., ref. 2. The reader is expected to have ref. 2 in his possession and to be familiar with its contents.

There are three principal differences between the input requirements of the two computer programs. The differences consist of the following additional data required by the unsteady flow program:

- (1) boundary condition data describing unsteady surface motion at the control points
- (2) wake paneling grid point data providing for harmonic variation in the transverse component of wake vorticity, and
- (3) mean steady component of flow data at the control points of the unsteady flow problem.

The input data is described in detail in sec. 5.2.

Output data is also similar to the output data of the steady flow program. The primary difference is that the output data of the unsteady flow program is complex. i.e., the program generates the real and imaginary parts of the complex amplitudes of the unsteady flow parameters. The output data is described in sec. 5.3.

### 5.1 GLOBAL COORDINATE SYSTEM

All geometric input describing network grid points is expressed in the global coordinate system, see sec. 1.0, ref. 2. The global and compressibility coordinate systems are related by a user supplied angle of attack (ALPC) in degrees and angle of sideslip (BETC) in degrees. From these two angular rotations, the program computes the components of a unit vector in the direction of the x-axis of the compressibility coordinate system. This unit vector is as follows:

$$\hat{c} = \text{COMP}(1)\hat{i} + \text{COMP}(2)\hat{j} + \text{COMP}(3)\hat{k} \quad (88)$$

where  $\hat{i}, \hat{j}, \hat{k}$  are the unit base vectors of the global coordinate system.

### 5.2 INPUT DATA REQUIREMENTS

#### 5.2.1 STEADY MEAN COMPONENT OF FLOW DATA

By reference to the boundary conditions equations, i.e., eqs. (31) and (34), it is seen that at each control point the following steady mean component of flow data is required:

---

† For computer system requirements refer to sec. 1.5 of ref. 2.

steady mean density,

$$\rho_s = \rho_o \left( 1 - \frac{M_o^2}{U_o} \hat{c} \cdot \vec{\nabla} \phi_s \right) \quad (89)$$

and steady mean mass flux vector,

$$\vec{W}_s = \rho_o \left( U_o \hat{c} + \vec{\nabla} \phi_s - \hat{c} M_o^2 \hat{c} \cdot \vec{\nabla} \phi_s \right) \quad (90)$$

In addition, the gradient of the mass flux vector is required to evaluate the second term of the boundary condition shown by eq. (31). That term is evaluated from second order derivatives of the steady velocity potential, with respect to the local panel coordinates, see app. E.

The user may elect to ignore the influence of the mean steady component of flow. This choice is set by the logical variable LSTDY in subroutine INPUT. If the statement LSTDY=.TRUE. appears in subroutine INPUT, the program expects mean steady flow data. If the statement LSTDY=.FALSE. appears, the steady mean density and steady mean mass flux vector are given their freestream values. The default value of LSTDY is .FALSE.

The steady mean flow data is provided by executing the steady flow program of refs. 1 and 2. The steady flow program must be executed using precisely the same geometry and paneling as that to be used in the unsteady flow program. The control point numbering and the control point locations are therefore identical with those to be used in the unsteady flow problem, and the following data is saved for each control point†:

JC, control point number;  
ICP, panel number containing JCth control point;  
PLCL(I), I=1, 2, 3, local panel coordinates of the control point;  
TSC(1), source strength;  
TSC(2), doublet strength;  
TSC(I), I=3,4,5 components of the gradient of the doublet strength in the global coordinate system;  
W(1), average potential;  
W(I), I=2,3,4 components of the perturbation mass flux vector in the global coordinate system;  
DDO(I), I=1,2 components of the gradient of doublet strength in local panel coordinate system;  
X1(I), I=1,2,3 second order derivatives of the doublet strength with respect to the local panel coordinate system.

In the unsteady flow program these quantities for each control point are contained in labeled common block STDY.

† This data must be saved in the subroutine OUTPUT, see fig. 1.12 of ref. 2, using the following statements:

For each case:

WRITE (8,8001) AMACH, ALPHA(IACASE), BETA(IACASE)

For each panel center control point:

WRITE (8,8001) JC,ICP,PLCL,TSC,W,DDO, (X1(I),I=4,6) 8001 FORMAT (4020)

The data is contained on an octal formatted file identified to the program as tape 13. The first record on the file contains the following values: AMACH, ALPHA(IACASE), BETA(IACASE). Subsequent records contain the data which is listed above and which appears in labeled common block, STDY. Tape 13 is read as a sequential file in the unsteady flow program and it is generated by the steady flow panel method program by inserting the previously mentioned WRITE statements. The steady flow program must be executed with NEXDGN=1 and bit number one must be set in the variable IFLAG (e.g., IFLAG = IFLAG. or .1).

### 5.2.2 BOUNDARY CONDITIONS

Boundary conditions are specified at each control point following the procedures of sec 2.4 of ref. 2. The general form of the boundary condition is identical with that of ref. 2, except that the flow parameters are complex as shown by eq. (79), i.e.,

$$c_u (\vec{w}_u^* \cdot \hat{n}_s) + \vec{T}_u \cdot \vec{\nabla} \phi_u^* + D_u \phi_u^* + c_\ell (\vec{w}_\ell^* \cdot \hat{n}_s) + \vec{T}_\ell \cdot \vec{\nabla} \phi_\ell^* + D_\ell \phi_\ell^* = \text{BET}^* \quad (91)$$

In certain cases the coefficient BET\* is represented by the value of the mass flux boundary condition shown by eq. (31). In these cases the coefficient BET\* is computed by Subroutine CBET by choosing option 5 of table 2.3, ref. 2. As shown by eq. (31), the normal component of mass flux is equated to

$$\text{BET}^* = \left[ -\vec{W}_s \cdot (\vec{\theta}^* \times \hat{n}_s) - (\vec{D}^* \cdot \vec{\nabla} \vec{W}_s) \cdot \hat{n}_s + \rho_s u_n^* \right] \frac{1}{\rho_0} e^{-i\vec{\omega} \hat{c} \cdot \vec{R}} M_0^2 / \beta^2 \quad (92)$$

where  $\vec{R}$  is the position vector of the control point in the global coordinate system. This equation contains the following complex amplitudes of the unsteady surface motion parameters: surface rotation,  $\vec{\theta}^*$ ; surface displacement,  $\vec{D}^*$ ; and surface rate of displacement,  $u_n^*$ . These parameters are related to time dependent quantities as follows:

$$\vec{\theta} = R(\vec{\theta}^* e^{i\omega t}), \quad \vec{D} = R(\vec{D}^* e^{i\omega t}), \quad \text{and } u_n = R(u_n^* e^{i\omega t})$$

Where  $\omega$  is the circular frequency in radians per second and  $R(\ )$  denotes the real part.

The circular frequency is input to the program in the following ratio:

$$\text{OMGBAR} = \omega / U_0 = \bar{\omega} \quad (93)$$

which is related to the reduced frequency as

$$k = \bar{\omega}c/2 \quad (94)$$

where  $c$  is a characteristic length expressed in the units of length used in defining the freestream velocity magnitude. From eqs. (93) and (94) it is clear that the input parameter is related to the reduced frequency of the unsteady motion as follows:

$$\text{OMGBAR} = 2k/c. \quad (95)$$

As an example of the computations carried out by subroutine CBET, consider the case of the configuration shown by fig. 41 undergoing pitch oscillations about its center of mass, i.e., its cg.

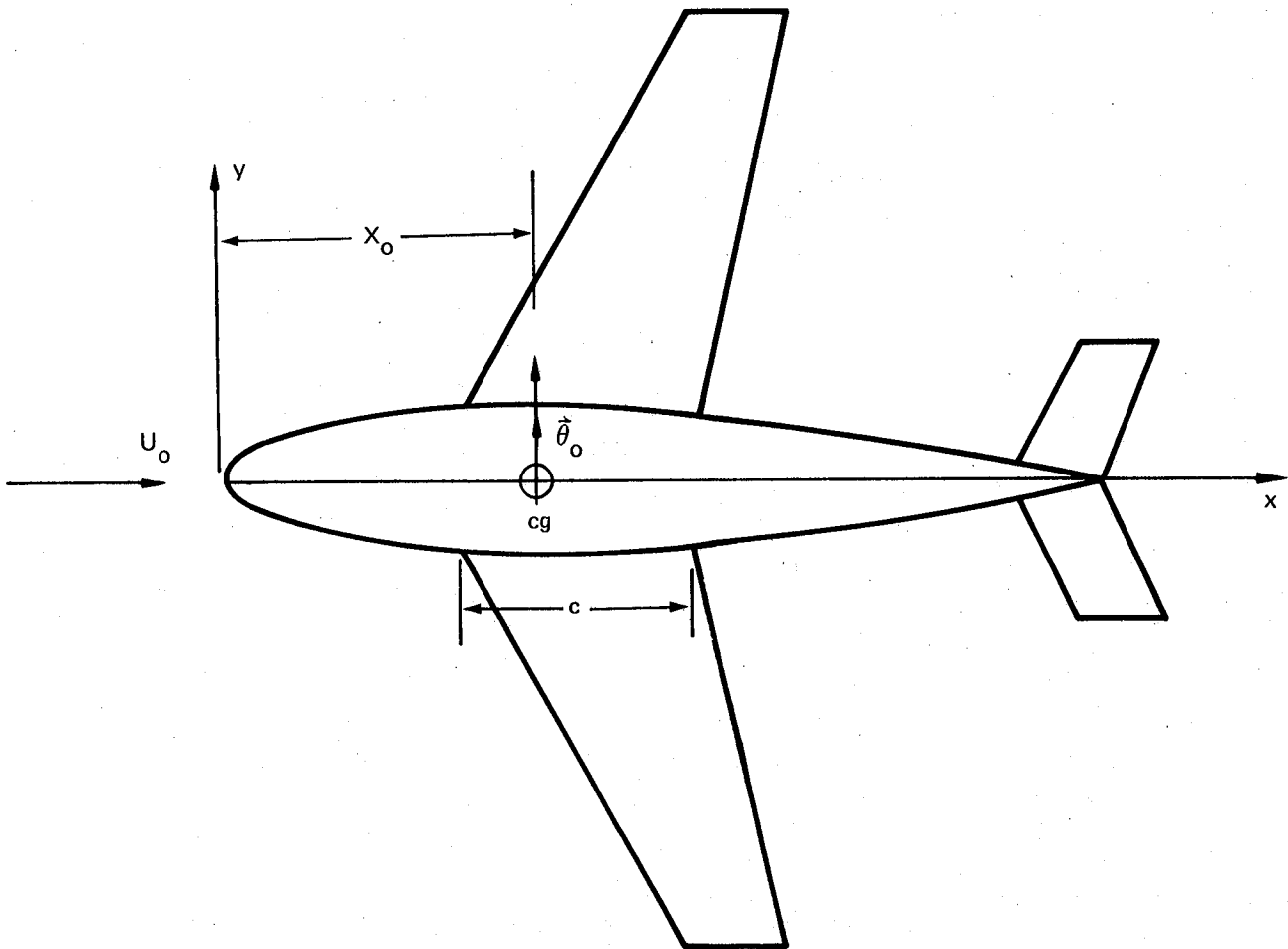


Figure 41. — Airplane Configuration Oscillating in Pitch

Assume the following values:

$$X_0 = 9.14 \text{ meters (30 ft),}$$

$$U_0 = 213.4 \text{ m/sec (700 ft/sec),}$$

$$|\vec{\theta}_0| = 3^\circ$$

$$C = 7.92 \text{ meters (26 ft), and}$$

$$k = 1.0$$

and assume that the x axis is parallel with the freestream and that the x axis passes through the cg. The frequency input value is given by eq. (95) as follows:

$$\begin{aligned} \text{OMGBAR} &= 2.0 (1.0)/13.0 \\ &= 0.07692 \end{aligned}$$

The surface displacement at the control point with position  $\vec{R}$  is

$$\vec{D}^*(\vec{R}) = \vec{\theta}_0 \times (\vec{R} - \vec{R}_0) \quad (96)$$

where

$$\begin{aligned} \vec{\theta}_0 &= (0.0)\hat{i} + (3.0/57.296)\hat{j} + (0.0)\hat{k} \\ &= (0.0)\hat{i} + (0.05236)\hat{j} + (0.0)\hat{k} \end{aligned} \quad (97)$$

and

$$\vec{R}_0 = (30.0)\hat{i} + (0.0)\hat{j} + (0.0)\hat{k}. \quad (98)$$

The surface rotation at the control point is

$$\vec{\theta}^*(\vec{R}) = \vec{\theta}_0^* \quad (99)$$

The surface displacement rate at the control point is

$$u_n^* = i\bar{\omega} U_0 \vec{D}^*(\vec{R}) \cdot \hat{n}_s. \quad (100)$$

Substituting into eq. 92 and using eq. 89 and 90, the right hand member of the boundary condition is seen to be given by

$$\begin{aligned} \text{BET}^* &= \left[ \left( U_0 \hat{c} + \vec{\nabla} \phi_s - \hat{c} M_0^2 \hat{c} \cdot \vec{\nabla} \phi_s \right) \cdot \left( \vec{\theta}_0^* \times \hat{n}_s \right) \right. \\ &\quad - \left( \vec{\theta}_0^* \times (\vec{R} - \vec{R}_0) \right) \cdot \vec{\nabla} \left( \vec{\nabla} \phi_s - \hat{c} M_0^2 \hat{c} \cdot \vec{\nabla} \phi_s \right) \\ &\quad \left. + \left( 1 - \frac{M_0^2}{U_0} \hat{c} \cdot \vec{\nabla} \phi_s \right) i\bar{\omega} U_0 \left( \vec{\theta}_0^* \times (\vec{R} - \vec{R}_0) \right) \cdot \hat{n}_s \right] e^{-i\bar{\omega} \hat{c} \cdot \vec{R} M_0^2 / \beta^2} \end{aligned} \quad (101)$$

This expression is evaluated in subroutine CBET at each control point storing the complex amplitude BET\* in the labeled common block BCOND.

Evaluation of BET\* for the example requires the FORTRAN code shown by fig. 42; however, the second term contained in the brackets of eq. (101) is not included in this computation. As shown by sec. 4.4, second order derivatives of the velocity potential are not evaluated with sufficient accuracy for this term to be included in the computations, and it is not included in any of the examples computed for this report.

As seen in fig. 42, the factor

$$e^{-i\bar{\omega}\hat{c}\cdot\vec{R}} M_o^2 / \beta^2 \quad (102)$$

is computed by a call to subroutine CMAB, computing the scalar product

$$(\text{FACTOR}) = \hat{c} \cdot \vec{R}$$

where the components of  $\hat{c}$  are contained in COMPD(I) while the components of  $\vec{R}$  are contained in ZC(I). The system subroutine CEXPI then computes the factor shown by eq (102). The subroutine CBET next computes the following cross products:

$$\vec{D}^* = \vec{\theta}_o^* \times (\vec{R} - \vec{R}_o)$$

$$\vec{c}_{xv}^* = \vec{\theta}_o^* \times \hat{n}_s$$

and the subroutine CRZAB computes the scalar products:

$$\text{CFAC} = \hat{c} \cdot (\vec{\theta}_o^* \times \hat{n}_s) \text{ and } \text{DN} = \vec{D}^* \cdot \hat{n}_s.$$

Finally, the operation

$$\text{CSUM} = \text{FSVM(I)} * (\text{DN} - \text{DFAC}),$$

appearing just before the text concerning the logical variable LSTDY, is equivalent to

$$\text{CSUM} = U_o \left[ i\bar{\omega} (\vec{\theta}_o^* \times (\vec{R} - \vec{R}_o)) \cdot \hat{n}_s - \hat{c} \cdot (\vec{\theta}_o^* \times \hat{n}_s) \right]. \quad (103)$$

This expression represents the bracketed quantity of eq. (101) when the influence of the steady component of flow is ignored.

```

SUBROUTINE CBET
COMMON/ACASE/ALPHA(5),BETA(5),FSVM(5),FSV(3,5),IACASE,NACASE
COMPLEX THETA
COMMON/BCDAT/R(3),THETA(3,5)
COMMON/CNTRO/ZC(3),ZNC(3),ZDC,IPC,ICC,JZC,JCN,KC
COMMON/COMPRS/AMACH,BETAMS,BETAM,SBETAM,ABETMS,ALPC,BETC,
COMP(3),AROTC(9),AROTCI(9),CZINV(3,3)
COMPLEX BET
COMMON/BCOND/CU,CL,TU(3),TL(3),DU,DL,BET(5),NCT,NLOPT,NROPT,NBIN
COMMON/FREQDT/OMGBAR,OMEGB,OMG
LOGICAL LSTDY
COMMON/OUTDAT/IFLAG,LSTDY
COMMON/STDY/JC;ICP,PLCL(3),TSC(6),W(4),DDO(2),X1(3)
COMPLEX CFAC,CSUM,CXV,CXPI,CZEXP,D,DN
DIMENSION CXV(3),D(3),PHES(3),IMP(3)
DATA THETA/(0.,0.),(.05236,0.),(0.,0.)/
DATA R/30.,0.,0./
CALL CMAB(ZC,COMP,FACTOR,1,3,1)
CZEXP=CXPI(FACTOR*OMEGB*(BETAMS-1.))
GA=CU+CL
GD=.5*(CU-CL)
DO 1000 I=1,NACASE
D(1)=THETA(2,I)*(ZC(3)-R(3))-THETA(3,I)*(ZC(2)-R(2))
D(2)=THETA(3,I)*(ZC(1)-R(1))-THETA(1,I)*(ZC(3)-R(3))
D(3)=THETA(1,I)*(ZC(2)-R(2))-THETA(2,I)*(ZC(1)-R(1))
CXV(1)=THETA(2,I)*ZNC(3)-THETA(3,I)*ZNC(2)
CXV(2)=THETA(3,I)*ZNC(1)-THETA(1,I)*ZNC(3)
CXV(3)=THETA(1,I)*ZNC(2)-THETA(2,I)*ZNC(1)
CALL CRZAB(D,ZNC,DN,1,3,1)
DN=DN*CMPLX(0.,OMGBAR)
CALL CRZAB(CXV,COMP,CFAC,1,3,1)
CSUM=FSVM(I)*(DN-CFAC)
IF(.NOT.LSTDY)GO TO 1000
CALL CSCAL(BETAMS,COMP,ZNC,TMP)
CALL CMAB(ZNC,TMP,FACTOR,1,3,1)
CALL VADD(TSC(3),TSC(1)/FACTOR,ZNC,TMP,3)
DO 100 J=1,3
100 PHES(J)=GA*W(J+1)+GD*TMP(J)
CALL CMAB(PHES,COMP,FACTOR,1,3,1)
FACTOR=FACTOR*(SETAMS-1.)
CALL VADD(PHES,FACTOR,COMP,TMP,3)
CALL CRZAB(CXV,TMP,CFAC,1,3,1)
1000 CSUM=CSUM+DN*FACTOR-CFAC
BET(I)=CSUM*CZEXP
RETURN
END

```

Figure 42. – Example Subroutine CBET

The logical variable LSTDY is supplied to the program as one of the input parameters in subroutine INPUT and it is contained in the common block labeled OUTDAT. If this variable has the value TRUE, then subroutine CBET computes the steady mass flux vector and the steady disturbance density; it then forms the following result:

$$\begin{aligned} \text{CSUM} = & \left[ \left( U_o \hat{c} + \vec{\nabla} \phi_s - \hat{c} M_o^2 \hat{c} \cdot \vec{\nabla} \phi_s \right) \cdot \left( \vec{\theta}_o^* \times \hat{n}_s \right) \right. \\ & \left. + \left( 1 - \frac{M_o^2}{U_o} \hat{c} \cdot \vec{\nabla} \phi_s \right) i\bar{\omega} U_o \left( \vec{\theta}_o^* \times \left( \vec{R} - \vec{R}_o \right) \right) \cdot \hat{n}_s \right] \end{aligned} \quad (104)$$

This operation is expressed as

$$\begin{aligned} \text{CSUM} = & \text{CSUM} - \left( \vec{\nabla} \phi_s - \hat{c} M_o^2 \hat{c} \cdot \vec{\nabla} \phi_s \right) \cdot \left( \vec{\theta}_o^* \times \hat{n}_s \right) \\ & - M_o^2 \hat{c} \cdot \vec{\nabla} \phi_s i\bar{\omega} \left( \vec{\theta}_o^* \times \left( \vec{R} - \vec{R}_o \right) \right) \cdot \hat{n}_s \end{aligned} \quad (105)$$

where CSUM on the right is given by eq. (103). Referring to figure 42, the call to subroutine CSCAL leads to an evaluation of the conormal to the surface; hence, the components of TMP(3) contain the components of  $\vec{n}_c$  after the call to CSCAL. The call to CMAB leads to an evaluation of the scalar product of the surface normal with the surface conormal, i.e.,

$$\text{(FACTOR)} = \hat{n} \cdot \vec{n}_c \quad (106)$$

The call to VADD leads to an evaluation of  $\vec{\nabla} \phi_s$  at the upper side of the surface. Recalling eq. (74), viz.,

$$\vec{v}_u = (\vec{v})_A + \frac{1}{2} \left( \vec{n}_c \sigma + \vec{\nabla} \mu \right) \quad (107)$$

and noting that

$$\text{TSC} (2 + J) = \vec{\nabla} \mu_s \quad \text{for } J = 1, 2, 3$$

while

$$\text{TSC} (1) = \sigma_s,$$

the call to VADD is seen to yield

$$\vec{n}_c \sigma_s + \vec{\nabla} \mu_s;$$

further, since

$$\text{CA} = 1.0 \text{ and } \text{CD} = 0.5,$$

regardless of whether Morino-type boundary conditions ( $\text{CU}=1.0, \text{CL}=-1.0$ ) or mass flux boundary

condition (CU=1.0, CL=0.0), the "do loop" leads to

$$\text{PHES}(J) = \vec{\nabla} \phi_s$$

evaluated at the upper side of the surface. The next subroutine call to CMAB evaluates the following scalar product:

$$\hat{c} \cdot \vec{\nabla} \phi_s$$

and the next operation yields

$$\begin{aligned} \text{FACTOR} &= \text{FACTOR} * (\text{BETAMS} - 1.0) \\ &= \hat{c} \cdot \vec{\nabla} \phi_s M_o^2. \end{aligned} \quad (108)$$

In turn, the calls to VADD and CRZAB yield

$$\text{TMP}(I) = \vec{\nabla} \phi_s - \hat{c} M_o^2 \hat{c} \cdot \vec{\nabla} \phi_s \quad (109)$$

$$\text{CFAC} = \left( \vec{\nabla} \phi_s - \hat{c} M_o^2 \hat{c} \cdot \vec{\nabla} \phi_s \right) \cdot \left( \vec{\theta}_o^* \times \hat{n}_s \right). \quad (110)$$

Recalling that

$$\text{DN} = \hat{n}_s \cdot \left( \vec{\theta}_o^* \times (\vec{R} - \vec{R}_o) \right) i\bar{\omega}, \quad (111)$$

the final operation, viz.,

$$\text{CSUM} = \text{CSUM} + \text{DN} * \text{FACTOR} - \text{CFAC}, \quad (112)$$

yields an evaluation of eq. (105).

The final operation of subroutine CBET, yields the boundary condition value, viz.,

$$\text{BET}^* = \text{CSUM} \left( e^{-i\bar{\omega} \hat{c} \cdot \vec{R}} M_o^2 / \beta^2 \right). \quad (113)$$

The preceding example describes a single boundary condition consisting of the rigid body mode shape: pitch oscillation. Provision is made for up to five boundary condition cases representing five different mode shapes; thus, for example, there is provision for introducing five different centers of rotation for the pitch oscillation or for introducing five completely different mode shapes. One must recognize, however, that the flow Mach number and reduced frequency are fixed and that these parameters are the same for each boundary condition case.

Two labeled common blocks, ACASE and BCON, contain the information related to multiple cases. ACASE contains the variable NACASE defining the total number of cases to be executed; it also contains the variable IACASE identifying the case currently being executed and three scalars and a vector which can be evaluated for each case. BCON contains the boundary condition defining parameters associated with any control point which are the coefficients appearing in eq. (91) and up to five values for BET\* are allowed for each of the two boundary conditions at a control point.

### 5.2.3 UNSTEADY WAKE REPRESENTATION

The unsteady wake representation available within the program provides capability for constructing an elaborate model of the unsteady wake vorticity convection. Wake surfaces are represented by doublet networks which, as noted in sec. 3.2, can be made to form a stream surface of the steady mean component of flow. The unsteady vorticity can be convected along the mean steady streamlines on the wake surface with the average mass flux of the mean steady flow.

As shown by eq. (37), viz.,

$$\mu^*(\ell, s) = \mu^*(c, s) e^{-\left[ (i\bar{\omega} / \beta^2) \int_c^\ell d\xi / w_s \right]} \quad (37)$$

the wake model determines the doublet distribution on an entire wake network in terms of the doublet strength along the upstream edge of the network. The integral contained in eq. (37) yields the time period, i.e.,

$$\Delta t = \frac{1}{\beta^2 U_0} \int_c^\ell d\xi / w_s \quad (114)$$

representing the period of time required for unsteady vorticity to be convected from point  $c$  on the network edge to the point  $\ell$  interior to the network. Writing eq. (37) in terms of the time delay, viz.,

$$\mu^*(\ell, s) = \mu^*(c, s) \left[ \cos(\omega \Delta t) - i \sin(\omega \Delta t) \right],$$

the doublet distribution is seen to be a harmonic function of the time period. Since the steady disturbance velocity is at least an order of magnitude less than the freestream velocity, the factor  $w_s$  is nearly unity (cf. the discussion preceding eq. (37) in sec. 3.1); hence, the unsteady wake vorticity varies nearly as a harmonic function of the  $x$  compressibility system coordinate, i.e.,

$$\mu^*(x, s) \approx \mu^*(c, s) \left[ \cos(\bar{\omega}(x-c)) - i \sin(\bar{\omega}(x-c)) \right] \quad (115)$$

where

$$x-c = U_0 \Delta t.$$

The doublet strength distribution on the wake is represented in terms of doublet panel distributions. As noted in sec. 3.4, a doublet panel distribution is a quadratic function of the local panel coordinates, c.f. eq. (50), and the quadratic is determined by its least squares fit to the values of the actual doublet distribution at the evaluation points shown in fig. 12. As shown above, at a wake surface the actual doublet distribution is very nearly a harmonic function of the downstream distance, see fig. 43. A quadratic can approximate a

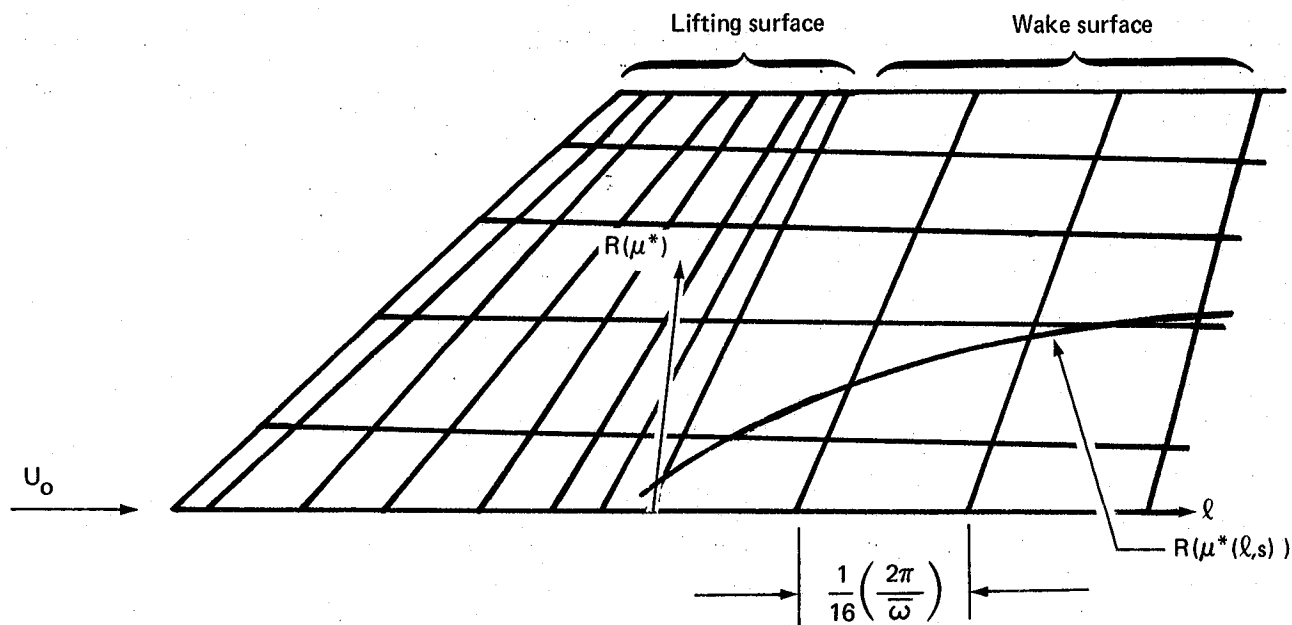


Figure 43. — Wake Panel Spacing

harmonic function to within three significant figures over a domain which is one sixteenth of the wave length of the harmonic function; therefore, the length of a wake panel in the streamwise direction should not be greater than one sixteenth of  $(2\pi/\bar{\omega})$  in regions where that level of accuracy is required.

The wake networks are defined in subroutine INPUT and they are paneled like any other doublet network defining the grid points of the panel corner points, sec. 1.1, ref. 2. Control points are defined and boundary conditions are specified only along the upstream edge of a wake network, sec. 1.3.2 of ref. 2. The time period contained in eq. (37), for evaluation the downstream wake doublet strength, is introduced at each doublet singularity parameter point in subroutine DASPL. Eq. (37) is expressed as

$$\mu^*(I) = \mu^*(J) e^{-i(\bar{\omega}/\beta^2)TDLY(I)} \quad (116)$$

where

$$TDLY(I) = \int_{\ell(J)}^{\ell(I)} d\xi / w_s \quad (117)$$

where  $\ell(J)$  is the wake streamline coordinate of the network edge singularity parameter upstream of the  $I$ th singularity parameter on the wake, the latter, having the wake streamline coordinate  $\ell(I)$ , fig 44.

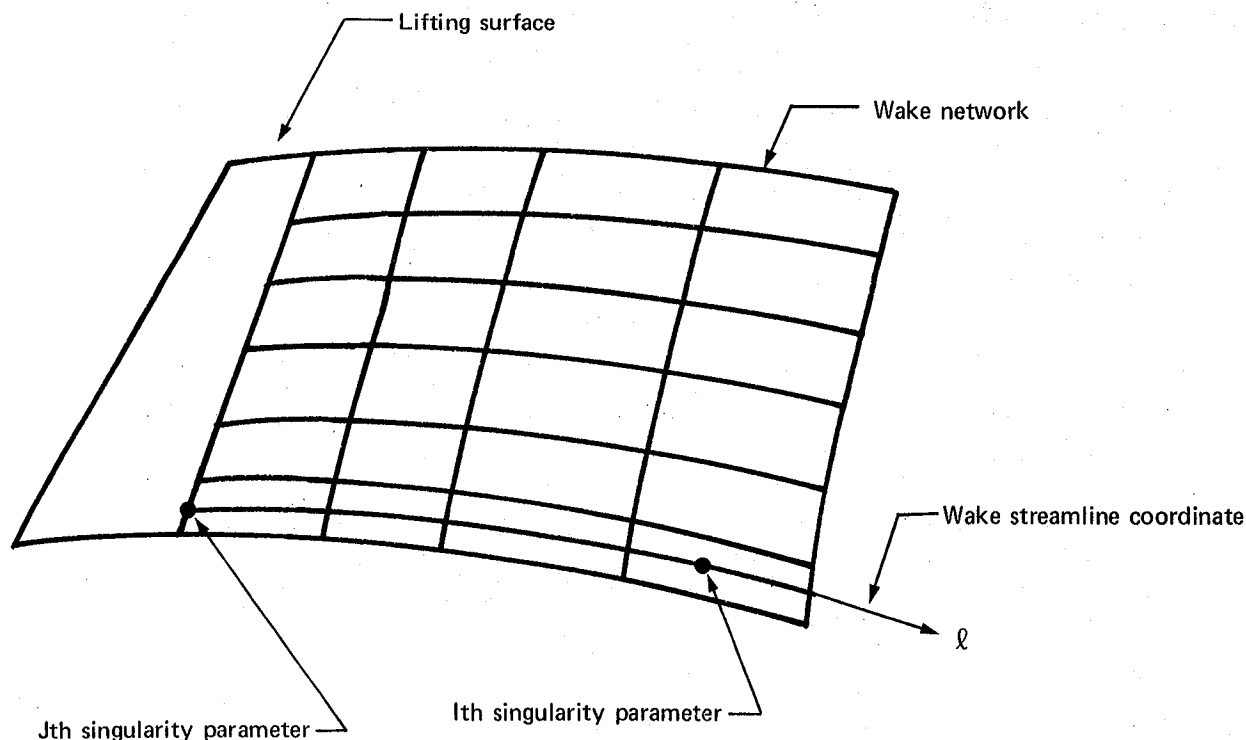


Figure 44. - Singularity Parameters Along Wake Streamline Coordinates

In its present form, subroutine DASPL generates TDLY(I) as follows:

$$TDLY(I) = \hat{c} \cdot (\vec{R}(I) - \vec{R}(J)) \quad (118)$$

where  $\hat{c}$  is the unit vector in the compressibility direction, eq. (88), while  $\vec{R}(I)$  and  $\vec{R}(J)$  are the position vectors, respectively, of the downstream and upstream singularity parameters. This expression approximates the wake vorticity convection time period, ignoring the effect of the average mean steady disturbance mass flux vector. This approximation is used because the analysis capability of the steady flow panel method does not currently provide for an evaluation of eq. (108).

### 5.3 OUTPUT DATA DESCRIPTION

With the exception of pressure data, the output data of the unsteady flow panel method is a subset of the steady flow panel method as listed in Table 3-1 of ref. 2. Of course, values of all unsteady flow parameters are expressed as the real and imaginary parts of their complex amplitudes. The following pressure coefficients are output.

*Linear, Unsteady Disturbance Pressure*

	Upper Surface	Lower Surface	Difference
Real	CPLINU	CPLINL	CPLIND
Imaginary	CPLNUI	CPLNLI	CPLNDI

$$C_p^* = -\frac{2}{U_0} (i\bar{\omega}\phi^* + \hat{c} \cdot \vec{\nabla}\phi^*) \quad (119)$$

*Quadratic, Unsteady Disturbance Pressure*

	Upper Surface	Lower Surface	Difference
Real	CP2NDU	CP2NDL	CP2NDD
Imaginary	CP2DUI	CP2DLI	CP2DDI

$$C_p^* = -\frac{2}{U_0} \left( i\bar{\omega} \rho_s \phi^* / \rho_0 + (\vec{W}_s / \rho_0 U_0) \cdot \vec{\nabla}\phi^* \right) \quad (120)$$

where

$$\rho_s = \rho_0 \left( 1 - \frac{M_0^2}{U_0} \hat{c} \cdot \vec{\nabla}\phi_s \right) \quad (17)$$

and

$$\vec{W}_s = \rho_0 \left( U_0 \hat{c} + \vec{\nabla}\phi_s - M_0^2 \hat{c} \cdot \vec{\nabla}\phi_s \right) \quad (10)$$

*Linear, Total Disturbance Pressure*

	Upper Surface	Lower Surface	Difference
Real	CPLNUT	CPLNLT	CPLNDT
Imaginary	CPLUTI	CPLLLTI	CPLDTI

$$C_p^* = C_p^* (119) - \frac{2}{U_0} \hat{c} \cdot \vec{\nabla}\phi_s \quad (121)$$

where  $C_p^*$  (119) denotes the value of  $C_p^*$  computed from eq. (119)

*Quadratic, Total Disturbance Pressure*

	Upper Surface	Lower Surface	Difference
Real	CP2DUT	CP2DLT	CP2DDT
Imaginary	CP2UTI	CP2LTI	CP2DTI

$$C_p^* = C_p^* (120) - \frac{1}{U_0} \left( 2 \hat{c} \cdot \vec{\nabla} \phi_s + \frac{1}{U_0} \vec{w}_s \cdot \vec{\nabla} \phi_s \right) \quad (122)$$

where

$$\vec{w}_s = \vec{\nabla} \phi_s - M_0^2 \hat{c} \cdot \vec{\nabla} \psi_s \quad (11)$$

and  $C_p^* (120)$  denotes the value of  $C_p^*$  computed from eq. (120)

## 6.0 CONCLUSIONS

An advanced panel method for solving subsonic unsteady potential flow boundary value problems has been presented. The method is shown to be applicable to small disturbance flows when the flow can be described with adequate accuracy by a solution to the linear, first order approximation to the unsteady potential flow equation. The method is also shown to be applicable to arbitrary configurations.

The principal feature of the method which required validation is a kernel function approximation. Solutions to the unsteady flow equation are related to solutions to Helmholtz's equation by a coordinate transformation and a change of dependent variable. Using this relationship, a solution to an unsteady flow problem is expressed in terms of an integral equation derived from Helmholtz's theorem. The panel method is based on a reduction of this integral equation to a system of linear, complex algebraic equations and the reduction is accomplished by a typical panel method approximation leading to a panel by panel evaluation of the integral expression appearing in the integral equation. The kernel function approximation is required for the closed form evaluation of the integrals.

The validity of the kernel function approximation has been examined both theoretically and empirically. The theoretical examination consists of a direct error analysis. The empirical examination consists of comparisons of computed panel method results with results from alternative computational methods. The alternative methods do not contain kernel function approximations of the same nature as that of the panel method. The comparisons include solutions to unsteady flow problems of thin, planar wings and for T-tails; they demonstrate that the panel method solution tends to converge to the correct solution as the number of panels is increased.

In the analysis of unsteady flow on thin, planar wings the panel method yields aerodynamic forces which converge nearly monotonically with increasing panel density. Monotonic convergence for a sequence of thin wing solutions tended to occur only for a particular set of panel density distributions. In the case of the more complex T-tail, however, the panel method tended to converge with increased panel density but convergence was not always monotonic. This condition is thought to result from the particular choice of panel density distribution. Finding the panel density distribution leading to monotonic convergence may not be plausible except for very simple configurations undergoing very simple modes of motion.

The validity of the panel method for computing unsteady flow about bodies of finite thickness was tested by an indirect comparison. The unsteady flow was evaluated about a wing having a finite (but small) thickness (viz., 4.8 percent) with the wing oscillating in pitch. The unsteady flow was evaluated for the case of thick wing theory with the panels located on the actual wing surface and with the flow boundary conditions satisfied at the actual wing surface. The unsteady flow was evaluated a second time but to provide a comparison case using thin wing theory. In thin wing theory the panels lie on a flat mean wing surface

and the flow boundary conditions at the actual surface are satisfied only to a first order approximation; but, since accurate alternate methods are available for its evaluation, thin wing theory provides a reliable comparison case. The lifting pressure distributions for these two cases are compared and found to be in very close agreement. This close agreement shows that the panel method is valid for bodies of finite thickness.

Application of the method to complex configurations was demonstrated by computing the unsteady flow about a wing-body-tail-nacelle configuration undergoing pitch oscillation. Results from this computation are compared with equivalent results computed using the well known doublet-lattice method. The comparisons are in sufficient agreement to indicate validity of the panel method and the capability to analyze very complicated geometries.

## APPENDIX A

### GENERAL THEORY OF FLOW

#### A.1 INTRODUCTION

This appendix contains a derivation of the general theory of compressible, inviscid, nonconducting, irrotational, isentropic flow expressed as a boundary value problem. The derivation leads to a single, nonlinear partial differential equation governing the flow; and it leads to the analytical expressions for boundary conditions appropriate to solid, aerodynamic surfaces and to wake surfaces. The derivation proceeds from results appearing in ref. 14 and its purpose is to provide a convenient reference for the development of the approximate theory of flow appearing in app. B.

#### A.2 FLOW EQUATION

The derived governing equation (called, as usual, the flow equation) is a single equation in terms of a single flow parameter, viz., the velocity potential, but it is derived here from a system of six equations in terms of six variables: the components of velocity, pressure, density, and internal energy. The system of six equations, taken as the primitive statement of the theory, represents the conservation laws (in their forms appropriate to an inviscid, nonconducting fluid undergoing an isentropic process) along with the constitutive relation for the fluid, the latter being an equation relating internal energy to the pressure (a mechanical variable) and the density (a deformation variable). The flow equation is derived by a process of reduction wherein the primitive system of equations are combined so as to eliminate the explicit appearance of the original variables. In the reduction process two additional variables are introduced by two additional equations which express the constraints imposed to obtain irrotational and isentropic flow.

In the statement of the primitive system of equations and in the derivation involving those equations, the laws of conservation of mass, momentum, and energy are stated independently of one another, for example, the law of conservation of momentum is expressed without asserting that mass is conserved. This independence is retained because of the particular requirements of the development in app. B which leads to an approximate theory. In the development contained in app. B approximations are postulated regarding the conservation laws. The interdependence of those approximations is examined using the equations of app. A; therefore, the laws of conservation are initially stated (cf., eqs. (A.2a) and (A.3a)) as independent relations.

The primitive system of equations is as follows:

- Continuity equation (eq. 5.4), ref. 14—

$$\frac{\partial \rho}{\partial t} + \vec{\nabla} \cdot (\rho \vec{Q}) = 0 \quad (\text{A.1})$$

This equation follows from the law of conservation of mass and relates the dilatation rate of the fluid to its rate of change of mass density as

$$\vec{\nabla} \cdot \vec{V}_c = -\frac{1}{\rho} \frac{d\rho}{dt} \quad (\text{A.1a})$$

where

$$\frac{d}{dt} \equiv \frac{\partial}{\partial t} + \vec{V}_c \cdot \vec{\nabla}.$$

- Euler's equations of motion eq. (6.9), ref. 14—

$$\frac{d\vec{V}_c}{dt} + \frac{1}{\rho} \vec{\nabla} p = 0. \quad (\text{A.2})$$

These equations follow from the law of conservation of linear momentum when mass is conserved causing the law of conservation of linear momentum, viz.,

$$\vec{V}_c \left( \frac{d\rho}{dt} + \rho \vec{\nabla} \cdot \vec{V}_c \right) + \rho \frac{d\vec{V}_c}{dt} + \vec{\nabla} p = 0, \quad (\text{A.2a})$$

to reduce to eq. (A.2).

- Energy equation eqs. (34.2) and (34.3), ref. 14—

$$\rho \frac{de}{dt} + p \vec{\nabla} \cdot \vec{V}_c = 0. \quad (\text{A.3})$$

This equation follows from the law of conservation of energy when eqs. (A.1) and (A.2) are satisfied causing the law of conservation of energy, viz.,

$$\left( e + \frac{1}{2} \vec{V}_c \cdot \vec{V}_c \right) \left( \frac{d\rho}{dt} + \rho \vec{\nabla} \cdot \vec{V}_c \right) + \rho \vec{V}_c \cdot \left( \frac{d\vec{V}_c}{dt} + \frac{1}{\rho} \vec{\nabla} p \right) + \rho \frac{de}{dt} + p \vec{\nabla} \cdot \vec{V}_c = 0, \quad (\text{A.3a})$$

to reduce to eq. (A.3).

- Constitutive relation —

$$\frac{de}{dt} = \frac{1}{\gamma-1} \frac{d}{dt} (p/\rho). \quad (\text{A.4})$$

This equation is derived from the perfect gas relations (sec. 31, ref. 14) viz.,

$$\frac{de}{dt} = C_v \frac{dT}{dt} \quad (\text{A.5})$$

and

$$p = \rho RT, \quad (\text{A.6})$$

where

$$R = C_p - C_v \text{ and } \gamma = C_p / C_v.$$

Eqs.(A.1), (A.2), (A.3), and (A.4) are a determinate system of six equations in terms of six flow parameters, namely,

$$\rho, p, e, \vec{V}_c.$$

The specific internal energy  $e$  is eliminated as an explicit dependent variable by combining eqs. (A.3) and (A.4) to obtain

$$\frac{1}{\gamma-1} \frac{d}{dt} (p/\rho) = -(p/\rho) \vec{\nabla} \cdot \vec{V}_c.$$

Introducing eq. (A.1a) to eliminate the dilatation rate, after some manipulation, the pressure and density are found to be related as follows:

$$\frac{dp}{dt} = \gamma (p/\rho) \frac{dp}{dt}. \quad (\text{A.7})$$

This result is integrated, following the motion of a specific but arbitrarily chosen fluid particle, to find the well known isentropic pressure-density relation, viz.,

$$(p/\rho_0) = (\rho/\rho_0)^\gamma. \quad (\text{A.8})$$

Equations (A.1), (A.2) and (A.8) form a determinate system of five equations in terms of five flow parameters, namely,

$$\rho, p, \vec{V}_c.$$

For the case of irrotational flow the system of equations governing the flow may be combined to eliminate explicit appearance of the velocity by introducing a new flow parameter, namely, the velocity potential. Letting the flow be a disturbance from a uniform freestream and introducing the kinematical constraint of irrotationality, viz.,  $\vec{\nabla} \times \vec{V}_c = 0$ , the flow velocity may be expressed in terms of a potential as follows:

$$\vec{V}_c = \vec{U}_0 + \vec{\nabla}\phi. \quad (\text{A.9})$$

Also, as shown by eqs. (3.5) and (17.1), ref. 14, the fluid particle acceleration may be expressed as

$$\frac{d\vec{V}_c}{dt} = \vec{\nabla}\psi + \vec{\omega} \times \vec{V}_c$$

where

$$\vec{\omega} \equiv \vec{\nabla} \times \vec{V}_c \quad \text{and} \quad \psi \equiv \frac{\partial \phi}{\partial t} + \frac{1}{2} \vec{V}_c \cdot \vec{V}_c;$$

thus, for irrotational flow in which  $\vec{\omega}$  vanishes, the acceleration terms of Euler's equations of motion, viz., eq. (A.2), can be expressed as the gradient of a scalar:

$$\vec{\nabla} \left( \frac{\partial \phi}{\partial t} + \frac{1}{2} \vec{V}_c \cdot \vec{V}_c \right) + \frac{1}{\rho} \vec{\nabla} p = 0. \quad (\text{A.10})$$

Noting, further, that eq. (A.8) supplies a unique relation between pressure and density (i.e., the flow is barotropic), the following relation follows from the rule for differentiating a definite integral taken along an arbitrary path in space from a point where the pressure and density are uniform:

$$\vec{\nabla} \int_{p_0}^{p(x,y,z,t)} \frac{dp}{\rho(p)} = \int_{p_0}^{p(x,y,z,t)} \vec{\nabla} \left( \frac{1}{\rho(p)} \right) dp + \frac{1}{\rho(p(x,y,z,t))} \vec{\nabla} p(x,y,z,t) - \frac{1}{\rho(p_0)} \vec{\nabla} p_0 = \frac{1}{\rho} \vec{\nabla} p$$

where  $\vec{\nabla} p(\rho)$  vanishes because the dependence of pressure on density is independent of position and  $\vec{\nabla} p_0$  vanishes because the lower limit of the integral is assumed to be at a spatial point where the pressure is uniform. Using this result, Euler's equations of motion are expressed entirely as the gradient of a scalar quantity:

$$\vec{\nabla} \left( \frac{\partial \phi}{\partial t} + \frac{1}{2} \vec{V}_c \cdot \vec{V}_c + \int_{p_0}^p \frac{dp}{\rho} \right) = 0.$$

Integrating this expression over an arbitrary path from a point in the undisturbed fluid, Bernoulli's integral to Euler's equations of motion is found by introducing eq. (A.9) and choosing the potential  $\phi$  to be zero in the undisturbed fluid. The result appears as follows:

$$\frac{D\phi}{Dt} + \frac{1}{2} \vec{\nabla} \phi \cdot \vec{\nabla} \phi + \int_{p_0}^p \frac{dp}{\rho} = 0 \quad (\text{A.11})$$

where

$$\frac{D\phi}{Dt} = \frac{\partial\phi}{\partial t} + \vec{U}_0 \cdot \vec{\nabla}\phi.$$

Further, substituting eq. (A.9) into the continuity equation yields the following expression in which the velocity components are eliminated as explicit variables:

$$\nabla^2 \phi = -\frac{1}{\rho} \frac{d\rho}{dt}. \quad (\text{A.12})$$

Finally, eqs. (A.8), (A.11), and (A.12) provide a determinate system of three equations in terms of three flow variables, namely,

$$\rho, p, \phi.$$

The pressure and density are eliminated as explicit variables by introducing the speed of sound as a new variable (c.f. sec. 35, ref. 14) viz.,

$$c^2 = \frac{dp}{d\rho}. \quad (\text{A.13})$$

Combining eq. (A.7) with eq. (A.13), the speed of sound is found to be given by the following ratio:

$$c^2 = \gamma p/\rho. \quad (\text{A.14})$$

Since eq. (A.14) is a property of the fluid, the differential with respect to time following a fluid particle can be expressed as

$$\frac{d}{dt}(c^2) = (\gamma-1) \frac{1}{\rho} \frac{d\rho}{dt};$$

and, on integrating, following the motion of a specific but arbitrarily chosen particle, the speed of sound is evaluated as follows:

$$+\vec{\nabla} \cdot (\rho \vec{V}_c) = 0 \quad c^2 - c_0^2 = (\gamma-1) \int_{p_0}^p \frac{dp}{\rho}$$

where  $c_0$  and  $p_0$  appear as a result of having chosen a path of integration beginning at an undisturbed point in the flow. This result is combined with eq. (A.11) to obtain the speed of sound in terms of the velocity potential, viz.,

$$c^2 = c_0^2 - (\gamma-1) \left( \frac{D\phi}{Dt} + \frac{1}{2} \vec{\nabla}\phi \cdot \vec{\nabla}\phi \right). \quad (\text{A.15})$$

Pressure and density are eliminated by using eq. (A.13) to express the continuity equation (as given by eq. (A.12)) in terms of the speed of sound. The result is as follows:

$$\nabla^2 \phi = -\frac{1}{c^2} \frac{1}{\rho} \frac{dp}{dt}$$

Differentiating Bernoulli's integral (as given by eq. (A.11)) and combining the result with this form of the continuity equation, a determinate system of two equations, consisting of eq. (A.15) and

$$\nabla^2 \phi = \frac{1}{c^2} \frac{d}{dt} \left( \frac{D\phi}{Dt} + \frac{1}{2} \vec{\nabla} \phi \cdot \vec{\nabla} \phi \right), \quad (\text{A.16})$$

is found in terms of two flow parameters, namely,

$$\phi \text{ and } c.$$

The desired result, viz., a single equation in terms of a single flow parameter, is obtained by eliminating the speed of sound between eq. (A.15) and eq. (A.16) to find the following equation in terms of the disturbance velocity potential:

$$\nabla^2 \phi = \left[ c_0^2 - (\gamma-1) \left( \frac{D\phi}{Dt} + \frac{1}{2} \vec{\nabla} \phi \cdot \vec{\nabla} \phi \right) \right]^{-1} \frac{d}{dt} \left( \frac{D\phi}{Dt} + \frac{1}{2} \vec{\nabla} \phi \cdot \vec{\nabla} \phi \right) \quad (\text{A.17})$$

this equation is termed the "flow equation."

The fluid pressure is evaluated in terms of the velocity potential by substituting the isentropic pressure-density relation (i.e., eq. (A.7)) into Bernoulli's integral (i.e., eq. (A.11)) and carrying out the indicated integration. When the result is expressed in terms of a pressure coefficient, it appears as follows:

$$\begin{aligned} C_p &= (p - p_0) / \left( \frac{1}{2} \rho_0 U_0^2 \right) \\ &= \frac{2}{\gamma M_0^2} \left\{ \left[ 1 - (\gamma-1) \frac{1}{c_0^2} \left( \frac{D\phi}{Dt} + \frac{1}{2} \vec{\nabla} \phi \cdot \vec{\nabla} \phi \right) \right]^{\gamma/\gamma-1} - 1 \right\}. \end{aligned}$$

### A.3 BOUNDARY CONDITIONS

The equations of the preceding section govern the kinematics and dynamics of the fluid flow; as such, they represent conditions which must be satisfied at every point of the flow field. This section introduces additional conditions which must be satisfied on surfaces which form the boundaries of the flow field.

The bounding surfaces are of three types. They consist of the aerodynamic surface of the aircraft, the surfaces of its wake, and a far-field surface which completely surrounds the aerodynamic surface, but which is at a large distance from it. The aerodynamic surface has the characteristics of the surface of a solid body; therefore, fluid particles do not penetrate this surface. In addition, the aerodynamic force on an aircraft is the result of the fluid pressure acting on the aerodynamic surface. The wake has two surfaces which are adjacent to one another and are separated by an infinitesimal distance. These wake surfaces form two sides of a vortex sheet; fluid particles do not pass through them and the component of velocity tangent to them is discontinuous. Disturbances to the fluid flow are required to propagate toward the far-field surface and are required to become vanishingly small there.

### A.4 AERODYNAMIC SURFACE

Let  $S$  denote the aerodynamic surface of the aircraft at the present instant of time, and denote the volume enclosed by this surface as  $V$ . In the analytical representation of the flow problem the fluid is continuous and fills the entire space; hence, the surface  $S$  encloses the mass of fluid,  $M$ , computed as follows:

$$M = \iiint_V \rho \, dv .$$

In the case of an arbitrary motion of  $S$ , the mass  $M$  may vary with time; and, assuming mass is conserved, this variation implies that there is motion of fluid through  $S$  in violation of the aerodynamic surface boundary condition. Spatial points of the surface  $S$  have a velocity denoted as  $\vec{u}$ , see sec. 3.1; hence, the time rate of change of the mass contained in  $V$  is given by

$$\begin{aligned} \frac{dM}{dt} &= \lim_{\Delta t \rightarrow 0} \left\{ \frac{1}{\Delta t} \left[ \iiint_{V'} \rho(x,y,z,t + \Delta t) \, dv + \iint_{S'} \rho(x,y,z,t + \Delta t) \Delta t \vec{u} \cdot \hat{n} \, ds - \iiint_{V'} \rho(x,y,z,t) \, dv \right] \right\} \\ &= \iiint_{V'} \frac{\partial \rho}{\partial t} \, dv + \iint_{S'} \rho \vec{u} \cdot \vec{n} \, ds \end{aligned} \quad (\text{A.19})$$

where  $S'$  and  $V'$  are spatially fixed but coincident with the moving surface and volume ( $S$  and  $V$ ) at the instant of time  $t$ , see fig. 45.

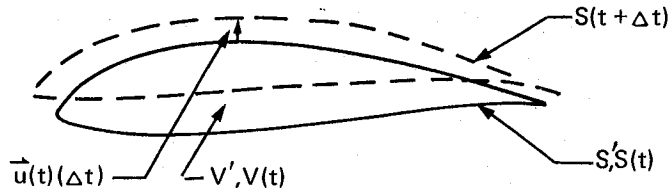


Figure 45. — Aerodynamic Surface Variation in Time

Since mass is conserved, the continuity equation, i.e., eq. (A.1), is introduced and the volume integral contained in eq. (A.19) is as follows:

$$\iiint_{V'} \frac{\partial \rho}{\partial t} dv = - \iiint_{V'} \nabla \cdot (\rho \vec{V}_c) dv .$$

Applying the divergence theorem leads to

$$\iiint_{V'} \frac{\partial \rho}{\partial t} dv = - \iint_{S'} \rho \vec{V}_c \cdot \hat{n} ds$$

so that on substituting this expression into eq. (A.19), the time rate of change of mass is found as follows:

$$\frac{dM}{dt} = \iint_{S'} (\rho \vec{u} \cdot \hat{n} - \rho \vec{V}_c \cdot \hat{n}) ds . \quad (A.20)$$

This equation shows that the time rate of change of enclosed mass is evaluated by the surface integral sum of

$$d\left(\frac{dM}{dt}\right) = (\rho \vec{u} \cdot \hat{n} - \rho \vec{V}_c \cdot \hat{n}) ds .$$

If there is to be no exchange of fluid from  $V$ , interior to  $S$ , with the fluid exterior to  $S$ , then this differential quantity must vanish at every point of  $S$ ; therefore, the aerodynamic surface boundary condition is given by

$$\rho u_n = \vec{M} \cdot \hat{n} \text{ on } S \quad (A.21)$$

where

$$u_n \equiv \vec{u} \cdot \hat{n}$$

and

$$\vec{M} \equiv \rho \vec{V}_c \quad (\text{A.22})$$

is the fluid mass-flux vector.

In the case of steady flow, wherein  $u_n = 0$ , the boundary condition is found by integrating the steady flow continuity equation over  $V$  to find

$$\iiint_V \vec{\nabla} \cdot \vec{M} \, dv = 0.$$

Applying the divergence theorem, the aerodynamic surface boundary condition is found to be

$$\vec{M} \cdot \hat{n} = 0 \text{ on } S. \quad (\text{A.23})$$

The aerodynamic force acting on the surface  $S$ , see fig. 46, is found as

$$\vec{F}_s = - \iint_S p \hat{n} \, ds. \quad (\text{A.24})$$

Let  $S_c$  be a control surface, moving with the fluid and surrounding  $S$ , and let  $V$  be the volume of fluid between  $S_c$  and  $S$ . The total force acting on this volume of fluid must vanish; hence,

$$\vec{F} = - \iint_{S_c} p \hat{n} \, ds - \iint_S p \hat{n} \, ds + \frac{d}{dt} \iiint_V \rho \vec{V}_c \, dv = 0 \quad (\text{A.25})$$

Applying the transport theorem (ref. 14, sec. 4), the volume integral becomes

$$\frac{d}{dt} \iiint_V \rho \vec{V}_c \, dv = \frac{\partial}{\partial t} \iiint_V \rho \vec{V}_c \, dv + \iint_S \rho \vec{V}_c \vec{V}_c \cdot \hat{n} \, ds + \iint_{S'_c} \rho \vec{V}_c \vec{V}_c \cdot \hat{n} \, ds$$

where  $S'_c$  is chosen to be a spatially fixed surface coinciding with  $S_c$  at time  $t$ . In steady flow the first two terms on the right vanish (the first by definition and the second by virtue of eq. (A.23)); hence,

$$\frac{d}{dt} \iiint_V \rho \vec{V}_c \, dv = \iint_{S'_c} \rho \vec{V}_c \vec{V}_c \cdot \hat{n} \, ds$$

Substituting this result and eq. (A.24) into eq. (A.25), the force acting on  $S$  is found in terms of an integral over the spatially fixed control surface,  $S'_c$ , as follows:

$$\vec{F}_s = \iint_{S'_c} \left( \rho \vec{V}_c \vec{V}_c \cdot \hat{n} + p \hat{n} \right) ds. \quad (\text{A.26})$$

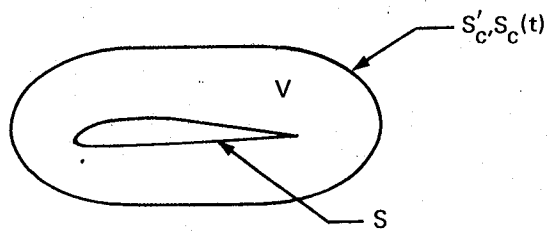


Figure 46. — Control Surface for Computing Aerodynamic Force

Eq. (A.26) also follows directly from Euler's equations of motion and the continuity equation. In steady flow these expressions are given by

$$\vec{\nabla} \cdot \vec{V}_c + \vec{\nabla} p = 0 \quad (\text{A.27})$$

and

$$\vec{\nabla} \cdot \vec{M} = 0 ; \quad (\text{A.28})$$

thus, eq. (A.27) can be written as follows:

$$\vec{\nabla} \cdot (\vec{M} \vec{V}_c) + \vec{\nabla} p = 0 . \quad (\text{A.29})$$

Integrating over the volume  $V$  and applying the divergence theorem, eq. (A.29) leads to

$$\iint_{S_c + S} [(\vec{V}_c \vec{M}) \cdot \hat{n} + p \hat{n}] ds = 0 .$$

Introducing the steady aerodynamic surface condition shown by eq. (A.23) and the definition shown by eq. (A.24), the aerodynamic force on  $S$  is found again as

$$\vec{F}_s = \iint_{S_c} (\rho \vec{V}_c \vec{V}_c \cdot \hat{n} + p \hat{n}) ds .$$

In steady flow, therefore, if the mass flux vector, velocity vector, and pressure satisfy eqs. (A.27) and (A.28), then eqs. (A.23) and (A.26) are valid expressions for the aerodynamic surface conditions.

The above results are well known and appear in most standard texts on fluid mechanics. They are developed here to provide a special emphasis for app. B, where approximations are introduced. The approximations are imposed on the relationships governing the pressure and density in the flow. In steady flow they lead to an approximate mass-flux vector which satisfies eqs. (A.28) and (A.29) exactly even though mass and momentum are not conserved exactly. As a result, the surface conditions shown by eqs. (A.23) and (A.26) are taken to be valid in the approximate theory of flow.

## A.5 WAKE SURFACE

The wake surface is a vortex sheet containing the vorticity shed from the trailing edge of a lifting surface; and as such, it is the idealization of the real flow which was originally introduced by Prandtl (ref. 15 sec. 19.1). The boundary layers at either side of a lifting surface separate from the surface and form a thin wake region of viscous flow trailing downstream. Like the thickness of the boundary layers, the thickness of the thin wake region of viscous flow tends to zero in the limit of zero viscosity. As noted by sec. 2.7, ref. 7, there is also a jump in potential across the wake surface along its upstream edge where it is attached to the lifting surface, and this jump in potential is equal to the circulation on the lifting surface. Since, in general, there can be both a spanwise and timewise variation in circulation on the lifting surface, there can be a gradient in the jump in potential along the wake surface. This gradient represents the vorticity shed from the lifting surface into the wake surface.

The wake is a free vortex sheet except along its upstream edge where it is attached to the lifting surface; also, the wake surface does not propagate through the fluid with at least the speed of sound. It follows from these two conditions (ref. 14, sec. F) that the fluid pressure is continuous across the wake surface, i.e.,

$$\llbracket p \rrbracket = 0 \text{ on } W. \quad (\text{A.30})$$

Additionally, in view of the discontinuity in potential across the wake, there may be a discontinuity in fluid velocity across the wake, viz.,

$$\llbracket \vec{V}_c \rrbracket \neq 0 \text{ on } W. \quad (\text{A.31})$$

Eqs. (A.30) and (A.31) cause the wake to be a particular type of surface of discontinuity. Formal procedures for analyzing the flow in the neighborhood of a surface of discontinuity are described by ref. 16, chapter C, and those procedures make use of the geometry shown by fig. 47. In fig. 47 the quantity  $S$  denotes a material surface surrounding the material volume  $V$ . This volume of fluid is divided into two parts,  $V^+$  and  $V^-$ , by the surface  $s$  and this dividing surface need not be a material surface. The volume  $V^+$  is surrounded by the surface  $S^+ + s$  and the volume  $V^-$  is surrounded by the surface  $S^- + s$ . Finally, the speed of surface displacement along the surface normal is given by the following expression:

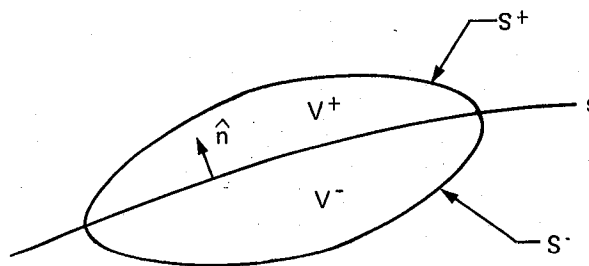


Figure 47. — Surface of Discontinuity

$$\vec{u}^+ \cdot \hat{n} = \begin{cases} \vec{V}_c \cdot \hat{n} & \text{on } S^+ \\ u_n & \text{on } s \end{cases}$$

$$\vec{u}^- \cdot \hat{n} = \begin{cases} \vec{V}_c \cdot \hat{n} & \text{on } S^- \\ u_n & \text{on } s. \end{cases}$$

As shown by ref. 14, eq. (6.1), momentum is conserved interior to the surface  $S$  if

$$\frac{d}{dt} \iiint_V \rho \vec{V}_c \, dv = - \iint_S p \hat{n} \, ds.$$

Introducing the transport theorem (ref. 14, eq. (4.1)), the volume integral can be expressed as follows:

$$\frac{d}{dt} \iiint_V \rho \vec{V}_c \, dv = \iiint_V \left[ \frac{\partial(\rho \vec{V}_c)}{\partial t} + \vec{V}_c \cdot \nabla(\rho \vec{V}_c) + \rho \vec{V}_c \nabla \cdot \vec{V}_c \right] dv;$$

and, by applying the divergence theorem, it follows that

$$\frac{d}{dt} \iiint_V \rho \vec{V}_c \, dv = \iiint_V \frac{\partial(\rho \vec{V}_c)}{\partial t} \, dv + \iint_S \rho \vec{V}_c \vec{V}_c \cdot \hat{n} \, ds.$$

Introducing the volume subdivision, these expressions yield

$$\begin{aligned} & \iiint_{V^+} \frac{\partial(\rho \vec{V}_c)}{\partial t} \, dv + \iiint_{V^-} \frac{\partial(\rho \vec{V}_c)}{\partial t} \, dv + \iint_{S^+} \rho \vec{V}_c \vec{V}_c \cdot \hat{n} \, ds \\ & + \iint_{S^-} \rho \vec{V}_c \vec{V}_c \cdot \hat{n} \, ds - \iint_s (\rho \vec{V}_c)^+ u_n \, ds + \iint_s (\rho \vec{V}_c)^- u_n \, ds \\ & = - \iint_{S^+} p \hat{n} \, ds - \iint_{S^-} p \hat{n} \, ds; \end{aligned}$$

hence, letting  $S^+$  and  $S^-$  approach  $s$  and noting that  $V^+$  and  $V^-$  vanish in the limit, while noting the arbitrariness in the choice of the integral over  $s$ , this equation becomes

$$\llbracket \rho \vec{V}_c (\vec{V}_c \cdot \hat{n} - u_n) \rrbracket + \llbracket p \rrbracket \hat{n} = 0. \quad (\text{A.32})$$

A development identical to that above, but applied to conservation of mass, leads to the Stokes-Christoffel condition (ref. 16, eq. 189.14), viz.,

$$\llbracket \rho (\vec{V}_c \cdot \hat{n} - u_n) \rrbracket = 0. \quad (\text{A.33})$$

This result may be used in conjunction with eq. (A.32) to obtain

$$\llbracket p \rrbracket \hat{n} - \rho^\pm U^\pm \llbracket \vec{V}_c \rrbracket = 0 \quad (\text{A.34})$$

where  $U$  is the speed of propagation of  $s$ :

$$U = u_n - \vec{V}_c \cdot \hat{n}.$$

Introducing the requirement that the pressure be continuous across the wake, viz., eq. (A.30), it follows from eq. (A.34) that

$$\rho^\pm U^\pm \llbracket \vec{V}_c \rrbracket = 0 \text{ on } W.$$

From eqs. (A.34) and (A.30) it follows that only the tangential component of velocity can be discontinuous across the wake surface, viz.,

$$\llbracket \vec{V}_c \cdot \hat{n} \rrbracket = 0 \text{ on } W$$

and

$$\llbracket \vec{V}_c \cdot \hat{t} \rrbracket \neq 0 \text{ on } W$$

where  $\hat{t}$  is an arbitrary unit vector tangent to the wake surface. These equations also show that the discontinuity in tangential component of flow must vanish unless the speed of propagation vanishes at either side of the wake surface; hence,

$$\rho^\pm u_n = (\rho \vec{V}_c)^\pm \cdot \hat{n} \text{ on } W. \quad (\text{A.35})$$

Eq. (A.35) is an analytical statement of the requirement which must be satisfied for the wake surface to be a material surface.

Let Bernoulli's integral, i.e., eq. (A.11), be evaluated at either side of the wake surface and form the difference of the two resulting integrals to obtain

$$\left[ \frac{\partial \phi}{\partial t} \right] + \vec{U}_0 \cdot \left[ \vec{\nabla} \phi \right] + \frac{1}{2} \left[ \vec{\nabla} \phi \cdot \vec{\nabla} \phi \right] = - \int_0^{p^+} dp/\rho + \int_0^{p^-} dp/\rho = - \int_0^{\llbracket p \rrbracket} dp/\rho$$

where  $p^+$  and  $p^-$  denote the pressure at either side of the wake surface. As a consequence of eq. (A.30), it follows that

$$\left[ \frac{\partial \phi}{\partial t} \right] + \vec{U}_0 \cdot \left[ \vec{\nabla} \phi \right] + \frac{1}{2} \left[ \vec{\nabla} \phi \cdot \vec{\nabla} \phi \right] = 0;$$

and, recognizing that

$$\frac{1}{2} (\vec{V}_c \cdot \vec{V}_c - \vec{U}_0 \cdot \vec{U}_0) = \vec{U}_0 \cdot \vec{\nabla} \phi + \frac{1}{2} \vec{\nabla} \phi \cdot \vec{\nabla} \phi,$$

Bernoulli's integral is found to lead to

$$\left[ \frac{\partial \phi}{\partial t} \right] + \frac{1}{2} \left[ \vec{V}_c \cdot \vec{V}_c \right] = 0 \text{ on } W. \quad (\text{A.36})$$

This condition must be satisfied if the wake surface is to be, simultaneously, a material surface and a surface of velocity discontinuity.

In the following the wake boundary condition shown by eq. (A.36) is developed into a partial differential equation governing the value of  $\llbracket \phi \rrbracket$  on the wake surface. This development follows a consideration of the kinematics of the fluid flow at the wake. To this end consider the two positions of the wake surface shown by fig. 48. One position is that of the wake surface at time  $t$ ; the other is its position a short interval of time,  $\Delta t$ , later. The two positions are denoted  $W(t)$  and  $W(t + \Delta t)$ .

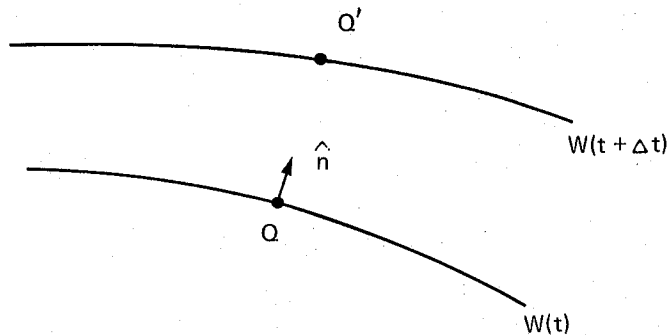


Figure 48. — Wake Surface Motion

The unit vector,  $\hat{n}$ , normal to  $W(t)$  at  $Q$  is directed at a surface point  $Q'$  of  $W(t + \Delta t)$ . Let  $Q$  have the compressibility system coordinates  $(x, y, z)$  and let the compressibility system coordinates of  $Q'$  be denoted as  $(x + \Delta x, y + \Delta y, z + \Delta z)$ . The quantities  $(\Delta x, \Delta y, \Delta z)$  represent the coordinate differences of the two surface points.

Let  $\Delta[\phi]$  denote the difference in the value of  $[\phi]$  at points  $Q$  and  $Q'$  so that

$$\begin{aligned} \frac{\Delta[\phi]}{\Delta t} &= \frac{[\phi]' - [\phi]}{\Delta t} \\ &= \frac{(\phi'^+ - \phi'^-) - (\phi^+ - \phi^-)}{\Delta t} \\ &= \frac{\phi'^+ - \phi^+}{\Delta t} - \frac{\phi'^- - \phi^-}{\Delta t} \\ &= [\Delta\phi/\Delta t] \end{aligned}$$

where the prime denotes evaluation at the point  $Q'$  while the absence of the prime denotes evaluation at the surface point  $Q$ . Taking the limit as  $\Delta t$  tends to zero leads to the result

$$\frac{\delta[\phi]}{\delta t} = \left[ \frac{\delta\phi}{\delta t} \right] \quad (\text{A.37})$$

where the operator  $\delta / \delta t$  denotes the time rate of change apparent to an observer moving with the component of velocity of the surface along its normal.

With  $\phi$  expressed as a function of the compressibility coordinates, the change in the value of  $\phi$  during the interval of time  $\Delta t$  is given by

$$\Delta\phi = \Delta t u_n \hat{n} \cdot \vec{\nabla}\phi + \frac{\partial\phi}{\partial t} \Delta t ;$$

hence, dividing by  $\Delta t$  and taking the limit as  $\Delta t$  tends to zero results in

$$\frac{\delta\phi}{\delta t} = u_n \hat{n} \cdot \vec{\nabla}\phi + \frac{\partial\phi}{\partial t} . \quad (\text{A.38})$$

Evaluating eq. (A.38) at either side of the wake surface and forming the difference of the two expressions yields

$$\left[ \frac{\delta\phi}{\delta t} \right] = u_n \hat{n} \cdot \left[ \vec{\nabla}\phi \right] + \left[ \frac{\partial\phi}{\partial t} \right] . \quad (\text{A.39})$$

Introducing eq. (A.37) into eq. (A.39) leads to

$$\frac{\delta}{\delta t} [\phi] = u_n \hat{n} \cdot \left[ \vec{\nabla}\phi \right] + \left[ \frac{\partial\phi}{\partial t} \right] . \quad (\text{A.40})$$

This result is called the kinematical condition of compatibility (ref. 16) and this condition must be satisfied if the discontinuity is to persist in time.

Noting that

$$\hat{n} \cdot \llbracket \vec{\nabla} \phi \rrbracket = \llbracket \hat{n} \cdot \vec{V}_c \rrbracket \quad (\text{A.41})$$

the requirement that the normal component of velocity be continuous leads to

$$\hat{n} \cdot \llbracket \vec{\nabla} \phi \rrbracket = 0$$

and the kinematical condition of compatibility given by eq. (A.40) reduces to

$$\frac{\delta}{\delta t} \llbracket \phi \rrbracket = \llbracket \frac{\partial \phi}{\partial t} \rrbracket \quad (\text{A.42})$$

on the wake surface. The wake boundary condition given by eq. (A.36), therefore, can be expressed as

$$\frac{\delta}{\delta t} \llbracket \phi \rrbracket + \frac{1}{2} \llbracket \vec{V}_c \cdot \vec{V}_c \rrbracket = 0 \text{ on } W. \quad (\text{A.43})$$

The objective, here, is to reduce the wake boundary condition to a partial differential equation in terms of the discontinuity in the velocity potential. The kinematical condition of compatibility shown by eq. (A.42) has accomplished this objective for the first term. The second term is expressed in the desired form by expressing  $\llbracket V_c^2 \rrbracket$  in terms of the average flow velocity at the wake surface, viz.,

$$\vec{V}_m = \frac{1}{2} (\vec{V}_c^+ + \vec{V}_c^-). \quad (\text{A.44})$$

Using this definition, deviation velocities at the wake may be defined as

$$\vec{q}^+ \equiv \vec{V}_c^+ - \vec{V}_m \text{ and } \vec{q}^- \equiv \vec{V}_c^- - \vec{V}_m \quad (\text{A.45})$$

with the result that

$$\vec{q}^+ = -\vec{q}^- \quad (\text{A.46})$$

The deviation velocities contain the wake velocity discontinuity; hence, the average flow velocity is continuous at the wake, i.e.,

$$\llbracket \vec{V}_m \rrbracket = 0 \text{ on } W; \quad (\text{A.47})$$

and it is tangent to the wake surface, i.e.,

$$\vec{V}_m \cdot \hat{n} = 0 \text{ on } W. \quad (\text{A.48})$$

Consider the second term in the wake boundary condition as shown by eq. (A.43) and apply the above conditions. Since

$$[[V_c^2]] = \vec{V}_c^+ \cdot \vec{V}_c^+ - \vec{V}_c^- \cdot \vec{V}_c^- \text{ on } W,$$

introducing eq. (A.44) leads to

$$[[V_c^2]] = V_m^2 + 2\vec{V}_m \cdot \vec{q}^+ + \vec{q}^+ \cdot \vec{q}^+ - V_m^2 - 2\vec{V}_m \cdot \vec{q}^- - \vec{q}^- \cdot \vec{q}^-;$$

and, because eq. (A.45) leads to

$$\vec{q}^- \cdot \vec{q}^- = \vec{q}^+ \cdot \vec{q}^+,$$

it follows that

$$[[V_c^2]] = 2\vec{V}_m \cdot [[\vec{q}]] \text{ on } W. \quad (\text{A.49})$$

Further, since

$$\vec{U}_0 + \vec{\nabla}\phi = \vec{V}_m + \vec{q},$$

then

$$[[\vec{q}]] = [[\vec{\nabla}\phi]].$$

It, therefore, follows that

$$[[V_c^2]] = 2\vec{V}_m \cdot [[\vec{\nabla}\phi]];$$

and, on applying Hadamard's lemma given by pp. 492 and 493, ref. 16, this result reduces to

$$[[V_c^2]] = 2\vec{V}_m \cdot \vec{\nabla}[\phi]. \quad (\text{A.50})$$

Finally, combining this result with eq. (A.43), the wake surface boundary condition is found as

$$\frac{\delta}{\delta t} [\phi] + \vec{V}_m \cdot \vec{\nabla} [\phi] = 0 \text{ on } W. \quad (\text{A.51})$$

This is the desired result: a partial differential equation governing  $[\phi]$  on  $W$ .

The wake surface is shown by eq. (A.51) to be a surface of convection on which the quantity  $[\phi]$  varies in time as a result of  $[\phi]$  being convected downstream with the mean flow velocity tangent to the wake surface,  $W$ . Given the wake location, the average flow velocity, and the value of  $[\phi]$  along the upstream edge of the wake, eq. (A.51) can be integrated to find the value of  $[\phi]$  at any point on the surface. The upstream edge of the wake surface is the trailing edge of a lifting surface. The spanwise value of  $[\phi]$  along this edge is known to be equal to the spanwise value of the circulation on the lifting surface (ref. 7, eq. 7-39). Eq. (A.51), therefore, does not represent an independent boundary condition. The flow conditions on the wake are completely determined by eq. (A.51) in conjunction with the flow equation and the independent boundary conditions on the aerodynamic surface.

## APPENDIX B

### APPROXIMATE LINEAR THEORY OF FLOW

#### B.1 INTRODUCTION

An approximate, linear theory of flow is formulated in this appendix starting from the fundamental postulate that all nonlinear terms of the flow equation, viz., eq.(A.17), are sufficiently small as to be negligible. This postulate reduces the flow equation to the following linear approximation:

$$\nabla^2 \phi = \frac{1}{c_0^2} \frac{D^2 \phi}{Dt^2}. \quad (\text{B.1})$$

Recall that the flow equation (for the case of irrotational flow) is equivalent to the following system of six equations (cf. app. A):

continuity,

$$\vec{\nabla} \cdot (\rho \vec{V}_c) = - \frac{\partial \rho}{\partial t}; \quad (\text{A.1a})$$

conservation of linear momentum,

$$\vec{V}_c \left( \frac{\partial \rho}{\partial t} + \vec{\nabla} \cdot (\rho \vec{V}_c) \right) + \rho \frac{d\vec{V}_c}{dt} + \vec{\nabla} p = 0; \quad (\text{A.2a})$$

conservation of energy,

$$\begin{aligned} & \left( e + \frac{1}{2} \vec{V}_c \cdot \vec{V}_c \right) \left( \frac{\partial \rho}{\partial t} + \vec{\nabla} \cdot (\rho \vec{V}_c) \right) + \rho \vec{V}_c \cdot \left( \frac{d\vec{V}_c}{dt} + \frac{1}{\rho} \vec{\nabla} p \right) \\ & + \rho \frac{de}{dt} + p \vec{\nabla} \cdot \vec{V}_c = 0; \end{aligned} \quad (\text{A.3a})$$

and the ideal gas relation,

$$\frac{de}{dt} = \frac{1}{\gamma-1} \frac{d}{dt} (p/\rho). \quad (\text{A.7})$$

Since the fundamental postulate is imposed on the exact flow equation, the approximations to each of the equations in this equivalent system of six equations are indeterminate; also, since both the aerodynamic surface and wake surface boundary conditions follow from the requirements of the laws of conservation of mass and linear momentum at those surfaces (cf. sec. A.4 and A.5), the approximate flow theory cannot be derived without choosing additional postulates which determine the approximations to those two conservation laws.†

The additional postulates are chosen assuming the unsteady flow to have a steady mean component so that the flow may be viewed as an unsteady small disturbance superimposed on a steady small disturbance flow. The additional postulates are chosen such that the steady mean component of the flow satisfies the boundary value problem of the linear, steady flow theory of ref. 1, summarized in sec. B.2. As shown in sec. B.2, the additional postulates are stated as approximations to two relations: (1) the relationship between mass density and velocity potential, viz.,

$$\rho = \rho(\phi),$$

and (2) the relationship between pressure and velocity potential, viz.,

$$p = p(\phi).$$

These approximate relations are chosen such that mass and linear momentum are conserved when there is no unsteady component of flow.

Consistent with these objectives, the unsteady flow is described by a velocity potential such that the unsteady flow velocity is given by

$$\vec{V}_c = \vec{U}_o + \vec{\nabla}(\phi_s + \phi_u) \quad (\text{B.2})$$

where  $\vec{U}_o$  is the velocity of the uniform freestream,  $\phi_u$  is the velocity potential of the unsteady small disturbance component of flow, and  $\phi_s$  is the velocity potential of the steady small disturbance component of flow.

## B.2 MEAN, STEADY COMPONENT OF FLOW

For the steady mean component of flow to be predicted by the theory of ref. 1 it must satisfy the following boundary value problem derived in sec. 3 of ref. 1:

Governing differential equation —

$$\vec{\nabla} \cdot \vec{W}_s = 0 \quad (\text{B.3})$$

where

$$\vec{W}_s = \rho_o (\vec{U}_o + \vec{w}_s) \quad (\text{B.4})$$

† This is a significant point and should be recognized as such. The additional postulates lead to the so-called "mass flux boundary conditions" and the use of the second order approximation to Bernoulli's integral to Euler's equations of motion.

and

$$\vec{w}_s = \vec{\nabla} \phi_s - M_o^2 (\phi_s)_x \hat{i};$$

whence, eq. (B.3) becomes

$$\nabla^2 \phi_s - M_o^2 (\phi_s)_{xx} = 0. \quad (B.5)$$

Aerodynamic surface boundary condition – (see eq. (A.23))

$$\vec{W}_s \cdot \hat{n}_s = 0 \text{ on } S_s \quad (B.6)$$

where, as shown by fig. 5,  $S_s$  denotes the steady mean location of the aerodynamic surface and  $\hat{n}_s$  is a unit vector normal to  $S_s$ .

Wake surface boundary condition – (see eqs. (A.30) and (A.35))

$$\vec{W}_s \cdot \hat{n}_s = 0 \text{ and } [C_{ps}] = 0 \text{ on } W_s \quad (B.7)$$

where, as shown by fig. 5,  $W_s$  denotes the steady mean location of the wake surface and

$$C_{ps} = \frac{p_s - p_o}{\frac{1}{2} \rho_o U_o^2}$$

$$= -\frac{1}{U_o^2} \left[ 2U_o (\phi_s)_x + \vec{\nabla}(\phi_s) \cdot \vec{\nabla}(\phi_s) - M_o^2 ((\phi_s)_x)^2 \right]. \quad (B.8)$$

Far field boundary condition –

$$\phi_s \rightarrow 0 \text{ as } \vec{R} \rightarrow \infty \quad (B.9)$$

where  $\vec{R}$  is the position of a field point relative to an arbitrarily chosen point on  $S_s$ .

As shown by ref. 1, when  $\phi_s$  satisfies eqs. (B.5), (B.6), (B.8), and (B.9), the steady mean flow has the following characteristics:

- (1) Mass is conserved because the continuity equation, (A.1a), is satisfied.
- (2) Conservation of linear momentum, eq. (A.2a), reduces to Euler's equations of motion, viz.,

$$\vec{W}_s \cdot \vec{\nabla}(\vec{U}_o + \vec{\nabla}\phi_s) + \vec{\nabla}p_s = 0, \quad (B.10)$$

because the continuity equation is satisfied.

- (3) Euler's equations of motion are satisfied when the pressure coefficient is approximated by eq. (B.8); and, therefore, Euler's momentum theorem holds, cf. ref. 14.
- (4) A solution to the linear flow equation (viz. eq. (B.5)) in the domain  $V$  surrounded by the closed surface  $\Sigma$  is uniquely determined if  $\phi_s$  and  $\vec{W}_s$  are uniquely specified on  $\Sigma$ .

Several additional characteristics of the flow are important to the purpose of the following section, i.e., the derivation of the unsteady flow theory. One of these characteristics is the approximation to the relation between mass density and velocity potential. That approximation is derived by expressing the continuity equation as

$$\vec{\nabla} \cdot \vec{\nabla}_c = -\frac{1}{\rho_s} \vec{\nabla}_c \cdot \vec{\nabla} \rho_s. \quad (\text{B.11})$$

This expression shows (cf. ref. 14, sec. 3 and 4) that the steady dilatation rate is proportional to the rate of convection of the fluid mass density. The steady dilatation rate is also evaluated by writing the flow equation (i.e., eq. (B.4)) as follows:

$$\vec{\nabla} \cdot \vec{\nabla}_c = M_0^2 (\phi_s)_{xx}$$

These two expressions for dilatation rate combine to express the rate of mass density convection as follows:

$$\frac{1}{\rho_s} \vec{\nabla}_c \cdot \vec{\nabla} \rho_s \approx -M_0^2 (\phi_s)_{xx} \quad (\text{B.12})$$

This result can be expressed in terms of the disturbance mass density, viz.,

$$\rho_s' = \rho_s - \rho_0, \quad (\text{B.13})$$

and that expression appears as

$$-M_0^2 (\phi_s)_{xx} = \frac{1}{\rho_0} (1 - \rho_s'/\rho_0 + \dots) (\vec{U}_0 + \vec{\nabla} \phi_s) \cdot \vec{\nabla} \rho_s'$$

where the series is the result of a binomial expansion. The order of magnitude of the disturbance mass density is evaluated from this expression to find

$$\rho_s'/\rho_0 = O(\phi_s/U_0);$$

thus, to a first order approximation

$$-M_0^2 (\phi_s)_{xx} \approx \frac{1}{\rho_0} \vec{U}_0 \cdot \vec{\nabla} \rho_s. \quad (\text{B.14})$$

Writing eq. (B.14) as

$$\left( \rho_s + \rho_o \frac{M_o^2}{U_o} (\phi_s)_x \right)_x \approx 0,$$

integrating with respect to  $x$ , and evaluating the constant of integration in the freestream, the desired approximation to the relation between the flow mass density and velocity is found to be as follows:

$$\rho_s \approx \rho_o \left( 1 - \frac{M_o^2}{U_o} (\phi_s)_x \right). \quad (\text{B.15})$$

Substituting this approximation into the expression for mass flux, viz.,

$$\vec{W}_s = \rho_s (\vec{U}_o + \vec{\nabla} \phi_s),$$

and neglecting terms of second order in  $\phi_s$  leads to the approximate mass flux vector shown by eq. (B.4); hence, eq. (B.15) is consistent with the theory of ref. 1.

The derivation of the unsteady flow theory also requires an evaluation of the order of magnitude of the disturbance pressure. That evaluation follows from the law of conservation of energy (viz., eq. (A.3a)) and the ideal gas relation (viz., eq. (A.4)). Since both mass and linear momentum are conserved, conservation of energy (i.e., eq. (A.3a)) reduces to the usual energy equation, viz.,

$$\vec{W}_s \cdot \vec{\nabla} e_s + p_s \vec{\nabla} \cdot \vec{V}_c = 0. \quad (\text{B.16})$$

As a consequence, the energy equation can be combined with the ideal gas relation to find the isentropic pressure-density relation, cf. app. A.,

$$(p_s/p_o) = (\rho_s/\rho_o)^\gamma. \quad (\text{A.8})$$

The isentropic pressure-density relation is now expanded in a Taylor series about the freestream conditions to find

$$\frac{p_s - p_o}{\rho_o} \approx c_o^2 \left( \frac{\rho_s - \rho_o}{\rho_o} \right) + \frac{1}{2} (\gamma-1) c_o^2 \left( \frac{\rho_s - \rho_o}{\rho_o} \right)^2 + \dots$$

where

$$c_o^2 = (dp/d\rho)_o = \gamma (p_o/\rho_o).$$

On neglecting terms which are shown by eq. (B.15) to be second and higher order in  $\phi_s$ , a first order approximation is found, viz.,

$$\frac{p_s - p_o}{\rho_o} \approx c_o^2 \left( \frac{\rho_s - \rho_o}{\rho_o} \right). \quad (\text{B.17})$$

Combining eq. (B.17) with eq. (B.15), the order of magnitude of the disturbance pressure is found to be given by

$$p_s - p_o = \rho_o c_o^2 \phi_s / U_o. \quad (\text{B.18})$$

### B.3 UNSTEADY FLOW APPROXIMATIONS

Approximations for the unsteady flow theory, which are consistent with the approximations of the preceding, are deduced by following the procedure leading to eqs. (B.15) and (B.18). The continuity equation is expressed in terms of the divergence of the mass flux, i.e.,

$$\vec{\nabla} \cdot (\rho \vec{V}_c) = - \frac{\partial \rho}{\partial t}; \quad (\text{A.1})$$

and an unsteady disturbance mass flux is deduced by writing the mass flux in terms of steady and unsteady components, viz.,

$$\rho \vec{V}_c = \vec{W}_s + \vec{w}_u, \quad (\text{B.19})$$

so that the continuity equation becomes

$$\vec{\nabla} \cdot (\vec{w}_u) = - \frac{\partial \rho}{\partial t} \quad (\text{B.20})$$

because the steady flow component satisfies the continuity equation, i.e.,

$$\vec{\nabla} \cdot \vec{W}_s = 0.$$

The unsteady flow equation, i.e., eq. (B.1), is now written as follows:

$$\vec{\nabla} \cdot \left( \vec{\nabla} \phi_u - \frac{M_o^2}{U_o} \frac{D}{Dt} (\phi_u) \hat{i} \right) = \left( \frac{M_o}{U_o} \right)^2 \frac{\partial}{\partial t} \left( \frac{D}{Dt} (\phi_u) \right).$$

Comparing this form with eq. (B.20), the following hypothesis is asserted:

$$\vec{w}_u \approx \rho_o \left( \vec{\nabla} \phi_u - \hat{i} \frac{M_o^2}{U_o} \frac{D}{Dt} (\phi_u) \right) \quad (\text{B.21})$$

and

$$\frac{\partial \rho}{\partial t} \approx - \left( \frac{M_o}{U_o} \right)^2 \frac{\partial}{\partial t} \left( \frac{D}{Dt} (\phi_u) \right) \quad (B.22)$$

On integrating eq. (B.22) with respect to time, the unsteady mass density is found to be given by the following:

$$\rho \approx - \rho_o \left( \frac{M_o}{U_o} \right)^2 \frac{D}{Dt} (\phi_u) + \rho_s \quad (B.23)$$

As a test of the validity of the above hypothesis, consider  $\phi_u$  to be independent of time. The disturbance mass flux approximation shown by eq. (B.21) then reduces to that of the steady flow theory, viz., that shown by eq. (B.4); also, the disturbance mass density approximation shown by eq. (B.23) reduces to that of the steady flow theory shown by eq. (B.15). The hypothesis therefore is seen to be consistent with the steady flow theory of ref. 1.

For the purpose of deducing an approximation to the unsteady pressure coefficient, recall Bernoulli's integral to Euler's equations of motion, viz.,

$$\frac{D\phi}{Dt} + \frac{1}{2} \vec{\nabla} \phi \cdot \vec{\nabla} \phi + \int_{p_o}^p \frac{dp}{\rho} = 0 \quad (A.11)$$

Assuming that Euler's equations of motion are satisfied at least to a first order approximation, the isentropic pressure-density relation can be expressed as follows:

$$\left( \frac{p - p_o}{\rho_o} \right) = c_o^2 \left( \frac{\rho - \rho_o}{\rho_o} \right) + \frac{1}{2} (\gamma - 1) c_o^2 \left( \frac{\rho - \rho_o}{\rho_o} \right)^2 + \dots \quad (B.24)$$

Substituting eq. (B.24) into eq. (A.11), the integral with respect to pressure is evaluated to find

$$\int_{p_o}^p \frac{dp}{\rho} = \left( \frac{p - p_o}{\rho_o} \right) - \frac{1}{2 c_o^2} \left( \frac{p - p_o}{\rho_o} \right)^2 + \dots \quad (B.25)$$

Bernoulli's integral, in terms of this series, is inverted by letting

$$\frac{p - p_0}{\rho_0} = \sum_{n=1}^{\infty} a_n (f(\phi))^n \quad (\text{B.26})$$

where

$$f(\phi) = \frac{D\phi}{Dt} + \frac{1}{2} \vec{\nabla}\phi \cdot \vec{\nabla}\phi$$

and evaluating the coefficients  $a_n$  using the uniqueness property of the power series. The result of substituting those coefficients into eq. (B.26) provides the desired result, namely,

$$\frac{p - p_0}{\rho_0} = - \left( \frac{D\phi}{Dt} + \frac{1}{2} \vec{\nabla}\phi \cdot \vec{\nabla}\phi \right) + \frac{1}{2c_0^2} \left( \frac{D\phi}{Dt} + \frac{1}{2} \vec{\nabla}\phi \cdot \vec{\nabla}\phi \right)^2 + \dots$$

Introducing  $\phi = \phi_s + \phi_u$  and neglecting terms which are of second order in  $\phi_u$ , the unsteady disturbance pressure is found by subtracting eq. (B.8). The result is the following approximation to Bernoulli's integral:

$$\frac{p - p_s}{\rho_0} \approx - \left[ \left( 1 - \frac{M_0^2}{U_0} (\phi_s)_x \right) (\phi_u)_t + \left( \vec{U}_0 + \vec{\nabla}\phi_s - M_0^2 (\phi_s)_{xx} \hat{i} \right) \cdot \vec{\nabla}(\phi_u) \right] \quad (\text{B.27})$$

which, by reference to eqs. (B.4) and (B.15), can be expressed as

$$p - p_s \approx - \left( \rho_s (\phi_u)_t + \vec{W}_s \cdot \vec{\nabla}(\phi_u) \right) \quad (\text{B.28})$$

Comparing eq. (B.28) with the usual approximation of linear, unsteady flow theory, viz.,

$$p - p_s \approx - \left( \rho_0 (\phi_u)_t + \rho_0 U_0 (\phi_u)_x \right) \quad (\text{B.29})$$

the freestream values of the mass density and the mass flux are seen to be replaced in the present theory by the values of those quantities evaluated in the steady mean component of flow. As a point of information which should be recognized, eq. (B.28) represents an approximation to Bernoulli's integral to Euler's equations of motion. In the present context Euler's equations of motion are approximated. Equation (B.28) therefore is the appropriate approximation for evaluating aerodynamic forces at the boundaries of a flow; however, if the pressure is viewed as one of the flow parameters, then the pressure is related to the velocity potential by eq. (B.24) truncated as

$$\left( \frac{p - p_0}{\rho_0} \right) \approx c_0^2 \left( \frac{\rho - \rho_0}{\rho_0} \right)$$

and eq. (B.23) expressed in terms of the total disturbance density, i.e.,

$$\frac{\rho - \rho_0}{\rho_0} \approx -\frac{M_0^2}{U_0^2} \frac{D\phi}{Dt} \quad (\text{B.30})$$

Combining these two expressions leads to the expression for the unsteady pressure evaluated as a parameter of the flow, viz.,

$$\frac{p - p_0}{\rho_0} \approx -\frac{D\phi}{Dt}$$

This result is identical with eq. (B.29) (i.e., the usual approximation of linear, unsteady flow theory), and this is the expected result in view of the fundamental postulate of the approximate theory, namely, that terms, having an order of magnitude smaller than  $O(\phi/U_0)$ , are neglected in the governing differential equations. Because of the fundamental postulate, Euler's equations of motion are represented only to a linear, first order approximation in  $(\phi / U_0)$ ; products of  $\phi_s$  and  $\phi_u$  appear in eq. (B.28) only because eq. (B.28) is an integral to a linear system of equations in which  $\phi_s$  appears as a parameter.

#### B.4 AERODYNAMIC SURFACE BOUNDARY CONDITION APPROXIMATION

The aerodynamic surface boundary condition, which was derived in app. A, states the following requirement: Fluid particles located at the aerodynamic surface  $S$  must have a motion satisfying eq. (A.21), viz.

$$\rho u_n = \vec{W} \cdot \hat{n} \quad (\text{A.21})$$

An approximate form of this equation is now derived for the case of unsteady, small disturbances from a steady mean flow.

The unsteady flow is a consequence of a small, unsteady disturbance motion of the surface  $S$  relative to its steady mean location  $S_s$ , fig. 49. A point  $P$  on  $S$  has position  $\vec{R}$  and becomes the point  $Q$  on  $S_s$  with position  $\vec{R}_s$  when the unsteady motion ceases. The point  $Q$  is said to be undergoing a displacement, i.e., a change in position, computed as follows:

$$\vec{D} = \vec{R} - \vec{R}_s \quad (\text{B.31})$$

The displacement of points on  $S_s$  are assumed to be sufficiently small that the value of a flow parameter evaluated at  $P$  can be approximated by a truncated Taylor series expansion about  $Q$ , e.g.,

$$\phi(P, t) \approx \phi(Q, t) + (\vec{\nabla}\phi)_Q \cdot \vec{D}. \quad (\text{B.32})$$

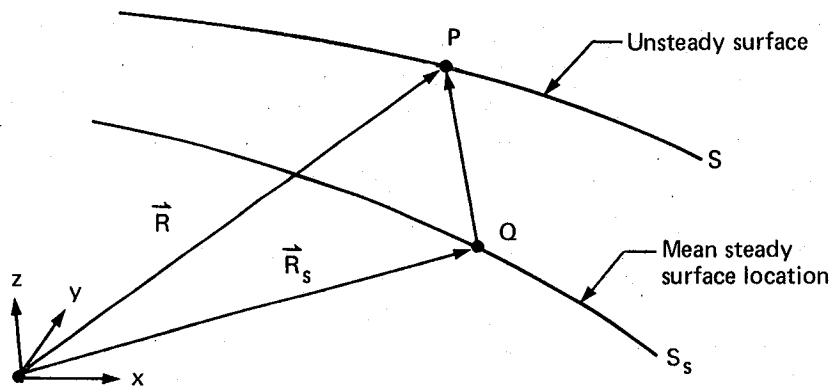


Figure 49. – Unsteady Surface Displacement

The velocity of the point  $P$  relative to the point  $Q$  is given by

$$\vec{u} = \frac{\partial \vec{D}}{\partial t} \quad (\text{B.33})$$

and the unsteadiness of the motion is assumed to be such that its Fourier representation has a reduced frequency band whose upper bound has the order of magnitude unity or less. As a consequence, the velocity of a surface point, when normalized by the freestream velocity, has an order of magnitude which is equal to or less than that of its displacement. Further, because of the assumed small displacement, the rotation of the surface at point  $P$  may be linearly approximated, viz.,

$$\vec{\theta} \approx \frac{1}{2} \vec{\nabla} \times \vec{D}; \quad (\text{B.34})$$

and the unit vector normal to  $S$  may be approximated, viz.,

$$\hat{n} \approx \frac{\hat{n}_s + \vec{\theta} \times \hat{n}_s}{|\hat{n}_s + \vec{\theta} \times \hat{n}_s|} \approx \hat{n}_s + \vec{\theta} \times \hat{n}_s. \quad (\text{B.35})$$

In turn, the normal component of surface velocity is approximated as follows:

$$u_n = \hat{n} \cdot \frac{\partial \vec{D}}{\partial t} \approx \hat{n}_s \cdot \frac{\partial \vec{D}}{\partial t} \quad (\text{B.36})$$

Substituting eqs. (B.35) and (B.36) into eq. (A.21), the surface boundary condition is approximated as follows:

$$\rho u_n \approx \vec{W} \cdot (\hat{n}_s + \vec{\theta} \times \hat{n}_s) \text{ on } S.$$

Introducing eqs. (B.19) and (B.23), this result becomes

$$(\rho_u + \rho_s) u_n \approx (\vec{W}_s + \vec{w}_u) \cdot (\hat{n}_s + \vec{\theta} \times \hat{n}_s) \text{ on } S \quad (\text{B.37})$$

where

$$\rho_u \approx -\rho_o \frac{M_o^2}{U_o^2} \frac{D\phi_u}{Dt}$$

The truncated expansion of the flow parameters, cf. eq. (B.32), leads to an expression evaluated on the steady mean surface, viz.,

$$\rho_s u_n \approx \vec{W}_s \cdot (\hat{n}_s + \vec{\theta} \times \hat{n}_s) + (\vec{D} \cdot \vec{\nabla} \vec{W}_s) \cdot \hat{n}_s + \vec{w}_u \cdot \hat{n}_s \text{ on } S_s$$

where all nonlinear terms involving unsteady quantities are neglected as small; further, as a consequence of eq. (B.6), the unsteady disturbance mass flux is found to be required to satisfy the following boundary condition on the steady mean surface:

$$\vec{w}_u \cdot \hat{n}_s \approx -\vec{W}_s \cdot (\vec{\theta} \times \hat{n}_s) - (\vec{D} \cdot \vec{\nabla} \vec{W}_s) \cdot \hat{n}_s + \rho_s u_n \text{ on } S_s \quad (\text{B.38})$$

where

$$\vec{w}_u \approx \rho_o \left( \vec{\nabla} \phi_u - \frac{M_o^2}{U_o} \frac{D}{Dt} (\phi_u) \hat{i} \right), \quad (\text{B.21})$$

$$\vec{W}_s \approx \rho_o \left( U_o \hat{i} + \vec{\nabla} \phi_s - M_o^2 (\phi_s)_x \hat{i} \right), \text{ and} \quad (\text{B.4})$$

$$\rho_s \approx \rho_o \left( 1 - \frac{M_o^2}{U_o} (\phi_s)_x \right). \quad (\text{B.15})$$

## B.5 WAKE SURFACE BOUNDARY CONDITION APPROXIMATION

The jump in potential across the wake surface is represented by a doublet sheet; hence, the wake boundary condition, i.e., eq. (A.51), is expressed as follows:

$$\frac{\delta\mu}{\delta t} + \vec{V}_m \cdot \vec{\nabla}\mu = 0 \text{ on } W \quad (\text{B.39})$$

where

$$\mu = \llbracket \phi \rrbracket \quad (\text{B.40})$$

is the strength of the doublet sheet. If eq. (B.39) is multiplied by the flow mass density, the boundary condition is an expression in terms of mass flux, i.e.,

$$\rho \frac{\delta\mu}{\delta t} + \vec{W}_m \cdot \vec{\nabla}\mu = 0 \text{ on } W. \quad (\text{B.41})$$

This result follows from continuity of pressure across the wake surface, i.e.

$$\llbracket p \rrbracket = 0 \text{ on } W, \quad (\text{A.30})$$

and the isentropic pressure-density relation, i.e., eq. (A.8); whereby,

$$\llbracket \rho \rrbracket = 0 \text{ on } W$$

so that the average mass density across  $W$  is equal to the mass density at either side of the wake.

The flow parameters appearing in eq. (B.41) and evaluated at a point  $P$  on  $W$  can be expressed by a Taylor series expansion about the steady mean location of  $P$  on  $W_s$ . The result appears as follows:

$$\begin{aligned} & \left( \rho + \vec{D} \cdot \vec{\nabla}\rho + \dots \right) \left( \frac{\partial\mu}{\partial t} + \frac{\partial\vec{D}}{\partial t} \cdot \vec{\nabla}\mu + \vec{D} \cdot \vec{\nabla} \frac{\partial\mu}{\partial t} + \dots \right) \\ & + \left( \vec{W}_m + \vec{D} \cdot \vec{\nabla}\vec{W}_m + \dots \right) \cdot \vec{\nabla} \left( \mu + \vec{D} \cdot \vec{\nabla}\mu + \dots \right) = 0 \text{ on } W_s. \end{aligned}$$

Introducing

$$\rho = \rho_u + \rho_s, \quad \vec{W}_m = (\vec{W}_s)_m + (\vec{w}_u)_m, \quad \text{and} \quad \mu = \mu_s + \mu_u$$

and noting that  $\mu_s$  satisfies the steady mean wake boundary condition, viz., eq. (B.7), after deleting products of unsteady quantities, the unsteady wake boundary condition is expressed as follows:

$$\rho_s \frac{\partial \mu_u}{\partial t} + \left( \vec{W}_s \right)_m \cdot \vec{\nabla} \mu_u = 0 \text{ on } W_s. \quad (\text{B.42})$$

Recalling eq. (B.40) and comparing eq. (B.42) with eq. (B.28), the unsteady wake boundary condition, as approximated by eq. (B.42), imposes the requirement that the approximate disturbance pressure be continuous across the wake. The approximation shown by eq. (B.42) is therefore consistent with the approximation for pressure.

## APPENDIX C

### DERIVATION OF INTEGRAL EQUATION FORMULATION OF THE UNSTEADY FLOW PROBLEM

The objectives of this appendix are twofold. The first objective is to provide a derivation of the integral equation which is shown as eq. (38). The second objective is to express that integral equation in terms of panel integrals by introducing a change of variable and a coordinate transformation. These panel integrals are evaluated by the methods of app. D to generate the unsteady aerodynamic influence coefficients which appear in sec. 3.4

In sec. C.1 the unsteady flow equation, shown as eq. (30), is shown to be identical in form with a particular form of Helmholtz's equation. This form of Helmholtz's equation follows from the application of the Prandtl-Glauert transformation to Helmholtz's equation when it is expressed in rectangular Cartesian coordinates. The application is such that two units of measure for distance are introduced into the formulation. One of these is the measure associated with the rectangular Cartesian coordinates of Helmholtz's equation; the second is that of the compressibility coordinate system in which the flow problem is defined. †

Section C.2 introduces the theorems of Helmholtz which provide an integral equation satisfying Helmholtz's equation. The integral equation is expressed in invariant form such that it can be expanded in terms of any coordinate system related to a rectangular Cartesian reference frame by an admissible transformation of coordinates. The Prandtl-Glauert transformation is admissible; and, in sec. C.3, the form of the integral equation satisfying the flow equation is derived. This derivation includes the definition of the conormal of the surface of integration.

Section C.4 delineates the line vortex integrals which arise at the perimeter of a surface having a doublet distribution.

Section C.5 introduces a change of variables for the integral equation. The operation provides a form for the integrals allowing them to be made independent of the compressibility factor,  $\beta$ .

Section C.6 derives the transformation from the compressibility coordinate system to the local coordinate system for each panel. Applying this transformation to the integral equations provides the panel integrals which are evaluated in app. D.

#### C.1 PRANDTL-GLAUERT TRANSFORMATION

The Prandtl-Glauert transformation is used in the following to relate solutions to Helmholtz's equation with solutions to the unsteady flow equation, eq. (30). Using indicial notation and summation convention (ref. 5, sec. 7), the transformation is expressed as follows:

$$\bar{x}^i = E_j^i x^j \quad (C.1)$$

† This distinction in measure and its consequence, viz., the introduction of two different unit vectors which are both normal to the same surface, tends to cause confusion in following the development of the panel method; it should be carefully noted.

where the compressibility coordinates are denoted as

$$x^1 = x, x^2 = y, x^3 = z \quad (\text{C.2})$$

and

$$E_1^1 = 1, E_2^2 = \beta, E_3^3 = \beta, E_j^i = 0 \text{ otherwise}; \quad (\text{C.3})$$

and the Prandtl-Glauert transformation is introduced choosing the  $\bar{x}^i$  system as the reference frame (ref. 5, pg 8). The metric tensor (ref. 5, sec. 29) of the compressibility system, therefore, is given by

$$g_{ij} = \frac{\partial \bar{x}^k}{\partial x^i} \frac{\partial \bar{x}^k}{\partial x^j} \quad (\text{C.4})$$

where, by eq. (C.3),

$$g_{11} = 1, g_{22} = \beta^2, g_{33} = \beta^2, g_{ij} = 0 \text{ otherwise}; \quad (\text{C.5})$$

while, its contravariant form (ref. 5, sec. 30), viz.,

$$g^{ij} = \frac{G^{ij}}{g} \quad (\text{C.6})$$

where  $G^{ij}$  are the cofactors of  $g_{ij}$  and  $g$  is the determinant of  $g_{ij}$ ,

$$g \equiv |g_{ij}|, \quad (\text{C.7})$$

has the components

$$g^{11} = 1, g^{22} = 1/\beta^2, g^{33} = 1/\beta^2, g^{ij} = 0 \text{ otherwise}. \quad (\text{C.8})$$

Helmholtz's equation (ref. 3, pg. 239), viz.,

$$\nabla^2 \phi^* + \Omega^2 \phi^* = 0, \quad (\text{C.9})$$

is expressed in terms of the contravariant metric tensor, eq. (C.6), by introducing the following identity (ref. 5, eq. (90.7)):

$$\nabla^2 \phi^* = g^{ij} \phi^*_{,ij} \quad (\text{C.10})$$

where (ref. 5, sec. 33) the comma denotes covariant differentiation. For the case of linear transformations, such as the Prandtl-Glauert transformation, covariant differentiation reduces to partial differentiation; hence,

$$\phi^{*,ij} = \frac{\partial^2 \phi^*}{\partial x^i \partial x^j} \quad (C.11)$$

Substituting eq. (C.11) into eq. (C.10) and substituting the result into eq. (C.9), Helmholtz's equation becomes

$$g^{ij} \frac{\partial^2 \phi^*}{\partial x^i \partial x^j} + \Omega^2 \phi^* = 0; \quad (C.12)$$

and, introducing eq. (C.2) and eq. (C.8), this form of Helmholtz's equation is expressed as

$$\phi_{xx}^* + \frac{1}{\beta^2} (\phi_{yy}^* + \phi_{zz}^*) + \Omega^2 \phi^* = 0. \quad (C.13)$$

Helmholtz's equation, as given by eq. (C.13), when multiplied by  $\beta^2$ , is identical with the unsteady flow equation, eq. (30). As a consequence of this identity, solutions to Helmholtz's equation expressed in the compressibility coordinate system (regarding the scaled coordinates,  $\bar{x}^1$ , as the reference frame) are solutions to the unsteady flow equation.

In the scaled coordinates,  $\bar{x}^1$ , Helmholtz's equation appears as follows:

$$\frac{\partial^2 \bar{\phi}^*}{\partial \bar{x}^k \partial \bar{x}^k} + \Omega^2 \bar{\phi}^* = 0; \quad (C.14)$$

or, letting

$$\bar{x} = \bar{x}^1, \bar{y} = \bar{x}^2, \bar{z} = \bar{x}^3, \quad (C.15)$$

Helmholtz's equation becomes

$$\bar{\phi}_{\bar{x}\bar{x}}^* + \bar{\phi}_{\bar{y}\bar{y}}^* + \bar{\phi}_{\bar{z}\bar{z}}^* + \Omega^2 \bar{\phi}^* = 0. \quad (C.16)$$

If

$$\bar{\phi}^*(\bar{x}, \bar{y}, \bar{z}) = \bar{\phi}^*(x, \beta y, \beta z) = \phi^*(x, y, z) \quad (C.17)$$

where  $\bar{\phi}^*$  is a solution to eq. (C.14), then, on substituting eq. (C.17) into eq. (C.14), the chain rule for differentiation leads to

$$\frac{\partial^2 \phi^*}{\partial x^i \partial x^j} \frac{\partial x^i}{\partial \bar{x}^k} \frac{\partial x^j}{\partial \bar{x}^k} + \Omega^2 \phi^* = 0. \quad (C.18)$$

Introducing the inverse Prandtl-Glauert transformation, viz.,

$$x^i = \epsilon_j^i \bar{x}^j \quad (C.19)$$

where

$$\epsilon_1^1 = 1, \epsilon_2^2 = 1/\beta, \epsilon_3^3 = 1/\beta, \epsilon_j^i = 0 \text{ otherwise,} \quad (C.20)$$

eq. (C.18) becomes eq. (C.13); hence, if  $\bar{\phi}^*$  is a solution to Helmholtz's equation expressed in the scaled coordinates regarded as the reference frame, the change of variables shown by eq. (C.17) provides a solution to the unsteady flow equation.

## C.2 HELMHOLTZ'S THEOREMS

Solutions to Helmholtz's equation are provided by the theorems of Helmholtz which appear in the following. Since the preceding has shown that solutions to Helmholtz's equation can be related to solutions of the unsteady flow equation by the Prandtl-Glauert transformation, the following theorems provide a means for constructing solutions to the unsteady flow problem.

Helmholtz's theorems (ref. 3, pg. 240) are based on a division of all space into two volumes  $V$  and  $V'$  by the closed surface  $\Sigma$  enclosing  $V$ ; thus,  $P$ , an arbitrary point in space, is either interior to  $\Sigma$  (i.e.,  $P \in V$ ) or exterior to  $\Sigma$  (i.e.,  $P \in V'$ ) or on  $\Sigma$  (i.e.,  $P \in \Sigma$ ). Letting

$$\psi^* = - \frac{1}{4\pi R} e^{-i\Omega R} \quad (C.21)$$

where  $R$  is the distance from  $P$  to a point  $Q$  on  $\Sigma$  and noting that eq. (C.21) satisfies eq. (C.12), then, if  $\phi^*$  is a second solution, the first theorem of Helmholtz states that

$$\begin{aligned} \phi^*(P) &= \iint_{\Sigma} \left( \frac{\partial \phi^*}{\partial n'} (Q^+) \psi^* - \phi^*(Q^+) \frac{\partial \psi^*}{\partial n'} \right) ds' \text{ if } P \in V \\ \phi^*(P) &= 0 \text{ if } P \in V' \\ \phi^*(P) &= \infty \text{ if } P \in \Sigma \end{aligned} \quad (C.22)$$

where  $\phi^* (Q^+)$  denotes the limiting value of  $\phi^*$  as the point of evaluation approaches Q from V,  $n'$  is the normal coordinate of  $\Sigma$  and is positive in V, and the prime denotes operations involving the coordinates of Q. The second theorem states that

$$\begin{aligned}\phi^* (P) &= - \iint_{\Sigma} \left( \frac{\partial \phi^*}{\partial n'} (Q^-) \psi^* - \phi^* (Q^-) \frac{\partial \psi^*}{\partial n'} \right) ds \text{ if } P \in V' \\ &= 0 \text{ if } P \in V \\ &= \infty \text{ if } P \in \Sigma\end{aligned}\tag{C.23}$$

where  $\phi^* (Q^-)$  denotes the limiting value of  $\phi^*$  as the point of evaluation approaches Q from V'.

Combining eqs. (C.22) and (C.23) leads to a third theorem:

$$\phi^* (P) = \iint_{\Sigma} \left( \left[ \frac{\partial \phi^*}{\partial n'} \right] \psi^* - \llbracket \phi^* \rrbracket \frac{\partial \psi^*}{\partial n'} \right) ds' \text{ if } P \in V' \cup V\tag{C.24}$$

where, for example,

$$\llbracket \phi^* \rrbracket \equiv \phi^* (Q^+) - \phi^* (Q^-)\tag{C.25}$$

because  $\phi^*$  and  $\partial \phi^* / \partial n'$  are not finite at the surface. The elementary source,  $\psi^*$ , leads to a discontinuous normal derivative for the potential; while the elementary doublet,  $\partial \psi^* / \partial n'$ , leads to a discontinuous potential. Noting that  $\phi^*$  and  $\partial \phi^* / \partial n'$  represent, respectively, the complex amplitudes of the potentials induced by unit sources and unit doublets distributed on  $\Sigma$ , one may define

$$\sigma^* (Q) \equiv \left[ \frac{\partial \phi^*}{\partial n'} \right]\tag{C.26}$$

and

$$\mu^* (Q) = \llbracket \phi^* \rrbracket\tag{C.27}$$

so that

$$\phi^* (P) = \phi_S^* (P) + \phi_D^* (P)\tag{C.28}$$

where

$$\phi_S^*(P) \equiv \iint_{\Sigma} \sigma^* \psi^* ds' \quad (\text{C.29})$$

and

$$\phi_D^*(P) \equiv - \iint_{\Sigma} \mu^* \frac{\partial \psi^*}{\partial n'} ds' \quad (\text{C.30})$$

Further, the complex amplitude of induced velocity can be expressed as

$$\vec{v}^*(P) = \vec{\nabla} \phi^* = \vec{v}_S^*(P) + \vec{v}_D^*(P) \quad (\text{C.31})$$

where

$$\vec{v}_S^*(P) = - \iint_{\Sigma} \sigma^* \vec{\nabla}' \psi^* ds' \quad (\text{C.32})$$

and

$$\vec{v}_D^*(P) = \iint_{\Sigma} \mu^* \vec{\nabla}' \frac{\partial \psi^*}{\partial n'} ds' \quad (\text{C.33})$$

because

$$\vec{\nabla} \psi^* = - \vec{\nabla}' \psi^* \quad (\text{C.34})$$

where the prime denotes differentiation with respect to the coordinates of the point Q, while the unprimed gradient operator denotes differentiation with respect to the coordinates of the point P.

Eqs. (C.28) through (C.33) describe the complex amplitudes of the potential and velocity induced at the field point P by harmonically fluxuating sources and doublets distributed on the closed surface  $\Sigma$ . These induced quantities satisfy the form of Helmholtz's equation shown by eq (C.12); and, eqs. (C.28) through (C.33), like eq. (C.12), are valid in terms of any coordinate system which is the result of an admissible transformation (ref. 5, sec. 19 and 20) from the reference frame. The reference frame has been chosen, in sec. C.1, to be the scaled coordinates,  $\bar{x}^i$ .

### C.3 CONORMAL VECTOR

As noted in the preceding section, the integral equation, i.e., eq. (C.24), which provides a means for evaluating the unsteady flow problem, is expressed in terms of geometric quantities whose measure is that of the scaled coordinates,  $\bar{x}^i$ . This use of measure is illustrated by writing

$$\frac{\partial \phi^*}{\partial n} ds = \hat{n} \cdot \vec{\nabla} \phi^* ds \quad (C.35)$$

where the magnitude of  $\hat{n}$  is unity in the measure of the scaled coordinates and  $ds$  is the differential surface element in the scaled coordinates. The objective of this section is to derive the following identity:

$$\hat{n} \cdot \vec{\nabla} \phi^* ds = \vec{n}_c \cdot \vec{\nabla} \phi^* dS \quad (C.36)$$

where  $\vec{n}_c$  is the conormal vector with components

$$\left( \beta^2 N_1, N_2, N_3 \right),$$

where the components of  $\vec{N}$  satisfy

$$\sqrt{(N_1)^2 + (N_2)^2 + (N_3)^2} = 1 \quad (C.37)$$

in the measure of the compressibility coordinates,  $x^i$ , and  $dS$  is the differential surface element in the compressibility coordinates. The vectors,  $\hat{n}$  and  $\vec{N}$ , are both normal to the same surface; hence, when they are evaluated at the same surface point,

$$\hat{n} = \vec{N}/N \quad (C.38)$$

where  $N$  is the magnitude of  $\vec{N}$  in the measure of the scaled coordinates,  $\bar{x}^i$ . Further, the two differential surface elements are shown to be related as

$$dS = N \sqrt{g} ds. \quad (C.39)$$

As a preliminary to the derivation, consider the reciprocal base systems (ref. 5, sec. 45). In the reference frame, again, taken to be the scaled coordinates,  $\bar{x}^i$ , position is described as follows:

$$\vec{r} = \bar{x}^i \hat{b}_i \quad (C.40)$$

where (ref. 5, eq. (45.2)) the vectors,  $\hat{b}_i$ , are the unit base vectors of the scaled coordinates such that

$$\hat{b}_i \cdot \hat{b}_j = \delta_{ij}. \quad (\text{C.41})$$

The covariant base vectors of the compressibility coordinates (ref. 5, eq. (45.6)) are defined as

$$\vec{a}_i = \frac{\partial \vec{r}}{\partial x^i}; \quad (\text{C.42})$$

and, since

$$\vec{a}_i \cdot \vec{a}_j = g_{ij}, \quad (\text{C.43})$$

these are not unit vectors in the measure of the scaled coordinates.

Contravariant base vectors are introduced by eq. (45.8), ref. 5, and these can be written in the following convenient form:

$$\vec{a}^i \epsilon_{ijk} = \vec{a}_j \times \vec{a}_k \quad (\text{C.44})$$

where (ref. 5, pg. 138)

$$\epsilon_{ijk} \equiv \sqrt{g} e_{ijk} \quad (\text{C.45})$$

and  $e_{ijk}$  is the permutation symbol defined in sec. 40 of ref. 5. Similarly, from eq. (45.9), ref. 8,

$$\vec{a}_i \epsilon^{ijk} = \vec{a}^j \times \vec{a}^k \quad (\text{C.46})$$

where (ref. 5, pg. 138)

$$\epsilon^{ijk} = \frac{1}{\sqrt{g}} e^{ijk}. \quad (\text{C.47})$$

Returning to the derivation, as noted by eq. (90.5) of ref. 5,

$$\frac{\partial \phi^*}{\partial n} ds = n^i \frac{\partial \phi^*}{\partial x^i} ds \quad (\text{C.48})$$

where  $n^i$  denotes the contravariant components of the unit normal vector,  $\hat{n}$ . An expression for evaluating  $n^i$  is obtained from the description of the surface,  $\Sigma$ , in Gaussian form (ref. 5, sec. 52), viz.,

$$x^i = x^i(u^1, u^2) \quad (C.49)$$

where  $u^\alpha$  (for  $\alpha = 1, 2$ ) are parameters which, when varied independently, describe curves on the surface which are surface coordinates. The base vectors of the surface coordinates (ref. 5, eq. (54.6)) are given by

$$\vec{a}_\alpha = \frac{\partial \vec{r}}{\partial u^\alpha} \quad (C.50)$$

where  $\vec{r}$  denotes position on the surface, i.e.,

$$\vec{r} = \bar{x}^i(u^1, u^2) \hat{b}_i = x^i(u^1, u^2) \vec{a}_i \quad (C.51)$$

where the following has been used:

$$\hat{b}_i = \frac{\partial \vec{r}}{\partial x^j} \frac{\partial x^j}{\partial \bar{x}^i}$$

so that, by eq. (C.40) and (C.20),

$$\hat{b}_i = \mathcal{E}_i^j \vec{a}_j \quad (C.52)$$

and

$$\mathcal{E}_i^j \bar{x}^i(u^1, u^2) = x^j(u^1, u^2). \quad (C.53)$$

Since  $\vec{a}_1$  and  $\vec{a}_2$  are vectors tangent to the surface along the surface coordinate curves, the unit normal vector is given by (ref. 5, eq. (65.2))

$$\hat{n} = \frac{\vec{a}_1 \times \vec{a}_2}{|\vec{a}_1 \times \vec{a}_2|} \quad (C.54)$$

The components of the unit normal vector are derived using eq. C.50 and C.51 to write the surface coordinate base vectors as

$$\vec{a}_\alpha = \frac{\partial x^i}{\partial u^\alpha} \vec{a}_i. \quad (\text{C.55})$$

Their cross product, using eq. (C.44), is then expressed as

$$\vec{a}_1 \times \vec{a}_2 = \frac{\partial x^j}{\partial u^1} \frac{\partial x^k}{\partial u^2} (\vec{a}_j \times \vec{a}_k) = \epsilon_{ijk} \frac{\partial x^j}{\partial u^1} \frac{\partial x^k}{\partial u^2} \vec{a}_i; \quad (\text{C.56})$$

hence, defining

$$\sqrt{a} \equiv |\vec{a}_1 \times \vec{a}_2|, \quad (\text{C.57})$$

the covariant components of the unit normal are found to be

$$n_i = \frac{1}{\sqrt{a}} \epsilon_{ijk} \frac{\partial x^j}{\partial u^1} \frac{\partial x^k}{\partial u^2} \quad (\text{C.58})$$

while the contravariant components are

$$n^i = g^{ij} n_j \quad (\text{C.59})$$

(ref. 5, sec. 45).

As shown by sec. 54, ref. 5, the differential surface element is given by

$$ds = |\vec{a}_1 \times \vec{a}_2| du^1 du^2; \quad (\text{C.60})$$

and, introducing eq. (C.57),

$$ds = \sqrt{a} du^1 du^2. \quad (\text{C.61})$$

Combining eq. (C.58) and (C.61), the covariant components, viz.,

$$n_i ds = \epsilon_{ijk} \frac{\partial x^j}{\partial u^1} \frac{\partial x^k}{\partial u^2} du^1 du^2, \quad (\text{C.62})$$

are seen to be the components of the vector formed by the cross product of the following two tangent vectors:

$$\vec{dr}_1 \equiv \vec{a}_1 du^1 = dx_1^i \vec{a}_i \quad (C.63)$$

and

$$\vec{dr}_2 = dx_2^i \vec{a}_i. \quad (C.64)$$

Consider the following vector product:

$$\hat{N} dS = \vec{dr}_1 \times \vec{dr}_2$$

in the measure of the compressibility coordinates; thus,

$$\hat{N} dS = e_{ijk} dx_1^j dx_2^k \hat{a}^i. \quad (C.65)$$

Introducing eq. (C.62) and recalling eq. (C.45), eq. (C.65) leads to

$$\hat{N} dS = \sqrt{g} n_i dS \hat{a}^i. \quad (C.66)$$

Taking the norm of this result in the measure of the scaled coordinates, wherein

$$(n_i \vec{a}^i) \cdot (n_j \vec{a}^j) = n_i g^{ij} n_j = 1 \quad (C.67)$$

and

$$(N_i \vec{a}^i) \cdot (N_j \vec{a}^j) = N_i g^{ij} N_j = (N)^2, \quad (C.68)$$

the two differential surface elements and the covariant components of the two normal vectors are found to be related as follows:

$$ds = \sqrt{g} N dS \quad (C.69)$$

and

$$n_i = N_i / N. \quad (C.70)$$

Eqs. (C.69) and (C.70) verify the expressions shown as eqs. (C.38) and (C.39).

Recalling eq. (C.59) and introducing eq. (C.70),

$$n^i = g^{ij} N_j / N ; \quad (C.71)$$

thus, since (ref. 5, eq. (92.5))

$$\frac{\partial \phi^*}{\partial n} ds = n^i \frac{\partial \phi^*}{\partial x^i} ds , \quad (C.72)$$

eqs. (C.69) and (C.71) lead to

$$\frac{\partial \phi^*}{\partial n} ds = \sqrt{g} g^{ij} N_j \frac{\partial \phi^*}{\partial x^i} dS \quad (C.73)$$

which can be written as

$$\frac{\partial \phi^*}{\partial n} ds = n_c^i \frac{\partial \phi^*}{\partial x^i} dS = \frac{\partial \phi^*}{\partial n_c} dS \quad (C.74)$$

where

$$n_c^i \equiv \sqrt{g} g^{ij} N_j ; \quad (C.75)$$

and, on introducing eq. (C.8), (C.5), and (C.7),

$$n_c^1 = \beta^2 N_1 , n_c^2 = N_2 , n_c^3 = N_3 . \quad (C.76)$$

From eq. (C.76) the vector  $\vec{n}_c$  is seen to be the vector usually called the conormal to the surface.

The integral equation shown as eq. (38) follows directly from eq. (C.25) by making the substitution shown as eq. (C.74); thus,

$$\phi^*(P) = \iint_{\Sigma} \left( \sigma^* \psi^* - \mu^* \frac{\partial \psi^*}{\partial n_c} \right) dS \quad (C.77)$$

where

$$\sigma^* \equiv \left[ \frac{\partial \phi^*}{\partial n_c} \right] \quad \mu^* \equiv \left[ \phi^* \right] . \quad (C.78)$$

#### C. 4 ELIMINATION OF PANEL EDGE LINE VORTICES

The integrals shown by eqs. (C.29) through (C.34) are expressed by the sum of the panel integrals shown by eq. (37) through (60). In the case of eq. (60), viz.,

$$\vec{v}_D^* (P) = - \iint_{\Sigma_e} \mu_e^* \frac{\partial}{\partial n_c} (\vec{\nabla}' \psi^*) dS',$$

a decomposition is introduced such that

$$\vec{v}_D^* = \vec{v}_d^* + \vec{v}_v^* \tag{C.79}$$

where the term  $\vec{v}_v^*$  represents the velocity induced by a line vortex lying on the perimeter of the panel, viz.,  $\partial \Sigma_e$ . When panels are joined together to form a continuous surface of integration, the line vortices at the edges of panels abutting one another are equal in strength and opposite in sign; hence, the velocity  $\vec{v}_v^*$  induced by one panel edge is canceled by the velocity induced by the other, abutting, panel edge. As a result, the line vortex induced velocities need not be computed and the doublet panel induced velocities (i.e., eq. (60)) are computed from the regular part of eq. (C.79), viz.  $\vec{v}_d^*$ .

The decomposition of eq. (60), which leads to eq. (C.79), is formed from a corollary to Stoke's theorem. Stoke's theorem is expressed by eq. (92.15) of ref. 5 which, on interchange of dummy indices  $j$  and  $k$ , is written as follows:

$$\iint_{\Sigma} \epsilon^{ijk} F_{k,j} n_i ds = \int_{\partial \Sigma} F_k \frac{dx^k}{dc} dc \tag{C.80}$$

where  $\partial \Sigma$  denotes the perimeter of the surface,  $\Sigma$ ;

$$x^i = x^i(c)$$

represents a parametric description of  $\partial \Sigma$ ; and  $F_k$  represents the covariant components of an arbitrary vector. The corollary is obtained by letting

$$F_k = \epsilon_{\ell km} \mu^* g^{mn} \psi_{,n}^* \text{ for } \ell = 1, 2, 3;$$

whereby, eq. (C.56) becomes

$$\iint_{\Sigma} \epsilon^{ijk} \epsilon_{\ell km} g^{mn} (\mu^* \psi_{,n}^*)_{,j} n_i ds = \iint_{\partial \Sigma} \epsilon_{\ell km} \mu^* g^{mn} \psi_{,n}^* \frac{dx^k}{dc} dc \tag{C.81}$$

where use has been made of Ricci's theorems (ref. 5, sec. 35), viz.,

$$g_{ij,k} = 0 \text{ and } g^{ij},_{k} = 0,$$

whence

$$(\epsilon_{\ell km})_{,j} = (\sqrt{g})_{,j} \epsilon_{\ell km} = \frac{1}{2\sqrt{g}} |g_{pq,j}| \epsilon_{\ell km} = 0.$$

Expanding (C.81) leads to

$$\begin{aligned} \int_{\partial\Sigma} \epsilon_{\ell km} \mu^* g^{mn} \psi_{,n}^* \frac{dx^k}{dc} dc &= \iint_{\Sigma} \epsilon^{ijk} \epsilon_{\ell km} g^{mn} \mu^* \psi_{,n}^* n_i ds \\ &+ \iint_{\Sigma} \mu^* \epsilon^{ijk} \epsilon_{\ell km} g^{mn} \psi_{,nj}^* n_i ds. \end{aligned} \quad (C.82)$$

The vector form of the integrand of the second integral is deduced using the reciprocal base system shown by eqs. (C.44) and (C.46). The result is a triple vector product which is then revised using the following vector product identity:

$$(\vec{a} \times \vec{b}) \times \vec{c} = \vec{b} (\vec{a} \cdot \vec{c}) - \vec{a} (\vec{b} \cdot \vec{c}).$$

These operations appear in the following sequence:

$$\begin{aligned} \mu^* \epsilon^{ijk} \epsilon_{\ell km} g^{mn} \psi_{,nj}^* n_i \vec{a}^{\ell} &= \mu^* \epsilon^{ijk} (\vec{a}_k \times \vec{a}_m) g^{mn} \psi_{,nj}^* n_i \\ &= -\mu^* (\vec{a}^i \times \vec{a}^j) \times \vec{a}_m g^{mn} \psi_{,nj}^* n_i \\ &= -\mu^* (\hat{n} \times \vec{\nabla}) \times \vec{\nabla} \psi^* \\ &= -\mu^* (\hat{n} \cdot \vec{\nabla}) \vec{\nabla} \psi^* + \mu^* (\vec{\nabla} \cdot \vec{\nabla} \psi^*) \\ &= -\mu^* g^{ij} n_i \psi_{,lj}^* \vec{a}^{\ell} + \mu^* n_{\ell} g^{ij} \psi_{,ij}^* \vec{a}^{\ell}. \end{aligned} \quad (C.83)$$

Also, from eq. (C.12),

$$g^{ij} \psi_{,ij}^* = -\Omega^2 \psi^*; \quad (C.84)$$

and, because the first term is identical with integrand of eq. (60), viz.,

$$\mu^* g^{ij} n_i \psi_{,ij}^* \vec{a}^\ell = \mu^* \frac{\partial}{\partial n_c} (\vec{\nabla} \psi^*),$$

eq. (C.79) becomes

$$\vec{v}_D^* = \vec{v}_d^* + \vec{v}_v^*$$

where

$$\begin{aligned} \vec{v}_d^* &= \iint_{\Sigma_e} \epsilon^{ijk} \epsilon_{lkm} g^{mn} \mu^*_{,j} \psi^*_{,n'} n_i ds' \vec{a}^\ell + \Omega^2 \iint_{\Sigma_e} n_\ell \mu^* \psi^* ds' \vec{a}^\ell \\ &= \iint_{\Sigma_e} (\hat{n} \times \vec{\nabla} \mu^*) \times \vec{\nabla}' \psi^* ds' + \Omega^2 \iint_{\Sigma_e} \hat{n} \mu^* \psi^* ds' \end{aligned} \quad (C.85)$$

$$\vec{v}_v^* = - \int_{\partial \Sigma_e} \epsilon_{lkm} \mu^* g^{mn} \psi^*_{,n'} \frac{dx'}{dc} dc \vec{a}^\ell = \int_{\partial \Sigma_e} \mu^* d\vec{r} \times \vec{\nabla}' \psi^* \quad (C.86)$$

where

$$\psi^*_{,i} = - \psi^*_{,i'}, \quad \vec{\nabla} \psi^* = - \vec{\nabla}' \psi^*,$$

and

$$d\vec{r}' = \frac{dx'^k}{dc} dc \vec{a}_k.$$

### C.5 CHANGE OF VARIABLE

In section C.1 it was noted, eq. (C.18), that solutions to the flow equation could be related to solutions to Helmholtz's equation through a change of variables: thus, if  $\phi^*(x,y,z)$  is a solution to the flow equation, then

$$\bar{\phi}^*(\bar{x}, \bar{y}, \bar{z}) = \bar{\phi}^*(\bar{x}, \bar{y}/\beta, \bar{z}/\beta) \quad (C.87)$$

is a solution to Helmholtz's equation expressed in the scaled coordinates, viz.,

$$\bar{\phi}^*_{\bar{x}\bar{x}} + \bar{\phi}^*_{\bar{y}\bar{y}} + \bar{\phi}^*_{\bar{z}\bar{z}} + \Omega^2 \bar{\phi}^* = 0. \quad (C.17)$$

The advantage accrued through this change of variables, when the solution to the flow equation is the integral equation shown by eq. (C.77), is that the integrals do not contain the compressibility factor,  $\beta$ , except that the compressibility factor appears in the Helmholtz's coefficient, viz.,

$$\Omega = \bar{\omega} M_0 \beta^2, \quad (30)$$

which appears in the exponential function contained in  $\psi^*$ .

Recalling eq. (C.77), the panel induced complex potential amplitudes at the field point,  $P$ , are given by

$$\phi_D^*(P) = - \iint_{\Sigma_e} \mu^* \frac{\partial \psi^*}{\partial n'_c} dS' \quad (C.88)$$

and

$$\phi_S^*(P) = \iint_{\Sigma_e} \sigma^* \psi^* dS. \quad (C.89)$$

Under the change of variables eqs. (C.74), (C.72) and (C.59) yield the expression

$$\frac{\partial \psi^*}{\partial n'_c} dS = n_i g^{ij} \frac{\partial \psi^*}{\partial x'^i} dS$$

which becomes

$$\frac{\partial \psi^*}{\partial n'_c} dS = n_i \frac{\partial \bar{\psi}^*}{\partial \bar{x}'^i} dS \quad (C.90)$$

where

$$\bar{n}_i = \mathcal{E}_i^j n_j, \quad \frac{\partial \bar{\psi}^*}{\partial \bar{x}'^i} = \mathcal{E}_i^j \frac{\partial \psi^*}{\partial x'^j},$$

and

$$g^{ij} \mathcal{E}_i^k \mathcal{E}_j^\ell = \delta^{k\ell};$$

hence, the doublet panel integral becomes

$$\phi_D^*(P) = \bar{\phi}_D^*(\bar{P}) \quad (C.91)$$

where

$$\bar{\phi}_D^* (\bar{P}) = - \iint_{\bar{\Sigma}_e} \bar{\mu}^* \frac{\partial \bar{\psi}^*}{\partial \bar{n}'} ds' \quad (C.92)$$

when

$$\frac{\partial}{\partial \bar{n}} \equiv \bar{n}_i \frac{\partial}{\partial \bar{x}^i}$$

Recalling eq. (C.69), the source panel integral becomes

$$\phi_S^* (P) = J \bar{\phi}_S^* (\bar{P}) \quad (C.93)$$

where

$$J \equiv \frac{1}{\sqrt{g} N}$$

and

$$\bar{\phi}_S^* (\bar{P}) = \iint_{\bar{\Sigma}_e} \bar{\sigma}^* \bar{\psi}^* ds' \quad (C.94)$$

Having the potentials expressed in the scaled coordinates, a convenient means for computing the velocity components in the compressibility coordinates is obtained by the following operations:

$$v_i^* = \frac{\partial \phi^*}{\partial x^i} = \frac{\partial \bar{\phi}^*}{\partial \bar{x}^j} \frac{\partial \bar{x}^j}{\partial x^i} = E_i^j \frac{\partial \bar{\phi}^*}{\partial \bar{x}^j} \quad (C.95)$$

Noting, again, that

$$\frac{\partial \bar{\psi}^*}{\partial \bar{x}^j} = - \frac{\partial \bar{\psi}^*}{\partial \bar{x}'^j}$$

the source panel induced velocity components are given by

$$\bar{v}_{Si}^* (\bar{P}) = J E_i^j \bar{v}_{Sj}^* (\bar{P}) \quad (C.96)$$

where

$$\bar{v}_{Si}^* (\bar{P}) = - \iint_{\Sigma_e} \bar{\sigma}^* \frac{\partial \bar{\psi}^*}{\partial \bar{x}'^i} ds' \quad (C.97)$$

The doublet panel induced velocity components are given by eq. (C.85) whereby

$$\bar{v}_{Dl}^* (\bar{P}) = \iint_{\Sigma_e} e^{ijk} e_{lkm} \frac{\partial \bar{\mu}^*}{\partial \bar{x}'^j} \frac{\partial \bar{\psi}^*}{\partial \bar{x}'^m} \bar{n}_i ds' + \Omega^2 \iint_{\Sigma_e} \bar{n}_l \bar{\mu}^* \bar{\psi}^* ds' \quad (C.98)$$

so that

$$\bar{v}_{Di}^* (\bar{P}) = E_i^l \bar{v}_{Dl}^* (\bar{P}) \quad (C.99)$$

The influence of a panel edge line vortex, eq. (C.86), becomes

$$\bar{v}_{vl}^* (\bar{P}) = \int_{\bar{\Sigma}_e} \mu^* e_{lmn} \frac{d\bar{x}^m}{dc} dc \frac{\partial \bar{\psi}^*}{\partial \bar{x}'^n} \quad (C.100)$$

## C.6 PANEL, LOCAL COORDINATE SYSTEMS

Eqs. (C.91) through (C.100) of section C.5 contain the integrals which must be evaluated to determine the panel influence at field points. This section introduces local coordinate systems in which these integrals assume forms which are particularly convenient for that evaluation. The coordinate lines of a local system are denoted as  $\xi, \eta, \zeta$  and the system is defined such that the  $\xi, \eta$  coordinate plane is parallel with the panel plane and such that the  $\zeta$  coordinate is along (and in the direction of) the panel normal,  $\hat{n}$ .

Letting the coordinate lines be denoted as

$$\xi^1 = \xi, \xi^2 = \eta, \xi^3 = \zeta, \quad (C.101)$$

the local system is expressed by a transformation of the compressibility coordinates as follows:

$$\xi^i = A_j^i x^j \quad (C.102)$$

with the inverse:

$$x^i = A_j^i \xi^j. \quad (\text{C.103})$$

This is a linear transformation since it is a combination of the Prandtl-Glauert transformation, viz.,

$$\bar{x}^k = E_j^k x^j, \quad (\text{C.1})$$

and an orthogonal transformation,

$$\xi^i = t_k^i \bar{x}^k, \quad (\text{C.104})$$

such that

$$A_j^i = t_k^i E_j^k \quad (\text{C.105})$$

where, because of the orthogonal nature of the transformation,

$$\bar{x}^k = T_i^k \xi^i \quad (\text{C.106})$$

and

$$T_i^k = t_k^i. \quad (\text{C.107})$$

The orthogonal transformation is derived by noting that, if  $\hat{\alpha}_i$  are unit base vectors for the local system, then they are related to the base vectors of the scaled system by the transformation rule for covariant tensors (ref. 5, sec. 24), viz.,

$$\hat{\alpha}_i = \frac{\partial \vec{r}}{\partial \xi^i} = \frac{\partial \vec{r}}{\partial \bar{x}^j} \frac{\partial \bar{x}^j}{\partial \xi^i} = T_i^j \hat{b}_j. \quad (\text{C.108})$$

The unit base vectors of the local system are chosen as follows:

$$\begin{aligned} \hat{\alpha}_2 &= \frac{\hat{n} \times \hat{c}}{|\hat{n} \times \hat{c}|} \\ \hat{\alpha}_1 &= \hat{\alpha}_2 \times \hat{n} \\ \hat{\alpha}_3 &= \hat{n} \end{aligned} \quad (\text{C.109})$$

where  $\hat{n}$  is the unit vector normal to the panel plane defined by eq. (C.54) and  $\hat{c}$  is a unit vector in the direction of the freestream flow, viz., in the direction of  $\bar{x}$  and  $x$ . Because of the form of the Prandtl-Glauert transformation, the vector  $\hat{c}$  is a unit vector in the measure of both the scaled system and the compressibility system, and its covariant and contravariant components are identical to one another. Using these characteristics of the vector  $\hat{c}$  along with eq. (C.38), the unit base vectors of the local system are seen to be given by

$$\begin{aligned}\hat{\alpha}_2 &= \frac{\vec{N} \times \hat{c}}{|\vec{N} \times \hat{c}|} \\ \hat{\alpha}_1 &= \frac{1}{N} \hat{\alpha}_2 \times \vec{N}\end{aligned}\tag{C.110}$$

and

$$\hat{\alpha}_3 = \frac{1}{N} \vec{N}$$

where it should be noted that these vectors can be formed directly from vectors expressed in the measure of the compressibility system.

The expansion required by eq. (C.108) is obtained by writing the cross products using the reciprocal base systems (viz. eqs. (C.44) and (C.46)); thus,

$$\vec{N} \times \hat{c} = e^{ijk} N_j c_k \vec{a}_i.\tag{C.111}$$

Introducing

$$v^i \equiv e^{ijk} N_j c_k\tag{C.112}$$

and

$$\alpha \equiv |\vec{N} \times \hat{c}| = \sqrt{v^i g_{ij} v^j},\tag{C.113}$$

because the local system has the measure of the scaled coordinates, wherein

$$\vec{a}_i \cdot \vec{a}_j = g_{ij},$$

the unit base vectors of the local system are found to be as follows:

$$\hat{\alpha}_2 = \frac{1}{\alpha} V^i \vec{a}_i,$$

$$\hat{\alpha}_1 = \frac{1}{\alpha N} U^i \vec{a}_i, \quad (\text{C.114})$$

and

$$\hat{\alpha}_3 = \frac{1}{N} N_j \vec{a}^j = \frac{1}{N} N_j g^{ji} \vec{a}_i$$

where

$$U^i \equiv e^{ijk} V_j N_k; \quad (\text{C.115})$$

because, in the measure of the compressibility system,

$$V^i = V_i. \quad (\text{C.116})$$

Since, again, by the law of transformation for covariant tensors,

$$\vec{a}_i = \frac{\partial \vec{r}}{\partial x^i} = \frac{\partial \vec{r}}{\partial \bar{x}^i} \frac{\partial \bar{x}^j}{\partial x^i} = E_i^j \hat{b}_j, \quad (\text{C.117})$$

the local system base vectors become as follows:

$$\hat{\alpha}_2 = \frac{1}{\alpha} V^i E_i^j \hat{b}_j$$

$$\hat{\alpha}_1 = \frac{1}{\alpha N} U^i E_i^j \hat{b}_j$$

$$\hat{\alpha}_3 = \frac{1}{N} N_k g^{ki} E_i^j \hat{b}_j. \quad (\text{C.118})$$

The orthogonal transformation shown by eq. (C.106) is deduced from eqs. (C.108) and (C.118) with the result that

$$\bar{x}^j = \frac{1}{\alpha N} U^i E_i^j \xi^1 + \frac{1}{\alpha} V^i E_i^j \xi^2 + \frac{1}{N} N_k g^{ki} E_i^j \xi^3. \quad (\text{C.119})$$

Similarly, the transformation, eq. (C.103), which is the inverse of eq. (C.102), is found from eq. (C.114) as

$$x^i = \frac{1}{\alpha N} U^i \xi^1 + \frac{1}{\alpha} V^i \xi^2 + \frac{1}{N} N_j g^{ji} \xi^3. \quad (\text{C.120})$$

Using the characteristics of the orthogonal transformation shown by (C.107), the transformation shown by eq. (C.104) is found as

$$\xi^1 = \frac{1}{\alpha N} U^i E_1^j \bar{x}^j,$$

$$\xi^2 = \frac{1}{\alpha} V^i E_1^j \bar{x}^j,$$

and

$$\xi^3 = \frac{1}{N} N_k g^{ki} E_1^j \bar{x}^j. \quad (\text{C.121})$$

Finally, introducing eq. (C.1) into eq. (C.121) and noting eq. (C.4), viz.,

$$g_{ij} = E_i^k E_j^k,$$

and noting from eq. (C.6) that

$$g_{ij} g^{jk} = \delta_i^k,$$

the transformation shown by eq. (C.102) is found to be

$$\xi^1 = \frac{1}{\alpha N} U^i g_{ij} x^j,$$

$$\xi^2 = \frac{1}{\alpha} V^i g_{ij} x^j,$$

and

$$\xi^3 = \frac{1}{N} N_j x^j. \quad (\text{C.122})$$

Matrix notation provides a useful form for presenting the operations involved in computing the components of  $A_j^i$  and its inverse,  $A_j^i$ , viz.,

$$[A_j^i] = \left[ \frac{1}{\alpha N} \{U^i\} \middle| \frac{1}{\alpha} \{V^i\} \middle| \frac{1}{N} [g^{ij}] \{N_j\} \right] \quad (C.123)$$

and

$$[A_j^i]^T = \left[ \frac{1}{\alpha N} [g_{ij}] \{U^i\} \middle| \frac{1}{\alpha} [g_{ij}] \{V^i\} \middle| \frac{1}{N} \{N_j\} \right] \quad (C.124)$$

where

$$\begin{aligned} \{U^i\} &= \text{components of } (\vec{N} \times \hat{c}) \times \vec{N}, \\ \{V^i\} &= \text{components of } (\vec{N} \times \hat{c}) \text{ and} \\ \{N_j\} &= \text{components of } \vec{N}. \end{aligned} \quad (C.125)$$

Expanding eq. (C.95) and noting eq. (C.105), the velocity components are found to transform as follows:

$$v_i^* = E_i^j \frac{\partial \bar{\phi}^*}{\partial \bar{x}^j} = E_i^j \frac{\partial \xi^k}{\partial \bar{x}^j} \frac{\partial \tilde{\phi}^*}{\partial \xi^k} = E_i^j t_j^k \frac{\partial \tilde{\phi}^*}{\partial \xi^k} = A_i^k \tilde{v}_k^* \quad (C.126)$$

where  $\tilde{\phi}^*$  denotes the complex amplitude of the modified potential expressed in the local system and

$$\tilde{v}_k^* = \frac{\partial \tilde{\phi}^*}{\partial \xi^k} \quad (C.127)$$

denotes the components of the velocity in the local system. Using eq. (C.126), eqs. (C.97) through (C.100), describing the panel influences, become as follows:

(1) Source panel induced potential:

$$\phi_S^*(P) = J \tilde{\phi}_S^*(\tilde{P}) \quad (C.128)$$

where

$$\tilde{\phi}_S^*(\tilde{P}) = - \iint_{\tilde{\Sigma}_e} \tilde{\sigma}^* \tilde{\psi}^* d\xi' d\eta' \quad (C.129)$$

(2) Doublet panel induced potential:

$$\phi_D^*(P) = \tilde{\phi}_D^*(\tilde{P}) \quad (C.130)$$

where

$$\tilde{\phi}_D^*(\tilde{P}) = \iint_{\tilde{\Sigma}_e} \tilde{\mu}^* \frac{\partial \tilde{\psi}}{\partial \xi'} d\xi' d\eta' \quad (C.131)$$

(3) Source panel induced velocity components

$$v_{Si}^* = A_i^j \tilde{v}_{Sj}^* \quad (C.132)$$

where

$$\tilde{v}_{Sj}^* = - \iint_{\tilde{\Sigma}_e} \tilde{\sigma}^* \frac{\partial \tilde{\psi}^*}{\partial \xi'^j} d\xi' d\eta' \quad (C.133)$$

(4) Doublet panel induced velocity components

$$v_{Di}^* = A_i^l \tilde{v}_{Dl}^* \quad (C.134)$$

where (for Greek indices ranging over 1,2)

$$\tilde{v}_{D\delta}^*(\tilde{P}) = \iint_{\tilde{\Sigma}_e} -e^{\alpha\beta} e_{\delta\beta} \frac{\partial \tilde{\mu}^*}{\partial \xi^\alpha} \frac{\partial \tilde{\psi}^*}{\partial \xi'} d\xi' d\eta' \quad (C.135)$$

because the components of the normal are given by

$$\tilde{n}_1 = 0, \quad \tilde{n}_2 = 0, \quad \tilde{n}_3 = 1$$

and

$$e^{3jk} e_{\delta km} = -e^{\alpha\beta} e_{\delta\beta m} = -e^{\alpha\beta} e_{\delta\beta}$$

while

$$\tilde{v}_{D3}^*(\tilde{P}) = \iint_{\tilde{\Sigma}_e} e^{\alpha\beta} e_{\beta\delta} \frac{\partial \tilde{\mu}^*}{\partial \xi^\alpha} \frac{\partial \tilde{\psi}^*}{\partial \xi'^\delta} d\xi' d\eta' + \Omega^2 \iint_{\tilde{\Sigma}_e} \tilde{\mu}^* \tilde{\psi}^* d\xi' d\eta' \quad (C.136)$$

because

$$e^{3jk} e_{3km} = e^{3\alpha\beta} e_{3\beta\delta} = e^{\alpha\beta} e_{\beta\delta}.$$

(5) Doublet panel edge induced velocity components:

$$v_{vi}^* = A_i^{\ell} \tilde{v}_{v\ell}^* \quad (\text{C.137})$$

where (for Greek indices ranging over 1,2)

$$\tilde{v}_{v\delta}^* (P) = \iint_{\partial\tilde{\Sigma}_e} \tilde{\mu}^* e_{\delta\alpha} \frac{d\xi^\alpha}{dc} dc \frac{\partial\tilde{\psi}^*}{\partial\xi'^\delta} \quad (\text{C.138})$$

while

$$\tilde{v}_{v3}^* (\tilde{P}) = - \iint_{\partial\tilde{\Sigma}_e} \tilde{\mu}^* e_{\alpha\beta} \frac{d\xi^\alpha}{dc} dc \frac{\partial\tilde{\psi}^*}{\partial\xi'^\beta} \quad (\text{C.139})$$

## APPENDIX D

### EVALUATION OF AERODYNAMIC INFLUENCE COEFFICIENTS

This appendix describes the theory underlying the procedure used to evaluate the panel influences shown by eqs. (C.128) through (C.136) of app. C.

Panel singularity distribution functions are introduced in sec. D.1. These functions reduce the panel influences of app. C to influence coefficients relating the induced flow potential and velocity at a field point, P, to the coefficients of a Taylor series expansion of the distribution function, cf. eq. (49) and (52). The end result is a set of integral equations for the panel influences which are in terms of panel integrals having integrands of nine basic types. The remainder of the appendix is directed toward deriving evaluation procedures for those nine integrals.

Section D.2 introduces two coordinate systems: (1) a panel edge coordinate system describing position in the panel plane in terms of distance along and normal to a panel edge and (2) a polar coordinate system. In the following sections of the appendix the panel integrals are expressed in polar coordinates. The panel edge coordinates are then introduced as a change of variables. The result is a convenient expression for the integral in terms of the distance along the panel edge.

Section D.3 contains a reduction of the integrals involved in the panel influence coefficients. The reduction is based, in part, on a separation of the unsteady kernel function into a steady component and an unsteady component. The unsteady kernel function, viz.,

$$\psi^* = -\frac{1}{4\pi R} e^{-i\Omega R},$$

is expressed as

$$\psi^* = \psi_0 + {}^*\psi$$

where the steady component is given by

$$\psi_0 = -\frac{1}{4\pi R}$$

and the unsteady component is given by

$${}^*\psi = -\frac{1}{4\pi} (e^{-i\Omega R} - 1) \frac{1}{R}.$$

The steady component is evaluated in closed form and the unsteady component is further reduced to a dependence on two fundamental integrals which cannot be evaluated directly in closed form.

The integrands of the two fundamental integrals are approximated in sec. D.4 by polynomials containing terms which are closed form integrable. Sec. D.5 describes the polynomial estimation procedure for the approximation introduced in sec. D.4 and sec. D.6 contains an error analysis to the approximation.

Finally, sec. D.7 contains a derivation of the influence coefficient evaluation procedure used in the far field. The fundamental idea underlying the far field evaluation is that of approximating the kernel function (or its gradient) with a truncated Taylor series expansion which is a valid approximation when the field point is sufficiently far from the influencing panel. The section presents the criteria used to establish validity.

### D.1 PANEL SINGULARITY STRENGTH DISTRIBUTION FUNCTIONS

For the purpose of introducing the singularity distributions,  $\sigma^*(Q)$  and  $\mu^*(Q)$ , the panel influence integrals are expressed in terms of the following representation of the field point, P, and the surface point, Q: P' is the point representing the projection of the field point onto the panel plane and  $\vec{h}$  is a vector along the panel normal from P to P', figure 50. A local origin,  $Q_0$ , with coordinates  $\xi_0, \eta_0, \zeta_0$  is introduced and P' and Q have the positions  $\vec{\delta}$  and  $\vec{r}$  relative to  $Q_0$ . The vector  $\vec{R}$  is then given by

$$\vec{R} = \vec{\rho} + \vec{h}. \quad (D.1)$$

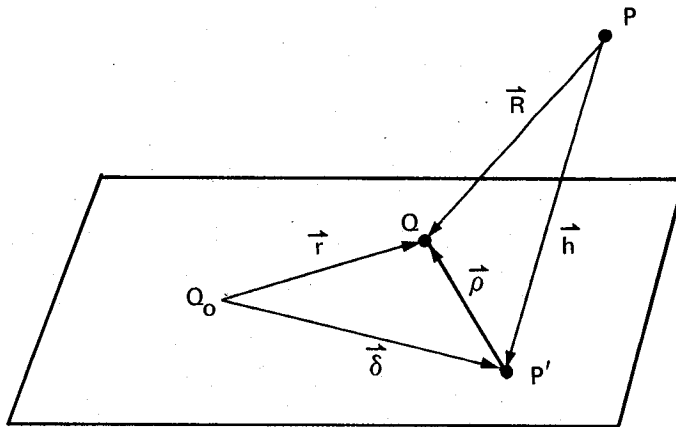


Figure 50. — Representation of Field and Surface Points

Indical notation and summation convention (ref. 5, sec. 7) are used in the following; hence, the following notation is introduced for the coordinates of points:

$$\begin{aligned}\xi^1 &= \xi', \quad \xi^2 = \eta' : \text{coordinates of Q} \\ \xi_0^1 &= \xi_0, \quad \xi_0^2 = \eta_0 : \text{coordinates of } Q_0 \\ z^1 &= \xi, \quad z^2 = \eta : \text{coordinates of } P'\end{aligned}\tag{D.2}$$

The components of the vectors in the panel plane (viz.,  $\vec{r}$ ,  $\vec{\rho}$ , and  $\vec{\delta}$ ) are given by

$$\begin{aligned}r^\alpha &= \xi^\alpha - \xi_0^\alpha, \\ \rho^\alpha &= r^\alpha - \delta^\alpha, \\ \delta^\alpha &= z^\alpha - \xi_0^\alpha\end{aligned}\tag{D.3}$$

where, and in the following, Greek indices have the range  $\alpha = 1, 2$ .

The panel singularity strength distribution functions, c.f. eqs. (49) through (52), are expressed in terms of the above notation as follows\*:

$$\sigma^*(Q) = \sigma_0^* + \sigma_{0,\alpha}^* r^\alpha\tag{D.4}$$

and

$$\mu^*(Q) = \mu_0^* + \mu_{0,\alpha}^* r^\alpha + \frac{1}{2} \mu_{0,\alpha\beta}^* r^\alpha r^\beta + \frac{1}{6} \mu_{0,\alpha\beta\gamma}^* r^\alpha r^\beta r^\gamma.$$

For the purpose of evaluating the integrals of eq. (C.128) through (C.136), however, it is convenient to expand  $\sigma^*$  and  $\mu^*$  in a Taylor series about the point  $P'$  (viz., the projection of the field point onto the panel plane); thus,

$$\sigma^*(Q) = \sigma_0 + \sigma_\alpha \rho^\alpha$$

and

$$\mu^*(Q) = \mu_0 + \mu_\alpha \rho^\alpha + \frac{1}{2} M_{\alpha\beta} \rho^\alpha \rho^\beta + \frac{1}{6} m_{\alpha\beta\gamma} \rho^\alpha \rho^\beta \rho^\gamma\tag{D.5}$$

\* Terms which are of third degree in the spatial coordinates are included in the doublet distribution function for evaluating the quasi-near-field approximation described in sec. D.7.

where

$$\begin{aligned}
\sigma_0 &\equiv \sigma_0^* + \sigma_{0,\alpha}^* \delta^\alpha \\
\sigma_\alpha &\equiv \sigma_{0,\alpha}^* \\
\mu_0 &\equiv \mu_0^* + \mu_{0,\alpha}^* \delta^\alpha + \mu_{0,\alpha\beta}^* \delta^\alpha \delta^\beta \\
\mu_\alpha &\equiv \mu_{0,\alpha}^* + \mu_{0,\alpha\beta}^* \delta^\beta + \frac{1}{2} \mu_{0,\alpha\beta\gamma}^* \delta^\beta \delta^\gamma \\
M_{\alpha\beta} &\equiv \mu_{0,\alpha\beta}^* + \mu_{0,\alpha\beta\gamma}^* \delta^\gamma \\
m_{\alpha\beta\gamma} &\equiv \mu_{0,\alpha\beta\gamma}^* .
\end{aligned} \tag{D.6}$$

Introducing eq. (D.5), eqs. (C.128) through (C.136) are written as follows:

$$\tilde{\phi}_S^* = - \left[ \sigma_0 \psi(1) + \sigma_\alpha \psi(\rho^\alpha) \right] \tag{D.7}$$

$$\tilde{\phi}_d^* = \left[ \mu_0 \omega(1) + \mu_\alpha \omega(\rho^\alpha) + \frac{1}{2} M_{\alpha\beta} \omega(\rho^\alpha \rho^\beta) + \frac{1}{6} m_{\alpha\beta\gamma} \omega(\rho^\alpha \rho^\beta \rho^\gamma) \right] \tag{D.8}$$

$$\tilde{v}_{S\beta}^* = \left[ \sigma_0 \tilde{W}_\beta(1) + \sigma_\alpha \tilde{W}_\beta(\rho^\alpha) \right] \tag{D.9}$$

$$\tilde{v}_{S3}^* = \left[ \sigma_0 \omega(1) + \sigma_\alpha \omega(\rho^\alpha) \right] \tag{D.10}$$

$$\tilde{v}_{d\alpha}^* = \left[ \mu_\alpha \omega(1) + M_{\alpha\beta} \omega(\rho^\beta) + \frac{1}{2} m_{\alpha\beta\gamma} \omega(\rho^\beta \rho^\gamma) \right] \tag{D.11}$$

$$\begin{aligned}
\tilde{v}_{ds}^* = & - \left[ \mu_\alpha \tilde{W}_\alpha(1) + M_{\alpha\beta} \tilde{W}_\alpha(\rho^\beta) + \frac{1}{2} m_{\alpha\beta\gamma} \tilde{W}_\alpha(\rho^\beta \rho^\gamma) \right] \\
& + \Omega^2 \left[ \mu_0 \psi(1) + \mu_\alpha \psi(\rho^\alpha) + \frac{1}{2} M_{\alpha\beta} \psi(\rho^\alpha \rho^\beta) + \frac{1}{6} m_{\alpha\beta\gamma} \psi(\rho^\alpha \rho^\beta \rho^\gamma) \right]
\end{aligned} \tag{D.12}$$

where

$$\psi(f) \equiv \iint \psi^* f d\xi' d\eta' \tag{D.13}$$

$$\omega(f) \equiv \iint \frac{\partial \psi^*}{\partial \xi'} f d\xi' d\eta' \quad (\text{D.14})$$

$$\tilde{W}_\alpha(f) \equiv \iint \frac{\partial \psi^*}{\partial \xi'^\alpha} f d\xi' d\eta' \quad (\text{D.15})$$

The problem of evaluating the panel influences reduces to the evaluation of the following integrals:

$$\psi(1), \psi(\rho^\alpha)$$

$$\omega(1), \omega(\rho^\alpha), \omega(\rho^\alpha \rho^\beta), \omega(\rho^\alpha \rho^\beta \rho^\gamma)$$

$$\tilde{W}_\alpha(1), \tilde{W}_\alpha(\rho^\beta), \tilde{W}_\alpha(\rho^\beta \rho^\gamma)$$

## D.2 PANEL EDGE COORDINATE SYSTEMS

The corners of a panel are enumerated by the subscript  $e$  in a counter clockwise direction. Their positions are denoted  $\vec{r}_e$ . The  $e$ th edge of a panel is described by the vector

$$\vec{T}_e = \vec{r}_{e+1} - \vec{r}_e, \quad (\text{D.16})$$

and

$$\hat{t}_e = \vec{T}_e / |\vec{T}_e| \quad (\text{D.17})$$

is a unit vector tangent to the  $e$ th edge. In indicial form

$$\hat{t}_e = t_e^\alpha \hat{\alpha}_\alpha \quad (\text{D.18})$$

where  $\hat{\alpha}_\alpha$  denotes the unit base vectors of the local system, cf. eq. (C.109). A normalized edge normal vector is then introduced as

$$\hat{n}_e = e_{\alpha\beta} t_e^\alpha \hat{\alpha}_\beta \quad (\text{D.19})$$

such that

$$n_e^1 = t_e^1, n_e^2 = -t_e^1$$

and

$$\hat{n}_e \times \hat{t}_e = e_{\alpha\beta} n_e^\alpha t_e^\beta = n_e^1 t_e^2 - n_e^2 t_e^1 = 1$$

The orthogonal unit vectors  $\hat{n}_e$  and  $\hat{t}_e$  are used to write

$$\vec{\rho} = a_e \hat{n}_e + V \hat{t}_e \quad (\text{D.20})$$

whence,

$$d\vec{\rho} = \hat{t}_e dc \quad (\text{D.21})$$

where  $dc$  is the differential arc length along an edge; also,

$$dc = dV. \quad (\text{D.22})$$

Recalling eq. (D.1) and introducing eq. (D.20),

$$\vec{R} = a_e \hat{n}_e + v \hat{t}_e + \vec{h}; \quad (\text{D.23})$$

whence,

$$R^2 = a_e^2 + v^2 + h^2.$$

Introducing polar coordinates, viz.,

$$\rho^1 = \rho \cos \phi \quad \text{and} \quad \rho^2 = \rho \sin \phi \quad (\text{D.24})$$

where

$$\rho \equiv |\vec{\rho}|.$$

then

$$\vec{\rho} \times d\vec{\rho} = \vec{\rho} \times \left[ \frac{\vec{\rho}}{\rho} d\rho + \rho d\phi \left( -\sin \phi \hat{\alpha}_1 + \cos \phi \hat{\alpha}_2 \right) \right].$$

Letting

$$\vec{v} = \rho d\phi \left( -\sin \phi \hat{\alpha}_1 + \cos \phi \hat{\alpha}_2 \right)$$

$$\vec{\rho} \times \vec{v} = e_{\alpha\beta} \rho^\alpha v^\beta = \rho^1 v^2 - \rho^2 v^1 = \rho^2 d\phi \left( \cos^2 \phi + \sin^2 \phi \right) = \rho^2 d\phi; \quad (\text{D.25})$$

thus,

$$\vec{\rho} \times d\vec{\rho} = \rho^2 d\phi .$$

Alternately,

$$\vec{\rho} \times d\vec{\rho} = (a_e \hat{n}_e + v \hat{t}_e) \times \hat{t}_e dv = a_e dv ; \quad (D.26)$$

hence, combining eqs. (D.25) and (D.26),

$$d\phi = \frac{a_e dv}{a_e^2 + v^2} \quad (D.27)$$

provides a relationship between the differential of the phase angle,  $\phi$ , and the edge coordinates.

### D.3 REDUCTION OF THE PANEL INTEGRALS TO FUNDAMENTAL INTEGRALS

Proceeding to a consideration of the integrals to be evaluated, consider first the relationship which can be established between  $\omega(\rho^\alpha f)$  and  $\tilde{W}_\alpha(f)$ .

Since

$$\frac{\partial \psi^*}{\partial \xi^\alpha} = \frac{\partial \psi^*}{\partial R} \frac{\partial R}{\partial \xi^\alpha} = \left( \frac{1}{R} \frac{\partial \psi^*}{\partial R} \right) \rho^\alpha, \quad \tilde{W}_\alpha(f) = \iint \rho^\alpha \left( \frac{1}{R} \frac{\partial}{\partial R} \psi^* \right) f d\xi' d\eta' ;$$

while, on the other hand, since

$$\frac{\partial \psi^*}{\partial \xi'} = \frac{\partial \psi^*}{\partial R} \frac{\partial R}{\partial \xi'} = - \left( \frac{1}{R} \frac{\partial \psi^*}{\partial R} \right) h ,$$

it follows that

$$\omega(\rho^\alpha f) = -h \iint \rho^\alpha \left( \frac{1}{R} \frac{\partial \psi^*}{\partial R} \right) d\xi' d\eta' .$$

Consequently, the two integrals are related as

$$\omega(\rho^\alpha f) = -h W_\alpha(f) ;$$

and, by induction,

$$\omega(\rho^\alpha) = -h W_\alpha(1)$$

$$\omega(\rho^\alpha \rho^\beta) = -h W_\alpha(\rho^\beta) \tag{D.28}$$

$$\omega(\rho^\alpha \rho^\beta \rho^\gamma) = -h W_\alpha(\rho^\beta \rho^\gamma)$$

The remaining integrals (viz.,  $\psi$ ,  $\omega$ ,  $\tilde{W}_\alpha$ ) are evaluated in terms of the cylindrical coordinates; whence,

$$d\xi d\eta = \left| \frac{\partial(\xi, \eta)}{\partial(\rho, \phi)} \right| d\rho d\phi = \rho d\rho d\phi. \tag{D.29}$$

In general, these integrals are not convergent; rather, their correct evaluation must be performed using the theory of finite parts.

Consider the integral performed for each edge, viz.,

$$\int_{\phi_e^-}^{\phi_e^+} d\phi \int_0^{\rho_e(\phi)} g\rho d\rho$$

where (figure 51)  $\phi_e^-$  and  $\phi_e^+$  denote the coordinates of the end points of the edge, while  $\rho_e(\phi)$  is simply the value of  $\rho$  expressed as a function of  $\phi$  along the eth edge.

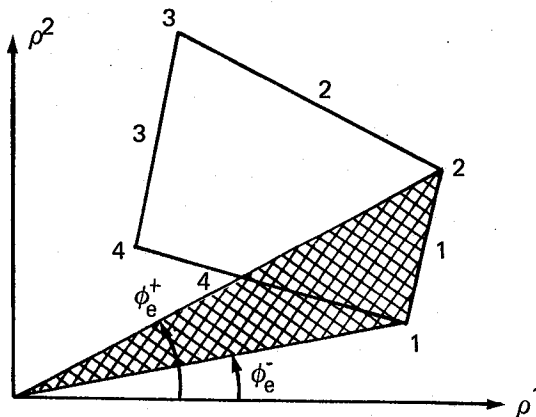


Figure 51. — Region of Integration Corresponding to a Panel Edge

Using these concepts,

$$\psi(1) = \sum_e \int_{\phi_e^-}^{\phi_e^+} d\phi \int_0^{\rho_e(\phi)} \psi^* \rho d\rho. \quad (D.30)$$

Defining

$$X(R) \equiv \int_0^R \psi R' dR' \quad (D.31)$$

and using the notation

$$R_e(\phi) = R|_{\rho = \rho_e(\phi)}, \quad (D.32)$$

it follows that

$$\psi(1) = \sum_e \int_{\phi_e^-}^{\phi_e^+} d\phi [X(R) - X(|h|)] = \sum_e \int_{\phi_e^-}^{\phi_e^+} d\phi X(R) - 2\pi C_0 X(|h|) \quad (D.33)$$

where  $C_0$  denotes the winding number, if the origin of the  $\rho^\alpha$  coordinates is interior to the panel,  $\Sigma_e$ . The winding number  $C_0$  is defined by the following relation:

$$\int_{\partial\Sigma_e} d\phi = 2\pi C_0 = \begin{cases} 0 & \text{(the boundary of } \Sigma_e \text{ does not} \\ & \text{encircle the origin)} \\ 2\pi & \text{(the boundary of } \Sigma_e \text{ does} \\ & \text{encircle the origin)} \end{cases} \quad (D.34)$$

Consider, now, the integral

$$\begin{aligned} \psi(\rho^\alpha f) &= \iint \rho^\alpha \psi^* f d\xi' d\eta' = \iint \left(\frac{\rho^\alpha}{\rho}\right) \left(\frac{\rho}{R}\right) (R \psi^*) (f) d\xi' d\eta' \\ &= \iint \left(\frac{\partial\rho}{\partial\xi^\alpha}\right) \left(\frac{\partial R}{\partial\rho}\right) \left(\frac{\partial X}{\partial R}\right) f d\xi' d\eta' = \iint \frac{\partial X}{\partial\rho^\alpha} f d\xi' d\eta'. \end{aligned}$$

Integrating by parts using Gauss' theorem,

$$\psi(\rho^\alpha f) = \int_{\partial} n_\alpha X f dc' - \iint X \frac{\partial f}{\partial \xi^\alpha} d\xi' d\eta';$$

thus, by induction,

$$\psi(\rho^\alpha) = \int_{\partial} n_\alpha X dc' \quad (D.35)$$

$$\psi(\rho^\alpha \rho^\beta) = \int_{\partial} \rho^\beta n_\alpha X dc' - \iint X d\xi' d\eta' \quad (D.36)$$

$$\psi(\rho^\alpha \rho^\beta \rho^\gamma) = \int_{\partial} \rho^\beta \rho^\gamma n_\alpha X dc' - \delta_{\beta\alpha} \iint \rho^\gamma X d\xi' d\eta' - \delta_{\gamma\alpha} \iint \rho^\beta X d\xi' d\eta' \quad (D.37)$$

where

$$\begin{aligned} \delta_{\alpha\beta} &= 1 \text{ if } \alpha = \beta \\ &= 0 \text{ if } \alpha \neq \beta. \end{aligned}$$

The integrals

$$\iint X d\xi' d\eta' \text{ and } \iint \rho^\alpha X d\xi' d\eta'$$

may be treated in a fashion identical to that given to  $\psi(1)$  and  $\psi(\rho^\alpha)$ .

Defining

$$\theta \equiv \int_0^R X R' dR', \quad (D.38)$$

$$X(1) \equiv \iint X d\xi' d\eta' = \sum_e \int_{\phi_e^-}^{\phi_e^+} \theta d\phi - 2\pi C_0 \theta \quad (|h|) \quad (D.39)$$

and

$$X(\rho^\alpha) \equiv \iint \rho X d\xi' d\eta' - \int_{\partial} n_\alpha \theta dc'. \quad (D.40)$$

Turning now to the treatment of  $\omega(1)$  and  $\tilde{W}_\alpha(f)$  and recalling that

$$\begin{aligned} \frac{\partial R}{\partial \xi'} &= -\frac{h}{R}, \quad \omega(1) = \iint \frac{\partial \psi^*}{\partial \xi'} d\xi' d\eta' \\ &= -h \iint \frac{1}{R} \frac{\partial \psi^*}{\partial R} d\xi' d\eta' = -h \sum_e \int_{\phi_e^-}^{\phi_e^+} d\phi \int_0^{\rho_e(\phi)} \frac{1}{R} \frac{\partial \psi^*}{\partial R} \rho d\rho. \end{aligned}$$

But,

$$\rho d\rho = R dR;$$

hence,

$$\omega(1) = -h \left\{ \sum_e \int_{\phi_e^-}^{\phi_e^+} \psi^* d\phi - 2\pi C_0 \psi^* (|h|) \right\}.$$

Next,

$$\tilde{W}_\alpha(f) = \iint f \frac{\partial \psi^*}{\partial \xi^\alpha} d\xi' d\eta' = \int_{\partial} n_\alpha \psi^* f ds' - \iint \psi^* \frac{\partial f}{\partial \xi^\alpha} d\xi' d\eta'; \quad (D.41)$$

consequently, by induction,

$$\tilde{W}_\alpha(1) = \int_{\partial} n_\alpha \psi^* ds' \quad (D.42)$$

$$\tilde{W}_\alpha(\rho^\beta) = \int_{\partial} \rho^\beta n_\alpha \psi^* ds' - \iint \psi^* d\xi' d\eta' \quad (D.43)$$

$$\tilde{W}_\alpha(\rho^\beta \rho^\gamma) = \int_{\partial} \rho^\beta \rho^\gamma n_\alpha \psi^* ds' - \delta_{\beta\alpha} \iint \rho^\gamma \psi^* d\xi' d\eta' - \delta_{\gamma\alpha} \iint \rho^\beta \psi^* d\xi' d\eta' \quad (D.44)$$

where the integrals on the right are given by eq. (D.28)

All of the required integral evaluations are now seen to be in terms of the following two operators:

the panel operator:

$$J(f) = \sum_e \int_{\phi_e^-}^{\phi_e^+} f d\phi - 2\pi C_0 f(|h|) \quad (D.45)$$

the edge operators:

$$I_e(g) = \int_{E_e} g ds' \quad (D.46)$$

$$\psi(1) = J(X) \quad (D.47)$$

$$\psi(\rho^\alpha) = \sum_e I_e(X)(n_e)_\alpha \quad (D.48)$$

$$\psi(\rho^\alpha \rho^\beta) = \sum_e I_e(\rho^\beta X)(n_e)_\alpha - J(\theta) \quad (D.49)$$

$$\psi(\rho^\alpha \rho^\beta \rho^\gamma) = \sum_e I_e(\rho^\beta \rho^\gamma X)(n_e)_\alpha - \delta_{\beta\alpha} \sum_e I_e(\theta)(n_e)_\gamma - \delta_{\gamma\alpha} \sum_e I_e(\theta)(n_e)_\beta \quad (D.50)$$

$$\omega(1) = -hJ(\psi^*) \quad (D.51)$$

$$\tilde{W}_\alpha(1) = \sum_e I_e(\psi^*)(n_e)_\alpha \quad (D.52)$$

$$\tilde{W}_\alpha(\rho^\beta) = \sum_e I_e(\rho^\beta \psi^*)(n_e)_\alpha - \psi(1) \quad (D.53)$$

$$\tilde{W}_\alpha(\rho^\beta \rho^\gamma) = \sum_e I_e(\rho^\beta \rho^\gamma \psi^*)(n_e)_\alpha - \delta_{\beta\alpha} \psi(\rho^\gamma) - \delta_{\gamma\alpha} \psi(\rho^\beta) \quad (D.54)$$

A careful examination of the integrals appearing in eqs. (D.47) through (D.54) reveals that the only integrals which need be evaluated are the following:

$$\begin{array}{cccc} hJ(\psi^*) & I_e(\psi^*) & I_e(\rho^\alpha \psi^*) & I_e(\rho^\alpha \rho^\beta \psi^*) \\ J(X) & I_e(X) & I_e(\rho^\alpha X) & I_e(\rho^\alpha \rho^\beta X) \\ J(\theta) & I_e(\theta) & & \end{array} \quad (D.55)$$

Before attacking this list of integrals, consider explicit expressions for the functions  $X$  and  $\theta$ , viz.,

$$X = -4\pi \int_0^R \psi^* R' dR' = \int_0^R e^{-i\Omega R'} dR' = \frac{e^{-i\Omega R} - 1}{(-i\Omega)} \quad (D.56)$$

and

$$\begin{aligned} \theta &= \int_0^R X R' dR' = \frac{1}{(-i\Omega)} \int_0^R R' (e^{-i\Omega R'} - 1) dR' \\ &= \frac{1}{(i\Omega)^2} \left\{ (-i\Omega R) [e^{-i\Omega R} - 1 - (-i\Omega R)] \right. \\ &\quad \left. - [e^{-i\Omega R} - 1 - (-i\Omega R) - (-i\Omega R)^2 / 2] \right\}. \end{aligned} \quad (D.57)$$

Introducing the abbreviated notation

$$x \equiv -i\Omega R, \quad (D.58)$$

then

$$-4\pi\psi^* = e^x / R; \quad (D.59)$$

$$X = R \left( \frac{e^x - 1}{x} \right); \quad (D.60)$$

and

$$\theta = R^3 \left\{ (e^x - 1 - x) / x^2 - (e^x - 1 - x - x^2 / 2) / x^3 \right\} \quad (D.61)$$

From these expressions  $\theta$  can be seen to be related to  $\psi^*$  and  $X$  as

$$\begin{aligned} \Omega^2 \theta &= 4\pi R^2 \psi^* + R x / 2 + X \\ &= 4\pi R^2 \psi^* - i\Omega R^2 / 2 + X. \end{aligned} \quad (D.62)$$

Returning to the problem of evaluating eq. (D.55), recall eqs. (D.20) and (D.22) so that, on referring to eq. (D.46),

$$\begin{aligned} I_e(\vec{\rho}\psi^*) &= \int_{E_e} (a_e \hat{n}_e + v \hat{t}_e) \psi^* dv = \hat{n}_e a_e I_e(\psi^*) + \hat{t}_e \int_{E_e} v \psi^* dv \\ &= \hat{n}_e a_e I_e(\psi^*) + \hat{t}_e X \Big|_{v^-}^{v^+}. \end{aligned} \quad (D.63)$$

Similarly,

$$I_e(\vec{\rho}X) = a_e \hat{n}_e I_e(X) + \hat{t}_e \theta \Big|_{v^-}^{v^+}. \quad (D.64)$$

Next,

$$\begin{aligned} I_e(\vec{\rho}\vec{\rho}\psi^*) &= \int_{E_e} (a_e \hat{n}_e + v \hat{t}_e) \vec{\rho}\psi^* dv \\ &= a_e \hat{n}_e I_e(\vec{\rho}\psi^*) + \hat{t}_e \int \vec{\rho} dX \\ &= a_e \hat{n}_e I_e(\vec{\rho}\psi^*) + \hat{t}_e \vec{\rho} X \Big|_{v^+}^{v^-} - \hat{t}_e \int X dv \\ &= a_e \hat{n}_e I_e(\vec{\rho}\psi^*) + \hat{t}_e \rho X \Big|_{v^+}^{v^-} - \hat{t}_e \hat{t}_e I_e(X). \end{aligned} \quad (D.65)$$

Similarly,

$$I_e(\vec{\rho}\vec{\rho}X) = a_e \hat{n}_e I_e(\vec{\rho}X) + \hat{t}_e \vec{\rho}\theta \Big|_{v^-}^{v^+} - \hat{t}_e \hat{t}_e I_e(\theta). \quad (D.66)$$

Recalling that eq. (D.12) contains a term multiplied by  $\Omega^2$  and noting that the term contains  $I_e(\theta)$ , eq. (D.12) involves eq. (D.62); hence, consider

$$\Omega^2 I_e(\theta) = -I_e(R^2\psi^*) - \frac{i\Omega}{2} I_e(R^2) + I_e(X). \quad (D.67)$$

Each term of eq. (D.67) is treated separately as follows:

$$\begin{aligned} I_e(R^2\psi^*) &= \int (v^2 + a_e^2 + h^2) \psi^* dv = \int v dX + (a_e^2 + h^2) I_e(\psi^*) \\ &= vX \Big|_{v^+}^{v^-} - \int X dv + (a_e^2 + h^2) I_e(\psi^*) = vX \Big|_{v^+}^{v^-} - I_e(X) + (a_e^2 + h^2) I_e(\psi^*) \\ I_e(R^2) &= (v^3/3) \Big|_{v^-}^{v^+} + (a_e^2 + h^2)(v^+ - v^-); \end{aligned}$$

thus,

$$\Omega^2 I_e(\theta) = 2I_e(X) - (a_e^2 + h^2) I_e(\psi^*) - vX \left| \frac{v^+}{v^-} - \frac{i\Omega}{2} (v^3 / 3) \right| \frac{v^+}{v^-} + (a_e^2 + h^2)(v^+ - v^-). \quad (D.68)$$

Similarly, consider

$$\Omega^2 J(\theta) = -h^2 J(\psi^*) + J(X) - \sum_e a_e I_e(\psi^*) \quad (D.69)$$

The above results complete the reductions which are possible without becoming heavily involved in the theory of special functions. For the treatment of the remaining integrals, recourse is made to techniques that involve approximating the integrand with expressions that are integrable in closed form.

#### D.4 APPROXIMATIONS FOR EVALUATING THE FUNDAMENTAL INTEGRALS

This section treats in detail the computation of the fundamental integrals  $I_e(\psi)$ ,  $I_e(X)$ ,  $hJ(\psi)$ ,  $J(X)$ , and  $J(\theta)$ . The approach which is used is this: Treat singular parts of an integrand separately and use a high order polynomial approximation on the regular part of the integrand (also, functions of  $R$  are approximated by polynomials in  $R$ ).

For the evaluation of  $J$  integrals the operations are as follows:

The unsteady kernel function, viz.,

$$\psi^* = -\frac{1}{4\pi} \frac{e^{-i\Omega R}}{R},$$

is expressed as

$$\psi^* = \psi_0 + {}^*\psi$$

where

$$\psi_0 = -\frac{1}{4\pi R} \quad (D.70)$$

is the steady kernel function; hence,

$${}^*\psi = \psi^* - \psi_0 = (e^{-i\Omega R} - 1) / R. \quad (D.71)$$

The function  ${}^*\psi$  is an analytic function of  $R$ ; consequently, it can be estimated quite accurately by polynomial interpolation.

In general, the approximation procedure consists of determining the coefficients for the approximation having the following form:

$$*\psi \approx *\tilde{\psi} \equiv \sum_{n=0}^N C_n (*\psi) R^n. \quad (D.72)$$

All that is required of this approximation is that it be accurate for values of  $R$  ranging over the boundary of the panel. (The reason for this is shown below.) Recalling the definition of  $J$ , i.e., eq. (D.45),

$$J(*\psi) = \sum_e \int_{\phi_e^-}^{\phi_e^+} *\psi d\phi - 2\pi C_0 *\psi(lh); \quad (D.73)$$

since  $*\tilde{\psi}$  accurately approximates  $*\psi$  on the boundary,

$$\begin{aligned} J(*\psi) &\approx \sum_e \int_{\phi_e^-}^{\phi_e^+} *\tilde{\psi} d\phi - 2\pi C_0 *\psi(lh) \\ &\approx J(*\tilde{\psi}) - 2\pi C_0 \{*\psi(lh) - *\tilde{\psi}(lh)\} \\ &\approx \sum_{n=0}^N C_n (*\psi) J(R^n) - 2\pi C_0 \{*\psi(lh) - *\tilde{\psi}(lh)\} \end{aligned} \quad (D.74)$$

where the presence of the second term allows  $*\tilde{\psi}(lh)$  to be a relatively poor approximation to  $*\psi(h)$ .

In a similar fashion,  $X$  and  $\theta$  are approximated by the formulae:

$$X \approx \tilde{X} \equiv \sum_{n=0}^N C_n(X) R^n \quad (D.75)$$

$$\theta \approx \tilde{\theta} \equiv \sum_{n=0}^N C_n(\theta) R^n \quad (D.76)$$

where a higher degree polynomial is used for  $\theta$  than is used for either  $*\psi$  or  $X$  for two reasons: (i) it involves no greater computational cost and (ii) the limiting behavior of  $\theta$  as  $\Omega$  tends to zero is given by

$$\lim_{\Omega \rightarrow 0} \theta = R^3 / 3;$$

thus, if  $N = 1$ ,  $N + 2 = 3$  will be required to follow the behavior of  $\theta$  in the limit of small frequency. Using the approximations shown by eqs. (D.75) and (D.76),

$$J(X) \approx \sum_{n=0}^N C_n(X) J(R^n) - 2\pi C_0 \{ X(|h|) - \tilde{X}(|h|) \} \quad (D.77)$$

$$J(\theta) \approx \sum_{n=0}^N C_n(\theta) J(R^n) - 2\pi C_0 \{ \theta(|h|) - \tilde{\theta}(|h|) \} \quad (D.78)$$

The task of evaluating the integrals has now been reduced to one of computing  $hJ(\psi_0)$  and  $J(R^n)$  for  $n = 0, \dots, N+2$ . Those operations are facilitated by a recursion formula for  $J(R^n)$ . Using the definition of  $J(f)$ , i.e., eq. (D.45), and some of the identities derived in the preceding (viz., eqs. (D.1), (D.27), and (D.46)),

$$\begin{aligned} J(R^n) &= \sum_e \int_{\phi_e^-}^{\phi_e^+} R^n d\phi - 2\pi C_0 |h|^n = \sum_e \int_{\phi_e^-}^{\phi_e^+} (\rho^2 + h^2) R^{n-2} d\phi - 2\pi h^2 C_0 |h|^{n-2} \\ &= \sum_e \int_{\phi_e^-}^{\phi_e^+} \rho^2 R^{n-2} \frac{a_e dv}{\rho^2} + h^2 J(R^{n-2}) = \sum_e \int_{v^-}^{v^+} a_e R^{n-2} dv + h^2 J(R^{n-2}) \\ &= \sum_e a_e I_e(R^{n-2}) + h^2 J(R^{n-2}). \end{aligned} \quad (D.79)$$

For  $n = 1$ , note that

$$-\frac{1}{4\pi} h^2 J(R^{-1}) = h(hJ(\psi_0)); \quad (D.80)$$

consequently, eqs. (D.79) and (D.80) provide a recursive relation for evaluating  $J(R^n)$  for all  $n$  if  $J(\psi_0)$  and  $J(1)$  are known. From eq. (D.46)

$$J(1) = \sum_e \int_{\phi_e^-}^{\phi_e^+} d\phi - 2\pi C_0 = 0 \quad (D.81)$$

because the panel edges form a close curve; thus, only the integral  $hJ(\psi_0)$  is required.

The integral  $J(\psi_0)$  has been studied extensively and these studies (ref 17, appendix J.7, J.8; ref 19 appendix G) have led to two basic forms, called the standard rationalization and the special rationalization. The standard rationalization is given (the quantity  $J$  of equation J.8.98, ref. 17 is to be identified with  $hJ(\psi_0)$ ),

$$hJ(\psi_0) = -\text{sgn}(h) \left[ 2\pi - \sum_{\substack{\text{panel} \\ \text{corners, } c}} (\pi - \text{Ph}(X_c, Y_c)) \right] \quad (D.82)$$

where

$$X_c = -h^2 \hat{t}_c \cdot \hat{t}_{c-1} - a_c a_{c-1} \quad (D.83)$$

$$Y_c = |h| R_c \hat{t}_{c-1} \times \hat{t}_c$$

and the phase function,  $\text{Ph}(\cdot, \cdot)$ , defined by

$$\text{Ph}(X_c, Y_c) = \arg(X_c + iY_c), -\pi < \epsilon \leq \pi,$$

is essentially equivalent to the standard intrinsic Fortran function ATAN2. (It is pertinent to remark that the expression [  $-J(\psi_0)$  ] of this document is equal to the expression  $H(1,1,3)$  that figures so prominently in appendixes D and G of ref. 19.)

The edge integrals,  $I_e$ , are determined using eq. (D.79) for values of  $n=1,2,\dots,N+2$ .

The procedures for  $I_e(\psi)$  and  $I_e(X)$  follow by combining eqs. (D.71) and (D.72) to obtain

$$*\psi \approx *\hat{\psi} \equiv \sum_{n=0}^N C_n(*\psi) R^n. \quad (D.84)$$

Applying the operator  $I_e$  to this relation and to eq. (D.75) yields the following estimates:

$$I_e(\psi) \approx I_e(1/R) + \sum_{n=0}^N C_n(*\psi) I_e(R^n) \quad (D.85)$$

and

$$I_e(X) \approx \sum_{n=0}^N C_n(X) I_e(R^n); \quad (D.86)$$

consequently, the computation required consists of the evaluation of  $I_e(R^K)$  for  $K = -1, 0, \dots, N$ . This is exactly the same set of information which is required for the evaluation of the  $J$  integrals, cf. eq. (D.79).

The following provides a recursion formula for the required integrals:

$$I_e(R^k) = \int_{v_e^-}^{v_e^+} R^k ds' = \int_{v_e^-}^{v_e^+} (v^2 + g_e^2) R^{k-2} dv$$

for

$$g_e^2 \equiv \rho_e^2 + h^2$$

$$\begin{aligned}
I_e(R^k) &= \int_{v_e^-}^{v_e^+} v^2 R^{k-1} dv + g_e^2 I_e(R^{k-2}) \\
&= \left\{ v \left( \frac{R^k}{k} \right) \Big|_{v_e^-}^{v_e^+} + \int_{v_e^-}^{v_e^+} R^k dv + g_e^2 (R^{k-2}) \right\} \\
&= v \frac{R^k}{k} \Big|_{v_e^-}^{v_e^+} - \frac{1}{k} I_e(R^k) + g_e^2 (R^{k-2})
\end{aligned}$$

Rearranging terms yields the recursion formula as

$$\begin{aligned}
I_e(R^k) &= \frac{k}{k+1} \left\{ \frac{1}{k} v R^k \Big|_{v_e^-}^{v_e^+} + g_e^2 I_e(R^{k-2}) \right\} \\
&= \frac{1}{k+1} \Delta(v R^k) + \frac{k}{k+1} g_e^2 I_e(R^{k-2})
\end{aligned} \tag{D.87}$$

where

$$\Delta(v R^k) \equiv v R^k \Big|_{v_e^-}^{v_e^+}$$

This recursion relation reduces the requirement to that of evaluating  $I_e(1/R)$  and  $I_e(1)$ . These integrals are evaluated as

$$I_e(1) = \int_{E_e} dc' = \Delta V \tag{D.88}$$

where

$$\Delta V \equiv v_e^+ - v_e^-$$

while

$$\begin{aligned}
I_e(1/R) &= \int_{E_e} \frac{dV}{R} = \int_{E_e} \frac{dv}{\sqrt{v^2 + g_e^2}} \\
&= \frac{1}{2} \ln \left( \frac{v+R}{v-R} \right) \Big|_{v_e^-}^{v_e^+}
\end{aligned} \tag{D.89}$$

## D.5 POLYNOMIAL ESTIMATION PROCEDURES

The preceding provides the procedures for evaluating the near field panel influence coefficients with the exception of the polynomial estimation procedures for  ${}^*\psi, X, \theta$ . Those polynomial estimation procedures are derived in this section. One of the principal considerations in constructing the polynomial estimates is that they be analytically precise in the limit as  $\Omega$  tends to zero. Since the limiting forms of these functions are

$${}^*\psi \approx (-i\Omega) + \frac{1}{2} (i\Omega)^2 R \rightarrow 0$$

$$X \approx R - \frac{1}{2} i\Omega R^2 \rightarrow R$$

$$\theta \approx R^3/3 \rightarrow R^3/3,$$

motivation is provided for requiring (at least in the case of small frequencies)

$${}^*\tilde{\psi} + i\Omega = O(R)$$

$$\tilde{X} - R = O(R^2)$$

$$\tilde{\theta} - R^3/3 = O(R^4).$$

In fact, it is convenient to require a somewhat stronger condition for  ${}^*\tilde{\psi}$ , viz.,

$${}^*\tilde{\psi} + i\Omega - \frac{1}{2} (i\Omega)^2 R = O(R^2) \text{ as } R \rightarrow 0.$$

Consequently, if the estimates of  ${}^*\psi$ ,  $X$ , and  $\theta$  are required for values of  $R$  such that  $\Omega R < 1$ , the estimates can be chosen to have the following forms:

$$\left. \begin{aligned} {}^*\tilde{\psi} &= -i\Omega - \frac{1}{2} \Omega^2 R + R^2 P_{N-2}(R) \\ \tilde{X} &= R + R^2 P_{N-2}(R) \\ \tilde{\theta} &= R^3/3 + R^4 P_{N-2}(R) \end{aligned} \right\} \text{ for } \Omega R_{\min} < 1 \quad (\text{D.90})$$

where  $R_{\min}$  is the minimum value of  $R$  for which the approximations must be accurate and  $P_{N-2}$  denotes some polynomial (different for each function  ${}^*\tilde{\psi}, \tilde{X}$ , or  $\tilde{\theta}$ ) of degree

less than or equal to (N-2). Since a polynomial of degree (N-2) is determined by its value at (N-1) points, the functions  $^*\psi, X$ , and  $\theta$  must be sampled at (N-1) points in order to determine the precise forms of the approximations.

The reason now becomes clear why it is convenient to fit the first two terms of the Taylor expansion of  $^*\psi$  and the first four terms of the expansion of  $X$  while requiring the degree of  $\theta$  to be (N+2) rather than N. With this choice there is a fit to the analytical behavior of these kernels for small R while the number of the remaining degrees of freedom is identical for each of the three functions. Since the functions of  $^*\psi, X$ , and  $\theta$  are all structurally similar, all three functions can be evaluated at the same (N-1) points. This mode of evaluation requires substantially less computational effort than would be required were each function evaluated at a different set of points.

Eq.(D.90) describes the approximation procedure for the case when  $\Omega R_{\min} < 1$ . More generally, the following procedure is used.

- (1) Find the minimum value,  $R_{\min}$ , and the maximum value,  $R_{\max}$ , which R assumes on the boundary of the panel and define

$$R_0 = \begin{cases} R_{\min} & \text{if } \Omega R_{\min} > \epsilon \\ 0 & \text{if } \Omega R_{\min} \leq \epsilon \end{cases} \quad (\text{D.91})$$

where, nominally,  $\epsilon = 0.1$ .

- (2) The functions  $^*\psi, X, \theta$  are fitted, for  $R \in [R_0, R_{\max}]$ , by the polynomial forms

$$^*\tilde{\psi} = ^*\psi(R_0) + ^*\psi'(R_0)(R - R_0) + (R - R_0)^2 P_{N-2}(^*\psi) \quad (\text{D.92})$$

$$\tilde{X} = X(R_0) + X'(R_0)(R - R_0) + (R - R_0)^2 P_{N-2}(X) \quad (\text{D.93})$$

$$\tilde{\theta} = \sum_{j=0}^3 \theta^{(j)}(R_0) \frac{(R - R_0)^j}{j!} + (R - R_0)^4 P_{N-2}(\theta). \quad (\text{D.94})$$

- (3) The remaining (N-1) degrees of freedom are determined by sampling  $^*\psi, X$ , and  $\theta$  at "constrained Tchebysheff abscissae" points chosen to globally minimize the expected error in the estimation of  $^*\tilde{\psi}$  and  $\theta$ . The sample points, denoted as  $R_i$  have the form

$$R_i = R_0 + (R_{\max} - R_0) t_i^{(N-1)} \text{ for } i = 1, \dots, N-1 \quad (\text{D.95})$$

where  $t_i^{(n)}$  are normalized interpolation points which must be determined by solving  $J$  nonlinear equations in the following. When the functions have been sampled at these points, the remaining degrees of freedom are constrained by interpolation.

The value of  $N$ , the degree of the approximation, remains to be chosen by a careful error analysis of the above procedure, see sec. D.6.

Consider the following class of polynomials which are called "constrained Tchebycheff polynomials" and which are associated with the optimal choice of interpolation points for the constrained interpolation problem,

$$f(x) = f(0) + xf'(0) + x^2 P_{N-2}(x) \text{ for } 0 \leq x \leq 1. \quad (\text{D.96})$$

A set of basis polynomials is characterized as follows

$$P_0 = 1, P_1 = x, P_2 = x^2; \quad (\text{D.97})$$

and, for  $m > 0$ ,  $P_{m+2}$  is characterized by the conditions:

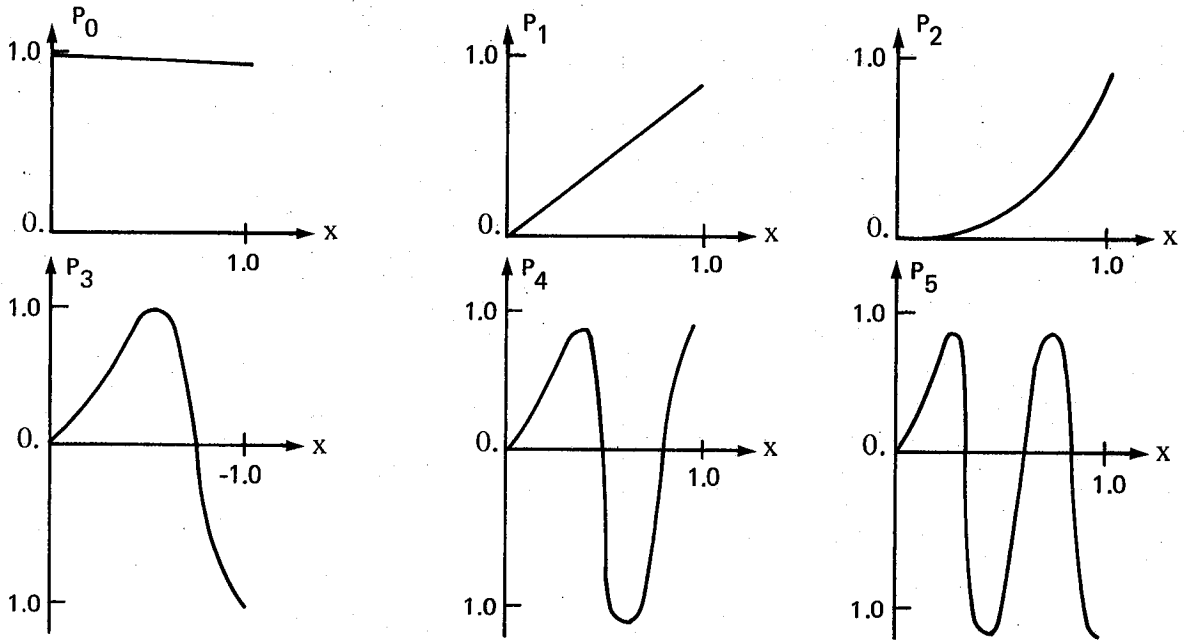
$$P_{m+2}(0) = P'_{m+2}(0) = 0, P_{m+2}(1) = (-1)^m, \quad (\text{D.98-a})$$

$P_{m+2}$  has  $m$  extrema between 0 and 1 at  $x_i$  for  $i = 1, \dots, m$  and these extrema satisfy

$$P'_{m+2}(x_i) = 0 \quad (\text{D.98-b})$$

$$P_{m+2}(x_i) = (-1)^{i-1} \quad (\text{D.98-c})$$

Diagrammatically, the basis polynomials appear as



The problem is to find the extremum points of  $P_{m+2}$  for all  $m$  and, in this way, characterize the family of basis polynomials. Once the basis polynomials are known, their roots can be determined to obtain the natural analogues of Tchebycheff abscissae. The roots of  $P_{n+1}$  (which are  $N-1$  in number in the interval  $0 \leq x \leq 1$ ) provide the evaluation points of  $f(x)$  for which the optimal solution to the problem is obtained.

The nonlinear algebraic equation which must be satisfied by the set of extremum points for  $P_{m+2}$  is derived as follows. Using the conditions eqs. (D.98a) and (D.98c), it is clear the  $P_{m+2}(x)$  may be expressed in terms of the numbers  $x_i$  by the following formula (Lagrange interpolation):

$$P_{m+2}(x) = \sum_{i=1}^m (-1)^{i-1} \delta_i(x) / \delta_i(x_i) + (-1)^m \delta_{m+1}(x) / \delta_{m+1}(1) \quad (D.99)$$

where

$$\delta_i(x) = x^2(x-1) \prod_{\substack{j=1 \\ j \neq i}}^m (x-x_j) \quad (D.100-a)$$

$$\delta_{m+1}(x) = x^2 \prod_{j=1}^m (x-x_j)$$

The actual positions of the points  $x_i$  are then determined by improving the constraint shown as eq. (D.98b). Computing  $P'_{m+2}(x_i)$ ,

$$\begin{aligned}
 P'_{m+1}(x_k) &= \sum_{\substack{i=1 \\ i \neq k}}^m (-1)^{i-1} (\delta_k / \delta_i) \frac{1}{x_k - x_i} \\
 &+ (-1)^{k-1} \left[ \frac{2}{x_k} + \frac{1}{x_{k-1}} + \sum_{\substack{i=1 \\ i \neq k}}^m \frac{1}{x_k - x_i} \right] \\
 &+ (-1)^m (\delta_k / \delta_{m+1}) \frac{1}{x_k - 1}
 \end{aligned} \tag{D.101}$$

where

$$\delta_k = \delta_k(x_k), \delta_{m+1} = \delta_{m+1}(1). \tag{D.102}$$

Eq. (D.101) motivates the definition of a function  $F$  as follows

$$\begin{aligned}
 F_k(x) &= \sum_{\substack{i=1 \\ i \neq k}}^m \frac{1}{(x_k - x_i)} \left[ \frac{(-1)^{i-1}}{\delta_i} + \frac{(-1)^{k-1}}{\delta_k} \right] \\
 &+ \frac{1}{(x_k - 1)} \left[ \frac{(-1)^m}{\delta_{m+1}} + \frac{(-1)^{k-1}}{\delta_k} \right] + (-1)^{k-1} \frac{2}{x_k \delta_k} \\
 &= (-1)^{k-1} \frac{2}{x_k \delta_k} + \sum_{\substack{i=1 \\ i \neq k}}^{m+1} \frac{1}{x_k - x_i} \left( \frac{(-1)^{i-1}}{\delta_i} + \frac{(-1)^{k-1}}{\delta_k} \right)
 \end{aligned}$$

$$P(x) = \sum_{i=1}^{m+1} (-1)^{i-1} \delta_i(x) / \delta_i(x_i)$$

$$\delta_i(x) = x^2 \prod_{\substack{j=1 \\ j \neq i}}^{m+1} (x - x_j)$$

$$x_{m+1} \equiv 1$$

$$P'(x) = \sum_{i=1}^{m+1} (-1)^{i-1} \frac{\delta'_i(x)}{\delta_i(x)} \frac{\delta_i(x)}{\delta_i(x_i)}$$

$$\frac{\delta'_i(x)}{\delta_i(x)} = \frac{2}{x} + \sum_{\substack{j=1 \\ j \neq i}}^{m+1} \frac{1}{x-x_j} \qquad \frac{\delta'_i(x_i)}{\delta_i(x_i)} = \frac{2}{x_i} + \sum_{\substack{j=1 \\ j \neq i}}^{m+1} \frac{1}{x_i-x_j}$$

$$\delta'_i(x_k) = x_k^2 \prod_{j \neq i, k} (x_k - x_j) = \delta_k / (x_k - x_i)$$

$$P'(x_k) = \sum_{\substack{i=1 \\ i \neq k}} (-1)^{i-1} \frac{\delta_k / \delta_i}{(x_k - x_i)} + (-1)^{k-1} \left[ \frac{2}{x_k} + \sum_{\substack{j=1 \\ j \neq k}} \frac{1}{x_k - x_j} \right]$$

$$= \frac{2(-1)^{k-1}}{x_k \delta_k} + \sum_{\substack{i=1 \\ i \neq k}} \frac{1}{x_k - x_i} \left[ \frac{(-1)^{k-1}}{\delta_i} + \frac{(-1)^{k-1}}{\delta_k} \right]$$

## D.6 ERROR ANALYSIS FOR CONSTRAINED POLYNOMIAL FITTING

In this section a rigorous error analysis is presented for the polynomial approximations to the functions  $^*\psi(R)$ ,  $X(R)$  and  $\theta(R)$ . The error bounds are relative error bounds; for  $^*\psi$ , the error bound takes the form

$$|^*\psi(R) - ^*\tilde{\psi}(R)| \leq |^*\psi,0| \eta.$$

Here,  $^*\psi(R)$  is the transcendental function to be approximated by a polynomial in  $R$ ,  $^*\tilde{\psi}(R)$  is the associated polynomial approximation, and  $^*\psi,0$  is a "gauge function" chosen so that the following approximate bound holds:

$$|^*\psi(R) / ^*\psi,0| \lesssim 1.$$

The small positive number  $\eta$  measures the relative accuracy of the approximation. It turns out that because the function  $^*\psi(R)$  is analytic in  $R$  with all of its derivations nicely bounded, a value of  $\eta = 10^{-10}$  can be achieved for all practical purposes by polynomials of degree less than or equal to 8.

Now, in the evaluation of aerodynamic influence coefficients, integrals of the form

$$\iint_{\Sigma_e} ^*\psi ds' \text{ and } \int_{E_e} ^*\psi d\phi$$

are approximated by computing the corresponding integrals for the polynomial approximations, that is,

$$\iint_{\Sigma_e} ^*\tilde{\psi} ds' \text{ and } \int_{E_e} ^*\tilde{\psi} d\phi$$

Using the relative error bound for  $^*\psi$  given above, the quality of these approximations is assessed by means of the following integral error bounds:

$$\left| \iint_{\Sigma_e} ^*\psi ds' - \iint_{\Sigma_e} ^*\tilde{\psi} ds' \right| \leq |^*\psi,0|_{\max} \eta \Delta s' \text{ and } \left| \int_{E_e} ^*\psi d\phi - \int_{E_e} ^*\tilde{\psi} d\phi \right| \leq |^*\psi,0|_{\max} \eta \pi$$

From this, it is easily seen that  $\eta$  provides an appropriate estimate of the relative accuracy of the integrals as well. Thus, a relative error bound for the polynomial approximation  ${}^*\tilde{\psi}$  translates directly into a similar relative error bound for the required integrals.

Having described (in a general sort of way) the nature and the purpose of the error bounds, it is now appropriate to present and derive the precise error bounds that are required. As a beginning, this presentation and derivation requires the development of some notation.

The functions  ${}^*\psi(R)$ ,  $X(R)$  and  $\theta(R)$  for which polynomial approximations are desired are given by

$${}^*\psi(R) = (e^{-i\Omega R} - 1) / R \quad (D.103)$$

$$X(R) = \int_0^R \psi(R')R'dR' = (e^{-i\Omega R} - 1) / (-i\Omega) \quad (D.104)$$

$$\begin{aligned} \theta(R) = \int_0^R X(R')R'dR' = R^3 \left\{ \left[ e^{-i\Omega R} - 1 - (-i\Omega R) \right] / (-i\Omega R)^2 \right. \\ \left. - \left[ e^{-i\Omega R} - 1 - (-i\Omega R) - \frac{1}{2}(-i\Omega R)^2 \right] / (-i\Omega R)^3 \right\}. \end{aligned} \quad (D.105)$$

Note that for small frequencies ( $\Omega \rightarrow 0$ ), the functions  ${}^*\psi$ ,  $X$  and  $\theta$  exhibit the following limiting behavior:

$${}^*\psi = -i\Omega + O(\Omega^2) \quad (D.106)$$

$$X = R + O(\Omega) \quad (D.107)$$

$$\theta = R^3 / 3 + O(\Omega) \quad (D.108)$$

These limiting properties motivate the definition of the "gauge functions":  ${}^*\psi_o$ ,  $X_o$ ,  $\theta_o$ , which will be used later in the statement of the error bounds. The definitions of the gauge functions are as follows:

$${}^*\psi_o \equiv -i\Omega \quad (D.109)$$

$$X_o \equiv R \quad (D.110)$$

$$\theta_o \equiv R^3 / 3. \quad (D.111)$$

Now, when approximations are desired for the  ${}^*\psi$ ,  $X$ , and  $\theta$  for  $R$  lying in the internal  $[R_0, R_{\max}]$ , the approximating polynomials are assumed to have the following structure:

$${}^*\tilde{\psi}(R) = {}^*\psi(R_0) + {}^*\psi'(R_0)(R - R_0) + (R + R_0)^2 P_{N-2}[{}^*\psi](R) \quad (D.112)$$

$$\tilde{X}(R) = X(R_0) + X'(R_0)(R - R_0) + (R - R_0)^2 P_{N-2}[X](R) \quad (D.113)$$

$$\tilde{\theta}(R) = \sum_{j=0}^3 \theta^{(j)}(R_0) (R - R_0)^j / j! + (R - R_0)^4 P_{N-2}[\theta](R). \quad (D.114)$$

Here,  $P_{N-2}[f](R)$  denotes a polynomial of degree  $N-2$  in the variable  $R$ , determined by the function  $f$ . (Note:  $N$  is restricted to be greater than or equal to 1. For  $N = 1$ ,  $N-2 = -1$  and the convention is adopted that  $P_{-1}[f](R) \equiv 0$ .) The coefficients of the polynomials  $P_{N-2}[{}^*\psi]$ ,  $P_{N-2}[X]$  and  $P_{N-2}[\theta]$  are determined by requiring that the polynomials  ${}^*\tilde{\psi}$ ,  $\tilde{X}$ ,  $\tilde{\theta}$  agree with the functions  ${}^*\psi$ ,  $X$ ,  $\theta$  at the  $N-1$  values of  $R$ , viz.,

$$R_i = R_0 + (R_{\max} - R_0) Z_i^{(N+1)} \quad i=1,2,\dots,N-1. \quad (D.115)$$

The numbers  $Z_i^{(N+1)}$ ,  $i = 1, \dots, N-1$  are the non-zero roots of a polynomial  $P_{N+1}(x)$  having the form

$$P_{N+1}(X) = K_{N+1} X^2 \prod_{i=1}^{N-1} (x - z_i^{(N+1)}). \quad (D.116)$$

The polynomial  $P_{N+1}(X)$  is a "constrained Tschebycheff basis polynomial" which is a family of polynomials that will be described below.

The accuracy of the polynomial approximations, i.e., eqs. (D.112), (D.113), and (D.114), is determined by two parameters:

- (i)  $N$ , which determines the degree of the various polynomial approximations, and
- (ii)  $\Delta\phi$ , the total phase variation experienced by the function  $e^{-i\Omega R}$  for  $R \in [R_0, R_{\max}]$

where it should be noted the  $\Delta\phi$  is given explicitly by

$$\Delta\phi = \left| \Omega (R_{\max} - R_0) \right|. \quad (D.117)$$

For  $R$  lying in the interval  $[R_0, R_{\max}]$ , the accuracy of the polynomial approximations, i.e., Eqs. (D.112), (D.113), and (D.114), can be described precisely by the following relative error bounds:

$$|(*\psi - *\tilde{\psi}) / *\psi_0| < \frac{C_{N+1}}{N+2} (\Delta\phi)^{N+1} \quad (\text{D.118})$$

$$|(X - \tilde{X}) / X_0| < D_{N+1} (\Delta\phi)^N \quad (\text{D.119})$$

$$|(\theta - \tilde{\theta}) / \theta_0| < \frac{3}{N+3} \left[ \frac{C_{N+1}}{N+2} (\Delta\phi)^{N+1} + D_{N+1} (\Delta\phi)^N \right]. \quad (\text{D.120})$$

The parameters  $C_{N+1}$ ,  $D_{N+1}$  (tabulated in Table 8) are called "truncation error coefficients"; they decrease rapidly with increasing  $N$ . The bounds, viz., eqs. (D.118) (D.119), and (D.120), clearly show that if  $N$  is chosen large enough that

$$\frac{C_{N+1}}{N+2} (\Delta\phi)^{N+1} < \eta \quad (\text{D.121})$$

and

$$D_{N+1} (\Delta\phi)^N < \eta, \quad (\text{D.122})$$

then the following relative error bounds will immediately follow:

$$|(*\psi - *\tilde{\psi}) / *\psi_0| < \eta$$

$$|(X - \tilde{X}) / X_0| < \eta$$

$$|(\theta - \tilde{\theta}) / \theta_0| < \frac{3}{2} \eta$$

Thus, for any specified error tolerance,  $\eta$ , an appropriate value of  $N$  is selected so that the two inequalities: eqs. (D.121) and (D.122), are enforced, consequently, assuring sufficient accuracy is obtained in the polynomial approximations: eqs. (D.112), (D.113), (D.114). It is pertinent to remark that for  $\Delta\phi = 2\pi / 6$  (so that  $[R_0, R_{\max}]$  spans  $1/6$  of a wave length) and  $\eta = 10^{-10}$  (10 significant digits), the inequalities eqs. (D.121) and (D.122) are satisfied provided  $N \geq 8$ . A fairly complete table of the maximum phase variation,  $\Delta\phi$ , allowable for a given  $N$  and  $\eta$  is presented in Table 9.

Table 8. — Truncation Coefficients\* and Zeros\*\* of Constrained Tschebycheff Polynomials\*\*\*

N	2	3	4	5	6
C(N+1)	.176488E-01	.788915E-03	.327165E-04	.120822E005	.396476E-07
D(N+1)	.333095E-01	.261056E-02	.168479E-03	.894424E-05	.399135E-06
1.	.894107456974979	.606717423814530	.418254069443174	.301674740674210	.226595419540605
2.		.951856618566651	.761423683974629	.590322089237812	.462063955210008
ℓ 3.			.971712927869628	.838296069702794	.694739789581133
4.				.981195629247498	.882789721841533
5.					.986532130357020
N	7	8	9	10	11
C(N+1)	.116355E-08	.307903E-10	.740598E-12	.163101E-13	.331018E-15
D(N+1)	.152913E-07	.511954E-09	.151990E-10	.404951E-12	.997958E-14
1.	.175946932336543	.140351289637167	.114455639954652	.095862800941203	.080180344720937
2.	.368204640983135	.298873937094264	.246743790067857	.095062800941203	.080180344720937
3.	.574775757973370	.477851060077372	.401168084345066	.340339265992784	.291682130160915
4.	.765287083020215	.656524898416237	.563272199092783	.485427407681714	.420942838028783
5.	.911009103656216	.813554821066919	.717353855456647	.630434630202327	.554690530009402
ℓ 6.	.989854498274183	.930077552626063	.848391222077275	.763662228532745	.683850675866850
7.		.992071284053473	.943584280361694	.874338729060653	.799639161635557
8.			.993627507931414	.953508620868845	.894174252256846
9.				.994763511480262	.961018408761163
10.					.995618902517403

\*C(N+1) and D(N+1)

$$** \left\{ z_{\ell}^{(N+1)} \right\}_{\ell=1}^{N-1}$$

\*\*\* $P_{N+1}(X), N=2, \dots, 11$

Table 9. — Maximum Admissible Phase Variation\*

N \ M**	M**				
	4	6	8	10	12
2	.0752	.0075	.0008	.00008	.0000075
3	.4992	.1075	.0232	.0050	.0011
4	1.3244	.4188	.1324	.0419	.0132
5	2.4179	.9626	.3832	.1526	.0607
6	3.6825	1.7093	.7934	.3682	.1709
7	5.0646	2.6232	1.3587	.7037	.3645
8	6.5074	3.6594	2.0578	1.1572	.6507
9	7.9904	4.7902	2.8717	1.7215	1.0320
10	9.5116	6.0014	3.7866	2.3892	1.5075
11	11.0543	7.2730	4.7852	3.1483	2.0714

\*Maximum phase variation,  $(\Delta\phi)_{\max}$ , for a polynomial approximation of a given order N and relative accuracy  $\eta$ .

\*\*  $\eta = 10^{-M}$   
 $-\log_{10}(\eta) [\eta]$  (significant digits)

Having stated and discussed the fundamental error bounds: eqs. (D.118), (D.119), (D.120), it is now appropriate to present a derivation and proof of their validity.

As a starting point for this discussion, consider a family of polynomials  $\{P_i\}_{i=0}^{\infty}$ , called "Constrained Tschebycheff basis polynomials." These polynomials are characterized by two properties:

- (i) For  $j \geq 2$ ,  $P_j(x) = 0(x^2)$  as  $x \rightarrow 0$  and  $P_j(x)$  has  $j-2$  zeroes in the interval  $(0,1)$  (Constraint property).
- (ii)  $P_j(x)$  oscillates between  $-1$  and  $+1$  for  $x \in [0,1]$  (Tschebycheff property).

The first of these two properties, the constraint property, allows one to write down immediately the formulae for  $P_j(x)$ ,

$$\left. \begin{aligned} P_0 &= 1 \\ P_1 &= x \\ P_2 &= x^2 \end{aligned} \right\} \text{(These are defined in this way by convention.)} \quad \text{(D.123)}$$

$$P_j = K_j x^2 \prod_{\ell=1}^{j-2} (x - z_{\ell}^{(j)}) .$$

The Tschebycheff property now determines the placement of the zeroes  $z_{\ell}^{(j)}$  and the value for the normalization constant  $K_j$ . In practice, the polynomial  $P_j(x)$  is found by computing the "external ordinates":

$$\left\{ x_{\ell}^{(j)} \right\}_{\ell=1}^{j-1} ,$$

viz., points satisfying the conditions

$$x_1^{(j)} < x_2^{(j)} < \dots < x_{j-2}^{(j)} < x_{j-1}^{(j)} = 1 \quad \text{(D.124)}$$

$$P_j'(x_{\ell}^{(j)}) = 0 \quad \ell = 1, 2, \dots, j-2 \text{ (extremal property)} \quad \text{(D.125)}$$

$$P_j(x_{\ell}^{(j)}) = (-1)^{\ell-1} \quad \ell = 1, 2, \dots, j-2 \text{ (oscillation property).} \quad \text{(D.126)}$$

Using the characterization shown by eq. (D.126) together with the constraint  $P_j(x) = Cx^2$  for small  $x$ ,  $P_j(x)$  can be written explicitly in terms of

$$\left\{ x_{\ell}^{(j)} \right\}_{\ell=1}^{j-1}$$

by using Lagrange interpolation basis functions (c.f. ref. 19, pp 284-285). One finds that

$$P_j(x) = \sum_{\ell=1}^{j-1} (-1)^{\ell-1} \delta_{\ell}(x) / \delta_{\ell}(x_{\ell}) \quad \text{(D.127-a)}$$

where  $\delta_\ell(x)$  are given, viz.,

$$\delta_\ell(x) = x^2 \prod_{\substack{j=1 \\ r=1 \\ r \neq \ell}} (x - x_r^{(j)}). \quad (\text{D.127-b})$$

This representation, coupled with the external conditions eq. (D.125), then provide (j-2) unknown external coordinates  $x_\ell^{(j)}$ ,  $\ell=1, \dots, j-2$ . Solving these equations numerically by Newton's method, eq. (D.127) provides an explicit representation of the function  $P_j(x)$ . The representation shown by eq. (D.123), in terms of the zeroes  $z_\ell^{(j)}$ , can then be obtained by solving the equations:

$$P_j(z_\ell^{(j)}) = 0$$

This has been done and the zeroes  $z_\ell^{(N+1)}$ ,  $\ell = 1, \dots, N-1$ ,  $N = 2, \dots, 11$  are tabulated in table 8. Having computed  $z_\ell^{(j)}$ , the condition eq. (D.126) with  $\ell = j-1$  provides an explicit and useful formula for the normalization constant  $K_j$ . One obtains

$$(-1)^{j-2} = P_j(x_{j-1}^{(j)}) = P_j(1) = K_j \prod_{\ell=1}^{j-2} (1 - z_\ell^{(j)})$$

so that

$$K_j = (-1)^j / \prod_{\ell=1}^{j-2} (1 - z_\ell^{(j)}) \quad (\text{D.128})$$

Having described the constrained Tschebycheff polynomials in sufficient detail, the error analysis can now begin.

Suppose that a function  $f(x)$  is approximated on  $[0,1]$  by a polynomial  $f_N(x)$  of degree  $N$  by requiring that  $f_N(x)$  interpolate the following  $(N+1)$  pieces of data:

$$f(0), f'(0), f(z_\ell^{(N+1)}), \ell = 1, 2, \dots, N-1.$$

Thus,  $f_N(x)$  satisfies,

$$\begin{aligned} f_N(0) &= f(0) \\ f_N'(0) &= f'(0) \\ f_N(z_\ell^{(N+1)}) &= f(z_\ell^{(N+1)}), \ell = 1, 2, \dots, N-1. \end{aligned}$$

When these conditions are satisfied, the standard error analysis for polynomial interpolation then provides the estimates (c.f. ref. 19, p. 278)

$$f(x) - f_N(x) = \frac{f^{(N+1)}(\xi)}{(N+1)!} x^2 (x - z_1^{(N+1)}) \dots (x - z_{N-1}^{(N+1)}) \quad (\text{D.129})$$

Using eq. (D.123) with  $j = N+1$ , one can then write

$$f(x) - f_N(x) = \frac{f^{(N+1)}(\xi) P_{N+1}(x)}{(N+1)! K_{N+1}}$$

Now, since  $|P_j(x)| \leq 1$  for all  $x \in [0,1]$ , the error bound

$$|f(x) - f_N(x)| \leq C_{N+1} |f^{(N+1)}(\xi)|, \quad \xi \in [0,1] \quad (\text{D.130})$$

follows directly provided the truncation coefficient  $C_{N+1}$  is defined by

$$C_{N+1} = 1 / [(N+1)! K_{N+1}] \quad (\text{D.131})$$

The bound eq. (D.130) is of fundamental importance in the subsequent error analysis. It shows that the error associated with the specified polynomial interpolation process is determined by a constant  $C_{N+1}$ , depending on the order of the fit, and the modulus of the  $(N+1)$ st derivative of  $f$ . The coefficients  $C_{N+1}$  decrease very rapidly with increasing  $N$ , an approximate formula being given by  $17.15 \times 2^{-4.86N} = 17.15 \times 10^{-1.46N}$ . Thus, each extra term in the polynomial approximation provides an improvement in accuracy of about 1-1/2 decimal digits.

Another useful bound can be obtained from the estimate eq. (D.129). This bound reads as follows

$$|f(x) - f_N(x)| \leq D_{N+1} |x| |f^{(N+1)}(\xi)| \quad (\text{D.132})$$

where  $D_{N+1}$  is defined by

$$D_{N+1} = \frac{1}{(N+1)!} \max_{0 \leq x \leq 1} \left| x (x - z_1^{(N+1)}) \dots (x - z_{N-1}^{(N+1)}) \right| \quad (\text{D.133})$$

The bound eq. (D.132) will be useful in obtaining the relative error bounds for X, viz., eq. (D.119). The coefficients  $D_{N+1}$  also decrease rapidly with increasing N, an approximate formula being given by

$$N_{N+1} = 27.9 \times 2^{-4.44} = 27.9 \times 10^{-1.34}$$

Finally, before applying our results to the functions  $*\psi$ , X and  $\theta$ , one final estimate is stated. Suppose that a function  $g(x)$  is approximated on  $[0,1]$  by a polynomial  $g_{N+2}(x)$  of degree N+1 by requiring that  $g_{N+2}(x)$  interpolate the following data:

$$g(0), g'(0), g''(0), g'''(0), g(z_\ell^{(N+1)}), \ell = 1, 2, \dots, N-1.$$

Then the standard error analysis for polynomial interpolation gives

$$g(x) - g_{N+2}(x) = \frac{g^{(N+3)}(\xi)}{(N+3)!} x^4 (x - z_1^{(N+1)}) \dots (x - z_{N-1}^{(N+1)}), \quad \xi \in [0,1] \quad (D.134)$$

Having obtained the fundamental estimates, viz., eqs. (D.129), (D.132), (D.134), the error bounds, i.e., eqs. (D.118), (D.119), (D.120), can now be obtained. Consider first the bound (D.118). Defining the variation of R, i.e.,  $\Delta R$ , as

$$\Delta R = R_{\max} - R_0, \quad (D.135)$$

a function  $R(x)$  is defined for  $x \in [0,1]$  by writing

$$R(x) = (R_0 + \Delta R x) \in [R_0, R_{\max}]. \quad (D.136)$$

Applying the estimate shown by eq. (D.129) to the function  $f(x)$ , i.e.,

$$f(x) = *\psi(R(x)) = (e^{-i\Omega R(x)} - 1) / R = (-i\Omega) \left[ (e^{-i\Omega R(x)} - 1) / (-i\Omega R) \right] \quad (D.137)$$

one obtains

$$|*\psi(R(x)) - *\tilde{\psi}(R(x))| = |f(x) - f_N(x)| \leq C_{N+1} |f^{(N+1)}(\xi)| \quad \text{for } \xi \in [0,1]. \quad (D.138)$$

Now  $f^{(N+1)}(x)$  can be easily computed from eq. (D.137) to find

$$f^{(N+1)}(x) = (-i\Omega) [-i\Omega \Delta R]^{N+1} \left( \frac{d}{dz} \right)^{N+1} \left[ (e^z - 1) / z \right] \Big|_{z = -i\Omega R}. \quad (D.139)$$

By a fairly straightforward computation, the identity

$$\left(\frac{d}{dz}\right)^p \left(\frac{e^z - 1}{z}\right) = \frac{1}{z^{p+1}} \int_0^z \xi e^{\xi} d\xi \quad (\text{D.140})$$

is easily proved. Applying this identity with  $p = N+1$  then yields

$$\left(\frac{d}{dz}\right)^{N+1} \left[\frac{e^z - 1}{z}\right] \Big|_{z = i\Omega R} = \frac{1}{(-i\Omega R)^{N+2}} \int_0^{-i\Omega R} \xi^{N+1} e^{\xi} d\xi = \int_0^1 \tau^{N+1} e^{-i\Omega R \tau} d\tau \quad (\text{D.141})$$

for  $\xi = -i\Omega R \tau$ .

The integral on the right has the following bound:

$$\left| \int_0^1 \tau^{N+1} e^{-i\Omega R \tau} d\tau \right| \leq \int_0^1 \tau^{N+1} |e^{-i\Omega R \tau}| d\tau \leq \int_0^1 \tau^{N+1} d\tau \leq \frac{1}{N+2}. \quad (\text{D.142})$$

Substituting this result into eq. (D.139) then yields the bound for  $f^{(N+1)}(x)$ , viz.,

$$\left| f^{(N+1)}(x) \right| \leq |\Omega| |\Omega \Delta R|^{N+1} \frac{1}{N+2}. \quad (\text{D.143})$$

Substituting this bound for the  $(N+1)^{\text{st}}$  derivative of  $f$  into eq. (D.138) then yields

$$\left| * \psi - * \tilde{\psi} \right| \leq C_{N+1} |\Omega| |\Omega \Delta R|^{N+1} \frac{1}{N+2}. \quad (\text{D.144})$$

Recalling that  $* \psi_{,0} = i\Omega$ ,  $\Delta \phi = |\Omega \Delta R|$ , the relative error bound follows directly as:

$$\left| (* \psi - * \tilde{\psi}) / * \psi_{,0} \right| \leq \frac{C_{N+1}}{N+2} |\Delta \phi|^{N+1}$$

as asserted by eq. (D.118).

Next, the error bound, shown as eq. (D.119) for  $X$ , is proved. Applying the bound shown as eq. (D.132) to the function  $f(x)$  defined by

$$f(x) = X(R(x)) \quad (\text{D.145})$$

one obtains

$$|X - \tilde{X}| \leq D_{N+1} X |f^{(N+1)}(\xi)|. \quad (D.146)$$

Now the (N+1)<sup>st</sup> derivative of this new f(x) is given as

$$\begin{aligned} f^{(N+1)}(x) &= \left(\frac{d}{dx}\right)^{N+1} \left[ \frac{e^{-i\Omega R(x)} - 1}{-i\Omega} \right] = \left(\frac{d}{dx}\right)^N [\Delta R e^{-i\Omega R(x)}] \\ &= (\Delta R) (-i\Omega \Delta R)^N e^{-i\Omega R(x)} \end{aligned}$$

so that

$$|f^{(N+1)}(x)| \leq \Delta R (\Delta \phi)^N. \quad (D.147)$$

Substituting this bound into eq. (D.146) and dividing by the gauge function, given by  $X_0 = R$ , yields the following bound:

$$|(X - \tilde{X}) / X_0| \leq \frac{1}{R} D_{N+1} X \Delta R (\Delta \phi)^N = D_{N+1} (\Delta \phi)^N \left( \frac{x \Delta R}{R(x)} \right).$$

This result directly implies the bound eq. (D.119) by virtue of the inequality

$$\frac{x \Delta R}{R(x)} = \frac{R(x) - R_0}{R(x)} = 1 - R_0 / R(x) < 1 \quad (D.148)$$

which implies

$$|x \Delta R / R| \leq 1.$$

Finally, the error bound, shown as eq. (D.120), is proved. Applying the estimate eq. (D.134) to the function g(x),

$$g(x) = \theta(R(x)) \quad (D.149)$$

one obtains

$$\theta(R(x)) - \tilde{\theta}(R(x)) = \frac{1}{(N+3)!} x^4 \prod_{\ell=1}^{N-1} (1 - z_\ell^{(N+1)}) \left(\frac{d}{dx}\right)^{(N+3)} [\theta(R(x))] \Big|_{x=\xi}. \quad (D.150)$$

A straightforward computation yields the following equation for the derivative expression:

$$\begin{aligned}
 \left(\frac{d}{dx}\right)^{N+3} [\theta(R(x))] &= \left(\frac{d}{dx}\right)^{N+2} [R(x)X(R(x))] \Delta R \\
 &= \left(\frac{d}{dx}\right)^{N+1} [X(R(x)) + \text{Re}^{-i\Omega R}] (\Delta R)^2 \\
 &= \left(\frac{d}{dx}\right)^N [(2 - i\Omega R)e^{-i\Omega R}] (\Delta R)^3 \\
 &= (N + 2 - i\Omega R)e^{-i\Omega R} (-i\Omega \Delta R)^N (\Delta R)^3.
 \end{aligned}$$

Substituting this into eq. (D.150) and dividing by the gauge function  $\theta_o = R^3/3$  yields

$$(\theta - \tilde{\theta}) / \theta_o = \frac{3}{(N+3)!} \frac{x^4}{R^3} \prod_{\ell=1}^{N-1} (x - z_\ell^{(N+1)}) \left[ \underbrace{(N+2)}_1 - \underbrace{i\Omega R}_2 e^{-i\Omega R} (-i\Delta\phi)^N \Delta R^3 \right].$$

Breaking this up into two terms as indicated yields

$$\begin{aligned}
 \frac{\theta - \tilde{\theta}}{\theta_o} &= \frac{3e^{-i\Omega R} (-i\Delta\phi)^N}{(N+3)!} \left[ (N+2) \left(\frac{x\Delta R}{R}\right)^3 \left(x \prod_{\ell=1}^{N-1} (x - z_\ell^{(N+1)})\right) \right. & 1 \\
 &\quad \left. + (-i\Omega \Delta R) \left(\frac{x\Delta R}{R}\right)^2 \left(x^2 \prod_{\ell=1}^{N-1} (x - z_\ell^{(N+1)})\right) \right] & 2
 \end{aligned}$$

Bounding this expression, one obtains

$$\left| \frac{\theta - \tilde{\theta}}{\theta_o} \right| \leq \frac{3 \cdot 1 \cdot \Delta\phi^N}{(N+3)!} \left[ (N+2) \cdot 1 \cdot [(N+1)! D_{N+1}] + |\Delta\phi| \cdot 1 \cdot [(N+1)! C_{N+1}] \right]. \quad (D.151)$$

In obtaining this bound, the definition of  $D_{N+1}$  shown by eq. (D.133) has been used together with the bound eq. (D.148) and the following identity:

$$\max_x \left| x^2 \prod_{\ell=1}^{j-2} (x - z_\ell^{(N+1)}) \right| = \max_x \left| \frac{P_{N+1}^{(x)}}{K_{N+1}} \right| = \frac{1}{K_{N+1}} = (N+1)! C_{N+1}.$$

Rearranging the bound eq. (D.151) slightly now yields the required form of the bound, cf. eq. (D.120):

$$\left| \frac{\theta - \tilde{\theta}}{\theta_0} \right| \leq \frac{3}{N+3} \left[ D_{N+1} (\Delta\phi)^N + \frac{C_{N+1}}{(N+2)} (\Delta\phi)^{N+1} \right]$$

## D.7 FAR-FIELD APPROXIMATIONS

Recall that the panel influences, viz., eqs. (C.128) through (C.139), describe the potential and the gradient of the potential induced at the field point  $P$  as the result of source and doublet distributions on quadrilateral surface panels. If the panel influence at the field point is evaluated, letting the field point recede to greater and greater distances from the panel, then the panel influence is found to depend less and less on the details of the panel source and doublet distributions; in fact, if the field point is sufficiently far from the panel, the panel influence appears to be that of a point source and a point doublet. This observation is the fundamental idea underlying the far field approximations to the panel influences.

The kernel function,  $\psi^*$ , and its gradient,  $\vec{\nabla}'\psi^*$ , are approximated by a truncated Taylor series expansion, and the panel influences are manipulated and separated into the sum of a product of two kinds of components. These two types of components are called kernel moments and panel moments. The kernel moments depend only upon the field point location relative to the point of expansion and are, in particular, independent of the geometry of the panel. The panel moments, on the other hand, depend only upon the geometry of the panel and may be computed once and for all before any panel influences are computed.

Because the kernel function,  $\psi^*$ , exhibits singular behavior as the field point of evaluation approaches the point of source or doublet definition, it is clear that the concept for far field expansions must break down as the field point approaches the point of kernel function definition. As a consequence, the far field expansion is applied only when the distance  $R$  from the field point  $P$  to every point  $Q$  on the panel is bounded substantially away from zero. Let  $\vec{q}_0$  denote the position of the point  $Q_0$  lying more or less in the panel center and let  $Q_0$  be the expansion point. Letting  $\vec{p}$  denote the position of the field point, the condition for bounding the field point away from the panel is expressed as

$$R(\vec{p}, \vec{q}_0) = |(\vec{p} - \vec{q}_0)| > K\bar{D} \quad (D.152)$$

where  $\bar{D}$  denotes the panel diameter measured in the scaled coordinate system, c.f. sec. C.1. The constant  $K$  has been chosen as follows:

$$K = \begin{cases} 1.5 \text{ quadrupole far-fields} \\ 4 \text{ dipole far-fields} \\ 12 \text{ monopole far-fields} \end{cases} \quad (D.153)$$

where the terms monopole, dipole, and quadripole refer to moments of the kernel function, and are defined in the following.

In addition to the condition shown by eq. (C.152), which is adequate to ensure that the function  $1/R$  is adequately approximated by a truncated Taylor series, it is also necessary to ensure that the total phase variation over the panel, viz.,

$$\Delta\phi = \Omega (R_{\max} - R_{\min}), \quad (\text{D.154})$$

is sufficiently small that adequate accuracy is achieved. Roughly, to indicate the nature of the requirements imposed by this condition, consider table 10 showing the value of  $\Delta\phi$  admissible for the monopole, dipole, and quadrupole approximations when the error in the approximation to the function,

$$e^{i\phi}$$

is less than or equal to  $\epsilon$ . The approximation is given by the truncated Taylor series:

$$e^{i\phi} \simeq e^{i\phi_0} \left\{ \sum_{j=0}^N \frac{[i(\phi - \phi_0)]^j}{j!} \right\}, \quad (\text{D.155})$$

and table 10 shows the value of  $\Delta\phi$  for which the approximation attains the accuracy  $\epsilon$  in the interval  $[\phi_0 - \Delta\phi, \phi_0 + \Delta\phi]$ . Since the absolute value of the error entailed in the approximation is provided by Lagrange remainder theorem, whence

$$\left| e^{i\phi} - e^{i\phi_0} \left\{ \sum_{j=0}^N \frac{[i(\phi - \phi_0)]^j}{j!} \right\} \right| = \frac{|\phi - \phi_0|^{N+1}}{(N+1)!},$$

the admissible range for  $\phi$  for a given  $N$  and a given  $\epsilon$  is

$$\Delta\phi = [(N+1)! \epsilon]^{1/(N+1)}. \quad (\text{D.156})$$

Table 10 is based on eq. (D.156).

These remarks are aimed at describing the accuracy of the procedure; the following describes the details of the procedure itself.

Table 10. — Admissible Panel Phase Variation \* Related to Truncation Errors

N \ ε	.001	.003	.01	.03	.1	.3
1, monopole	.045	.077	.141	.245	.447	.775
2, dipole	.182	.262	.391	.565	.843	1.216
3, quadrapole	.394	.518	.700	.921	1.245	1.638

\*Value of  $\Delta\phi$  such that, for  $(\phi_0 - \Delta\phi) \leq \phi \leq (\phi_0 + \Delta\phi)$ , the approximation

$$e^{i\phi} = e^{i\phi_0} \left\{ \sum_{j=0}^N \frac{[i(\phi - \phi_0)]^j}{j!} \right\}$$

is accurate to within  $\epsilon$

As stated above, the underlying principle of the far-field approximation follows from having replaced the actual kernel functions by truncated Taylor series approximations; therefore, as a starting point for describing the far-field approximation procedure, consider the Taylor series expansions for the kernel function and its gradient, viz.,

$$\psi^* = -\frac{1}{4\pi R} e^{-i\Omega R}$$

and

$$\vec{\nabla}' \psi^*,$$

where these expressions are in terms of the scaled coordinates introduced by sec. C.1. Proceeding in such a way as to preserve maximum symmetry, let

$$\psi^* = \psi^* (|\vec{p} - \vec{q}|) = \psi^* (|\vec{p} - \vec{q}_0 - (\vec{q} - \vec{q}_0)|) \quad (\text{D.157})$$

where  $\vec{p}$  is the position of the field point P and  $\vec{q}$  is the position of the surface point Q. The surface point  $Q_0$  with position  $\vec{q}_0$  will be the point of expansion; thus, letting

$$\vec{P} \equiv \vec{p} - \vec{q}_0 \text{ and } \vec{Q} \equiv \vec{q} - \vec{q}_0, \quad (\text{D.158})$$

$$P \equiv (P^i g_{ij} P^j)^{1/2} \text{ and } Q \equiv (Q^i g_{ij} Q^j)^{1/2}, \quad (\text{D.159})$$

$$P_i \equiv g_{ij} P^j \text{ and } Q_i \equiv g_{ij} Q^j, \quad (\text{D.160})$$

$$R \equiv [(P^i - Q^i) g_{ij} (P^j - Q^j)]^{1/2}, \quad (\text{D.161})$$

leads to the following expansion of the kernel function:

$$\psi^*(R) \doteq \psi^*(P) - Q^i \frac{\partial}{\partial P^i} \psi^*(P) + \frac{1}{2} Q^i Q^j \frac{\partial^2}{\partial P^i \partial P^j} \psi^*(P). \quad (\text{D.162})$$

Similarly,

$$\begin{aligned} \vec{\nabla}' \psi^* &= \vec{a}^k \frac{\partial \psi^*}{\partial Q^k} = -\vec{a}^k \frac{\partial \psi^*}{\partial P^k} = -\vec{a}_{\ell}^k g^{\ell k} \frac{\partial \psi^*}{\partial P^k} \\ &\doteq \vec{a}_{\ell}^k g^{\ell k} \left[ -\frac{\partial}{\partial P^k} \psi^*(P) + Q^i \frac{\partial^2}{\partial P^k \partial P^i} \psi^*(P) - \frac{1}{2} Q^i Q^j \frac{\partial^3}{\partial P^k \partial P^i \partial P^j} \psi^*(P) \right]. \end{aligned} \quad (\text{D.163})$$

Introducing the following identities:

$$\frac{\partial \psi^*}{\partial P^i} = \frac{\partial P}{\partial P^i} \frac{\partial \psi^*}{\partial P} = \frac{\partial}{\partial P^i} \left( P^\ell g_{\ell m} P^m \right)^{1/2} \frac{\partial \psi^*}{\partial P} = g_{im} \frac{P^m}{P} \frac{\partial \psi^*}{\partial P} = \frac{P_i}{P} \frac{\partial \psi^*}{\partial P}$$

$$\frac{\partial^2 \psi^*}{\partial P^i \partial P^j} = g_{ij} \frac{1}{P} \frac{\partial \psi^*}{\partial P} + P_i \frac{P_j}{P} \frac{\partial}{\partial P} \left( \frac{1}{P} \frac{\partial \psi^*}{\partial P} \right) = P_i P_j \left( -\frac{1}{P} \frac{\partial}{\partial P} \right)^2 \psi^* - g_{ij} \left( -\frac{1}{P} \frac{\partial \psi^*}{\partial P} \right)$$

$$\frac{\partial^3 \psi^*}{\partial P^i \partial P^j \partial P^k} = -P_i P_j P_k \left( -\frac{1}{P} \frac{\partial}{\partial P} \right)^3 \psi^* + \left[ g_{ij} P_k + g_{ik} P_j + g_{jk} P_i \right] \left( -\frac{1}{P} \frac{\partial}{\partial P} \right)^2 \psi^*$$

and defining the operator  $D$  by

$$D \equiv -\frac{1}{P} \frac{\partial}{\partial P}$$

and substituting it into eqs. (D.162) and (D.163) leads to the following truncated expansions of the kernel function and its gradient:

$$\psi^*(R) \doteq \psi^*(P) + Q^i P_i D \psi^* + \frac{1}{2} Q^i Q^j \left( P_i P_j D^2 \psi^* - g_{ij} D \psi^* \right) \quad (D.164)$$

$$\begin{aligned} \vec{\nabla} \psi^* \doteq \vec{a}_\rho g^{\rho k} \left\{ P_k D \psi^* + Q^i \left[ P_i P_k D^2 \psi^* - g_{ik} D \psi^* \right] \right. \\ \left. + \frac{1}{2} Q^i Q^j \left[ P_i P_j P_k D^3 \psi^* - \left( g_{ij} P_k + g_{ik} P_j + g_{jk} P_i \right) D^2 \psi^* \right] \right\} \quad (D.165) \end{aligned}$$

where the following identity has been used:

$$Q_i P^i = Q^i P_i.$$

Eqs. (D.164) and (D.165) lead to the definition of quantities which are termed kernel function moments, viz.,

$$\begin{aligned} G_{(0)} &= \psi^*(P) \\ G_{(1)}^i &= P^i D \psi^* \\ G_{(2)}^{ij} &= P^i P^j (D^2 \psi^*) - g^{ij} D \psi^* \\ G_{(4)}^{ijk} &= P^i P^j P^k (D^3 \psi^*) - \left( P^i g^{ik} + P^j g^{jk} P^k g^{ij} \right) D^2 \psi^* \quad (D.166) \end{aligned}$$

where each of these moments has the property of a tensor which is completely symmetric in its indices. In terms of the kernel moments the truncated expansions become

$$\psi^*(R) \doteq G_{(0)} + Q_i G_{(1)}^i + \frac{1}{2} Q_i Q_j G_{(2)}^{ij} \quad (D.167)$$

$$\vec{\nabla}' \psi^* \doteq \vec{a}_k \left( G_{(1)}^k + Q_i G_{(2)}^{ik} + \frac{1}{2} Q_i Q_j G_{(4)}^{ijk} \right). \quad (D.168)$$

Having obtained these approximations for the kernel function and its gradient, the panel influences shown by eqs. (C.128) through (C.139) can be evaluated for the far-field approximation. The result of that evaluation is expressed in terms of the following panel moments:

$$\begin{Bmatrix} E_n \\ E_{in} \\ E_{ijn} \end{Bmatrix} \equiv - \iint_{\Sigma_e} S_n \begin{Bmatrix} 1 \\ Q_i \\ \frac{1}{2} Q_i Q_j \end{Bmatrix} ds \text{ for } \sigma^* = \sum_n S_n \bar{\sigma}_n \quad (D.168)$$

$$\begin{Bmatrix} W_{kn} \\ W_{ikn} \\ W_{ijkn} \end{Bmatrix} \equiv - \iint_{\Sigma_e} m_n \begin{Bmatrix} 1 \\ Q_i \\ \frac{1}{2} Q_i Q_j \end{Bmatrix} n_k ds \text{ for } \mu^* = \sum_n m_n \bar{\mu}_n \quad (D.170)$$

$$\begin{Bmatrix} F_{\delta n} \\ F_{\delta in} \\ F_{\delta ijn} \end{Bmatrix} \equiv \iint_{\Sigma_e} -e^{\alpha\beta} e_{\delta\beta} \frac{\partial m_n}{\partial \xi^\alpha} \begin{Bmatrix} 1 \\ Q_i \\ \frac{1}{2} Q_i Q_j \end{Bmatrix} ds \text{ for } \begin{matrix} \alpha = 1,2 \\ \beta = 1,2 \\ \delta = 1,2 \end{matrix} \quad (D.171)$$

where it should be noted that the entries of the F-moments are vectors; moreover, all these moments are symmetric in the  $ij$  indices.

Using the above definitions, the panel influences are written in the following concise form:

$$\begin{aligned} \phi_S &= \sum_n \iint_{\Sigma_e} S_n \left( G_{(0)} + Q_i G_{(1)}^i + \frac{1}{2} Q_i Q_j G_{(2)}^{ij} \right) ds \bar{\sigma}_n \\ &= \sum_n \left( G_{(0)} E_n + G_{(1)}^i E_{in} + G_{(2)}^{ij} E_{ijn} \right) \bar{\sigma}_n \end{aligned} \quad (D.172)$$

$$\begin{aligned}
\phi_D &= \sum_n \iint_{\Sigma_e} m_n \left( G_{(1)}^k + Q_i G_{(2)}^{ki} + \frac{1}{2} Q_i Q_j G_{(4)}^{kij} \right) \vec{a}_k \cdot \hat{n} \, ds \, \bar{\mu}_n \\
&= \sum_n \left( G_{(1)}^k W_{kn} + G_{(2)}^{ik} W_{ikn} + G_{(4)}^{ijk} W_{ijkn} \right) \bar{\mu}_n
\end{aligned} \tag{D.173}$$

$$\begin{aligned}
\vec{v}_S &= \sum_n \iint_{\Sigma_e} S_n \left( G_{(1)}^k + Q_i G_{(2)}^{ki} + \frac{1}{2} Q_i Q_j G_{(4)}^{kij} \right) \vec{a}_k \, ds \, \bar{\sigma}_n \\
&= \vec{a}_i \sum_n \left( G_{(1)}^i E_n + G_{(2)}^{ij} E_{jn} + G_{(4)}^{ijk} E_{jkn} \right) \bar{\sigma}_n
\end{aligned} \tag{D.174}$$

$$\begin{aligned}
\vec{v}_{D_\delta}^* &= \sum_n \left( F_{\delta n} G_{(1)}^k + F_{\delta in} G_{(2)}^{ik} + F_{\delta ijn} G_{(4)}^{ijk} \right) n_k \, ds \, \bar{\mu}_n \\
\vec{v}_{D_3}^* &= \sum_n - \left( F_{\delta n} G_{(1)}^\delta + F_{\delta in} G_{(2)}^{i\delta} + F_{\delta ijn} G_{(4)}^{ij\delta} \right) \, ds \, \bar{\mu}_n
\end{aligned} \tag{D.175}$$

**APPENDIX E**  
**SECOND ORDER DERIVATIVES OF THE VELOCITY POTENTIAL**

The following terms appears in the boundary condition shown as equation eq. (31):

$$(\vec{D}^* \cdot \vec{\nabla} \vec{W}_s) \cdot \hat{n}_s$$

and this term contains the operations:

$$\vec{\nabla} \vec{W}_s = \vec{\nabla} (\vec{\nabla} \phi_s - \hat{c} M_o^2 \hat{c} \cdot \vec{\nabla} \phi_s) \quad (E.1)$$

which, in turn, contains second order derivatives of the velocity potential of the steady mean component of flow. The objective of this appendix is to present a means for evaluating those derivatives.

Recall that the doublet strength at a network surface point is equal to the jump in potential across the network surface, c.f., eq. (C.27). In the case of a thick body on which Morino-type boundary conditions are applied, c.f., sec. 3.4, the potential vanishes at the interior of the body; hence, the doublet strength at the body surface is equal to the value of the potential at the exterior side of the surface of the body, i.e.,

$$\phi_s = \mu_s \quad (E.2)$$

at the body surface. The steady flow panel method computes the doublet strength as a quadratic function of the surface coordinates, viz.,

$$\mu_s(Q) = \mu_o + \mu_\xi \xi + \mu_\eta \eta + \frac{1}{2} \mu_{\xi\xi} \xi^2 + \mu_{\xi\eta} \xi \eta + \frac{1}{2} \mu_{\eta\eta} \eta^2; \quad (E.3)$$

hence, the following second order derivatives of the velocity potential are readily evaluated:

$$\begin{aligned} (\phi_s)_{\xi\xi} &= \mu_{\xi\xi} \\ (\phi_s)_{\xi\eta} &= \mu_{\xi\eta} \\ (\phi_s)_{\eta\eta} &= \mu_{\eta\eta} \end{aligned} \quad (E.4)$$

Of the remaining second order derivatives  $(\phi_s)_{\xi\xi}$  can be evaluated using the flow equation, i.e.,

$$\nabla^2 \phi_s - M_o^2 \hat{c} \cdot \vec{\nabla} (\hat{c} \cdot \vec{\nabla} \phi_s) = 0. \quad (E.5)$$

Letting

$$\hat{g}_\xi, \hat{g}_\eta, \hat{g}_\zeta$$

represent the unit base vectors in the directions of the surface coordinates, it follows that

$$\begin{aligned} \phi_{\zeta\zeta} = & - \frac{1}{1 - (M_o \hat{c} \cdot \hat{g}_\zeta)^2} \left\{ \phi_{\xi\xi} \left[ 1 - (M_o \hat{c} \cdot \hat{g}_\xi)^2 \right] \right. \\ & \left. + \phi_{\eta\eta} \left[ 1 - (M_o \hat{c} \cdot \hat{g}_\eta)^2 \right] \right\}. \end{aligned} \quad (E.6)$$

The remaining second-order derivatives can be evaluated using the steady flow boundary condition applied at aerodynamic surfaces, viz.,

$$\vec{W}_s \cdot \hat{n}_s = 0,$$

which, when expressed in terms of the surface coordinates, becomes

$$\phi_\zeta = -U_o \hat{c} \cdot \hat{n}_s. \quad (E.7)$$

The surface is to be represented as a quadratic function of the surface coordinates at each panel, i.e.,

$$f(\xi, \eta, \zeta) = 0$$

where

$$f(\xi, \eta, \zeta) = \zeta - \left( \zeta_o + \zeta_{\xi\xi}\xi + \zeta_{\eta\eta}\eta + \frac{1}{2}\zeta_{\xi\xi\xi}\xi^2 + \zeta_{\xi\eta}\xi\eta + \frac{1}{2}\zeta_{\eta\eta\eta}\eta^2 \right), \quad (E.8)$$

and the vector normal to the surface is

$$\hat{n}_s = \frac{\vec{\nabla} f}{|\vec{\nabla} f|} \quad (E.9)$$

where

$$\vec{\nabla} f = - \left( \zeta_\xi + \zeta_{\xi\xi\xi}\xi + \zeta_{\xi\eta}\eta \right) \hat{g}_\xi - \left( \zeta_\eta + \zeta_{\eta\eta}\eta + \zeta_{\xi\eta}\xi \right) \hat{g}_\eta + \hat{g}_\zeta \quad (E.10)$$

and

$$|\vec{\nabla} f| = \sqrt{\left( \zeta_\xi + \zeta_{\xi\xi\xi}\xi + \zeta_{\xi\eta}\eta \right)^2 + \left( \zeta_\eta + \zeta_{\eta\eta}\eta + \zeta_{\xi\eta}\xi \right)^2 + 1}. \quad (E.11)$$

Finally, the two remaining second-order derivatives are formed by differentiating eq. E.7 to obtain the following:

$$\phi_{\xi\xi} = -U_o \hat{c} \cdot \left[ \left( -\xi_{\xi\xi} \hat{g}_{\xi\xi} - \xi_{\xi\eta} \hat{g}_{\xi\eta} \right) \left( 1 / |\nabla f| \right) - (\nabla f) (|\nabla f|_{\xi}) / (|\nabla f|)^2 \right] \quad (\text{E.12})$$

and

$$\phi_{\eta\xi} = -U_o \hat{c} \cdot \left[ \left( -\xi_{\xi\eta} \hat{g}_{\xi\xi} - \xi_{\eta\eta} \hat{g}_{\eta\eta} \right) \left( 1 / |\nabla f| \right) - (\nabla f) (|\nabla f|_{\eta}) / (|\nabla f|)^2 \right] \quad (\text{E.13})$$

Eqs. (E.4), (E.6), (E.12), and (E.13) provide a means for evaluating all nine components of the gradient of the mean steady flow velocity potential.

## REFERENCES

1. Ehlers, E.F., Epton, M.A., Johnson, F.T., Magnus, A.E., and Rubbert, P.E.: "A Higher Order Panel Method for Linearized Supersonic Flow," NASA CR-3062, 1979.
2. Moran, J., Tinoco, E.N., and Johnson, F.T.: "User's Manual, Subsonic/Supersonic Advanced Panel Pilot Code," NASA CR-152047, 1978.
3. Sneddon, I.N.: "Elements of Partial Differential Equations," McGraw-Hill Book Co., 1957.
4. Morino, L., Kuo, C.: "Subsonic Potential Aerodynamics for Complex Configurations: A General Theory," AIAA Journal, p. 191, 1974.
5. Sokolnikoff, I.S.: "Tensor Analysis," John Wiley and Sons, 1964.
6. Garrick, I.E.: "Nonsteady Wing Characteristics," Princeton Series in High Speed Aerodynamics and Jet Propulsion, Vol. VII, Section F, Princeton Univ. Press, 1957.
7. Ashley, H., and Landahl, M.: "Aerodynamics of Wings and Bodies," Addison-Wesley, 1965.
8. Rowe, W.S., Redman, F.E., Ehlers, F.E., and Sebastian: "Prediction of Unsteady Aerodynamic Loads Caused by Leading Edge and Trailing Edge Control Surface Motions in Subsonic Compressible Flow—Analysis and Results," NASA CR-2543, August 1975.
9. Forsching, H., Friebstein, H., Wagner, J.: "Pressure Measurements on a Harmonically Oscillating Swept Wing with Two Control Surfaces in Incompressible Flow," AGARD Conference Proceedings No. 80, 1971.
10. Clevenson, S.H., Leadbetter, S.A.: "Measurements of Aerodynamic Forces and Moments at Subsonic Speeds on a Simplified T-Tail Oscillating in Yaw about the Fin Midchord," NACA TN4402, 1958.
11. Davies, D.E.: "Generalized Aerodynamic Forces on a T-Tail Oscillating Harmonically in Subsonic Flow," Report No. Structures 295, Royal Aircraft Establishment, Ministry of Aviation, May 1964.
12. Stark, V.J.E.: "Aerodynamic Forces on a Combination of a Wing and a Fin Oscillating in Subsonic Flow," Report TN54, Saab Aircraft Co., Linkoping, Sweden, 1964.
13. Kalman, T.P., Rodden, W.P., and Giesing, J.P.: "Application of the Doublet-Lattice Method to Nonplanar Configurations in Subsonic Flow," AIAA Journal of Aircraft, Vol. 8, No. 6, June 1971.
14. Serrin, J.: "Handbuch der Physik, Mathematical Principles of Classical Fluid Mechanics," Springer-Verlag, 1960.

## REFERENCES (CONCLUDED)

15. Karamcheti, K.: "Principles of Ideal-Fluid Aerodynamics," John Wiley and Sons, 1966.
16. Truesdell, C., and Toupin, R.A.: "Handbuch der Physik, The Classical Field Theories," Springer-Verlag, 1960.
17. Magnus, A.E., Epton, M.A.: "PAN AIR – A Computer Program for Predicting Subsonic and Supersonic Linear Potential Flows about Arbitrary Configurations Using a Higher Order Panel Method," Vol. I—Theory Document (Ver. 1.0), NASA CR-3251, 1980.
18. Johnson, F.T.: "A General Panel Method for the Analysis and Design of Arbitrary Configurations in Incompressible Flows," NASA CR-3079, December 1975.
19. Dahlquist, G., Bjork, A.: "Numerical Methods," Prentice Hall, Inc., 1974.

